Isolation, characterization and pharmacological application of bioactive compound from leaves of *Alpinia nigra* (Gaertn.) B.L. Burtt

A thesis submitted by

Manish Kumar Gupta

For the award of the degree

of

Doctor of Philosophy

September 2022

Department of Biosciences and Bioengineering

Indian Institute of Technology Guwahati

Guwahati 781039, Assam, India

INDIAN INSTITUTE OF TECHNOLOGY GUWAHATI

Department of Biosciences and Bioengineering

Guwahati – 781039

STATEMENT

I do hereby declare that the matter embodied in this thesis entitled **"Isolation, characterization and pharmacological application of bioactive compound from leaves of *Alpinia nigra* (Gaertn.) B.L. Burtt"** is the result of investigations carried out by me in the Department of Biosciences and Bioengineering, Indian Institute of Technology Guwahati, India, under the guidance of Prof. Latha Rangan. In keeping with the general practice of reporting scientific observations, due acknowledgements have been made wherever the work described is based on the findings of other investigators.

September 2022

Manish Kumar Gupta

Department of Biosciences and Bioengineering

Indian Institute of Technology Guwahati

Guwahati 781039, Assam India

INDIAN INSTITUTE OF TECHNOLOGY GUWAHATI
Department of Biosciences and Bioengineering
Guwahati – 781039

CERTIFICATE

It is certified that the work described in this thesis, entitled **"Isolation, characterization and pharmacological application of bioactive compound from leaves of *Alpinia nigra* (Gaertn.) B.L. Burtt"**, done by Mr. Manish Kumar Gupta for the award of degree of Doctor of Philosophy is an authentic record of the results obtained from the research work carried out under my supervision in the Department of Biosciences and Bioengineering, Indian Institute of Technology Guwahati, India, and this work has not been submitted elsewhere for a degree.

September 2022

Prof. Latha Rangan
(Thesis Supervisor)
Department of Biosciences and Bioengineering
Indian Institute of Technology Guwahati
Guwahati 781039, Assam India

Dedicated to my beloved parents

ACKNOWLEDGEMENTS

Several people helped and encouraged me throughout my PhD duration, which enabled me to complete this doctoral thesis. Firstly, I am truly thankful to Prof. Latha Rangan for her scientific and moral guidance as mentor throughout my doctoral research. I wish to express sincere appreciation to the doctoral committee members Prof. Sumana Dutta, Dr. Rajkumar P. Thummer, Prof. Manish Kumar for their suggestions, practical advice, and timely guidance in completion of the thesis work. Furthermore, I would like to express my gratitude to Prof. Vikash Kumar Dubey, Prof. Ajay B. Kunnumakkara, Department of BSBE, IITG, for allowing me to complete a portion of my doctoral thesis work in their laboratories, as well as for their constant attention and excellent guidance in achieving the objectives with great scientific effort. My heartfelt gratitude and great respect go to Dr. Rakhi Chaturvedi, Head, Department of BSBE, IIT Guwahati, and former HOD Prof. Latha Rangan. I sincerely thank all the staff members of the Department of BSBE, especially Mr. Nurul Islam, Mr. Niranjan Barah, Ms. Prarthana Swargari and Mr. Dipankar Barman who had helped me by all the ways during my stay at IITG. The timely assistance and cooperation of CIF, IITG staff members are gratefully recognized here. All of these moves owe a debt of gratitude to the Ministry of Education, Government of India, for providing much-needed financial assistance during my PhD term.

My heartfelt gratitude to my friends and seniors, Dr. Rahul G. Shelke, Dr. Anuma Singh, Dr. Reshmi Das, Dr. Rajkumari Jobina, and Ms. S. Sanjana for their priceless cooperation and support. Members of our lab group have made a significant contribution to my personal and professional development during my stay at IITG. In addition, special thanks to Gaurav Bhatt, Alok Senapati, Heeramoni Boro, Nuzelu, Anamika and Rashmi Singh. The group has served as a stress reliever as well as a source of helpful information and collaboration.

I am eternally grateful to my parents, who allowed me to see this wonderful world and prove my scientific work. The prayers and blessings of my parents have enabled me to overcome all the challenges of life. I express my heartfelt gratitude to my sister and brother for their unwavering moral support, constant encouragement and faith in me.

A personal note of gratitude, love, and respect to everyone who has supported me with my PhD thesis work, whether directly or indirectly. Finally, I would want to express my gratitude to almighty God for his unwavering support throughout my time at IIT Guwahati.

September 2022 **Manish Kumar Gupta**

Table of contents

Graphical abstract

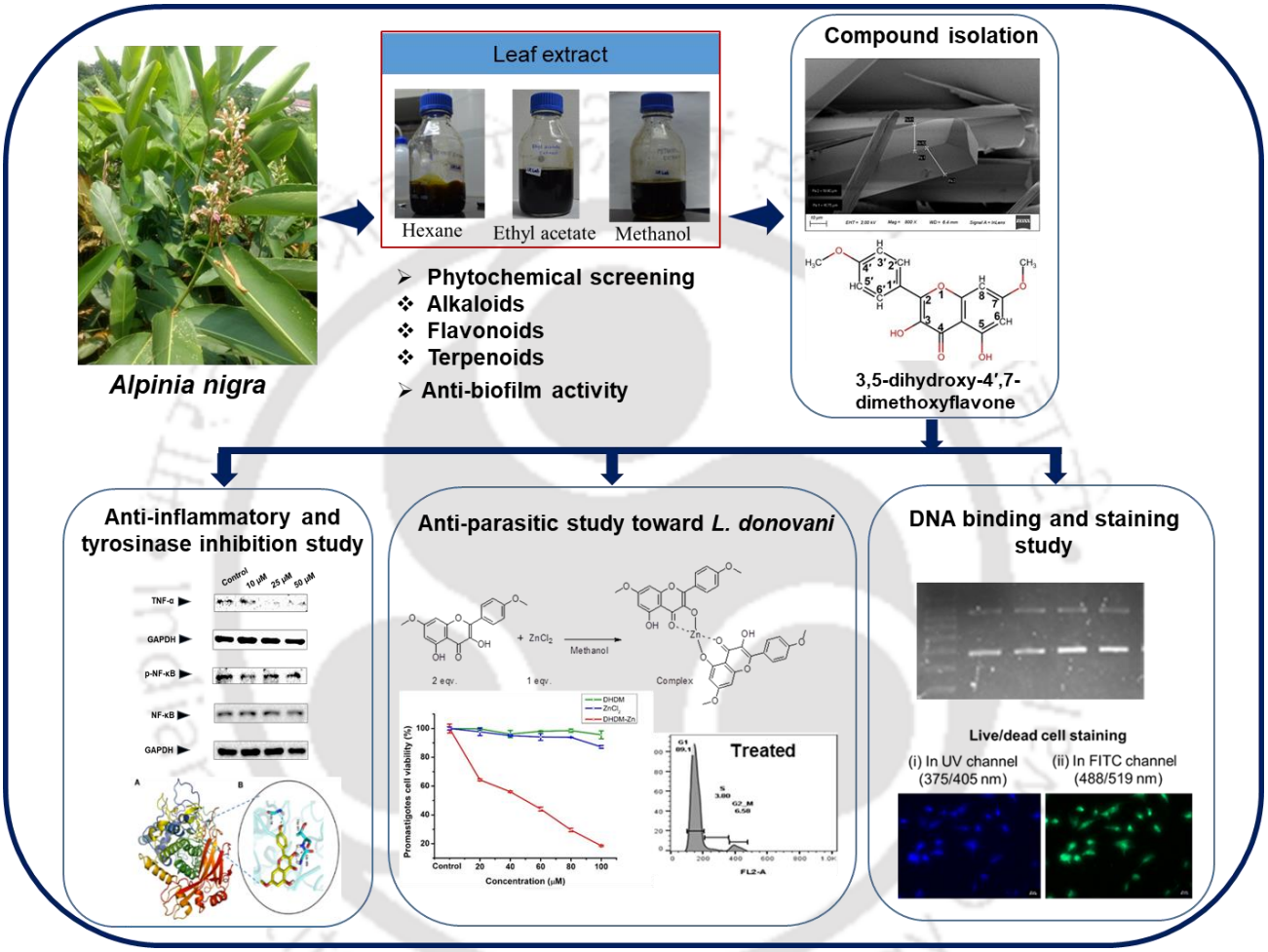

Abstract

The present study is focused on investigating the potential uses of the herbaceous plant *Alpinia nigra* (Gaertn.) B.L. Burtt (Zingiberaceae). Traditionally this plant is used in folk remedies for curing gastritis and infectious diseases. The plant leaves are used as a food-flavoring agent by tribal people in Northeast (NE) India. However, the scientific community has not explored the plant leaf for its medicinal properties. Thus in the present study, the leaf extracts hexane (L-Hex), ethyl acetate (L-EtAc), and methanol (L-Met) were subjected to phytochemical analysis. The antibacterial, anti-biofilm, and anti-quorum sensing activities of the L-EtAc extract was determined by *in-vitro* analysis and was found to be potential. Further, the compound 3, 5-dihydroxy 4′,7-dimethoxy flavone (DHDM) was purified from L-EtAc, crystallized, and structural characterization was performed using multispectroscopic techniques including HRMS, FTIR, Raman, SC-XRD, 1-D NMR, and 2-D NMR. The cell viability assay showed no inhibition of DHDM at ≤200 μM concentration in THP-1 (human macrophage) and ≤80 μM in HaCaT (human keratinocyte) cell lines. Additionally, strong antioxidant properties and reduced ROS generation suggested preventing oxidative damage and skin aging. Fluorescence quenching studies and molecular docking revealed strong binding of DHDM to tyrosinase leading to the conformational change. Further, the anti-tyrosinase activity of the isolated compound was observed at 42.5 μM (IC_{50}). Moreover, DHDM inhibited the expression of anti-inflammatory proteins like TNF-α and NF-κB. Furthermore, DHDM was evaluated as the antileishmanial agent, but the result was not significant. Therefore, a zinc derivative of DHDM was synthesized to enhance its anti-leishmanial effect. DHDM-Zn displayed considerable leishmanicidal activity (IC_{50} ~63±0.73 μM). Interestingly, significant growth inhibition in the promastigote cells was observed upon DHDM-Zn treatment. The flow cytometry analysis revealed promastigote's cell cycle arrest in the G1 phase. This may be due to the fact that the compound might bind with DNA and inhibit the DNA replication. The binding nature of DHDM with nucleic acid (DNA) was investigated using UV–visible spectrophotometer, Isothermal calorimetry thermodynamic (ITC), and agarose gel-based assay. Thus exploring its potential as an alternative dye for ethidium bromide (EtBr). The study also confirmed the differential staining of live/dead cell for fluorescence microscopic study.

Abbreviations

ANOVA	Analysis of variance
ADT	AutoDock Tools
BHT	Butylated hydroxyl toluene
BSA	Bovine serum albumin
BHK	Baby hamster kidney
CBB	Coomassie brilliant blue
CC	Column chromatography
COX	Cyclooxygenase
DNA	Deoxyribonucleic acid
DM	Diabetes mellitus
DFT	Density functional theory
DHDM	3,5-dihydroxy-4′,7-dimethoxyflavone
DM	Diabetes mellitus
DMSO	Dimethyl sulfoxide
DPPH	2, 2-diphenyl-1-picrylhydrazyl
DAPI	4′,6-diamidino-2-phenylindole
EDX	Energy dispersive X-ray
EtBr	Ethidium bromide
FC	Flow cytometry
FDA	Food and drug administration
FESEM	Field emission scanning electron microscopy
FTIR	Fourier transform infrared spectroscopy
GAE	Gallic acid equivalents
GC-MS	Gas chromatography mass spectrometry
GMP	Good manufacturing practices
GP63	Glycoprotein 63
HPA	Human pancreatic α-amylase
HPLC	High-performance liquid chromatography
HRMS	High resolution mass spectrometry
HaCaT	Human keratinocyte cells

HSA	Human serum albumin
IDF	International diabetes foundation
IC	inhibitory concentration
ITC	Isothermal calorimetry thermodynamic
IE	Interaction energy
KI	Kovat's indices
KBr	Potassium bromide
LB	Lineweaver-Burk
MBC	Minimum bactericidal concentration
MD	MolDock
MFI	Median fluorescence
MGAM	Maltase-glucoamylase
MIC	Minimal inhibitory concentration
MMP	Matrix metalloproteinases
MTT	3(4,5- dimethylthiazol-2-yl)-2,5-diphenyl tetrazolium bromide
MVD	Molegro virtual docker
NF-κB	Nuclear factor kappa B
NEI	North East India
NMR	Nuclear magnetic resonance
OD	Optical density
PBS	Phosphate buffer saline
PDB	Protein data bank
PCR	Polymerase chain reaction
PI	Propidium iodide
pNPG	p-Nitrophenyl- -D-glucopyranoside
RBC	Red blood cells
RNA	Ribonucleic acid
L-EtAc	Ethyl accetate extract of leaf
L-Hex	Hexane extract of leaf
L-Met	Methanolic extract of leaf

QS	Quorum sensing
RT	Retention time
R_f	retention factor
SEM	Scanning electron microscopy
Sc-XRD	Single-crystal X-ray diffraction
UV	Ultraviolet
VL	Visceral leishmaniasis
TNF-α	Tumor Necrosis Factor Alpha
THP-1	(human macrophage)
TLC	Thin-layer chromatography
TSP	Total soluble phenolics
WHO	World Health Organisation
Zn	Zinc

List of NMR units

Hz	Hertz
J	Coupling constant
M	Multiplet
MHz	Mega Hertz
PPM	Parts per million
S	Singlet
T	Triplet
δ	Chemical shift

Units

µg	Microgram
µg/µl	Microgram per microlitre
µg/mL	Microgram per milliliter
µl	Microlitre
µM	Micromolar
µS	Micro simen
ºC	Degree celsius
Å	Angstrom
a.u.	Arbitrary units
g	Gram
hr	Hour
kcal/mol	Kilocalorie per mole
mg	Milligram
mg/mL	Milligram per millilitre
min	Minute
mL	Milliliter
mM	Millimolar
pH	Negative log H+ ion
rpm	Revolution per minute
s	Second
v/v	Volume/volume
w/v	Weight/volume

List of figures

List of tables

Introduction

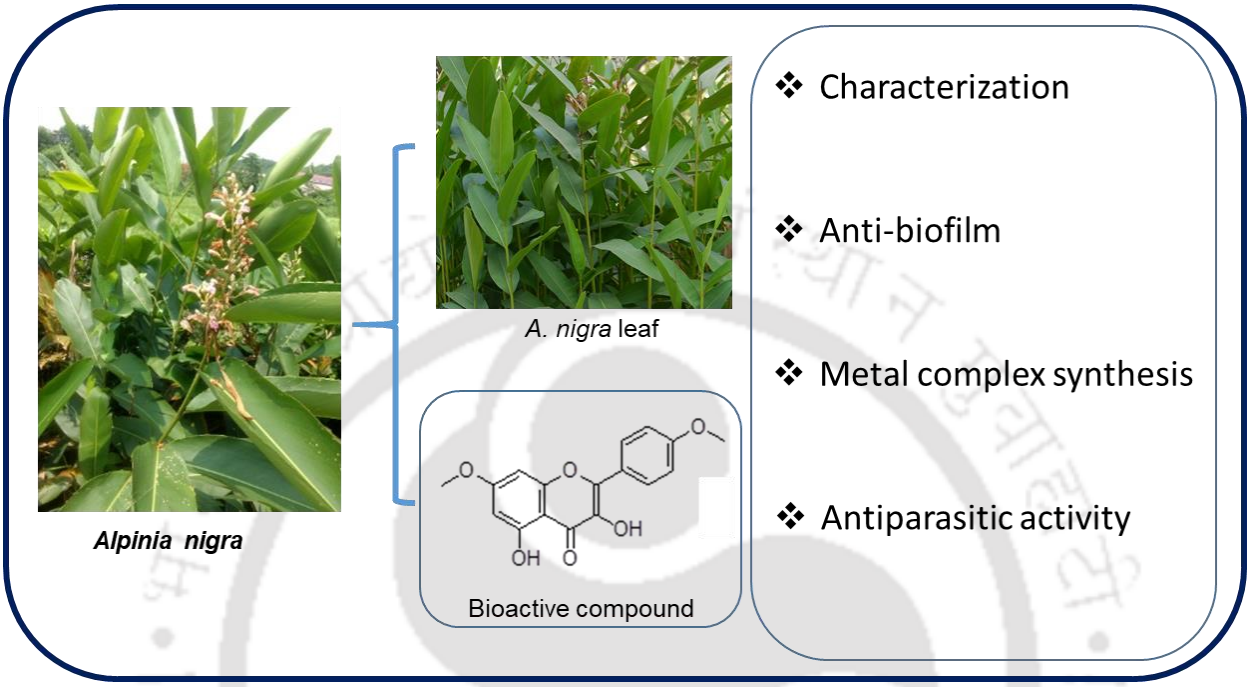

This chapter presents the background and inspiration for the current research and the role of plant-derived natural compounds for the treatment of various diseases. It also emphasizes the numerous ways that have been used to achieve specific objectives.

Chapter 1

Introduction

Plants are a source of therapeutic agents used to cure various diseases for centuries. Nature has continuously provided different range of secondary metabolites. The secondary metabolites found are mainly of complex mixture (crude extracts) containing various bioactive compounds. Currently, extensive research is being carried out on the different plant species and their therapeutic values, due to which traditional medicine has become popular all over the world. Plants contain many phytochemicals with various bioactivities, including antibacterial, antioxidant, anti-inflammatory, and anticancer activities. However, less than 10% of the world's biodiversity has been evaluated for potential biological activity (Cragg and Newman 2013). The continuing nature of several bacterial diseases is endorsed to the formation of biofilms that are intractable to antibiotic therapy. Biofilm-associated diseases have affected millions of people worldwide and are highly resistant to the host immune system due to frequent surface antigens and gene expression changes. Therefore, there is a need to find out an alternative approach to cure biofilm infections. Plant-derived bioactive compounds and its derivative have shown a significant role in combatting bacterial infection.

Zingiberaceae plant product and their derivative have reported efficacy against bacterial diseases (Tushar et al. 2010a). Recently, many plant-derived compounds were reported for their anti-biofilm effect (Kaverimanian and Heuertz 2019a). Furthermore, we note that natural compounds have been shown highly effective against many microbial pathogens. *Pseudomonas aeruginosa* is presumably involved in biofilm formation and protects from the host defensive mechanism. *P. aeruginosa* biofilm-forming bacteria produce many quorum sensing (QS) signals to form a colony and generate susceptibility against the external effect (Thi et al. 2020).

Medicinal plants have aided in the development of new and unique pharmacological entities by functioning as drug templates (Egbuna et al. 2020). Plants produce a wide range of phytochemicals that aid in biological process protection and repair. The diverse uses of plants in treating various diseases are estimated as beneficial for pharmaceutical industries. Phytochemicals such as flavonoids, tannin, saponin, terpenoid, cellulose, and some other phenolic compounds have varied industrial use and are thus economically valuable. The qualitative and quantitative estimation of these phytochemicals from the plant source will help to know the economical and medicinal value of plants (Egbuna et al. 2020). The previous reports

have revealed very few plants species investigated pharmacologically and phytochemically. According to Atanasov et al. (2015), only ~ 6% and ~15 % of existing plant species have been studied pharmacologically and phytochemically (Atanasov et al. 2015a). Therefore, ethnomedicinal knowledge of plants species has supported further investigations of plant-based secondary metabolites. The intricate chemical structure of secondary metabolites and its pharmacological consequences is critical for increasing the likelihood of success in new drug development. Nearly 69 small-molecule new drugs approved from 2005 to 2007 worldwide, 13 were evolved through natural sources by bioactive natural products. Bioactive natural compounds were responsible for over a quarter of contemporary medicine's development and evolution. Due to the difficulty of extracting natural compounds on a wide scale, only around 10% of the entire biodiversity of plants has been investigated for therapeutic purposes. However, many beneficial bioactive compounds derived from natural sources remain undiscovered (Yuan et al. 2016). Advanced analytical and spectroscopic techniques helps to understand the structure of many natural products and their complex chemical entities for novel drug discovery. Modern analytical techniques are also involved in the rapidity of compound isolation and elucidation of natural product structure. The spectroscopic studies also give insight for addressing the specificity and suitability of the therapeutics activity of natural bioactive products (Ghosh et al. 2013a).

Spectroscopic methods are frequently employed in the structure elucidation of the bioactive compounds. Manly spectroscopic methods like high-resolution mass spectrometry (HRMS), nuclear magnetic resonance (NMR), Raman, and Fourier transform infrared spectroscopy (FTIR) are used in the characterization procedure. Furthermore, single-crystal X-ray diffraction (Sc-XRD) and powder X-ray diffraction are mainly used to know crystal patterns of natural compounds (Abu Khalaf et al. 2019; Gupta et al. 2021). Raman and infrared spectroscopy techniques have created an accumulative assessment to identify and analyze the vibrational assignments of bioactive compounds. IR assignments spectra of the compound can be compared with the computational density functional theory (DFT) calculations for sufficiently high accuracy (Márquez et al. 2018). Scanning electron microscopy (SEM) and energy dispersive X-ray (EDX) analysis are also useful in knowing about the elemental composition of the derivatized compound (Scimeca et al. 2018).

Several proteins and enzymes have showed a potential affinity for natural compounds. Natural products like quercetin and kaempferol have been shown to bind to the proteins bovine serum albumin (BSA), Human serum albumin (HSA), and cholinesterase (Papadopoulou et al. 2005; Khan et al. 2009b). On the other hand, protein and enzyme disorders have resulted in a slew of diseases. In animal and plant systems, excessive enzyme production causes disease. Overexposure to sunlight and strong UV radiation causes excessive tyrosinase production in the skin in some diseases. Hyperpigmentation illnesses such as melasma, freckles, melanoma, and age spots in animals are caused by such conditions, which are referred to as photo aging (Tyrrell and Keyse, 1990). As a result, the development of a powerful tyrosinase inhibitor is vital.

Tyrosinase (EC 1.14.18.1) is a multifunctional enzyme that plays a role in the pigmentation of fruits and melanin formation in mammals. It is widely distributed in melanosomes of bacteria, fungi, and plants (Artés et al. 1998; Kim et al. 2017). Tyrosinase is involved in melanin synthesis in mammalian cells, but over-production of the enzyme causes hyperpigmentation disease (Schallreuter et al. 2008; Hridya et al. 2015). Revestrol and quercetin are some bioactive compounds isolated from plants that possess antioxidant activity as well as pharmacological impartment as a treatment for hyperpigmentation (Zimmermann Franco et al. 2012; Fan et al. 2017). Medicinal plants are also used in herbal-based therapeutics and are considered a rich source of ingredients (Lin et al. 2007). Since plants are rich sources of the chemical constituent, there is a need to explore and isolate bioactive components possessing the therapeutic potential for treating various hyperpigmentation diseases. Research is being carried out on tyrosinase inhibitors with the help of natural products due to the less toxic nature of the natural herbal product and its medicinal importance in applications like cosmetics, food, and pharmaceutical industries.

Recent reviews revealed the importance of natural products mainly towards contagious disease, which denotes >75% of the 97 new antibacterial drugs hosted and approved. These statistics/data noticeably reveal the continuous curiosity in natural product research. Apart from natural products, the Federal development agency (FDA) has also approved their semi-synthetic derivatives as sources of novel drugs or lead compounds for generating new drugs (Newman and Cragg 2016). Anti-ailment and disease treatments rely on a wide range of natural and semi-synthetic materials. Moreover, derivatized compounds with metal ions also played a vital role in the bioactivities of natural products (Tu et al. 2016). Plant natural product like flavonoids has

been extensively described as effective chelators for metal ions, such as iron, copper, platinum, and palladium (Malesev and Kuntic 2007; Kalinowska et al. 2016). Flavonoid-metal complexes possess a higher anticancer activity and are the potential candidate for anticancer agents than free flavonoids (Lee and Tuyet 2019). However, some metal ions are essential elements for the metabolic process and work as a cofactor of several enzymes. These essential elements are also helpful for cellular processes that regulate various biological functions. The bioavailability of essential elements maintain cellular homeostasis and plays a commanding role in cell proliferation, differentiation, and regulation mechanisms (Beyersmann and Haase 2001).

Plant-derived products are used traditionally for the cure of parasitic infections. For instance, Artemisinin isolated from *Artemisia annua* showed efficacy against cutaneous leishmaniasis (CL) (Sen et al. 2007). The essential oil derived from the plant has been explored for effective anti-leishmanial activity. Some studies revealed metalloproteinase (GP63) in the *Leishmania* parasite as the specific function of zinc in the cellular processes (Macdonald et al. 1995). Recently, the metal ion complex of flavonoids with metal ions like iron, zinc, and copper have been shown as effective antioxidant agents (Jeslin Kanaga Inba et al. 2013). However, the effect of zinc complexed flavonoids on the survival of *L. donovani* has been less explored to date.

Plant secondary metabolite especially flavonoids have widely been reported as less toxic and have shown to possess DNA (nucleic acids) binding properties (Hubbe et al. 2019). The detection and quantitation of nucleic acids, particularly DNA is a very common task in biotechnological research. Specialized research requires the differentiation of different types of nucleic acids like single standard DNA, double standard DNA, and plasmid DNA. The nucleic acid screening applications use presently available toxic and mutagenic fluorescent stains by compromising on safety. For decades, ethidium bromide (EtBr) has been the predominant dye used for nucleic acid screening in agarose gels because of its low cost and sufficient sensitivity (Karacan and Okay 2013). However, the costs of decontamination and waste disposal, as well as the potential dangers to researchers and the environment, could make the dye prohibitively expensive and hazardous. Therefore, investigation of the interaction of a flavone compound with DNA (nucleic acid) is needed. Biophysical techniques enable the user to get an insight and better understanding of the interaction mechanism. Analysis of UV–vis absorbance spectra and isothermal calorimetry thermodynamic (ITC) parameters indicates the formation of the complex

between flavone and DNA (Qais and Ahmad 2018). Additional experiments such as visualization of DNA in agarose gel-based method (Li et al. 2016), staining of the cell nucleus, and confirmation by microscopic study help confirm flavone-DNA binding. Furthermore, flavone-DNA binding might be helpful for the development of new stain for DNA visualization in agarose gel, cell nuclear visualization and viability of cell confirmation by microscopic and flow cytometric analysis.

Plant-based natural products used in folk remedies and bioactive small molecules are currently receiving more attention for their ethno medicinal uses (Tushar et al. 2010a). To increase the likelihood of discovering new, unique medications and minimize the expenses of drug research, ethno pharmacological knowledge of plants should be investigated. Medicinal plants are widly distributed in India. Due to this, India is known as the botanical garden of the world, providing a large number of herbal medicines (Kalaskar and Surana 2014). Meetei et al. (2012) generated a database related to medicinal plants' enormous prominence and abundance in NEI. The database covered information on numerous natural products from various medicinal plants of NEI and their medicinal properties (Meetei et al. 2012). Earlier, many research groups have described the uses of traditional medicinal plants of NEI for the curing of diseases like diabetes, parasitic infection, malaria, and other traditional remedies (Deb et al. 2015; Pratim Sarma 2017). Other studies also exhibited that medicinal plants of NEI can be used as cytotoxic constituent towards various cancer cell lines (Suhitha et al. 2015) and as antibacterial agents (Unni et al. 2009).

The family Zingiberaceae is well recognized for its versatile nature and extraordinary medicinal value in India. This family has 52 genera and 1,300 species found worldwide (Jain and Prakash 1995), of which 19 genera and about 88 species are present in North East India (NEI) (Ghosh and Rangan 2013). Unfortunately, the ethno medicinal value of Zingiberaceae plants has not been fully documented for future pharmacological applications in NEI. Among the Zingiberaceae family, the *Alpinia* genus is the largest genus constituting about 230 species dispersed around the tropical and subtropical region of Asia and the Pacific (Kress et al. 2005). Genus *Alpinia* retains a complex chemical profile. Many bioactive constituents such as alkaloids, flavonoids, terpenoids, and tannins contribute to its therapeutic efficacy against antimicrobial, anti-inflammatory, anticancerous, antidiabetic, and other diseases. To date, most of the research has been focused on *A. galanga*, *A. oxyphylla*, and other species viz. *A. speciosa*, *A. zerumbet*,

and many others for the isolation of bioactive compounds (Dash et al. 2020). Another important plant of genus *Alpinia* and a less explored member is *Alpinia nigra* (Gaertn.) B. L. Burtt, which is spread over a different region of NEI, commonly known as "Tora". The plant is also present in Thailand, China, and Southeast Asian states. Traditionally, this plant is used as a folk medicine to cure various diseases viz. trematocidal, gastric diseases, insect bites, dyspepsia (Roy and Tandon 1998). In recent years, researchers have explored this plant to isolate the natural product and cure intestinal helminth infection (Swargiary and Roy 2015).

Research on this plant is sparse, hence the current study was conducted in an effort to isolate and characterize the compounds extracted from leaves of the herbaceous plant *A. nigra* in order to better understand this plant's potential medicinal properties. Further, synthesis, derivatization, exploration and efficacy of the leaf crude extracts and purified bioactive compounds for their antibacterial, antityrosinase, anti-leishaminiasis, and DNA binding activities were carried out to explore the possibility of development of future therapeutics.

Objectives

Based on the earlier study and the medicinal importance of *A. nigra*. The present study was carried out with the following objectives.

The specific objectives are:

1) Phytochemical screening, antibacterial, anti-biofilm and quorum sensing inhibiting activity of *Alpinia nigra* leaf extract against infectious pathogen *Pseudomonas aeruginosa* PAO1.

2) Isolation, purification and characterization of 3,5-dihydroxy-4',7-dimethoxyflavone from the leaves of *A. nigra.*

3) Antioxidant, anti-tyrosinase, and anti-inflammatory activities of 3,5-dihydroxy-4′,7-dimethoxyflavone isolated from the leaves of *A. nigra*.

4) Synthesis and characterization of zinc derivatized 3, 5-dihydroxy 4′, 7-dimethoxyflavone and its anti leishmaniasis activity against *L. donovani*.

5) Proposed application of 3, 5-dihydroxy 4′, 7-dimethoxyflavone as a DNA binding dye.

Literature review

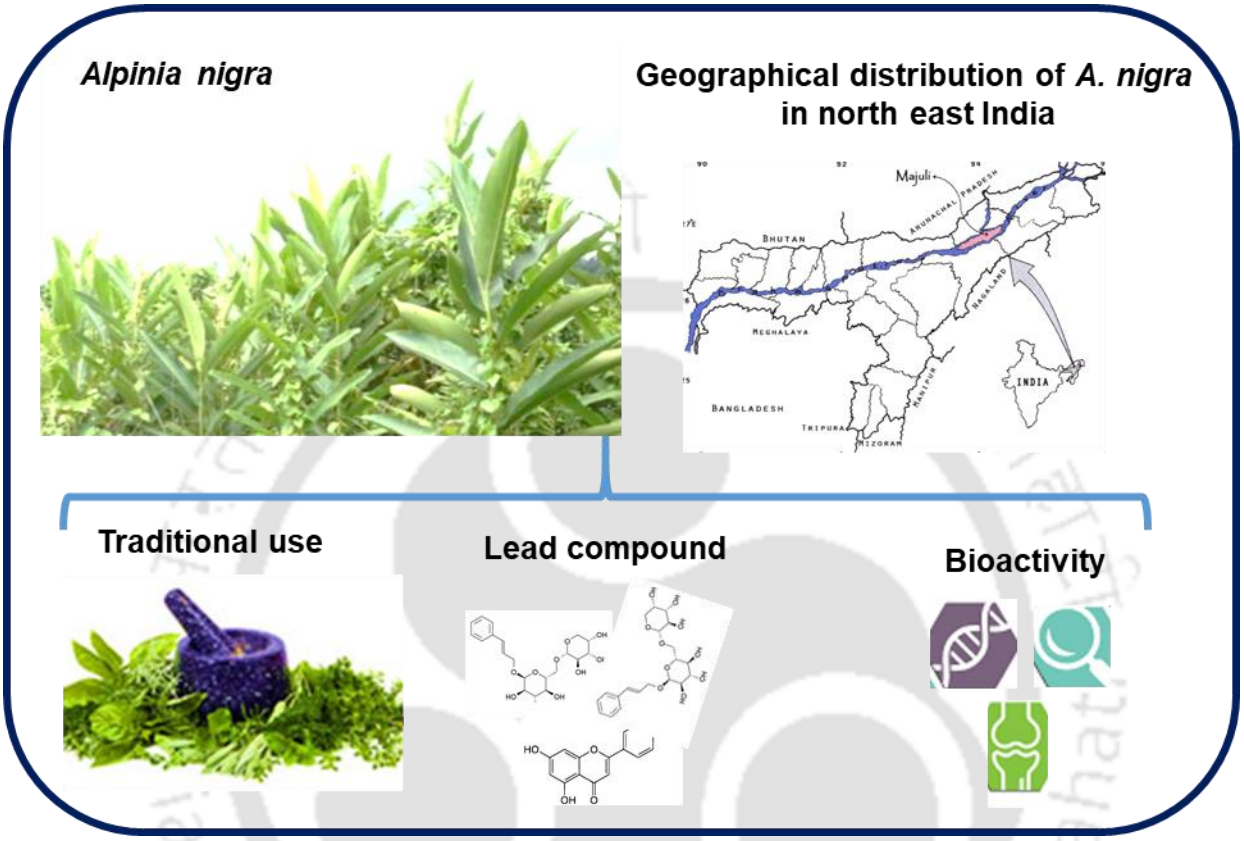

The history and current state of genus *Alpinia* in drug discovery are discussed in this chapter. This background information further emphasizes the significance of the genus *Alpinia* and its bioactive compounds for pharmaceutical applications.

Chapter 2

Literature review

2.1 Introduction

Plant-derived natural products are the primary source of therapeutics in the diverse traditional medicinal system that has been accepted for generations. The World Health Organization (WHO) has projected that over 60-65% of the world's population depends on the plant product as therapeutic agents (Ahmad Khan and Ahmad 2019). Plant-derived medicine has been assimilated into the so-called alternative remedial system, also known as “herbal medicine or phytomedicine.” About 60-70% of the modern drugs are derived from natural resources, and many synthetic analogs have been developed from the chemical entity of bioactive substances of plant origin that serves as the prototype for many synthetic analogs (Egbuna et al. 2020).

Medicinal plants are used in herbal-based therapeutics and considered as structurally diverse assortment of pharmacologically active compounds. Secondary metabolites of the plant have great potential to cure numerous diseases associated with bacterial, parasites, and viruses (Cragg and Newman 2013). Plant metabolites have recently been used in several studies. Numerous studies have demonstrated the efficacy of secondary metabolites like flavonoids, alkaloids, and terpenes in inhibiting the spread of pathogenic microorganisms. Progression in chemical analysis has guided researchers to explore and modify active constituents from plants. The efficacy of plant products have been validated using recent scientific techniques, which have assisted in the treatment of various severe health ailments. The medicinal plant's active compounds are either used directly for therapeutic effect or semisynthetically modified lead structures are used.

Essential oils, crude extracts, and purified bioactive compounds from plants are considered remarkable bioactive metabolite sources (Mashhadi Akbar Boojar 2019). Natural products have been extensively applied in the medicinal industry for developing novel drug entities against inflammation, oxidative process, and cancer. Many antiviral natural products have already been defined by the activity against several viral diseases such as Dengue virus, Hepatitis B, Enterovirus, and Influenza virus (Musarra-Pizzo et al. 2021). Recently, some plant metabolites have been found to be involved in the binding and inhibiting of the proteins involved in SARS-CoV-1 progression. The reported plant secondary metabolite such as tetrandrine,

fangcholine, cepharanthine alkaloids have shown binding affinity towards the reported protein and DNA intercalated from SARS-CoV-2 virus (Kim et al. 2019).

Some of the natural compounds have shown an excellent antagonistic effect towards resistance parasites and bacteria. The natural product, astragalin isolated from *Alpinia nigra* has demonstrated a good efficacy against *Fasciolopsis buski* parasite (Swargiary 2015). Hence, the present *in silico* technique for drug development, such as molecular docking, has been explored through many natural and synthetic compounds. The binding affinity of the natural compound towards the targeted infectious agent has been explored and reported (Cerqueira et al. 2021). Currently, the molecular structures, inoculation, and replication methods for a number of infectious organisms are known, therefore it is possible to produce medications that may battle the specific disease.

However, the development of any new drug, especially synthetic drugs, is accompanied by the problem of toxicity, which must be addressed. In other words, the drug should be target-specific and not harmful for host metabolism (Chakrabartty et al. 2021). Therefore, pharamaceutical industries prevail natural compounds due to less toxicity. Some natural products from flora and fauna have been examined in drug improvement since the outbreak of many chronic diseases (El-Seedi et al. 2021). Nowadays, scientists are mainly focused on the medicinal plant for the exploration of non-toxic natural products with high therapeutic efficacy. Therefore, the search for novel therapeutic agents from traditional medicinal plants continues for effective medication.

2.2 Plant-derived therapeutic compounds

Indigenous people utilize plants for curing diseases as a traditional healing method and as a food source. Ayurveda and Chinese herbal naturopaths used herbal crude extract in practices as traditional medicine system. Extracts of some natural products have been directed to the modern discovery of their active constituents and, ultimately, play an important role in developing novel drugs (Yuan et al. 2016).

These natural product crude extracts were widely used as a pivotal source for primary healthcare. The known confirmation of human intellect towards the use of plant extracts to treat/cure many diseases originated in the history of ancient Indian, Chinese and North African

civilizations. Nowadays, researchers are mainly focused on the isolation of principle bioactive compounds or active pharmaceuticals towards the treatment of various ailments and diseases.

During the 19th century, isolation and purification of the individual active constituent from traditionally used medicinal herbs were initiated. A remarkable revolution in the history of the medicinal plant was the "Quinine", isolated from *Cinchona* bark directed more attention towards bioactive products from plant sources (D.J. 2012; Semedo et al. 2021). Many other discoveries of plant-derived bioactive compounds drew much attention from the scientist of the New World, and explorations began to various parts of impassable forests in search of novel medicines. Another notable breakthrough in the history of the medicinal plant was the "Artemisinin", isolated from the *Artemisia* plant for curing malaria disease (Nigam et al. 2019).

2.3 Advancement of plant derived medicine

2.3.1. Traditional medicine

Plant-derived natural products have encouraged drug discovery. As such, natural products are the active constituents of many traditional medicines. Generally, natural products have shown less toxicity. Moreover, these plant-derived natural products are used as the backbone of synthetic drugs. Therefore, natural product is habitually used as starting points for drug discovery. Nature has been an essential source of drugs since time immemorial (Ghosh et al. 2014a). In the plant kingdom, Zingiberaceae is known as "pharmacy" as it is the hub of medicinal plants, which are mostly rhizomatous. These plants contain large amounts of essential oils in their tissues which are mainly responsible for their characteristic and stimulating odor. Due to its high medicinal and culinary value, this family has been immensely investigated by several researchers and scientists. *Zingiber officinale* root product has shown anti-inflammatory activity (Uz et al. 2009). Another genus *Alpinia* is well known for its enormous medicinal properties and used as essential spice and food flavoring products in different parts of Asia (Dash et al. 2020).

2.3.2. Natural product-derived medicine as a modern drug

Plant-derived pharmaceuticals make up many of the most routinely prescribed medicines today. Some of the bioactive natural product assembled drugs are analgesics. *Willow* tree bark extract has been recommended for its potential pain-relieving qualities. The presence of salicin, a

bioactive molecule that can be hydrolyzed and converted into salicylic acid, is responsible for this. The synthetic compound acetylsalicylic acid is known as aspirin (Desborough and Keeling 2017). Aspirin is derivative of salicylic acid and widely used as a pain reliever. The inhibition of the cyclooxygenase (COX) enzyme is key mechanism of action of acetylsalicylic acid (aspirin) (Patrono 2019).

A recent example is a ziconotide, obtained from the species *Conus magus*. It is typically an analgesic agent that is used for the core of chronic pain. Its mechanism of action is an N-type calcium channel blocker (Miljanich 2004). Another example is opium obtained from *Papaver somniferous*. It has the most potent narcotic component. The alkaloid morphine acts as an opioid receptor agonist (Rosso 2010).

The natural product has shown efficacy against pathogenic microorganisms by inhibiting cell wall formation. The first antibiotic, penicillin, was isolated from the mold *Penicillium*. Penicillin has a beta-lactam structure and has the effect on the DD-trans peptidase enzyme that is essential for the formation of cross-link peptidoglycan to form the bacterial cell wall (Perez-Llarena and Bou 2009). Some natural products target tubulin, which is a key part of the cytoskeleton. The natural product, colchicine, was isolated from the *Colchicum autumnale* (autumn crocus flowering plant) work as an inhibitor of tubulin polymerization. Therefore, colchicine is used to treat gout (Karamanou et al. 2018). In contrast, a natural product-based drug Paclitaxel exhibits a stabilizer of tubulin polymerization and is used as a chemotherapeutic drug. Paclitaxel drug is based on the terpenoid natural product taxol, which is isolated from *Taxus brevifolia* (the pacific yew tree) (Hasanpourghadi et al. 2016). A polyketide, mevastatin, isolated from *Penicillium citrinum*, is widely used to lower cholesterol due to its role in inhibiting HMG-CoA reductase (Kim et al. 2006b). Lastly, several natural product-based drugs are used to treat cancer, congestive heart failure, hypertension, bacterial and fungal infection.

Numerous antibacterial compound was isolated during and after world war II. Penicillium, cephalosporium, and streptomyces were reported during World War II and originated the antibiotics era. After World War II, many antibiotics have reported. Meanwhile, some bacteria have generated resistance against antibiotics. Therefore, the urgency is to discover a new and efficient drug for treating various bacterial diseases. Initially, crude extract of plant metabolites has shown promising efficacy against pathogenic bacteria. But some formulations show toxicity against normal and healthy cells. Therefore, the isolation of active ingredients

from the extract of natural products has led to the modern discovery and development of novel target drugs. Notably the discovery of "reserpine" from the *Rauwolfia serpentine* roots reformed the uses of anesthetics in healthcare (Ruyter et al. 1991; Srivastava et al. 2021). Similarly, the other remarkable discoveries of that time, "vincristine" and "vinblastine" were isolated from *Catharanthus roseus,* which were used for the treatment of cancer (Pham et al. 2020). Further, notable plant-derived medicines with potent antifungal, antibacterial, anticancer, antiparasitic, and anti-inflammatory agent has been tabulated below (**Table 2.1**).

2.4 Challenges in the plant-based drug development

Plant-based drugs can be discovered using a wide range of methods, including phytochemical screening, one or more specific biological assays, reported biological activity, ethnomedicinal background research, and traditional use of plants. Other challenges in the development of plant-based pharmaceuticals include the determination of enriched and standardized extracts and the suitable form (powdered, extract, or precipitate form) to utilize as a medication (Thomford et al. 2018).

Several challenges have been associated using a natural product for the development of new herbal drugs. Now, pharmaceutical companies are focusing on the bioactive compound, which is pure and follows pharmacological drug-like properties such as the Lipinski rule (Mao et al. 2016). Plant bioactive compound sources are often unpredictable to access and supply due to varying composition by sourcing seasonal and environmental condition.

The drug discovery from biological sources such as natural products from microorganisms, plant species, and insects evaluated for bioactivity remains unexplored. Scientists in the field of natural products will have to constantly optimize extraction, purification, and quality control of substances that are routed for drug development. However, the drug development process takes a long time, an average of 8 to 10 years. During the drug development process, a huge amount of money is spent on determining and discarding various unnecessary steps. It is projected that hardly one compound is successfully approved by clinical trials in more than 5000 lead natural bioactive compounds (Katiyar et al. 2012). During the drug discovery process, herbal products possess identification, optimization including combinatorial chemistry and medicinal, lead development (such as pharmacokinetics, toxicology, ADME, and drug delivery), and clinical trials, and all take considerable time (Atanasov et al. 2015b).

Table 2.1 Examples of plant-derived drugs developed on the basis of traditional use (Lopez 2011)

S.no.	Drug	Lead /Principal compound	Use for modern drug	Plant name	Traditional use (Origin)	Reference
1.	Arteeter	Artemisinin	Antimalarial	*Artemisia annua L.* (Asteraceae)	Antimalarial (China)	(Mueller et al. 2004)
2.	Atropine	(-)Hyosciamine	Anticholinergic	*Atropa belladonna L.* (Solanaceae)	Pan relief, asthma, (Europe)	(Griffin and Lin 2000)
3.	Colchicine	Colchicine	Antigout	*Colchicum autumnale L.* (Liliaceae)	Poison (Europe)	(Karamanou et al. 2018)
4.	Acetylsali-cylic acid	Salicin	Anti-inflammatory Antiagregant	*Salix sp* (Salicaceae)	Inflammation (Europe, Asia, America)	(Vlachojannis et al. 2011)
5.	Chromoglycate	Kellin	Anti-inflammatory, hyperoxaluria	*Ammi visnaga (L). Lam.* (Apiaceae)	Inflammatory conditions (North Africa)	(Badr et al. 2015)
6.	Galantamine	Galantamine	Colinesterase inhibitor (Alzheimer)	*Galanthus sp* (Amaryllidaceae)	Nerve pain (Eastern Europe)	(Birks 2006)
7.	Digoxin	Digoxin	Cardiotonic	Digitalis sp (*Scrophulariaceae)*	Dropsy (Europe)	(Patocka et al. 2020)

8.	Etoposide	Podophylotoxin	Antitumour	*Podophyllum peltatum* (Berberidaceae)	Laxative, skin infections (North America)	(Shah et al. 2021)
9.	Morphine	Morphine	Opioid analgesic	*Papaver somniferum L.* (Papaveraceae)	Pain relief (Western Mediterranean)	(Lachenmeier et al. 2010)
10.	Pseudoephedrine	Ephedrine	adrenergic agonist (nasal decongestant)	*Ephedra sinica Stapf* (Ephedraceae)	Cough suppressant (China)	(Fischer et al. 2006; Ma et al. 2007)
11.	Rivastigmine	Physostigmine	Cholinesterase inhibitor	*Physostigma venenosum Balf.* (Fabaceaea)	Poison (Africa)	(Somani 1990)
12.	Vinblastine, Vincristine Vinorelbine	Vinblastine, Vincristine	Antitumour	*Catharanthus roseus* (L.) G. Don. f. (Apocynaceae)	Hypoglucemiant (Madagascar)	(Salerni et al. 2010; Keglevich et al. 2012)

2.5 Chemical constituents of plant

The medicinal plant contains several bioactive components such as flavonoids, amides, tannins, saponins, glycosides, terpenoids, and phenolic compounds. These bioactive constituents have been widely investigated in the seeds, leaves, and stem bark of many medicinal plants. The pharmacological activities of these bioactive components serve as health-promoting and pharmaceutical agents.

Polyphenolic compounds have been extensively reported in several medicinal plants. These groups of compounds such as flavonoids, phenolic acids, tannins, stilbenes, and lignans contain aromatic rings with hydroxyl groups. Flavonoids are mainly characterized by two benzene rings, A and B, which are linked through a heterocyclic pyran ring. Flavonoids are classified as flavones and isoflavones based on the position of the benzenoid ring. Phenolic compounds have been widely reported to have beneficial effects on human health, such as anticancer, antimicrobial, antioxidant, and antimutagenic properties (Aboul-Enein et al. 2013). Phenolic acids such as vanillic, caffeic, ferulic, protocatechuic, and rosmarinic acid are present in several plant species (De Paula et al. 2017).

Alkaloids: Alkaloids are naturally occurring nitrogen-containing organic compounds. Alkaloids are primarily synthesized as secondary metabolites in plants and fungi. They have a wwide range of bioactivities. Alkaloids are mostly defined by their basicity, bitter taste, physiological actions, and plant origin. The common chemical feature of every alkaloid contains a minimum of one nitrogen atom. Alkaloids chemical structures have extremely divergent (Debnath et al. 2018). Alkaloids are one of the important secondary metabolites that showed therapeutic properties. The alkaloids have been classified by their heterocyclic ring system and biosynthetic precursor into several groups such as indole, imidazole, tropane, piperidine, purine, pyrrolizidine, quinolozidine, pyrrolidine, and isoquinoline (Wangchuk 2019).

Alkaloids can be easily classified by the starting ingredients of their biosynthetic pathways, such as the amino acids that provide nitrogen atoms. Thus, the identification of initial ingredients that synthesize an alkaloid is an important key for the classification of natural alkaloid compounds. Moreover, the species–metabolite relation database (KNApSAcK Core DB) has been well-known for its systematic understanding of the alkaloids. Alkaloids tend to prevent many degenerative diseases by scavenging the free radical or inhibiting the enzymatic reaction.

Several studies have been reported for its extensive pharmaceutical activities (Gutiérrez-Grijalva et al. 2020).

Terpenoids: Terpenoids are a modified class of terpenes, also recognized as isoprenoids. It is the most abundant and structurally diverse natural bioactive constituent found in many medicinal plants. It contains different functional groups and an oxidized methyl group at various positions. Terpenoids are classified into several classes: Hemiterpenoids, Monoterpenoids, Sesquiterpenoids, Diterpenoids, Sesterterpenoids, Triterpenoids, Tetraterpenoids, Polyterpenoids, on the basis of isoprene units. Most of the terpenoids are biologically active and used to treat various diseases worldwide (De Oliveira et al. 2013). Some terpenoids inhibited human cancer cells and exhibited anticancer drugs such as Taxol and its related derivatives. However, terpenoids have shown various roles in medicine, foods, cosmetics, vitamins, and so on.

Saponins belong to the subclass of terpenoids widely distributed in plants. It's a structurally linked compound containing a steroid and triterpenoid aglycone (sapogenin). It is historically isolated from soapwort (genus *Saponaria*), a flowering plant. They are characterized by foaming properties and their hemolytic activity. They are responsible for imparting a bitter taste and astringency to plant materials. Saponins are poorly immersed, and most of its component form insoluble complexes with 3-b-hydroxysteroids. They interact and form large micelles with cholesterol and bile acids. However, some saponins were revealed to lower cholesterol levels in some animal species. The effects towards hypocholesterolemic of saponins are more useful for human's health (He et al. 2019).

Some saponins are present in legume plant which called the soyasaponins. They are classified into groups A, B, and E saponins based on the aglycone chemical structure. Recently, dehydrosoyasaponin I was reported from chickpeas and other legumes and show activity as a potent calcium-activated potassium channel opener. The study also revealed that dehydrosoyasaponin I might be used for treating urological, cardiovascular, respiratory, neurological, and other disorders (Giangiacomo et al. 1998).

2.6 *Alpinia*: distribution and chemical constituents

Alpinia belongs to the, family Zingiberaceae. It is well known for its various medicinal properties and several food flavoring spices with high commercial values. It is distributed

worldwide with nearly 50 genera and 1,300 diverse species mainly found in South and Southeast Asia (Saha et al. 2020). India contains approximately 22 genera and 178 species in North Eastern, whereas the North East region alone contains 19 genera and 88 diverse species (Jain and Prakash 1995)

In the family Zingiberaceae, *Alpinia* is the most complex and largest genus, which was classified by Charles Plumier, the famous French botanist, and named after Prospero Alpino, the well-known Italian botanist of the 16th century. The genus *Alpinia* comprises 230-250 species spread over tropical and subtropical provinces of Asia and the Pacific. According to phylogeny, *Alpinia is* classified under the Angiosperm Phylogeny Group II (APG II) system and comes under the monocotyledonous plants, order Zingiberales, subfamily Alpinioideae, and tribe Alpinieae (Angiosperm Phylogeny Group 2003). DNA-based studies disclosed the genus as polyphyletic, characterized by six clades scattered across the tribe Alpinieae (Kress et al. 2005).

The *Alpinia* genus mostly possesses aromatic aerial, underground parts, and attractive inflorescence, which is generally subjected to different fractionation processes to extract essential oils, aqueous extract, and bioactive components. Various parts of this plant have significant potential to yield bioactive components towards the development of future herbal remedies.

Essential oil of the different plant parts of this genus contains many bioactive compounds that exhibited medicinal properties towards various therapeutics. Due to its versatile utility in therapeutics, the genus *Alpinia* attends more attention from the natural product scientist to develop potential herbal therapeutics against numerous diseases like diabetes, ulcer, cancer, and many parasitic diseases (Ghosh and Rangan 2013). Research continues to unveil the mechanism of action of the natural bioactive compounds isolated from different species of the genus in regulating the disease progression and cure. The bioactive components are shown in the following **Table 2.2**.

Table 2.2 The reported compounds from *Alpinia* species

S. No.	Species name	Reported Compounds	Part used	References
1.	*A. nigra*	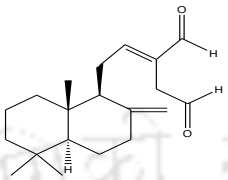 (E)-labda-8(17), 12-diene-15, 16-dial	Seed	(Ghosh et al. 2014a)
2.	*A. ligulata* and *A. nieuwenhuizii*	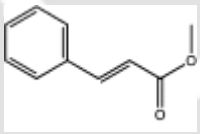 (E)-methyl cinnamate	Rhizome	(Yusoff et al. 2011)
3.	*A. mutica*	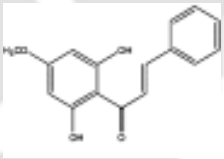 Pinostrobin chalcone	Rhizome	(Malek et al. 2011)
4.	*A. zerumbet*	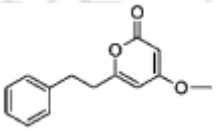 Dihydro-5,6-dehydrokawain	Leaves	(Upadhyay et al. 2011)

5.	*A. galanga*	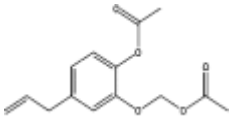	Rhizome	(Kaur et al. 2010)

1′-acetoxyeugenol acetate

6.	*A. katsumadai*	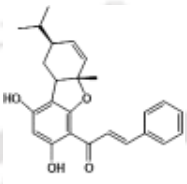	Seeds	(Hua et al. 2009)

Sumadain C

7.	*A. galanga*	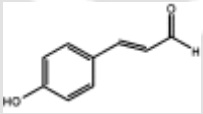	Rhizome	(Phitak et al. 2009)

P-hydroxycennaldehyde

8.	*A. oxyphylla*	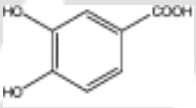	Kernels	(An et al. 2008)

Protocatechuic acid

9.	*A. officinarum*	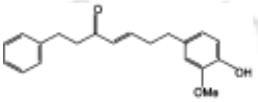	Rhizome	(Yadav et al. 2003)

Diarylheptanoid

10.	*A. speciosa*	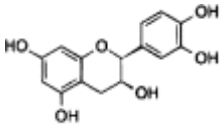	Rhizome	(Masuda et al. 2000)
		Epicatechin		
11.	*A. galanga*	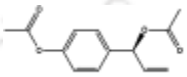	Rhizome	(Janssen and Scheffer 1985)
		Acetoxychavicol Acetate		

2.7 Genus *Alpinia:* therapeutics potential

The genus *Alpinia* showed its incredible biopharmaceutical potential, as evident from earlier published reports, and is gaining the attention of researchers from diverse disciplines. The presence of bioactive substances such as flavonoids, tannins, and terpenes is the key to its therapeutic efficiency. Brief accounts of various biological studies and the efficacy of diverse *Alpinia* member towards the therapeutic uses are described below.

2.7.1. Antibacterial and anti-biofilm activity

Alpinia plant products and their derivative have reported efficacy against bacterial diseases (Tushar et al. 2010a). Recently, many plant-derived compounds were reported for their anti-biofilm effect (Kaverimanian and Heuertz 2019a). Furthermore, it was shown that natural compounds are highly effective against many microbial pathogens. Biofilm-associated bacterial diseases are highly resistant to the host immune system. The control of bacterial infection continues to be a major challenge as bacteria evolve resistance against several potent antibacterial drugs (Brown and Wright 2016). Natural products have several chemical complexities which permit them to cross the cell membrane barrier in bacteria and several target molecules. This target molecule has its individual specificity leading to prominent antibacterial activities (Dai et al. 2020). Further, these accomplishments, only some new antibacterial classes like oxazolidinone mupirocin, linezolid, and lipopeptide, daptomycin have been accepted during the years 1985, 2000, and 2003, respectively (Liu and Karttunen 2018).

FDA has declined more than 50% of antibiotics approval in the last two decades (Kinch et al. 2014). However, the cure of bacterial infections is complicated daily due to resistance developed by bacteria to the antibacterial agents. The magnitude of bacterial resistance has increased due to the extensive usage of antibacterial drugs for many years.

Many natural products have been reported for the cure of several bacterial diseases, which were obtained from various members of the *Alpinia* genus. To date, *A. galangal* has been explored for most activity studies and several bioactive isolations. Antibacterial activity has been reported through essential oil extracted from rhizomes of *A. galangal* (Zhou et al. 2021). Rhizome ethanolic extract of *A. galangal* exhibited a cytological alteration in *Staphylococcus aureus* cells by changing the integrity of the outer membrane. Many potential antimicrobial activities also been reported and revealed their therapeutic potential against bacteria, yeast, fungi, and parasitic diseases (Eram et al. 2019).

A remarkable natural compound, acetoxychavicol acetate, has been isolated from rhizomes of *A. galanga* and shown prominent active against bacterial diseases (Latha et al. 2009). Further, other species of the *Alpinia* genus, viz. *A. oxyphylla, A. zerumbet, A. speciosa*, and several others, are getting attention due to the presence of various polyphenolic compounds with multifarious phytochemical profiles. A number of purified compounds have been reported against a wide range of bacterial pathogens. The major antibacterial activities of several fractions and purified compounds from *Alpinia* species are assembled in **Table 2.3**.

2.7.2 Anticancerous activity

In the past few years, natural products isolated from many bioresources have contributed a significant role in cancer therapeutics. Moreover, several natural products and their derivatives retaining antitumor activity have released new avenues in the research of natural products associated with cytotoxic agents (Empl et al. 2015). Additionally, for chronic cancer, many plant-derived natural products are currently being employed. The FDA has since approved ixabepilone, temsirolimus, and trabectedin, all of which have revolutionized cancer treatment using natural products (Aghajanian et al. 2018). Furthermore, combinatorial chemistry, in conjunction with natural product-derived competitors, has anticipated numerous other important developments and advancements, revealing its central role in drug discovery.

Table 2.3 Antibacterial, anti-biofilm activities of several fractions and purified compounds from *Alpinia* species.

S. No.	Species name	Parts used	Bioactive fractions/compounds	Bioactivity	References
1	*Alpinia galangal*	rhizome	1'-acetoxychavicolacetate	Anti-biofilm and Antibacterial	(Puhs et al. 2020)
2	*A. purpurata*	Flowers	Essential oils and aqueous extracts	Antibacterial	(Santos et al. 2012)
3	*A. ligulata* and *A. nieuwenhuizii*	Rhizome	Essential oil	Antibacterial	(Yusoff et al. 2011)
4	*A. pahangensis*	Leaves and rhizomes	Hydrodistilled essential oil	Antibacterial	(Awang et al. 2011)
5	*A. galanga*	Rhizome	1′-Acetoxy-chavicol acetate	Antibacterial	(Weerakkody et al. 2011)
6	*A. galanga*	Leaves and rhizomes	Methanol, acetone and diethyl ether extracts	Antibacterial	(Rao et al. 2010)
8	*A. conchigera*	Leaves, stem and rhizomes	Essential oil obtained from hydrodistillation	Antibacterial	(Ibrahim et al. 2009)
9	*A. galanga*	Rhizome	D,L-1-Acetoxychavicol acetate	Antimicrobial	(Oonmetta-aree et al. 2006)
11	*A. speciosa*	Leaves	Ethanol extract	Antimicrobial	(Wang and Huang 2005)

Plant survive in hostile circumstances and acquires a natural system of evolution that agrees them to synthesize several beneficial chemical entities such as flavonoids, alkaloids, terpenes, and combating hostile environmental conditions. Several alkaloids and flavonoids have been used in cancer therapeutics. A remarkable example is Vincristine, a vinca alkaloid isolated from *Catharanthus roseus* and revealed effectively against leukemia and Hodgkin's disease (Batra and Sharma 2013).

Many studies have been performed in various cancer cell lines, and animal models imitate the potential of diverse species of *Alpinia* as an anticancer agent. A notable compound, pinostrobin chalcone, has been purified from *A. mutica,* showing the cytotoxic potential to numerous carcinoma cell lines (MCF7, KB, and Caski cells) with significant anticancer properties (Malek et al. 2011).

2.7.3 Anti-inflammatory and analgesic activity

Inflammation is a healing process. It initiates the complex biological response of vascular tissues to damaging stimuli such as pathogens, injured cells, or external irritants (Eming et al. 2007). Anti-inflammatory drugs diminish infection without disturbing the central nervous system. Thus, anti-inflammatory medications refer to the property of an element that edges down inflammation.

Drug towards infection which is caused due to inflammation may be a steroid, immune selective anti-inflammatory derivatives (ImSAIDs), non-steroidal anti-inflammatory drugs (NSAID), and herbal drugs (Amparo et al. 2020). However, steroidal drugs have a side effect to inhibit natural hormones and liver dysfunction (Soleimanpour et al. 2016). Likewise, NSAID can cause gastric erosions, initiating stomach ulcers. Some NSAID has been reported to cause severe haemorrhage and extreme myocardial infarction, and stroke (Zadrazil 2010). Therefore, herbal drugs and ImSAIDs are more preferable in curing inflammation. Bioactive compounds, Galangin, and cardamomin have been isolated from *A. officinarum* and *A. conchigera* which showed anti-inflammatory and analgesic actions (Lee et al. 2006; Lu et al. 2007).

2.7.4 Antidiabetic activity

Diabetes is widely predominant in developed and developing nations. The International Diabetes Foundation (IDF) proposed that diabetes affects around 246 million people in the world and is expected to reach up to 693 million by the year 2045. Diabetes causes death about ~6% of total

global mortality worldwide (Cho et al. 2018). It is a metabolic disorder of the endocrine and is characterized by persistent hyperglycaemia. Due to defects in insulin secretion or action of both, it results in abnormalities of protein, fat, and carbohydrate metabolism. According to WHO classification, diabetes mellitus (DM) is divided into insulin-dependent diabetes mellitus (IDDM) or type 1 and non-insulin-dependent diabetes mellitus (NIDDM) or type 2.

NIDDM commonly appears during young age in life. The recent medicine towards the management of NIDDM leads to several side effects such as hypoglycemia, abdominal pain, hepatotoxicity, and diarrhea (Funamoto et al. 2019). The present drug showed less effectiveness due to resistance. Therefore, alternative medicine is necessary.

Many traditional medicines from plant sources have been used for the curing of diabetes. The natural product mainly plays a role in binding and inhibiting carbohydrate hydrolysis enzymes, viz. pancreatic glucosidase, and amylase. Enzyme inhibition resulted in reducing carbohydrate digestion and delaying the absorption of glucose. Over the decade, many research groups have isolated bioactive compounds from plants source and checked their efficacy towards amylase and alpha-glucosidase activity. To date, several bioactive compounds such as flavonoids, alkaloids, polyphenols, and their sugar derivatives showed inhibitory activities (Ademiluyi and Oboh 2013). The genus *Alpinia* has a high therapeutic impact due to its various biomedical applications. Meanwhile, the isolated compound, labdane diterpene, from the seed of *A. nigra* has been reported as an anti-diabetic agent (Ghosh and Rangan 2014a).

2.8 *Alpinia nigra* (Gaertn.) B.L. Burtt:

A. nigra (Gaertn.) Burtt is a herbaceous, medium-sized rhizomatous plant that grows commonly in wasteland and shady places (Sahoo et al. 2013). This plant belongs to the family Zingiberaceae. The taxonomical classification of this plant is given in **Table 2.4**. The leaves are simple, alternate, pointed at the ends with a very short petiole and very long leaf sheath. The plant has panicle type of inflorescence. Flowers are solitary, perfect, terminal, and white to pinkish in color. Fruit is berry (**Fig. 2.1**) green when young and black with maturity (Ghosh et al. 2013b).

Table 2.4 Taxonomical classification of *A. nigra*

Classification
Kingdom: Plantae
Phylum: Tracheophyta
Class: Angiosperm
Subclass: Monocotyledonae
Order: Zingiberales
Family: Zingiberaceae
Subfamily: Alpiniodeae
Genus: *Alpinia*
Species: *nigra*

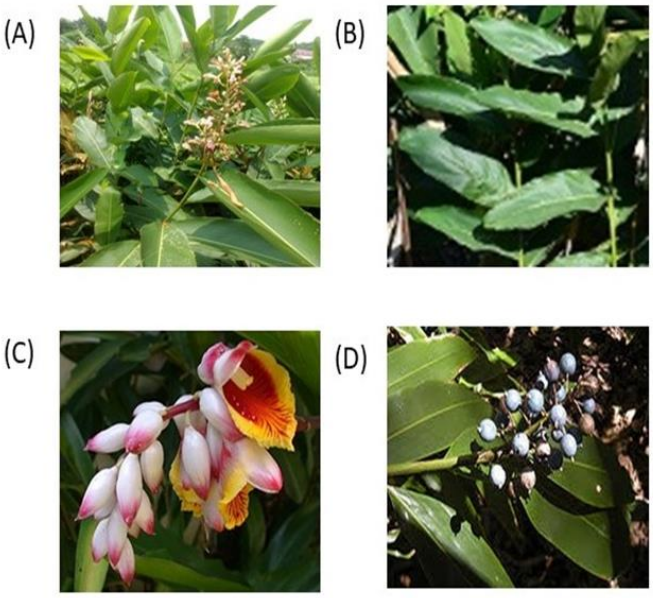

Fig. 2.1 *Alpinia nigra* (A) Whole plant; (B) Leaves; (C) Inflorescence and (D) Fruits

2.8.1 Therapeutic potential of *A. nigra*

The native people of Tripura consume aqueous extract of *A. nigra* shoot to cure the intestinal parasitic infection. The new leaves of the plant are also a favorite vegetable diet; however, in some parts of Manipur, it is used as a food flavoring product. Similarly, the aqueous juice of rhizome and shoot of *A. nigra* has been used for treating health problems like jaundice and gastric ulcers by the native people of Assam (Tushar et al. 2010b). The potential biological applications of *A. nigra* are depicted in **Fig. 2.2**.

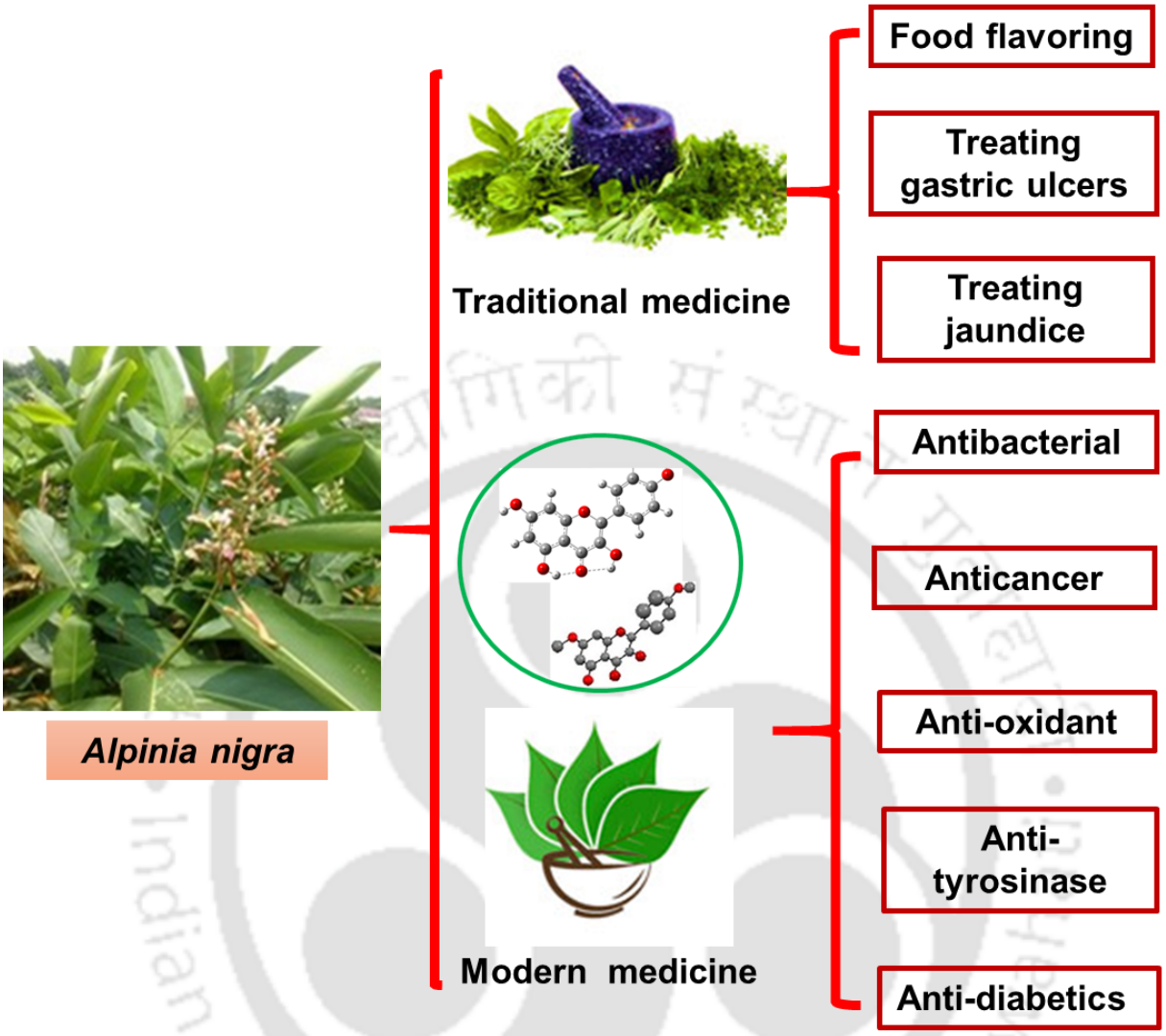

Fig. 2.2 Therapeutic potential of *A. nigra*

2.8.2 *A. nigra:* oil content and their constituent

A. nigra contains a complex chemical profile and possesses various types of bioactive compounds. Most plants from the genus *Alpinia* have a high content of essential oils and show a prominent amount of aromaticity. This suggests that the chemical compounds control the aromaticity of the plant (Monson and Baldocchi 2014). The oil content from the different parts of this plant has been tabulated (**Table 2.5**). Previous reports have suggested that the leaf' oil content is slightly higher compared to rhizome and flower (Ghosh et al. 2014a). Many of these natural bioactive compounds have been isolated from different parts of *A. nigra*. Some important bioactive compounds are enlisted in **Table 2.6**.

Table 2.5 Oil content estimated from different parts of *A. nigra* (Ghosh et al. 2014b; Islam et al. 2014)

Sr. No.	Parts used	Oil content (%)
1.	Rhizomes	0.15
2.	Dried fruits	1.25
3.	Flowers	0.06
4.	Leaves	0.23
5.	Seeds	0.76

Table 2.6 Compounds identified form *A. nigra* (Ghosh et al. 2017; Islam et al. 2014; Sethi et al 2015)

S. No.	NAME	STRUCTURE	MASS (Da)	FORMULA
1	(E)-labda-8(17), 12-diene-15, 16-dial	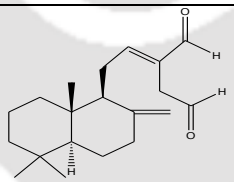	302.4510	$C_{20}H_{30}O_2$
2	(E)-8β ,17-Epoxylabd-12-ene-15, 16-dial	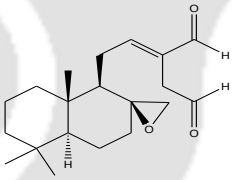	318.219495	$C_{20}H_{30}O_3$
3	1,5,9,9-Tetramethyl-1,4,7-cycloundecatriene	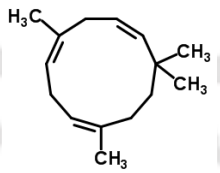	204.351	$C_{15}H_{24}$
4	6,6-Dimethyl-2-Methylene-Bicyclo(3.1.1)Heptane	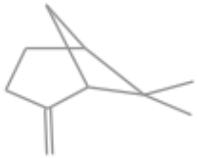	136.2340	$C_{10}H_{166}$

5	5-Amino-6-(2-fluoroanilino)furazano[3,4-b]pyrazine	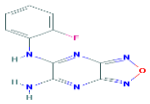	246.2006	$C_{10}H_7FNO$
6	4,11,11-Trimethyl-8-methylenebicyclo[7.2.0]undec-4-ene	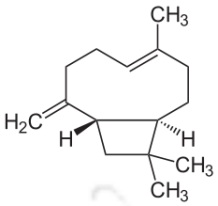	204.36	$C_{15}H_{24}$
7	6-(3-Fluorobenzyl)-1,2,3,4,5,6-hexamethyl-2,4-cyclohexadien-1-ol	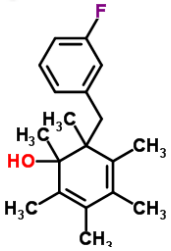	288.400	$C_{19}H_{25}FO$
8	1,6,10-Dodecatrien-3-ol,3,7,11-trimethyl-,(E)-	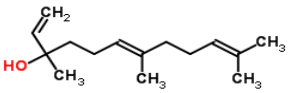	222.3663	$C_{15}H_{26}O$
9	Caryophyllene oxide	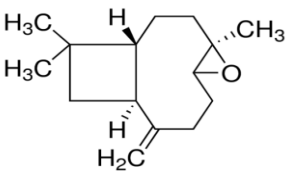	220.35	$C_{15}H_{24}O$
10	5,5-Dimethyl-4-[(1E)-3-methyl-1,3-butadienyl]-1-oxaspiro[2.5]octane	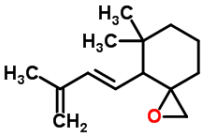	206.324	$C_{14}H_{22}O$
11	1,5,5,8-Tetramethyl-12-oxabicyclo[9.1.0]dodeca-3,7-diene	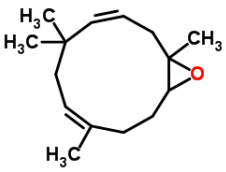	220.350	$C_{15}H_{24}O$

12	Sabinen	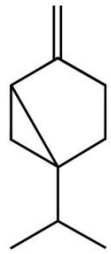	136.23	$C_{10}H_{16}$
13	D-Limonene	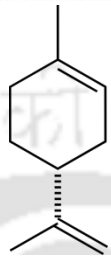	136.24	$C_{10}H_{16}$
14	α-cadinol	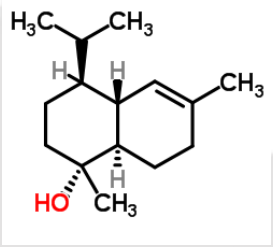	222.366	$C_{15}H_{26}O$
15	Stigmasterol	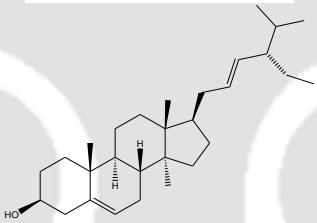	412.69	$C_{29}H_{48}O$
16	γ-Sitosterol	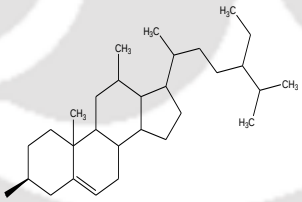	414.7067	$C_{29}H_{50}O$

2.8.3. Flavonoids from *A. nigra*

Flavonoid have been isolated from several parts of the plant. Generally, the flavonoids are involved in growth and defense against plaques by plants. They are low-molecular-weight phenolic compounds that are mostly distributed in the flower of this plant. Several flavonoids are easily recognized in the flower of Zingiberaceae family by their pigments. However, their existence is not only limited to flowers pigments but are found in leaves and several other parts

of the plant (Qiao et al. 2007; Ghosh et al. 2014a). The isolated flavonoids from *A. nigra* are tabulated below (**Table 2.7**).

Table 2.7 Flavonoid isolated from *A. nigra* (Qiao et al. 2007)

S. no.	Compound Name	Structure	Class of compound	Bioactivities
1.	Astraglin	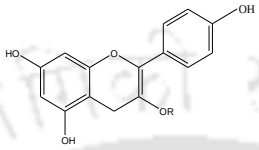 R= Glucose	Flavone glycoside	Antibacterial, antiprotozoal, antioxidant, hepato-protective
2.	Kaempferol-3-*O*-glucuronide	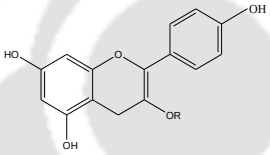 R= Glucouronic acid	Flavone glycoside	Antibacterial, antiprotozoal, antioxidant, hepato-protective

2.9. Flavonoids: As a source of therapeutics

Flavonoids are allied with a broad spectrum of health-promoting effects and are an essential constituent in an assortment of nutraceutical, medicinal, pharmaceutical, and cosmetic applications. Flavonoids belong to polyphenolic groups and have various promising biochemical and antioxidant effects associated with the cure of several diseases such as Alzheimer's disease (AD), cancer, atherosclerosis (Panche et al. 2016). Flavonoids are also found in beverages and foods of plant origin, such as vegetables, fruits, cocoa, tea, and wine; therefore, they are designated as dietary flavonoids. Flavonoids have several subgroups, including flavones, flavonols, chalcones, and isoflavones. This subclass of flavonoids have unique sources. For example, tea and onions leaves are major dietary sources of flavones and flavonols. The flavonoids are also present in the fruits and seeds of higher plants (Ullah et al. 2020). The therapeutic potential of flavonoids is tabulated below (**Table 2.8**).

Table 2.8 Flavonoids, their therapeutic potential, and rich dietary sources (Panche et al. 2016)

S. No.	Class	Compound name	Therapeutic potential	Dietary source	References
1.	Flavonols	Quercetin	Acetylcholinesterase inhibitor	Vegetables, fruits	(Ajiboye et al. 2018)
2.	Flavonols	Rutin	antioxidant	Green tea, red grape, grape seeds,	(Iacopini et al. 2008)
3.	Flavonols)	Myricetin	anticancer activity	Vegetables, fruits, nuts, berries, tea, red wine	(Yi et al. 2015)
4.	Xanthones	Macluraxanthone	Antibacterial	Maclura tinctoria (Hedge apple), Dyer's mulberry	(Yimdjo et al. 2004)
5.	Isoflavone	Genistein	Antibacterial	soyabeans,	(Hong et al. 2006)
6.	Isoflavone	Daidzein	Antioxidant	Soyabeans, tofu	(Dwiecki et al. 2009)
8.	Coumarin	Scopoletin	Anti-Inflammatory	Vinegar, dandelion coffee	(Ding et al. 2008)
10.	Flavanone	Naringenin	Anti-Sindbis activity	Grapes	(Paredes et al. 2003)
11.	Flavanone	Abyssinones	Anticancer activity	French bean seeds	(Farmer et al. 2010)
15.	Anthocyanidin	Peonidin	Antioxidant and prebiotic activity	purple sweet potatoes Cranberries, blueberries, grapes	(Sun et al. 2018)
18.	Flavanone	Hesperidin	Anti-inflammatory	Bitter orange, petit grain, orange, orange juice, lemon,lime	(Tejada et al. 2017)
19.	Flavan-3-ols	Epicatechin	cardiovascular and neuropsychological	Milk, chocolate, commercial, reduced fat	(Bernatova 2018)
22.	Flavones	Apigenin	anticancer	Milk, chocolate,	(Imran et al. 2020)

2.9.1 Chemistry and structure-function relationship of flavonoid

Flavonoids are benzo-ç-pyrone derivatives polyphenolic compounds that are commonly present in plants. More than 4000 flavonoids have been reported from plants, and most flavonoids are regular components of the human diet (Banjarnahor and Artanti 2015). The molecular structure of flavonoid contains a three-ring system, two aromatic rings/ phenyl rings (A and B), and an oxygenated heterocyclic ring (C ring). Generally, flavonoids have a 15-carbon skeleton chemical structure. In the IUPAC nomenclature, this 15-carbon structure is abbreviated as C6-C3-C6. Based on chemical structure, flavonoids can be classified into bioflavonoids, isoflavonoids, and neoflavonoids. Bioflavonoids are simple flavonoids consisting of a 15-carbon skeleton with two phenyl rings, one heterocyclic ring, and non-ketone polyhydroxy polyphenol. Meanwhile, isoflavonoids are derived from 3-phenylchromen-4-one (3-phenyl-1,4-benzopyrone) chemical structure. Neoflavonoids are derived from 4-phenylcoumarine (4-phenyl-1,2-benzopyrone) chemical structure (Rana and Gulliya 2019).

Flavonoids have been classified based on their chemical structure and are generally subdivided into several subgroups: Flavanones, Flavanonols, Anthocyanidins, Anthoxanthins, and Flavones (**Fig. 2.3**). The members of flavonoids are flavones, isoflavones, and the 2, 3-dihydroderivatives of flavone, namely flavanones, which are interconvertible with the isomeric chalcones. Flavanones undergo a series of transformation affecting the heterocyclic C ring to give rise to other family members of flavonoids, including anthocyanins and catechin (Panche et al. 2016).

Many flavonoids contain more than one catechol group and one phenolic group with a close carbonyl group that might work as conceivable chelating sites for the metal ion. Ortho-hydroxylation generally happens on the B-ring of the flavonoid molecule and 3-hydroxyl group, which is present in the C-ring at position a C2-C3, usually reveals the antiradical activities (Wang et al. 2018).

Several researchers have reported that flavonoids have the property of scavenging free radicals and inhibiting autoxidation reactions, but the relationship between their structure and activity remains unclear. Some studies revealed ortho-hydroxylation on the B-ring of the flavonoid molecule, and the 3-hydroxyl group present in the C-ring at position C2-C3 revealing the antiradical activities (López 2020). Several studies have shown the relationship between the chemical structure of the flavonoids and their ability to inhibit the free radical. Their efficacy as

the scavengers of 1,1-diphenyl-2-picrylhydrazyl (DPPH) free radicals. β-carotenelinoleic acid model system has been reported by Ray et al. (2007) as an antioxidant model system (Ray et al. 2007).

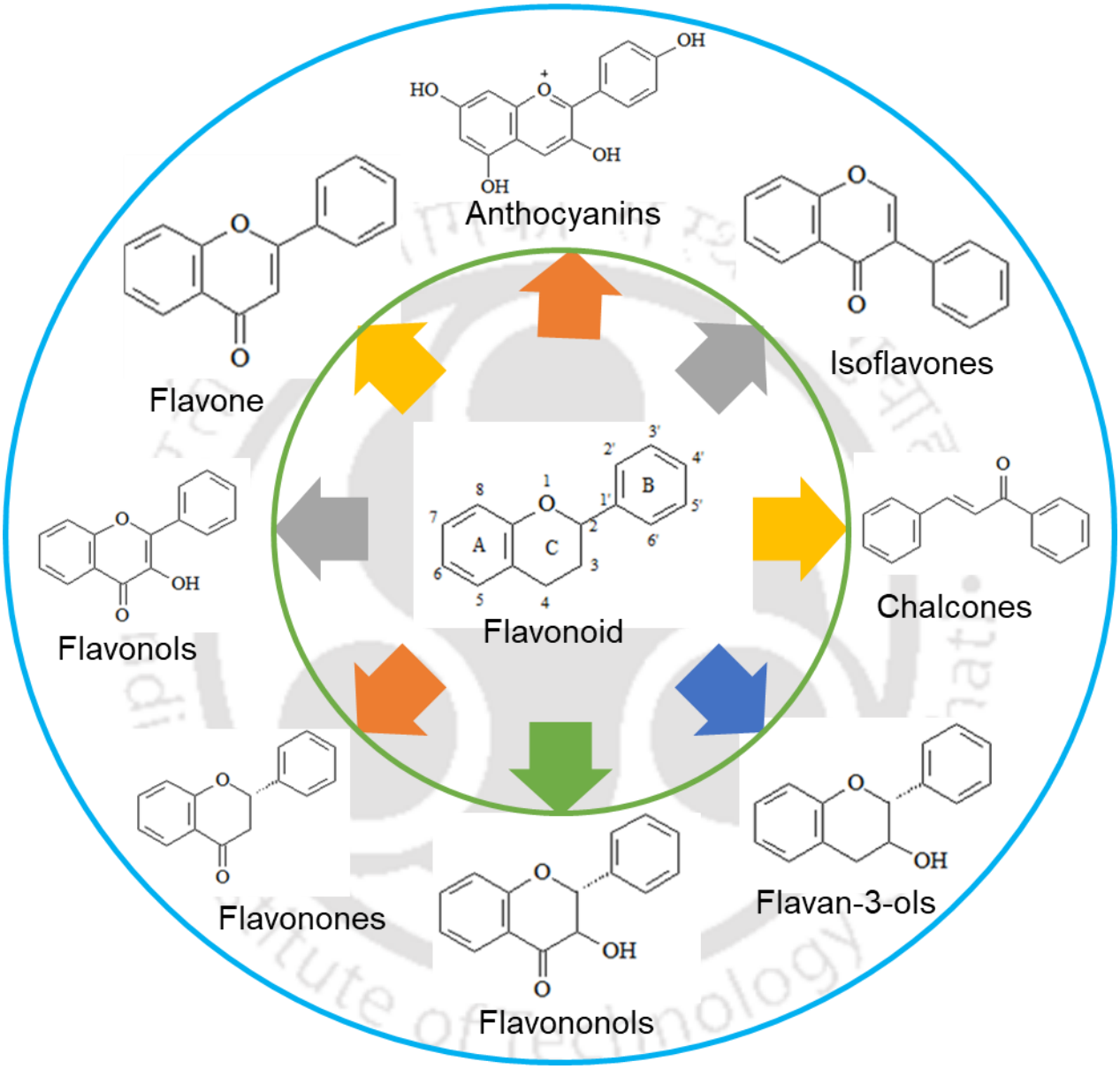

Fig. 2.3 Flavonoids basic structure and its subgroup

2.10 Therapeutic potential and recent advances in flavonoids

Currently, flavonoids are one of the possible bioactive compounds to combat several chronic diseases. Many researches on flavonoids report their medicinal properties, such as anti-bacterial, anti-aging, anti-inflammatory, anticholinesterase, etc. The therapeutic potential of flavonoids

reveal their capacity to control essential cellular enzyme functions involved in anti-inflammatory, anti-mutagenic, antioxidative, and anti-carcinogenic activity. They are also recognized as effective inhibitors for numerous enzymes, such as cyclo-oxygenase (COX), xanthine oxidase (XO), phosphoinositide 3-kinase and lipoxygenase.

2.10.1 Anti-cholinesterase activity

Acetylcholinesterase (AChE) is the main enzyme present in the central nervous system. The inhibition of AChE leads to rise of neural acetylcholine levels, which is one of the possible therapies for symptomatic relief of mild to moderate Alzheimer's disease (AD) (Saxena and Dubey 2019). Therefore, the inhibition of cholinesterases is one of the key focus for developing the new drug to combat AD. Many plant-derived flavonoids have been executed for their anti-cholinesterase activity. The *in vitro* inhibitory studies on several flavonoids such as quercetin, kaempferol 3-O-β-D-galactoside, rutin, and macluraxanthone showed anti-cholinesterase activity. The concentration-dependent inhibition study of quercetin and macluraxanthone has shown action against AChE and butyrylcholinsterase (BChE) (Ajiboye et al. 2018). The molecular docking studies revealed the intermolecular interaction of these two compounds. The enzyme kinetic studies executed that flavone compound quercetin inhibited AChE enzyme competitively (Khan et al. 2009b). Sheng et al. (2009) observed that most polyphenolic compounds such as flavone and its derivatives efficiently bind and inhibit the AChE.

2.10.2 Combating neurodegenerative diseases

Flavonoids exhibit an important role in the central nervous system. Many reported studies have shown that flavonoids isolated from different plants play an important role in the enzyme and receptor system of the brain. They executed significant effects on the central nervous system, like the anticipation of neurodegeneration-associated diseases such as Alzheimer's disease (AD) and Parkinson's disease (Magalingam et al. 2015; Hole and Williams 2021). Flavonoids can inhibit the enzymes, as there are strong reports about inhibitory enzymes such as phosphodiesterase, aldose reductase, Ca^{2+} ATPase, lipoxygenase, and COX in preventive neurodegenerative diseases. Some molecular docking reports have revealed that flavonoids bind with enzyme AChE and use therapeutics against AD (Shen et al. 2009). The reported paper by Shen et al. (2009) have designed a series of flavonoids and revealed potent AChE inhibitors.

Most of the flavonoids showed potent inhibitory activities against AChE. Further, the isoflavone skeleton was a capable structural template for the improvement of novel AChE inhibitors. Some other reports displaced the AChE- and BChE-inhibitory activities with four flavonoids: rutin, quercetin, kaempferol galactoside, and macluraxanthone. Out of these four flavonoids, macluraxanthone displayed a novel inhibitor of AChE and BChE (Khan et al. 2009a).

Molecular docking studies of some flavonoids revealed lower Alzheimer's Aβ production by inhibitory mechanism. It has been described that there exists a strong correlation between flavonoids and inhibitions of NF-κB-related mechanisms. In contrast, some researchers reported the molecular docking of flavones as BACE-1 inhibitors. Flavonoids strongly inhibit BACE-1 activity over the interactions of the BACE-1 catalytic center (Shimmyo et al. 2008).

2.10.3 Radical scavenging

Free radical scavenging property is one of the well-known properties of flavonoids. The free radical scavenging mechanism of flavonoids was explained by several research groups (Korkina and Afanas'ev 1997). According to the explained mechanism, the flavonoid hydroxyl group is highly reactive and oxidized by free radicals. Due to free radicals being scavenged by flavonoids, radical states are less reactive. In other words, the highly reactive hydroxyl group of the flavonoids makes free radicals inactive. The reaction mechanism between flavonoids and free radicals was described by the following equation as described by Korkina & Afanasev:

Flavonoid (OH) + r(O) + RH,

where O is an oxygen-free radical and R is a free radical.

Some published reports revealed that flavones could directly scavenge superoxides, while some flavones can scavenge peroxynitrite (Heim et al. 2002). Korkina and Afanasev et al, (1997) described that flavonoids such as epicatechin and rutin are powerful radical scavengers (Korkina and Afanas'ev 1997). Many researchers have also investigated the scavenging capacity of quercetin, kaempferol (Vellosa et al. 2011). *In vitro* study revealed flavonoids to prevent LDL oxidation by scavenging radicals and control atherosclerosis (Chen et al. 2019).

2.10.4 Metal chelating properties and its medicinal application

Metal ions play an imperative role in biological processes, and metal homeostasis is required for the maintenance of metal balance. Numerous diseases arise from the loss of homeostasis,

including metal overload and deficiency, which are caused by abnormal metal metabolism or metal absorption. Plant polyphenolic compounds have been extensively reported as effective chelators for metal ions, viz. iron, copper, zinc, platinum, and palladium (Broadley et al. 2007; Perez et al. 2009; Filipský et al. 2012). Plant polyphenolics like flavonoids possess higher chelating properties due to the presence of hydroxyl and the carbonyl groups of the C-ring. Hydroxyquinoline and its derivatives have been widely explored as a metal chelating agent and have shown various therapeutic potentials (Savić-Gajić and Savić 2020).

Many papers have reported the synthesis and the anticancer activity of complexes of flavonoids with metal such as Zn and Cu(II) ion (Tu et al. 2016). Some published data have described the possible site of flavonoids for conjugation of metal ions: the 3-hydroxyl or 5-hydroxyl and the 4-carbonyl groups of the C-ring. Copper and iron binding to flavonoids has been better studied. Some studies have explained that dietary flavonoids affect zinc homeostasis and transport (Jeslin Kanaga Inba et al. 2013).

The molecular skeleton of plant polyphenolic compounds (flavonoids) contains a three-ring system, two aromatic rings (A and B), and an oxygenated heterocycle (C ring). Many flavonoids contain more than one catechol group and one phenolic group with a close carbonyl group that might work as conceivable chelating sites for metal ions {Formatting Citation}. Determining the binding site and further structure confirmation of the complexes is critical, especially for polyphenols that have more than one possible metal-binding site. Therefore, more detailed studies are needed on the metal-binding properties of plant polyphenolic compounds to understand the effects at the molecular level.

2.10.5 Anti-cancer activity

Natural products are a major source of anti-tumoral agents, with 175 small molecules approved for cancer treatment between 1940 and 2014 (Newman and Cragg 2016). Plant-derived compounds, including taxanes, vinca alkaloids, camptothecins, and epipodophyllotoxins, are still at the forefront of therapeutic protocols in treating various cancers (Newman and Cragg 2016). Multifactorial properties of natural products can be advantageous to target-specific chemotherapeutic drugs, which usually result in resistance in cancer cells. Particular interest is polyphenols. These are abundantly present in plants and show attractive properties such as antioxidant, anti-inflammatory, and lack of substantial toxic effects (Bian et al. 2020).

2.11 Flavone: a novel source of bioactivity

Flavones are one of the important subgroups of flavonoids. Flavones are extensively present in flowers, leaves, and fruits. The flavone is mainly isolated from red peppers, chamomile, celery, parsley, mint, and *Ginkgo biloba*. The peels of citrus fruits are also a rich source of tageretin, sinensetin nobiletin, and polymethoxylated flavones (Manach et al. 2004). Flavone structure has a double bond between positions 2 and 3 and a ketone in position 4 of the C ring. Most flavones of vegetables and fruits have a hydroxyl group in position 5 of the A ring, while hydroxylation in other positions, for the most part in position 7 of the A ring or 3′ and 4′ of the B ring, may vary according to the taxonomic classification of the particular vegetable or fruit (Arfaoui 2021). Flavone has been shown to many bioactivities as anti-inflammatory, antioxidant, anticancer, and antibacterial, etc. (**Fig. 2.4**).

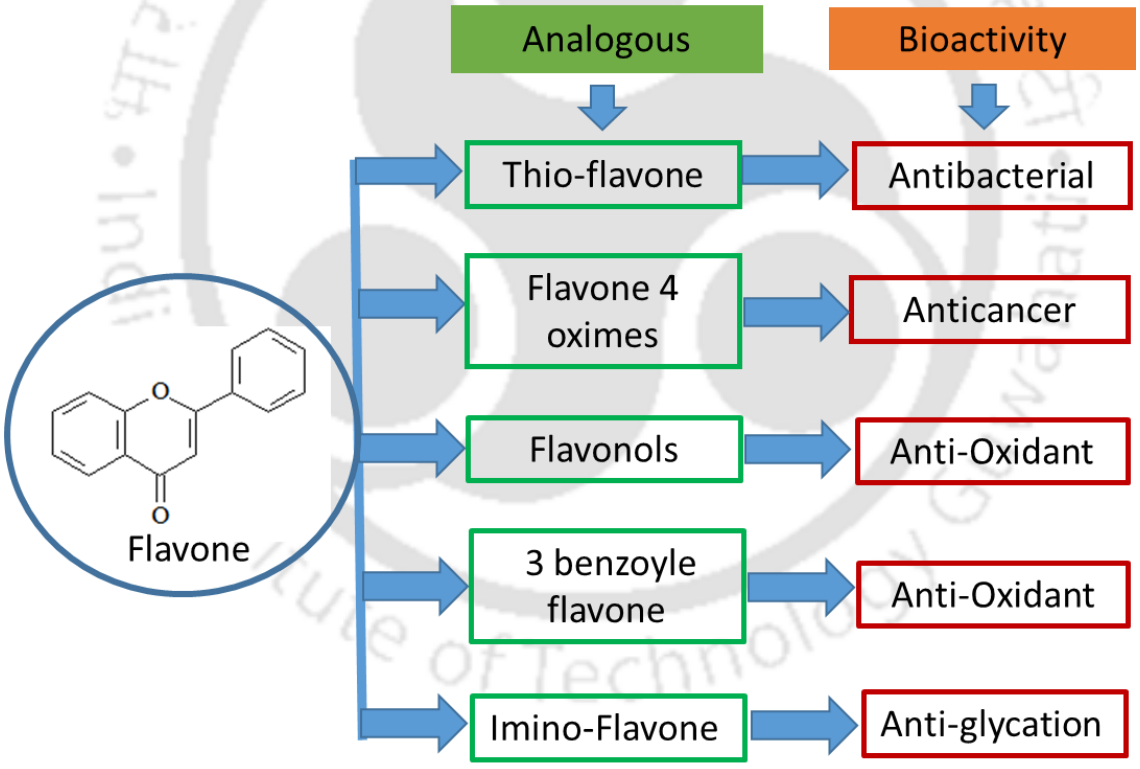

Fig. 2.4 Flavone, it's analogous and their bioactivity

2.12 Future research and the road ahead

Over the past few years' flavonoids have been receiving considerable attention in various possible benefits and therapeutic effects. Several studies have been reported towards therapeutics

and convoluted studies related *in vitro* and *in silico*. However, therapeutics potential towards many enzymes, proteins, and metal conjugate flavonoids effects is less explored. Hence, more studies are required to establish their usefulness.

The study on the polyphenolic compound is usually complex due to the heterogeneity of their molecular structures. Thus, less research data are available on the bioavailability of polyphenolic compounds like flavonoids. Furthermore, less methods existed to know and quantify the oxidative and reductive behavior of flavonoids. The measurement of flavonoid's effect and its mechanism *in vivo* remains difficult. So, there is an eminent need to develop new analytic techniques to countenance and assemble more information and data.

Many reports have emphasized that molecular docking studies are a prerequisite to classify and recognize the possible molecules of flavonoids for their usage in the cure of disease. The studies with molecular docking of flavonoids with receptor molecules are an important and noteworthy area of upcoming research. Further, more research is required to determine and discover the novel flavonoids from a natural source. This will substitute the use of synthetic medicines that are harmful to animal health. In this perspective, there is a necessity for research and development programmers linking *in vivo* and *in vitro* studies which will give an optimistic and safe picture for the development of several drugs in the future.

Phytochemical screening, antibacterial, anti-biofilm and quorum sensing inhibiting activity of *Alpinia nigra* leaf extract against infectious pathogen-*Pseudomonas aeruginosa* PAO1.

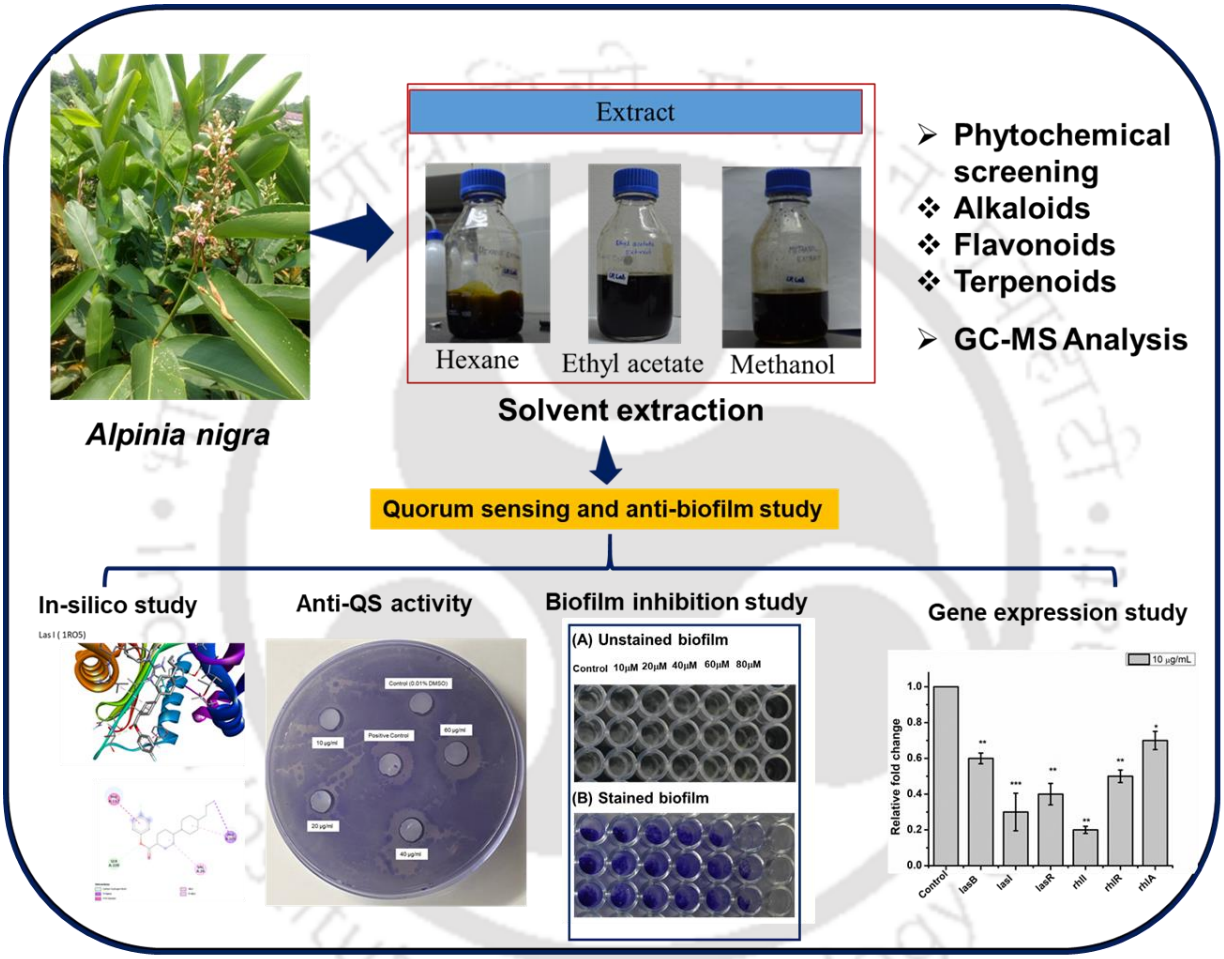

In this chapter, we performed phytochemical screening of *A. nigra* leaves extract and examined the potent compounds to evaluate the anti-biofilm activity towards *Pseudomonas aeruginosa*.

Chapter 3

Phytochemical screening, antibacterial, anti-biofilm and quorum sensing inhibiting activity of *Alpinia nigra* leaf extract against infectious pathogen *Pseudomonas aeruginosa* PAO1

3.1 Introduction

The multifaceted therapeutic applications of phytochemical based traditional medicine have amplified their usage worldwide, even when only about one tenth of the world's biodiversity has been assessed for biological activity (Cragg & Newman 2013). The antibacterial, antioxidant, anti-inflammatory and anti-oncogenic properties of phytochemicals offer the best counter offensive strategy against global antibiotic resistance escalation. The exponential production and indiscriminate prescription of antibiotics have engendered antibiotic resistance and rendered the treatment of infectious diseases far more challenging (Snow et al. 2016). Consequently, there is an increased preference of natural drugs for infection alleviation and a movement away from synthetic drugs and their adverse fallout (Mohammadi et al. 2020). Many plant secondary metabolites have proven pharmacological effects on animals and their systems (Silva et al. 2020). It is vital in the present context that the valuable cache of bioactive phytochemicals are documented and verified for diverse prophylactic application.

Efficacy of products and derivatives from the Zingiberaceae or ginger family against bacterial infections in traditional Indian medicine and their abundance in India have been well documented (Ghosh & Rangan 2013). The " Tora" of northeastern India and "Noh Kala" of Thailand is an aromatic medicinal species, *Alpinia nigra* B.L. Burtt, of the Zingiberaceae family. In general, *A. nigra* serves as an edible vegetable and restorative against dyspepsia, gastric disease, and insect bites. *A. nigra* raw juice from the leaf blades is even considered anthelmintic among the tribal people of Tripura (Roy & Tandon 1999).

The anti-biofilm properties of many plant-derived chemicals for documented and natural chemicals have evinced significant efficacy against a variety of microbial infections. The pathogenic *Pseudomonas aeruginosa* is implicated in biofilm formation, aided by the many quorum sensing (QS) signals that form a colony and afford protection against the host's defense mechanism (Kaverimanian & Heuertz 2019). Among the many QS signaling molecules, (S)-3-

(S)-butyl-homoserine lactone (BHL), oxododecanoyl-homoserine lactone (OdDHL), 2-heptyl-3-hydroxy-4(1H)-quinolone or Pseudomonas Quinolone Signal (PQS), and 2-heptyl-4(1H)-quinolone (HHQ) a PQS precursor are of particular significance. During *P. aeruginosa* infection, the cardinal receptor for BHL is *Rhl*R with *las*B forming an important extracellular virulence factor in its pathogenicity. The published reports revealed that PQS and HHQ molecules play key roles in signaling. Therefore, further investigation is needed for the inhibitory mode of action of PQS. Consequently, we explored compounds from *A. nigra* leaf extract for their antibacterial and biofilm limiting action.

3.2 Materials and methods

3.2.1 Sample collection and preparation of extract

The collection of mature leaves of *A. nigra* was carried out in the Indian Institute of Technology Guwahati (IITG) campus, Assam (26°12.476′N to 91°41.965′E). The collected leaves were subject to drying at room temperature in the shade, subsequently cut, and placed in a mechanical blender to obtain a fine leaf powder. Dried leaves powder (200 g) was packed into a Soxhlet apparatus and extracted was done according to the polar strength of the solvent (400 mL each) starting with non-polar (n-hexane) to polar (ethyl acetate and methanol) at 60–65°C. The extract was filtered through Whatman filter paper No. 1, and the extract was vacuum dried in a rotary evaporator (kolpammer, 210, Switzerland). The resultant dried leaf extract was weighed, placed in storage vials, and maintained at 4°C till required.

3.2.2 Phytochemical screening

The leaf extracts of the three different organic crude extract of plant\ under study were subjected to qualitative phytochemical analysis. The phytochemical constituents of the extracts were analyzed following the Richardson & Harborne (1985) method with some modification (Richardson and Harborne 1985). The alkaloids, flavonoids, saponins, terpenoids, and phenolics present in the extracts were qualitatively assessed by colorimetric methods.

3.2.2.1 Test for alkaloids

The organic extract (40 mg) was placed in a test tube, 2-5 drops of diluted HCl added, incubated for 5 minutes, and filtered. It was transferred to a fresh test tube, and 2-5 drops of Mayer's reagent were added.

3.2.2.2 Test for flavonoids

The dry crude extract (1 mg) was dissolved in 0.5 mL of aqueous 1N sodium hydroxide and heated at 40°C for 10 min. The appearance of yellow colouration indicated the presence of flavonoids; subsequently confirmed by an intense yellow colour on addition of a few drops of dilute H_2SO_4.

3.2.2.3 Test for saponins

The crude extract (2 mg) was dissolved in distilled water (5 mL). The solution was heated at 40°C for 15 min and vortexed for 2 minutes at room temperature. The formation of foam in the test tube revealed the presence of saponins.

3.2.2.4 Test for terpenoids

2ml chloroform was used to dissolve 2 mg of extract. Followed by addition of 1 mL each of acetic anhydride and concentrated H_2SO_4. Terpenoids were confirmed with the formation of a reddish-brown coloured interface.

3.2.2.5 Test for phenolics

0.5 mL of distilled water was used to dissolve 2 mg of the crude extracts. On addition of 5-6 drops of ferric chloride (5%) solution, the appearance of dark green colour in the solution indicated the presence of phenolic compounds.

3.2.2.6 Gas chromatography-mass spectrometry (GC-MS) analysis

The extract was investigated using 6890 series GC-MS equipped with MSD 5973 for analysis (Agilent Technologies, Alto, CA, USA). The sample was examined by using a sample injection volume of 1.0 µl (split ratio 1:100), in a column HP-5 (30m x 0.25mm x 0.25µm) at 70 eV ionization energy. Other parameters employed were constant flow rate of 1.1 mL/min for the

carrier gas helium (99.99%), and temperatures of 250°C for the injector and 230°C for ion source. A fused silica capillary column (rate of 3°C/min), with temperatures ranging from 100°C for 2 min to 290°C for 20 min, was used to separate the constituents. Mass spectra were scanned from 50 to 500 Da., at 70 eV with a scan-interval of 0.3 seconds. Identification of phytochemicals resulted from comparison of the spectral data with Wiley and NIST libraries (NIIST11.L).

3.2.3 Antibacterial activity

Testing of antibacterial activity was based on the earlier method (Song et al., 2019). In brief, bacterial cells (*P. aeruginosa* PA01) were seeded in 96-well plates, treated with 10 µg/mL to 80 µg/mL of L-EtAc, and incubated overnight in the shaking incubator (rpm 180) at 37°C. The absorbance recorded at 600 nm indicated the inhibitory concentration (IC_{50}) of extract against the bacterial pathogen (*P. aeruginosa* PA01).

3.2.4 Bacterial growth inhibition

P. aeruginosa was grown overnight in 10 mL sterilized NB medium at 37°C using a rotary incubator at 160 rpm. Subsequently, test organisms were transferred at a concentration of 1% in 200 µL NB broth and placed in 96-well plates. Various concentrations of L-EtAc (10-80 µg/mL) were added to each well, and the treated sample (0.01% DMSO) served as a control to track the normal growth of the microbial cells. Periodic recording of optical density (OD) was carried at intervals of 120 min using spectrophotometer at 600 nm from culture plates maintained at 37°C and 160 rpm. Plotting of OD versus time showcased the growth profile.

3.2.5 Biofilm inhibition

The polyvinyl chloride biofilm formation assay (Djordjevic et al. 2002) was applied to estimate impact of L-EtAc on biofilm formation. The pathogen cultures to be investigated underwent incubation at 37°C for 24 h, after resuspension in fresh NB medium with 10-80 µg/mL L-EtAc. The resultant biofilms in the microtiter plates were stained with crystal violet and quantified at OD 470 nm after using ethanol to dissolve the dye.

3.2.6 Inhibition of mature biofilms

P. aeruginosa biofilms were grown in microtitre plates for 48 h, subsequently treated with 20-60 µg/mL L-EtAc for 8 h. For quantification, the biofilms were dyed with crystal violet; ethanol was added to dissolve the dye, and OD was recorded at 470 nm.

3.2.7 Screening for anti-QS activity

The evaluation of anti-QS activity of L-EtAc was based on the standard agar well diffusion assay (Vasavi et al. 2016). About 100 µl *Chromobacterium violaceum* was added to 5 mL of molten NB agar (0.3%) and layered without delay on pre-poured NB agar plates. After solidification, L-EtAc ranging from 10 to 80 µg/mL were added prior to 24 h incubation at 37°C. The presence of a circular zone of inhibition of violacein endorsed anti-QS activity.

3.2.8 Inhibition of swarming motility and quantification of exopolysaccharide (EPS)

NA petri dishes treated with L-EtAc at 10 to 80 µg/mL were utilized in swarming motility assays. The inoculate of the strains under investigation was centrally placed on the agar surface for enhanced visibility of motility. For inhibition of EPS production, *P. aeruginosa* was grown and treated with L-EtAc (10 to 80 µg/mL) for 48 h. Subsequently, the culture was centrifuged, the supernatant filtered, 3 volumes of chilled 100% ethanol added to filtrate, and incubated for 24 h at 4°C. This procedure allowed EPS precipitation, followed by its quantification as per Liu et al., (2020).

3.2.9 Microscopic visualization of the biofilms

About 1% of pathogens under investigation (0.4 OD at 600 nm) derived from 24 h cultures were mixed with 1 mL of fresh NB medium with cover glass 1 cm^2; in the presence of 0.01 % DMSO (control) and L-EtAc (10 to 80 µg/mL). Post 48 h incubation, the cover glasses were washed three times with distilled water to discard planktonic cells. Roughly 200 µL of 1 % acridine orange stain (Sigma Aldrich) was added to the cover glasses, and the excess was removed by washing. The 20X visualization was enabled by fluorescence microscopy (Zeiss microscope, Zeiss, Germany).

3.2.10 *In silico* study

Molecular docking was performed using AutoDock Tools (ADT) (Morris et al. 2008). The protein crystal structures were downloaded from the Protein Data Bank (PDB) *las*I (PDB ID: 1RO5), *las*R (PDB ID: 6D6A), *rhl*I (PDB ID: 1KZF), and *las*B (PDB ID: 3DBK). The small molecules of *A. nigra* were selected from GC-MS data and all 3D structures of the ligands, were obtained from PubChem Open Chemistry Database. *In silico* evaluation of the interaction between phytochemical Caryophyllene oxide, 1,6,10-Dodecatrien-3-ol, 3,7,11-trimethyl-, Eucalyptol, Isolongifolol, (-)-Myrtenol, Spiro[4.5]dec-6-en-8-one, 1,7-dimethyl-4-(1-methylethyl)- and [1,1'-Bicyclohexyl]-4-carboxylic acid, 4'-propyl-, 4- fluorophenyl ester with four proteins, *las*I (PDB ID: 1RO5), *las*R (PDB ID: 6D6A), *rhl*I (PDB ID: 1KZF), and *las*B (PDB ID: 3DBK), associated with biofilm formation pathways of *P. aeruginosa* were carried out. Based on PDB, the active site residues of individual proteins were applied to configure the grid map (spacing 0.375 Å) and directed at active sites for docking score computation. Default settings at 40, 40, and 40 for X, Y, and Z, respectively, were maintained for grid box configurations. Each ligands was subject to 1000 docking runs for choosing target protein as rigid and the ligand as flexible. Ligand binding affinity evinced a negative score with units expressed as kcal/mol. Autodock docking outcomes were preserved as .pdbqt extension and .pdb extensions, respectively. Discovery Studio Visualizer tools helped analyze ligand and proteins interaction.

3.2.11 Biofilm-associated genes expression

The inoculum (OD600 of 0.05) derived from overnight cultures was introduced into fresh NB medium containing L-EtAc ranging from 10-40µg/mL and incubated at 37°C for 24 h. The trizol method was applied to extract and purify total RNA, measured at 260/280 nm by NanoDrop (ND1000 spectrophotometer). The first-strand cDNA was generated from a purified mRNA sample using cDNA synthesis kit (NEB), followed by qRT-PCR (Agilent, AriaMx Real-Time PCR) using Mastermix (Invitrogen) and carried out in triplicate. The initial reaction: 94°C for 10 minutes, 40 cycles of 94°C for 20 s, 59°C for 20 s, with first extension at 72°C for 20 s, and final at 72°C for 5 min. Primer sequences for *P. aeruginosa* QS genes and virulence genes are detailed in **Table 3.1**. 16s RNA, was utilized as a housekeeping gene to normalize qRT-PCR data and determine relative fold changes in gene expression. Agilent Manager Software helped

delineate amplification profiles. Cycle threshold (C*t*) values of individual target genes were normalized to the geometric mean of the C*t* of 16s RNA amplified from the corresponding sample. The fold change of target genes of individual groups against the control group was assessed by the ΔΔC*t* method.

Table 3.1 Primer sequences for *P. aeruginosa* QS genes**.**

Gene	Primer	Sequence (5′-3′)
lasI	Forward	GGCTGGGACGTTAGTGTCAT
	Reverse	AAAACCTGGGCTTCAGGAGT
lasR	Forward	ACGCTCAAGTGGAAAATTGG
	Reverse	TCGTAGTCCTGGCTGTCCTT
rhlI	Forward	AAGGACGTCTTCGCCTACCT
	Reverse	GCAGGCTGGACCAGAATATC
rhlR	Forward	CATCCGATGCTGATGTCCAACC
	Reverse	ATGATGGCGATTTCCCCGGAAC
lasB	Forward	GACCGAGAATGACAAAGTGGAA
	Reverse	GGTAGGAGACGTTGTAGACCAGTTG
rhlA	Forward	TGGCCGAACATTTCAACGT
	Reverse	GATTTCCACCTCGTCGTCCTT
16S rRNA	Forward	AGAGTTTGATCCTGGCTCAG
	Reverse	CTACGGCTACCTTGTTACGA

3.2.12 Statistical analysis

Every experiment was conducted in triplicate, and data was shown as mean values with standard deviation (SD).

3.3. Results and discussion

3.3.1 Organic extraction of leaf of *A. nigra*

The organic extract yield and biological activity of the plant extracts have a major relationship with the solvent used, mainly due to the different polarity of the phytochemical compounds (Moure et al. 2001). Therefore, choice of the most appropriate solvent is a determinant/ key

factor (Al-Farsi and Lee 2008). Hence, we have fractionated the organic extract of the leaves of *A. nigra* during subsequent steps of extraction by using gradient polarity of solvent system. Initially, the extraction was done with non-polar, n-hexane which yielded non-polar compounds. Then subjected to ethyl acetate and lastly methanol was used for extraction of semi polar and polar compound, respectively. After separate extraction of organic extract approximately 300-340 mL of solvent was recovered. The organic extract yield in terms of %were found to be 6.8 ± 0.2, 7.3 ± 0.8 and 4.5± 0.6 for L-Hex, L-EtAc and L-Met, respectively (**Table 3.2)**. Furthermore, by determining the yield of organic extract, the qualitative characterization of phyto constituents can be optimized for future biological applications.

Table 3.2 Optimization of yield-related parameters for organic solvent extract from *A. nigra* leaf

Parameter			
Sample	**Leaf of *A. nigra***		
Collection time	June-December		
Time for drying	30 days		
Solvent	**Hexane**	**Ethyl acetate**	**Methanol**
Sample weight (g)	200	200	200
Initial volume of solvent (mL)	400	400	400
Time for 1st cycle (min)	50	60	80
Time for next cycles (min)	30	40	45
Total no. cycle	80	80	80
Solvent recovery (mL)	300	340	320
Solvent recovery time (min)	60	80	110
Crude color	Yellowish green	Greenish brown	Dark brown
Total crude Yield %	6.8 ± 0. 2 %	7.3 ± 0.8 %	4.5± 0.6 %
Smell	Light oily	Bitter almond	Bitter sugary

3.3.2 Qualitative analysis of phytochemicals

A variety of biochemical tests formed an important part of the preliminary phytochemical screening of extract. Phytochemicals are well known for their multifaceted applications as

commercial bio-products, besides begin effective antimicrobial, antifungal, and antiparasitic agents (Ghosh et al. 2013b). Reports from *A. nigra* methanol seed extract has demonstrated anti-cancers and antiparasitic functions (Ghosh et al. 2016a). The phytochemical screening of the L-EaAc was found to be positive for alkaloids, tannins, terpenoids, phenols, and flavonoids. Saponins was not present in L- EtAc and L-Hex extract (**Table 3.3**). The presence of flavonoids, phenolic compounds, and tannins in significant levels signal antimicrobial activity, antioxidant activity, and wound healing properties (Abu Ahmed et al. 2015). It is noteworthy that L-EaAc of *A. nigra* leaves exhibited a high flavonoid content in this investigation.

Table 3.3 Phytochemical constituent analysis of leaf organic extract of *A. nigra*. (+) Present; (-) Absent.

S. no.	Chemical constituents	L-Hex	L-EtAc	L-Met
1	Phenolics	+	++	+
2	Flavonoids	+	+++	+
3	Alkaloids	+	++	+
4	Saponins	-	-	+++
5	Terpenoids	+	++	+

3.3.3 GC-MS analysis

The extract of *A. nigra* leaves was investigated by GC-MS to identify the possible bioactive compounds based on retention time (RT) and mass (M/Z) value. The present compounds in the organic solvent extract of *A. nigra* leaf were established based on recorded mass spectra versus spectral database sourced from NIST, Wiley library, besides other published reports. The GC data displayed 9, 23, and 20 major peaks at different RT in L-Hex (**Fig. 3.1**), L-EtAc (**Fig. 3.2**) and L-Met extract (**Fig. 3.3**), respectively. Further the compound peak signature was confirmed through MS, which showed individual compound on the basis of charge to mass ratio (M/Z), represented in **Table 3.4, Table 3.5, and Table 3.6**. The presence of labdane diterpenes like Eucalyptol, Isolongifolol, 1,6,10-Dodecatrien-3-ol, and 3,7,11-trimethyl-Caryophyllene oxide were confirmed from MS fragmentation patterns. Our results from GC-MS analysis of L-EtAc

show good correlation with previous studies. Thus, various derivatives of labdane diterpenes have been reported from seeds of *A. nigra*, and many other members of the Zingiberaceae family (Ghosh et al. 2016b). Labdane diterpenes are considered potent inhibitors of a wide range of enzymes with remarkable bactericidal and fungicidal activities (Demetzos and Dimas 2001). In addition to labdane diterpenes, many other unidentified compounds were detected in variable quantities in the L-EtAc of *A. nigra*. Similarly, among the 33 compounds detected from GC-MS analysis of *Alpinia mutica* leaf essential oil, 20 sesquiterpenes, and 10 monoterpenes were present (Sirat and Jani 2013). Further, investigations involving essential oils from *Alpinia. zerumbet* leaves and rhizome disclosed 1,8-cineole and terpinen-4-ol as major components, respectively (Leal-Cardoso et al. 2004).

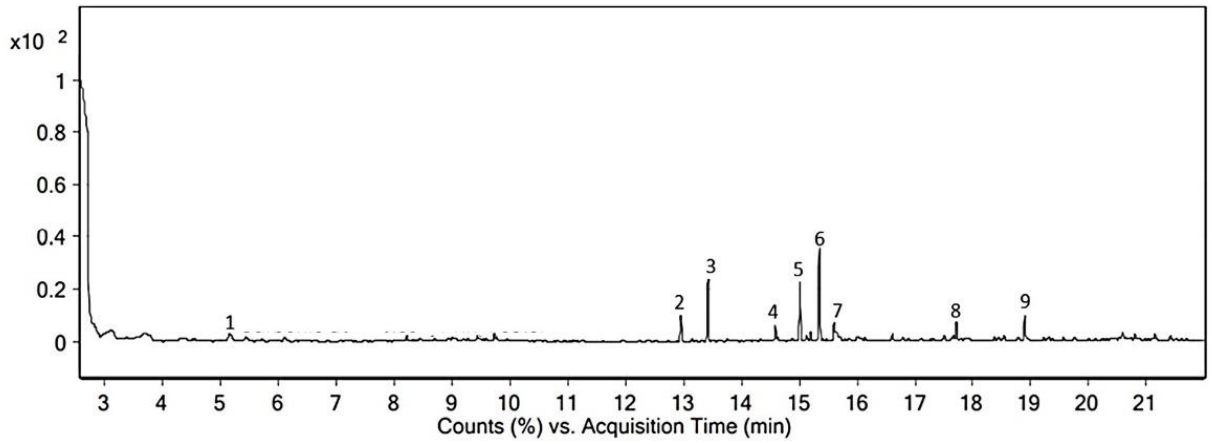

Fig. 3.1 GC-MS chemical profiling chromatograph of L-Hex extract.

Table 3.4 Compound identified from L-Hex extract

S. No.	Name	DB Formula	RT	Mass (m/z)
1.	1,2,6-Hexanetriol	$C_6H_{14}O_3$	5.158	134.1
2.	Caryophyllene	$C_{15}H_{24}$	12.952	204.3
3.	1,5,9,9-tetramethyl-1,4,7,-Cycloundecatriene	$C_{15}H_{24}$	13.421	204.3
4.	1,6,10-Dodecatrien-3-ol, 3,7,11-trimethyl-	$C_{15}H_{26}O$	14.585	222.3
5.	Caryophyllene oxide	$C_{15}H_{24}O$	15.017	220.3
6.	1,5,5,8-Tetramethyl-12-oxabicyclo[9.1.0]dodeca-3,7-diene	$C_{15}H_{24}O$	15.342	220.3
7.	10,10-Dimethyl-2,6-dimethylenebicyclo[7.2.0]undecan-5.beta.-ol	$C_{15}H_{24}O$	15.598	220.3
8.	6,10,14-trimethyl-2-Pentadecanone,	$C_{18}H_{36}O$	17.713	268.4
9.	2(3H)-Benzofuranone, 6-ethenylhexahydro-3,6-dimethyl-7-(1-methylethenyl)	$C_{15}H_{22}O_2$	18.782	234.1

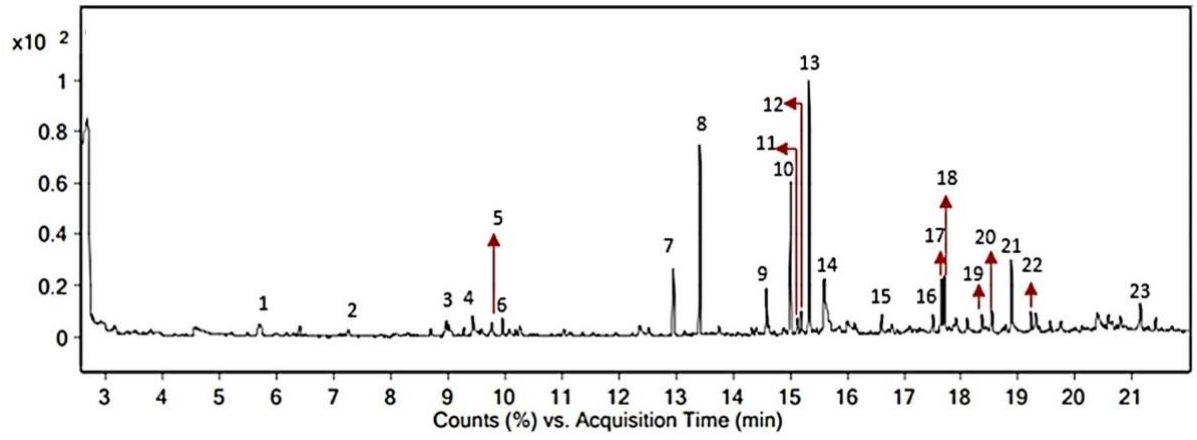

Fig. 3.2 GC-MS chemical profiling chromatograph of L-EtAc extract.

Table 3.5 Compound identified from L-EtAc extract

S. No.	Name	DB Formula	RT	Mass (m/Z)
1.	3-Carene	$C_{15}H_{24}$	5.702	136.2
2.	Eucalyptol	$C_{10}H_{18}O$	7.254	154.2
3.	trans-Verbenol	$C_{10}H_{16}O$	9.011	152.2
4.	Endo-Borneol	$C_{10}H_{18}O$	9.593	154.2
5.	(-)-Myrtenol	$C_{10}H_{16}O$	9.775	152.2
6.	Bicyclo[3.1.1]hept-3-en-2-one, 4,6,6-trimethyl	$C_{10}H_{14}O$	9.956	150.1
7.	Caryophyllene	$C_{15}H_{24}$	12.952	204.3
8.	1,5,9,9-tetramethyl-1,4,7,-Cycloundecatriene	$C_{15}H_{24}$	13.415	204.3
9.	1,6,10-Dodecatrien-3-ol, 3,7,11-trimethyl	$C_{15}H_{26}O$	14.579	222.3
10.	Caryophyllene oxide	$C_{16}H_{24}O$	15.01	220.3
11.	3,7-Cyclodecadien-1-one, 3,7-dimethyl-10-(1-methylethylidene)	$C_{15}H_{22}O$	15.123	218.3
12.	1,5,5,8-Tetramethyl-12-oxabicyclo[9.1.0]dodeca-3,7-diene	$C_{15}H_{24}O$	15.336	220.3
13.	Caryophylla-4(12),8(13)-dien-5.alpha-ol	$C_{16}H_{24}O$	15.598	220.3
14.	Undec-10-ynoic acid, tridec-2-yn-1-yl ester	$C_{24}H_{40}O_2$	16.606	360.6
15.	Ambrial	$C_{16}H_{26}O$	17.5	234.3
16.	Phytol, acetate	$C_{22}H_{42}O_2$	17.656	338.5
17.	6,10,14-trimethyl-2-pentadecanone	$C_{15}H_{26}O$	17.706	268.5

18.	3a,9-Dimethyldodecahydrocyclohepta[d]inden-3-one	$C_{16}H_{26}O$	18.532	234.3
19.	Spiro[4.5]dec-6-en-8-one, 1,7-dimethyl-4-(1-methylethyl)	$C_{15}H_{24}O$	18.782	220.3
20.	n-Hexadecanoic acid	$C_{16}H_{32}O$	18.882	256.4
21.	Hexadecanoic acid, ethyl ester	$C_{18}H_{36}O$	19.22	284.4
22.	Isolongifolol	$C_{15}H_{26}O$	19.308	222.3
23.	Octadecanoic Acid	$C_{18}H_{36}O_2$	21.134	284.4

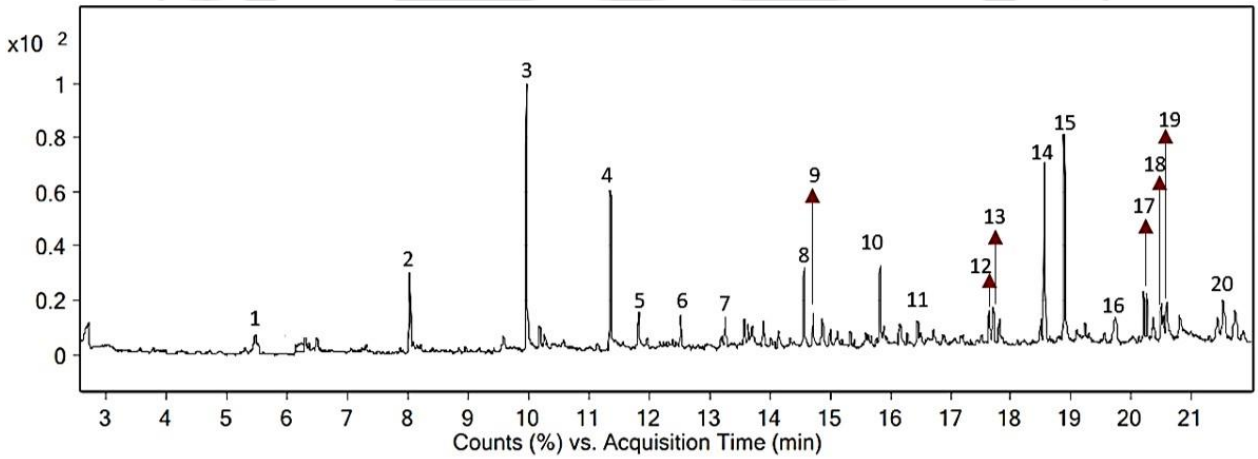

Fig. 3.3 GC-MS chemical profiling chromatograph of L-Met extract.

Table 3.6 Compound identified form L-Met extract.

S. No.	Name	DB Formula	RT	Mass (m/z)
1.	2-Methoxy-4-vinylphenol	$C_9H_{10}O_2$	5.471	150.1
2.	2,6-dimethoxyphenol	$C_8H_{10}O_3$	8.036	154.1
3.	Vanillin	$C_8H_8O_3$	10.187	152.0
4.	2-methoxy-4-propylphenol	$C_{10}H_{14}O_2$	11.357	150

5.	Coumarin, 3,4-dihydro-4,5,7-trimethyl	$C_{12}H_{14}O_2$	11.826	154
6.	2,4-Di-tert-butylphenol	$C_{14}H_{22}O$	12.527	206.3
7.	3',5'-Dimethoxyacetophenone	$C_{10}H_{12}O_3$	13.259	180.2
8.	Turmerone	$C_{15}H_{20}O$	14.566	216.3
9.	4-Propenyl-2,6-dimethoxyphenol	$C_{11}H_{14}O_3$	14.716	194.2
10.	(+)-Longicamphenylone	$C_{14}H_{22}O$	15.83	206.3
11.	Caffeine	$C_8H_{10}N_4O_2$	16.449	194.1
12.	Hexadecanoic acid, methyl ester	$C_{17}H_{34}O_2$	17.638	270.4
13.	Estra-1,3,5(10)-trien-17.beta.-ol	$C_{18}H_{24}O$	17.706	256.3
14.	Methyl 10-trans,12-cis-octadecadienoate	$C_{19}H_{34}O_2$	18.557	296.4
15.	13-Octadecenoic acid, methyl ester	$C_{19}H_{36}O_2$	18.882	296.5
16.	Heptadecanoic acid, 16-methyl-, methyl ester	$C_{19}H_{38}O_2$	19.727	298.5
17.	Bis(2-ethylhexyl) phthalate	$C_{24}H_{38}O_4$	20.252	390.5
18.	Cyclopentene-1-carboxylic acid, 4-[2-(diphenylmethyl)-2-propen-1-yl]-, methyl ester	$C_{23}H_{24}O_2$	20.49	332.4
19.	9,12-Octadecadienoic acid	$C_{18}H_{32}O$	20.578	280.4
20.	2,6-dimethoxyphenol,	$C_8H_{10}O_3$	21.71	207.1

3.3.4 Antibacterial activity

Antibacterial activity of L-EtAc was evaluated against the pathogens *P. aeruginosa* PAO1 by increasing the concentration of L-EtAc (from10-80 µg/mL) and evinced 26.38 µg/mL as the inhibitory concentration (IC_{50}) (**Fig. 3.4**). Previous studies have revealed a mild effect of *A. nigra* leaf extract (2 mg/disc) on *Bacillus cereus*, *B. subtilis*, *Staphylococcus aureus*, *Salmonella typhi*, *S. paratyphi*, *Escherichia coli*, *Vibrio cholerae*, and *Shigella sonnie* (Abu Ahmed et al. 2015). The present antibacterial activity was carried out on *P. aeruginosa* for determining the anti-quorum sensing and anti-biofilm activity as a better alternative.

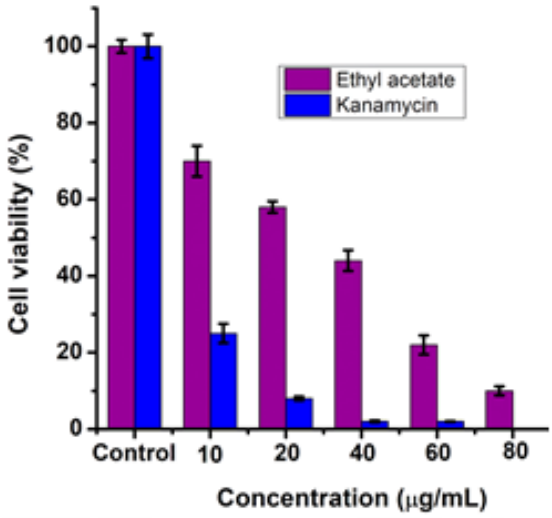

Fig. 3.4 Antibacterial activity of leaf ethyl acetate extract (L-EtAc) and kanamycin against *P. aeruginosa* PAO1.

3.3.5 Bacterial growth inhibition

The growth of bacteria was analyzed under control (0.01 % DMSO treated) condition and under the treatment of L-EtAc extract for knowing the extract's effect on bacterial growth. As opposed to the normal growth curve of *P. aeruginosa* in the absence of L-EtAc in control, the gradual shortening of log phase in a concentration-dependent manner was observed with treatment 10-80 μg/mL of L-EtAc (**Fig. 3.5**). This outcome possibly is due to significant decrease in growth rate and reduced bacterial colony formation. Our results are in good agreement with studies conducted by Ellen et.al. (2015), where treatment with ethanolic extract of *Zingiber officinale* rhizome, a medicinal plant, *P. aeruginosa* PAO1 displayed significant reduction in biofilm formation and corresponding growth rate (Ellen L Lagendijk 2015).

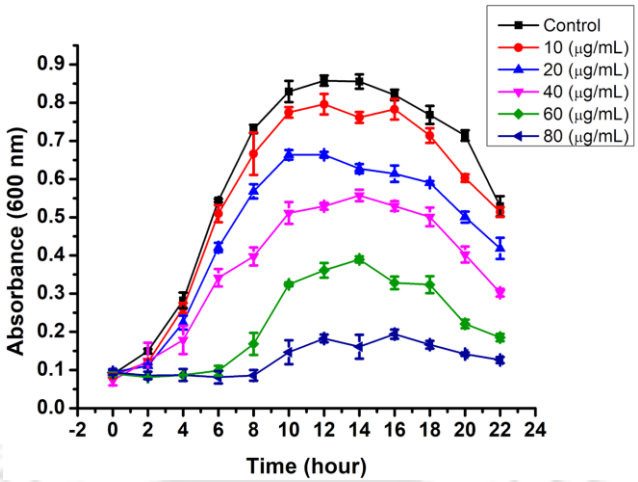

Fig. 3.5 Growth curve of *P. aeruginosa* in presence of various concentrations of L-EtAc extract (10-80 µg/mL).

3.3.6 Biofilm inhibition

The addition of L-EtAc that ranged from 10-80 µg/mL showed concomitant reduction in biofilm formation in *P. aeruginosa* (65 ± 1.05, 48 ± 2.05, 22 ± 1 %, 13 ± 2.6 %, 8 ± 1.35 %. and 2 ± 0.54 %) versus control (**Fig. 3.6**). Therefore, the data implied decreased swarming and EPS activity as evinced by diminished adhesion and maturation. These results are well supported by studies carried out by Hayat et. al. (2018); as reduced biofilm biomass downgrades opportunities for pathogen resistance augmentation (Hayat et al. 2018).

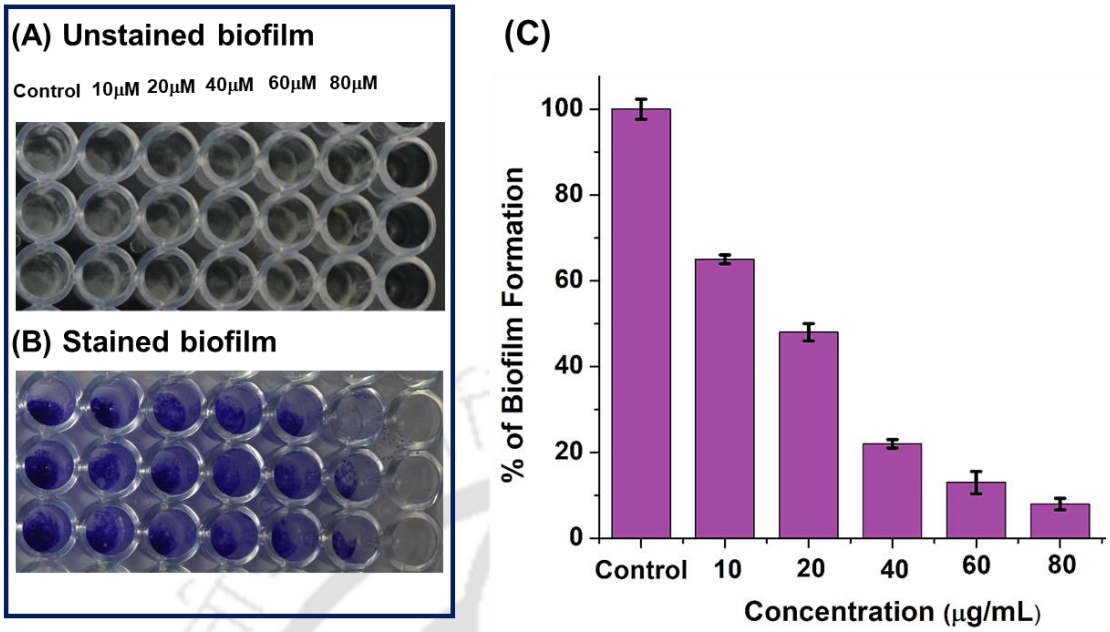

Fig. 3.6 Biofilms of *P. aeruginosa* formed in a microtiter plate at various concentrations of L-EtAc (10-80 µg/mL). (A) Unstained, (B) crystal violet stained and (C) percentage (%) biofilm inhibition.

3.3.7 Effect of L-EtAc on mature biofilm

After allowing biofilms of *P. aeruginosa* PAO1 to develop for 48 h, they were exposed to L-EtAc (20-60 µg/mL) for 8 h to induce disruption**. Figure 5** showcases the consequential lowering of biofilm production (62 % to 29 %) on L-EtAc treatment as evinced by crystal violet staining. In retrospect, disruption in biofilm production implies corresponding impairment of the QS mechanism, which is known to play a positive role in biofilm maturation. Consequently, the present findings draw support from studies with synthesized sulfur analogs that conspicuously disrupted mature biofilms of *P. aeruginosa* PAOI (Ganguly et al. 2011). In a similar manner, *Capparis spinosa* demonstrated considerable lowering of preformed biofilms of *E. coli, Proteus mirabilis, Serratia marcescens, and P. aeruginosa* PAO1 (Issac Abraham et al. 2011).

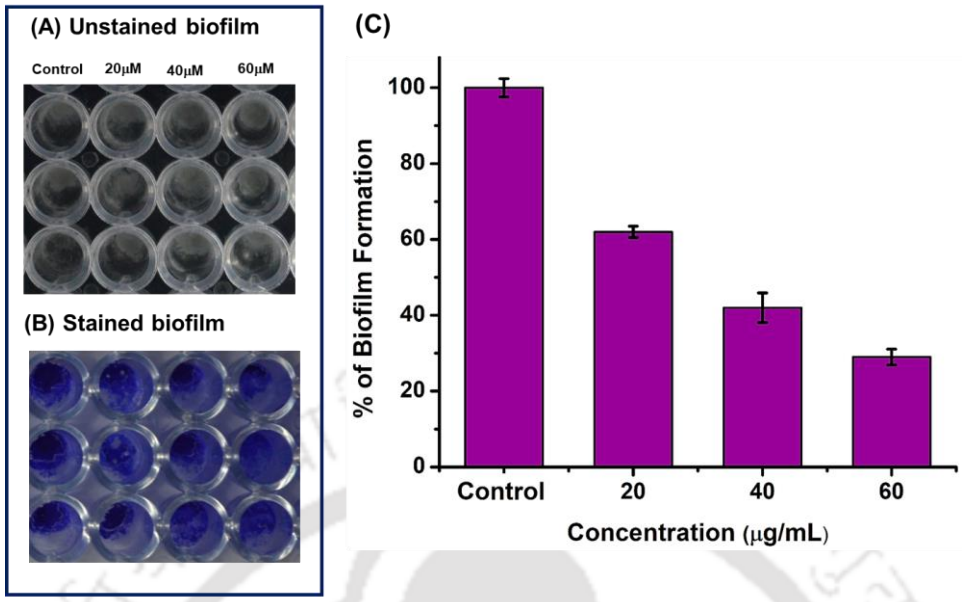

Fig. 3.7 Inhibition of mature biofilm on treatement with L-EtAc (20-60 μg/mL). (A) Unstained, (B) crystal violet stained and (C) peresentage biofilm inhibition.

3.3.8 Quorum sensing inhibitory activity

Concentration-dependent reduction in pigment production (transparent zones) was detected around the well loaded with L-EtAc (**Fig. 3.8**). The inhibitory zone assay showed a significant decrease of violacein pigment in all the applied concentrations (10-80 μg/mL) of L-EtAc. Thus, the QS inhibition role of L-EtAc was validated by violacein producing *C. violaceum* CV12472 biosensor strains. The violacein production is regulated by the CviIR-dependent quorum-sensing system. Consequently, suppression of violacein implied inhibition with AHL-regulated QS (Cauz et al., 2019). Our findings on QS inhibition in *C. violaceum* biosensor strains are endorsed by the 88.2 ± 0.1 % inhibition of violacein pigment documented with dietary flavonoid (Bali et. al. 2019). *P. aeruginosa* biofilm matrix is an alginate exopolysaccharide, known to be controlled by QS (Ryder et al. 2007).

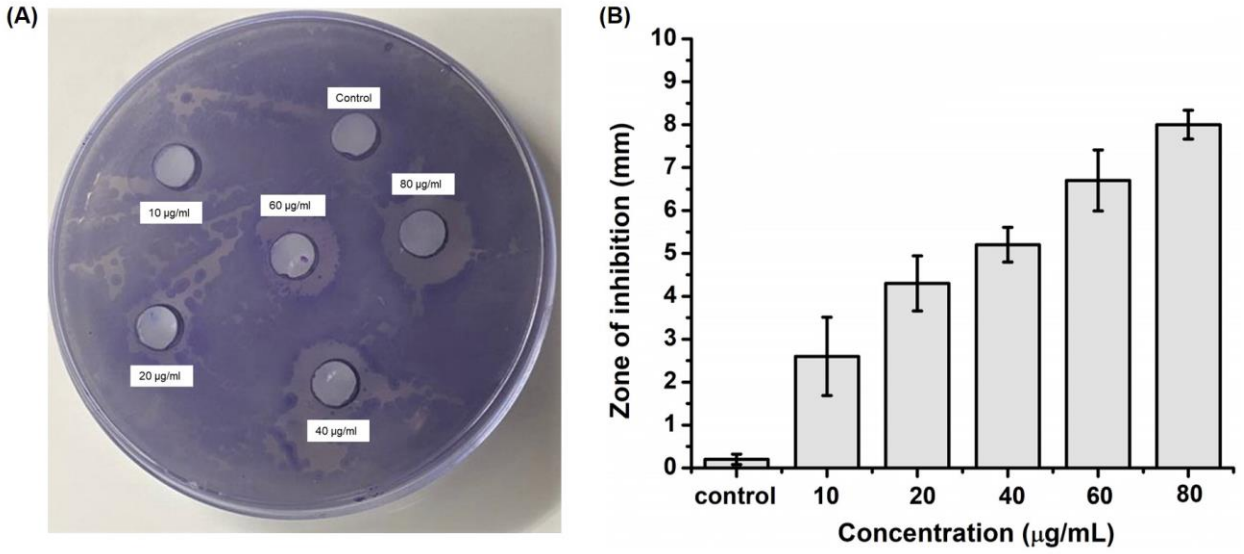

Fig. 3.8 (A) Inhibition of violacein pigment in presence of L-EtAc (10-80 µg/mL) (B) plate zone inhibition vs concentration.

3.3.9 Inhibition of swarming motility and EPS production

Flagella-driven swarming motility is a QS-dependent virulence function that triggers surface attachment during biofilm development (Othman et al., 2019). Therefore, it was pertinent in the present study to determine the L-EtAc concentrations (varied from 10-80 µg/mL) that incapacitated test pathogen migration and marked inhibition of flagella synthesis (**Fig. 3.9**). The significant reduction in EPS by L-EtAc endorsed the indirect disruption of AHL-regulated QS system, which blocked pathogen access to substratum and biofilm formation. Consequently, spectrometric analysis of EPS extracted from *P. aeruginosa* indicated a statistically significant reduction with all doses of L-EtAc (10 µg/mL to 80 µg/mL) (**Fig. 3.10**). EPS is vital for biofilm architecture and increases cellular resistance to stress (antibiotic, osmotic, and oxidative) (Merritt et al. 2010). Therefore, any disruption of EPS synthesis will inevitably impact biofilm architecture, reduce their resistance and expose bacteria to damage by antibiotics and drugs (Gao et al. 2012).

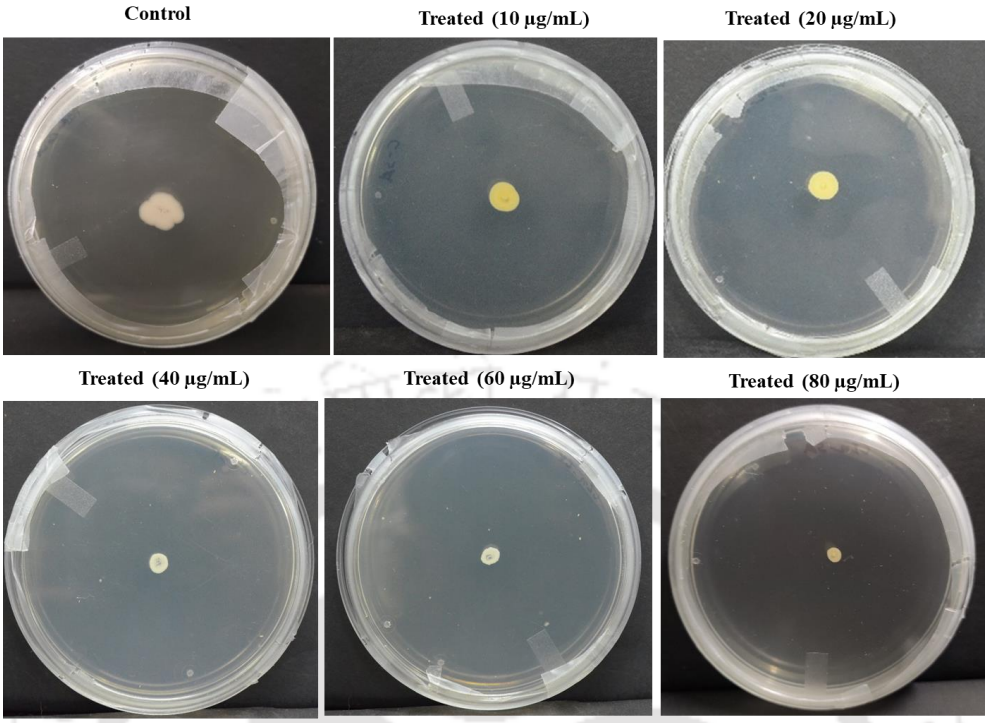

Fig. 3.9 Inhibition of swarming motility of *P. aeruginosa* in presence of different concentrations of L-EtAc (10-80 µg/mL).

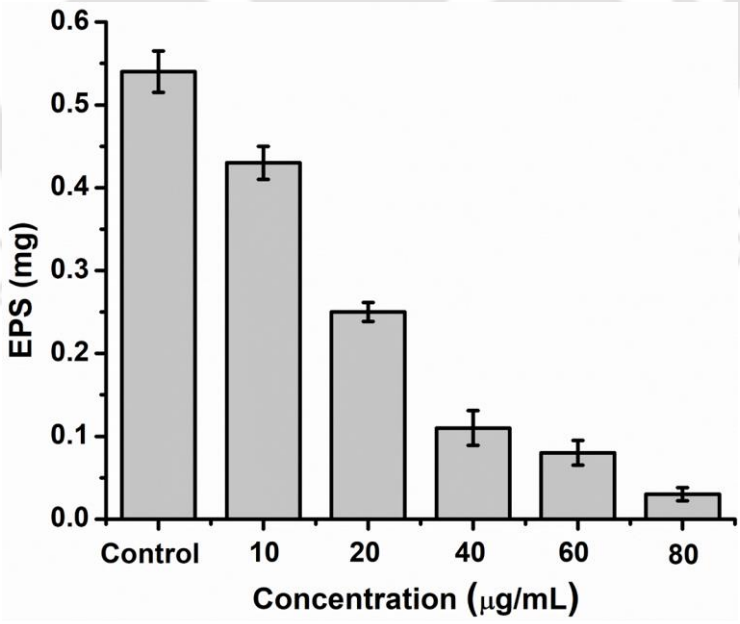

Fig. 3.10 Quantification of extracellular polymeric substance (EPS) in biofilm by treating with L-EtAc (10-80 µg/mL).

3.3.10 Microscopic visualization of the biofilms

Acridine orange was used to visualize the biofilm, bacterial cells, and the surrounding glycocalyx matrix. The biofilm on the outer surface of the glass slide displayed interlaced bacteria enfolded by a scaffolding network of extracellular matrix. On L-EtAc application, Bright field microscopy evinced reduction in number of micro bacterial colonies during the biofilm formation of test bacterial pathogens. Therefore, the treatment of bacterial pathogens with L-EtAc produced weak biofilms, a possible outcome of surface adhesion decrease and micro bacterial colony development. Microscopic examination of L-EtAc impacted biofilm architecture displayed decreased thickness, poor and weakened architecture in comparison to control (0.01% DMSO treated) biofilms of tested pathogens (**Fig. 3.11**). Our results are supported by work on ethyl acetate fraction of *Centella asiatica* L., at 400 µg/mL that enabled complete blocking of *C. violaceum* biofilm production (Vasavi et al. 2016). Further, *A. galangal* rhizome extract arrested biofilm formation, significantly affecting microbial cell viability (Puhs et al. 2020). The precise mechanism of biofilm inhibition by L-EtAc extract still needs extensive research. In an earlier attempt, Lee et al. (2009), used *P. aeruginosa* PAO1 as a model organism, and documented that CzcR, a bi-component response regulator is required for biofilm and pyocyanin inhibition (Lee et al. 2009). Since our results correlate well with the work of Lee et al. (2009), therefore, it is postulated that the same CzcR mechanism is operational in biofilm inhibition and increased hydrophobicity in *P. aeruginosa* PAO1.

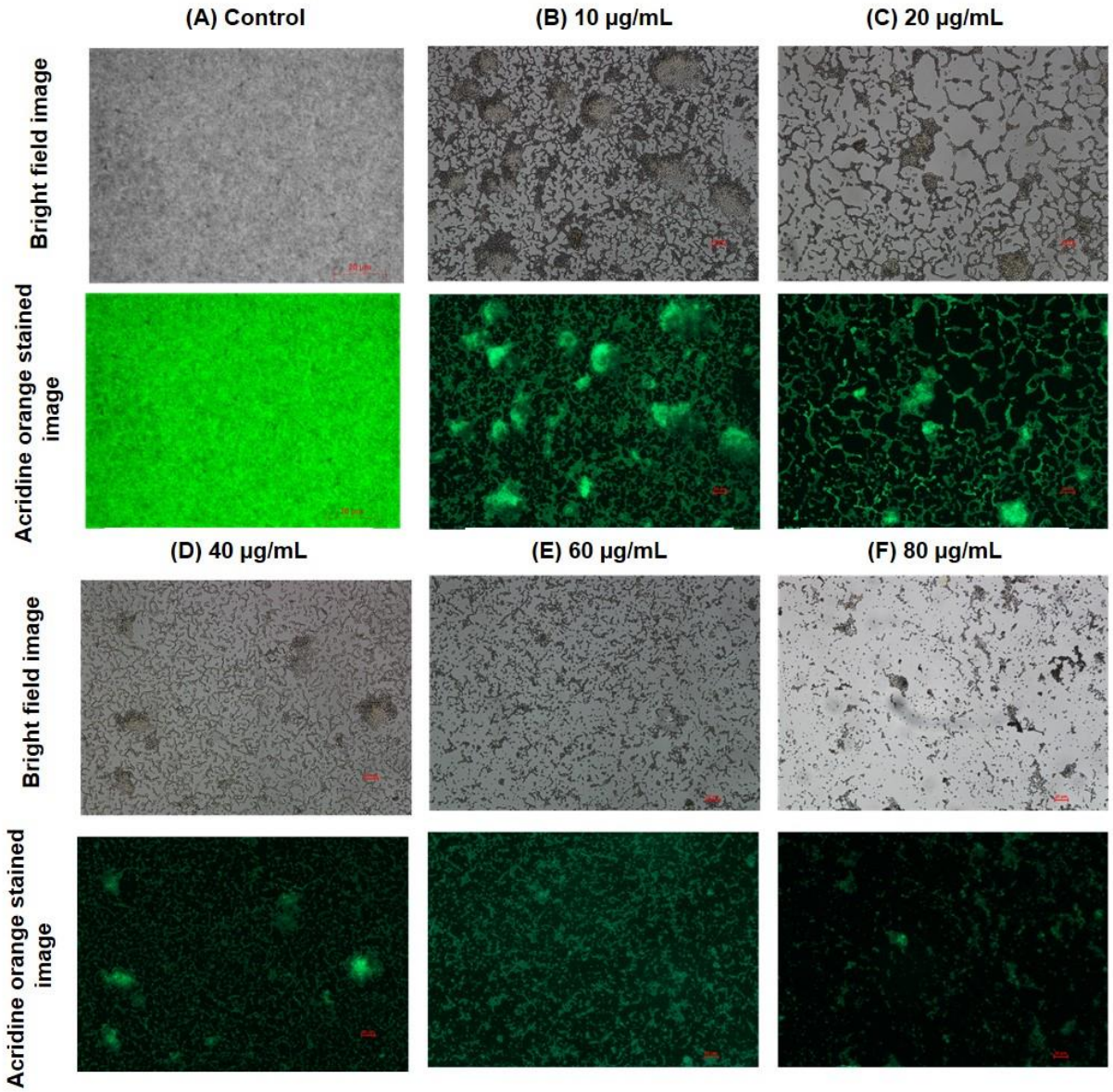

Fig. 3.11 Microscopic images of biofilm formation of test bacterial pathogens: Bright field and fluorescence (acridine orange stained) microscopic images of *P. aeruginosa* biofilm (A) control (untreated) and treated with L-EtAc (B) 10 µg/mL (C) 20 µg/mL (D) 40 µg/mL (E) 60 µg/mL (F) 80 µg/mL.

3.3.11 *In-silico* study

In this study, some molecules were selected from L-EtAc for molecular docking simulations to identify suitable inhibitors against the biofilm-associated proteins *las*I (PDB ID: 1RO5), *las*R (PDB ID: 6D6A), *rhl*I (PDB ID: 1KZF), and *las*B (PDB ID: 3DBK). *In silico* interaction

analysis of biofilm-associated proteins and phytochemicals such as Caryophyllene oxide, 1,6,10-Dodecatrien-3-ol, 3,7,11-trimethyl-, Eucalyptol, Isolongifolol, (-)-Myrtenol, Spiro[4.5]dec-6-en-8-one, 1,7-dimethyl-4-(1- methylethyl)- and [1,1'-Bicyclohexyl]-4-carboxylic acid, and 4'-propyl-, 4- fluorophenyl ester was carried out. The non-covalent interactions based on pi-alkyl, alkyl, carbon-hydrogen, and hydrogen bonds were analyzed in relation to the interaction of phytochemicals and amino acids. The binding energy from the interaction of protein and compounds are listed in **Table 3.7**. The molecular docking results indicate that the compounds under investigation showed biofilm inhibition activity. Proteins such as *las*I (PDB ID: 1RO5) demonstrated varied affinity to phytochemicals such as Eucalyptol, Myrtenol, and [1,1'-Bicyclohexyl]-4-carboxylic acid, 4'-propyl-,and 4- fluorophenyl ester; and docking calculations varying from -5.7 to -8.0 kcal/mol respectively. In the complex, ValA:26 residues of lasI interact with [1,1'-Bicyclohexyl]-4-carboxylic acid, 4'-propyl-, 4- fluorophenyl ester via alkyl bond; PheA:105 interacts with the ligand through the pi-alkyl bond formation; and SerA:109 forms the conventional hydrogen bond (**Fig. 3.12a**). Similar calculations were extracted for the interaction between *las*B PDB ID: (3DBK) and the phytochemicals molecule named [1,1'-Bicyclohexyl]-4-carboxylic acid, 4'-propyl-, 4- fluorophenyl ester, shows highest binding affinity of -8.0 kcal/mol with the pi-alkyl bond to TyrA:114, AlaA: 113, ValA:137, LeuA:197 (**Fig. 3.12b**).

Docking calculations for protein *rhl*I PDB ID: (1KZF) with phytochemicals exhibit the lowest and highest binding affinity of −5.7 to -7.6 kcal/mol, respectively. Among all compounds analyzed, TyrA:54 is involved in pi-alkyl solid interaction, while LeuA:12, ArgA:68, ArgA:100, and MetA:42 form an alkyl bonds with the ligand (**Fig. 3.12c**). *las*R PDB ID: (6D6A) displayed the highest affinity to phytochemical [1,1'-Bicyclohexyl]-4-carboxylic acid, 4'-propyl, and 4-fluorophenyl ester, with binding energy of -11.9 kcal/mol. In the complex, TrpG:60, TyrG:56 and TyrG:93 in the protein active site; interact with [1,1'-Bicyclohexyl]-4-carboxylic acid, and 4'-propyl-, 4- fluorophenyl ester, via the conventional hydrogen bond. Further, TyrG:47, TyrG:64, LeuG:110, and AlaG:105 are involved in pi-alkyl solid interactions, while LeuG:36, AlaG:50, AlaG:127, LeuG:40, and LeuG:125 forms alkyl bond with the ligand (**Fig. 3.12d**). Further, these findings are validated through the previous results demonstrated in compounds isolated from *Alstonia scholaris* leaf demonstrating binding affinity with *P. aeruginosa* protein *las*R (Abinaya & Gayathri 2019).

Table 3.7 The binding energy from the interaction of protein and compounds.

S. No.	Name of Compound	Binding Energy (kcal/mol)			
		LasI (1RO5)	**LasB (3DBK)**	**rhlI (1KZF)**	**LasR (6D6A)**
1	Caryophyllene oxide	-6.9	-5.9	-7.5	-8.2
2	1,6,10-Dodecatrien-3-ol, 3,7,11-trimethyl	-6.8	-5.7	-6.3	-8.0
3	Eucalyptol	-5.7	-5.1	-5.8	-6.2
4	Isolongifolol	-6.2	-6.3	-6.8	-6.7
5	(-)-Myrtenol	-5.8	-5.0	-5.7	-6.5
6	Spiro[4.5]dec-6-en-8-one, 1,7-dimethyl-4-(1-methylethyl)	-7.1	-6.0	-7.2	-8.5
7	[1,1'-Bicyclohexyl]-4-carboxylic acid, 4'-propyl-, 4- fluorophenyl ester	-8.0	-8.0	-7.6	-11.9

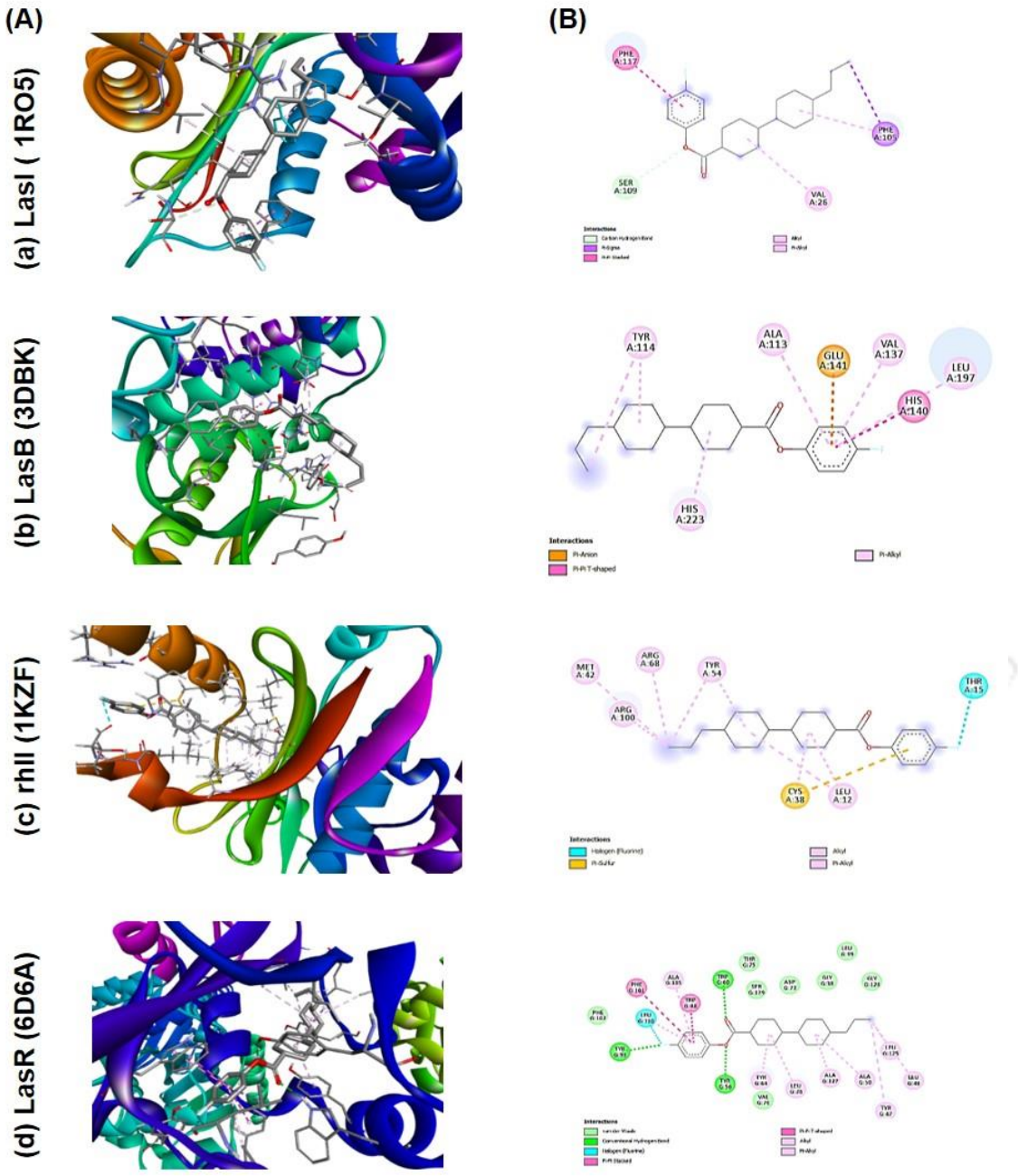

Fig. 3.12 (A) 3D representation of the interaction; (B) 2D representation of the interaction between screened phytochemical, [1,1'-Bicyclohexyl]-4-carboxylic acid, 4'-propyl-, 4-fluorophenyl ester with protein *las*I PDB ID: (1RO5), *las*B PDB ID: (3DBK), *rhl*I PDB ID: (1KZF), and *las*R PDB ID: (6D6A) displayed in figure (a, b,c and d) respectively. Dotted lines represent the various interactions, and the colour indicates the type of interaction. Residues are represented by coloured circles with their three letter code, chain identifier, and residue number.

3.3.12 Biofilm-associated genes expression

PCR techniques are applied to identify virulence factors by amplifying target virulence genes such as biofilm-associated genes using gene-specific primers. QS is the cardinal biofilm formation regulator of *P. aeruginosa*; consequently, the impact of L-EtAc extract on virulence of *P. aeruginosa* was an outcome of interference with QS. The mRNA expression level of QS genes and virulence genes of *P. aeruginosa,* including *rhl*I, *rhl*R, *las*I, *las*R (QS-associated genes), *las*B (encoding elastase), and *rhl*A (encoding rhamnosyltransferase), decreased significantly in dose dependent manner of L-EtAc extract (10-40 µg/mL) (**Fig. 3.13**). The previous reports demonstrated that down-regulation of QS-associated genes involve minimizing the virulence factors of *P. aeruginosa* (Kamali et al. 2020). Another report revealed α-galactosidase regulates the expression of 14 genes with biofilm association of starved *P. aeruginosa* in a dose-dependent manner (Balabanova et al. 2020). Therefore, in the final analysis, exogenous L-EtAc extract was able to down regulate QS-associated gene expression in *P. aeruginosa* PAO1.

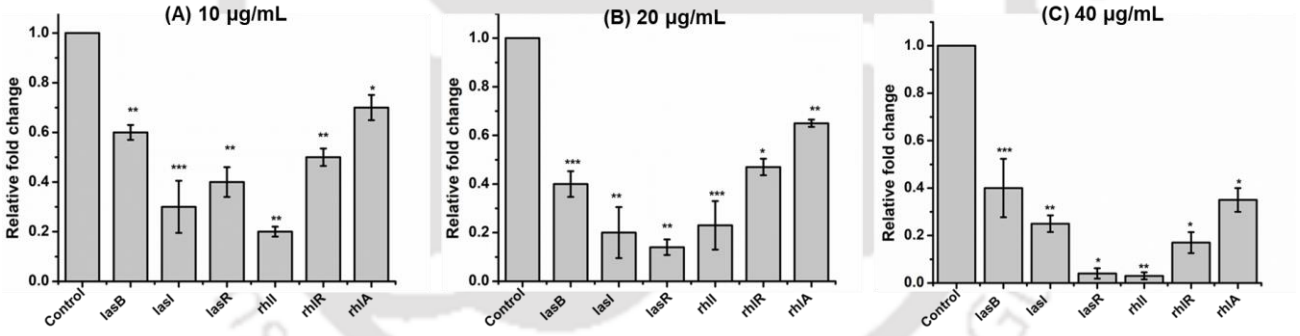

Fig. 3.13 Quantitative real-time PCR (qRT-PCR) was used to monitor the expression of QS-associated genes, treated with L-EtAC (A) 10 µg/mL and (B) 20 µg/mL (C) 40 µg/mL. Level of gene expression was presented as fold change relative to the control. 16s RNA expression was used for normalization. Assays were performed in triplicate. ** P<0.01 *** P<0.001.

3.4. Conclusion

The phytochemical screening of antibacterial, anti-biofilm, and QS inhibiting activity of *A. nigra* leaf extract against the pathogen *P. aeruginosa* PAO1 forms the central focus of this paper.

Towards achieving that objective, the investigation has been able to report the significant impact of L-EtAc in the reduction and inhibition potential of QS signaling, which plays a vital role in biofilm formation. Compounds contained in L-EtAc significantly reduced the biofilm development aided by decrease in swarming motility and EPS production in *P. aeruginosa* PAO1, a food pathogen. In addition, the considerable decrease evinced in preformed biofilms of tested bacterial pathogens post exposure to varied doses of L-EtAc is central to our results. To the best of our knowledge, this is probably the first report on the broad-spectrum inhibition of QS and biofilm by the L-EtAc extract compound of *A. nigra*, with the potential to contribute to the treatment of chronic diseases associated with the biofilm-forming pathogen, development of food packaging materials, and food preservatives.

Isolation, purification and characterization of 3,5-dihydroxy-4′,7-dimethoxyflavone from leaves of *Alpinia nigra*

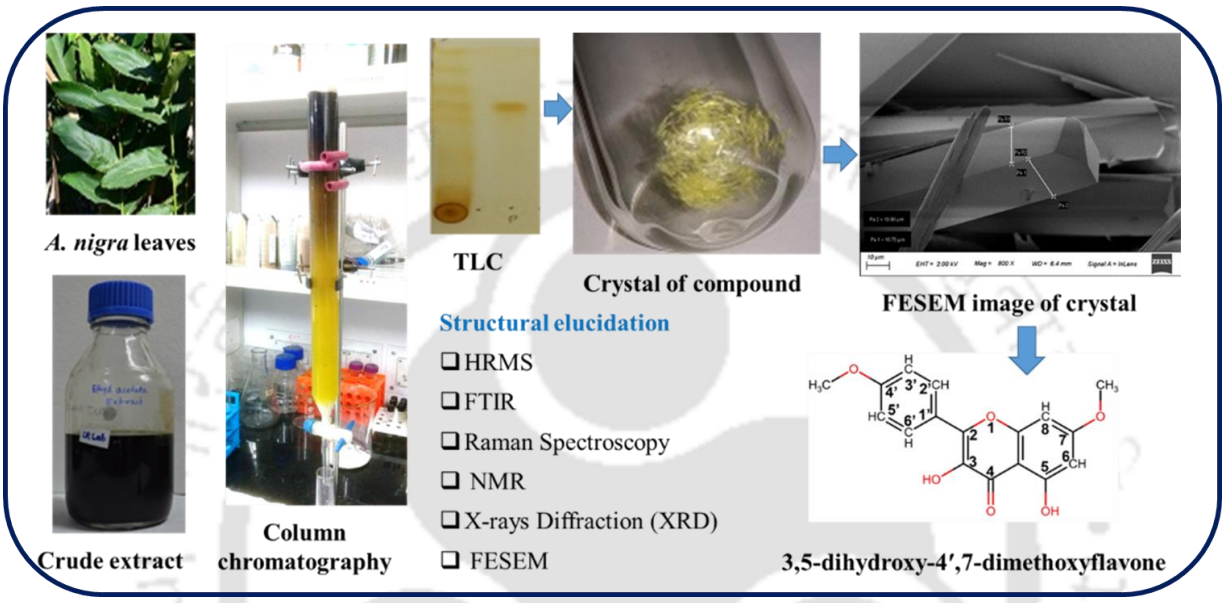

In this chapter, the compound was characterized and identified as a flavonoid, 3,5-dihydroxy 4′, 7-dimethoxyflevone (DHDM) from leaves of *Alpinia nigra* (family Zingiberaceae) for the first time from this plant.

Chapter 4

Isolation, purification and characterization of 3,5-dihydroxy-4',7-dimethoxyflavone from the leaves of *Alpinia nigra*

4.1 Introduction

Medicinal plant possesses various chemical compounds, known as natural compound. Natural compounds are the source of therapeutic agents in the pharmaceutical industries due to there less toxic effects compared to synthetic drugs. These compounds can be acquired from prokaryotic to higher eukaryotes like plants (Ahmad Khan and Ahmad 2019). The understanding of natural compounds led to significant contributions towards the development of many modern drugs by using natural products or their derivatives. The practice of using natural products as herbal therapy as alternative medicine is becoming an attractive approach for the treatment of various diseases. Medicinal plants are also used in herbal-based therapeutics and are considered a rich source of ingredients. Many plant secondary metabolites such as alkaloids, terpenoids, and flavonoids are reported as protectors against free radicals and tremendous biological activities such as antibacterial, anticancer, anti-inflammatory activity (Thomford et al. 2018; Ahmad Khan and Ahmad 2019). Flavonoid is a polyphenolic compound widely present in plant parts like seed, bark, flower, and leaves (Harborne and Williams 2000).

Zingiberaceae plants are well known for its medicinal use (Tushar et al. 2010b). The largest and most complex genus of this family is *Alpinia*, which has been used widely in different parts of the world in food, spices, dyes, perfume, and folk medicine (Ghosh and Rangan 2013). Genus *Alpinia* possesses the rich source of phytochemicals such as flavonoids (Sahoo et al. 2017), labdane diterpenes (Ghosh and Rangan 2014b), sesquiterpenes (Miyazawa et al. 2000), diarylheptanoids (Miyazawa et al. 2000; Ali et al. 2001b), and kava pyrone (Mpalantinos et al. 1998; Sirat and Jamil 1999). These natural compounds have been isolated and investigated for their biological applications against various diseases. However, the plant under study, *A. nigra* has limited information about the isolation and characterization of bioactive compounds and their application in therapeutics.

The two-flavone glycosides (astragalin and kaempferol-3-O-glucuronide) were isolated from seed clusters of *A. nigra*. kaempferol-3-O-glucuronide was presented as the major

compound in the fruit pulp (Qiao et al. 2007). The presence of two volatile oils, α-pinene and β -pinene, was reported in the fruits and rhizome of *A. nigra* (Qiao et al. 2000). The previous study reported the major constituents as β-pinene (56.27 %), α-caryophyllene (13.70 %), α-farnesene (7.92 %), and caryophyllene (6.46 %) as the principal constituent among other phyto-volatiles found inleaf essential oils of *A. nigra* as reveled in GC-MS analysis (Sahoo et al. 2017). Tribal people of NE India are also using leaves of this plant as a flavoring agent for food preparation, but less research has been carried out in other aspects. Therefore, ethyl acetate crude extract of leaves was explored for the isolation of bioactive compounds.

4.2 Material methods

4.2.1 Plant material

A. nigra plant leaves were collected from Indian Institute of Technology Guwahati (IITG) campus (26°12.476′N to 91°41.965′E), Assam. The mature leaves (1.0 kg) were harvested, rinsed off to remove debris, dried and cut into small pieces, and made powder with the help of a mixer grinder.

4.2.2 Isolation and purification of the compound

A. nigra dried leaves powder was subjected to soxhlet extraction using ethyl acetate solvent. The compound was isolated from the obtained crude extract using silica column chromatography and stored in 4°C until further use. The isolated compound was purified and confirmed through analytical chromatography (TLC Silica gel 60 F_{254}), UV visible spectroscopy (Genesys 10S UV-Vis spectrophotometers, Thermos Scientific), and High-Performance Liquid Chromatography (HPLC) (Shimadzu HPLC, shim-pack GWS 5µM C18 column).

4.2.3 Thin layer chromatography

Thin-layer chromatography (TLC) was carried out on pre-coated silica gel 60 F254 (0.25 mm, Merck, Germany). Crude extract of L-EtAc was diluted in ethyl acetate, and 10 µL was loaded on TLC plates. The mobile phase optimization was done with different percentages of n-hexane and ethyl acetate. The samples were allowed to run in a chromatographic chamber saturated with volatile binary solvent of the mobile phase. The individual spot on the plate was visualized under

UV and iodine fume. The retardation factor (R_f) of each spot on TLC plates was noted down. After a series of optimization (solvents to be used as mobile phase), crude extracts were subjected to column chromatography and solvent extraction.

4.2.4 Column chromatography

The glass column (3 × 50 cm) was sealed with cotton at the end of the column. The column was filled with slurry of silica gel (80 g, 60-120 mesh, Merck India) in hexane. Initially, 1 g of L-EtAc extract was dissolved in a minimum volume of dichloromethane (DCM), and dry silica gel was added further to form sample slurry. After evaporating DCM completely, the sample slurry was loaded onto the packed silica column. The column was eluted slowly at the rate of 1 mL/min and was collected in test tubes with appropriate labeling. Gradient elution with ethyl acetate and hexane (v/v) was used as a mobile phase for elution of different fractions. From L-EtAc, one major fraction was collected when the mobile phase reached at 9:91 [ethyl acetate: hexane (v/v)], and a small aliquot (10 µL) was loaded on TLC plate and visualized under UV light and iodine fume. Fractions having similar R_f values were pooled together and concentrated using a rotatory evaporator.

4.2.5 High-performance liquid chromatography

High-performance liquid chromatography (HPLC) analysis was done using Shimadzu's HPLC system with degassing unit (DGU 20ASR), auto sampler (SIL 20AHT) and liquid chromatogram (LC 20AD) system. The chromatographic purification of the compound was achieved with C-18G column having (250 × 4.6 mm) and 5 µm particle size. The eluted fraction obtained from column chromatography (10 mg/mL) was dissolved in acetonitrile, and filtered through a syringe filter (0.45 µm). The sample injection volume was 10 µL, and gradient elution was done at a 1mL/min flow rate. The program was run for 30 min with UV/Vis Detector (SPD-20A) set at wavelength 254 nm (Prabhu et al., 2002). Data was procured and processed using Shimadzu lab solutions. All the readings were taken in triplicate. Finally, the pure fractions were filtered, concentrated by a rotatory evaporator, and stored at 4°C for further study.

4.2.6 Structural characterization of compound

The purified compound structure was characterized by multi spectroscopy techniques such as high-resolution mass spectroscopy (HR-MS), Fourier transform infrared (FTIR), Raman and nuclear magnetic resonance (NMR) analysis. Further, the structure was confirmed by SC- XRD analysis.

4.2.7 High-resolution mass spectrometry

High-resolution mass spectrometry (HRMS) was carried out by using Agilent QTOF 6520 with electron spray ionization (ESI) technique. For mass spectral analysis, 1 mg of the pure isolated compound was dissolved in 1.5mL of methanol (HPLC grade). The spectra of mass were recorded in the range 0-1000 m/z ratio, in positive ESI mode.

4.2.8 Fourier transform infrared (FTIR) spectroscopy

FTIR analysis was carried out by the KBr pellet method through a spectrophotometer (Perkin Elmer spectrum two, Germany) (Li et al. 2014). For sample preparation, crystallized compound (2mg) was mixed with 20mg of KBr (potassium bromide; HiMedia, India) and made into a pellet. The spectrum was recorded in the range of 400–4000 cm^{-1}.

4.2.9 Raman spectroscopy

The Raman spectra of the crystallized compound were examined in a Raman spectrophotometer (Horiba Lab RAM HR) at an excitation wavelength of 514 nm of an argon-ion laser. The small amount of crystallized compound was kept on a glass slide and subjected to the inside of the instrument in dark light condition. The monochromatic light was implemented on the crystal surface. The Raman shift of crystalized compound was recorded in the range of 0–2000 cm^{-1}.

4.2.10 Field emission scanning electron microscopy (FESEM)

The edge and size of the crystallized compound were determined by FESEM (Carl Zeiss Ultra 55) at 3.0 kV. For sample preparation, a small amount of compound crystal was put on carbon tape then coated with gold for conductivity to avoid the charging effect.

4.2.11 Nuclear magnetic resonance

Nuclear magnetic resonance (NMR) was accomplished by dissolving the 20 mg of the crystallized compound in 600 µL of $CDCl_3$ (deprotonated solvent) and then transferred into 5 mm NMR tubes. 1D and 2D NMR were performed on a Bruker 600 MHz instrument. For spectral analysis of ^{1}H and ^{13}C NMR were recorded as an internal reference, trimethylsilane (TMS) for ^{13}CNMR acquisition and $CDCl_3$, solvent peak at $\delta = 7.26$ for ^{1}H NMR acquisition. For the distortionless enhancement by polarization transfer (DEPT) experiment, the decoupler pulse angle of 135° was used. The Top Spin 2.1 was used for NMR acquisition. MestReNova was used for spectral analysis. ^{1}H and ^{13}C spectral chemical shifts and coupling constants were expressed as δ and Hz, respectively. The chemical structure is drawn, and peaks were assigned using ChemDraw 8.0.3.

4.2.12 Single-crystal X-ray diffraction

The detailed structure of the purified compound was elucidated and confirmed by single-crystal XRD (CrysAlisPro Agilent Technologies, Germany). SC-XRD was performed by selecting a single crystal with the help of microscope and acquisition was performed in Agilent Single Crystal X-Ray Spectrometer and subjected on Eos diffractometer (SuperNova, Single source at offset) with MoKα radiation (λ = 0.7107 Å) in φ and ω scan modes, set at the temperature of 25ºC during data collection. Absorption correction was based on multiple and symmetry-equivalent reflections in the data set using the SADABS program (Bruker 2009). The structure was solved with the help of Superflip and refined with SHELXL-97 (Sheldrick 2008) and Olex2 (Dolomanov et al. 2009) software. The x-ray diffraction pattern was analyzed and structure of compound was confirmed with the help of Solex software.

4.3 Result and discussion

4.3.1 Isolation and purification of the compound

The compound was isolated from the leaf of *A. nigra* with the help of silica gel (mess size 60-120) column chromatography by using 9% ethyl acetate in hexane. The major compound was isolated from ethyl acetate extract by column chromatography with R_f value of 0.45 in 20:80 (ethyl acetate: hexane, v/v) (**Fig. 4.1**). Purification was evaluated by thin-layer chromatography (TLC), High-performance liquid chromatography (HPLC), and UV spectroscopy. HPLC was

carried out as a part of the purity assessment. Analytical HPLC with UV detector was performed to ascertain the purity of isolated compound as it offers high sensitivity and also because the majority of flavonoids are believed to have UV absorbance (Abu et al. 2019). The compound HPLC chromatogram showed 99.6% purity (**Fig. 4.2**).

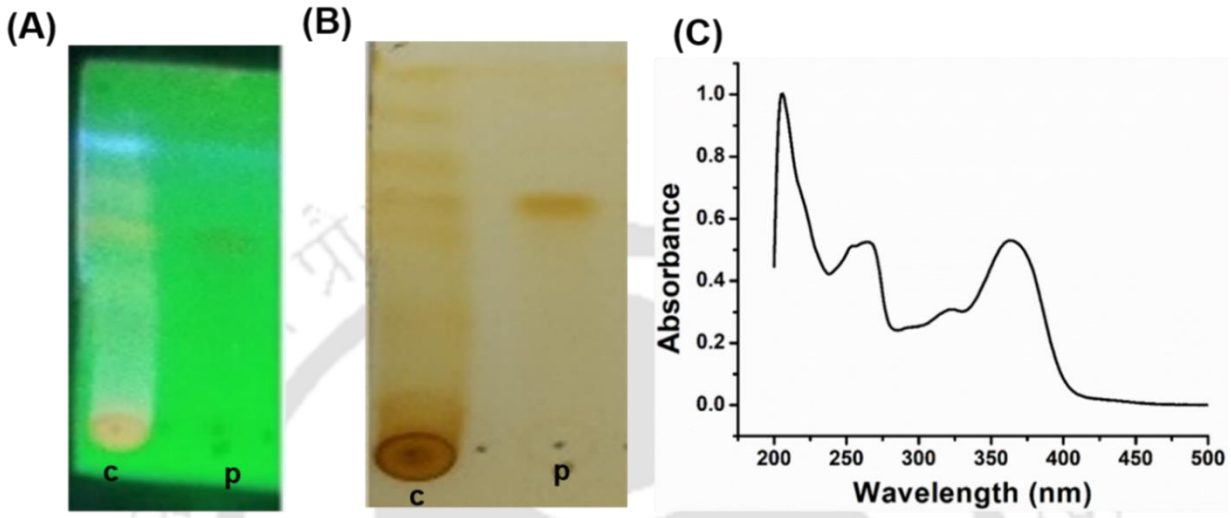

Fig. 4.1 (A) TLC plate of the isolated compound in UV light, showing UV absorption of isolated compound. (B) TLC of the isolated compound in iodine stain. (C) UV spectra of the isolated compound, displaying two intense peaks at λ_{264} nm and λ_{363} nm. In both fig (A) & (B), C represents crude extract and P purified compound.

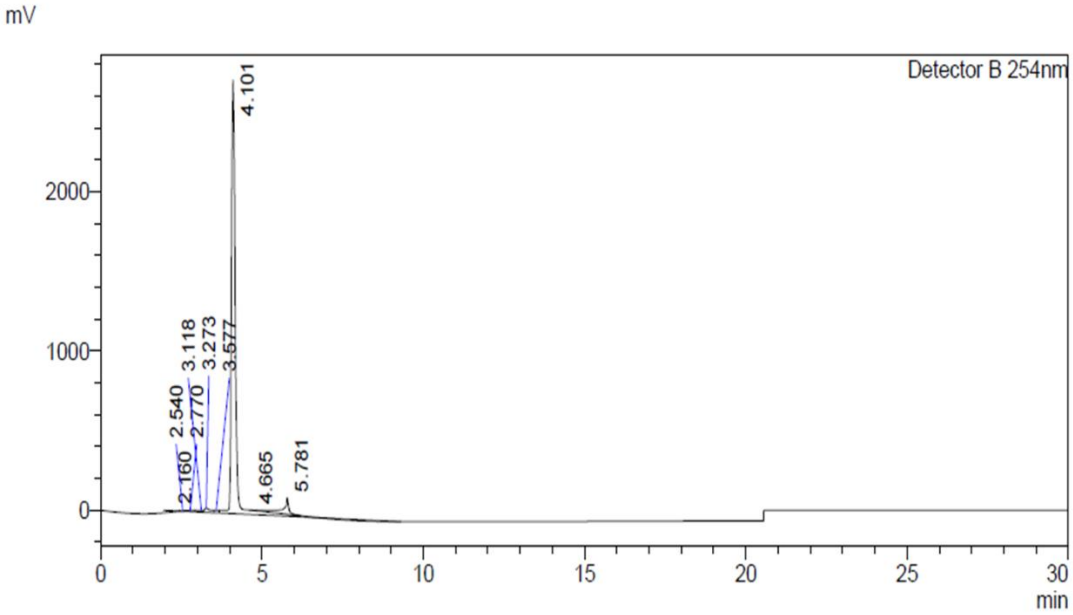

Fig. 4.2 HPLC spectra of the isolated compound indicate retention time at 4.1 min in the acetonitrile-water mobile phase.

4.3.2 Characterization of compound

The compound was yellow powder, and crystallization was done by slow evaporation method at room temperature. The mass of the isolated compound was confirmed by HRMS. The m/z of the isolated compound in positive mode $[M + H]^+$ was 315.0736 (**Fig. 4.3).**

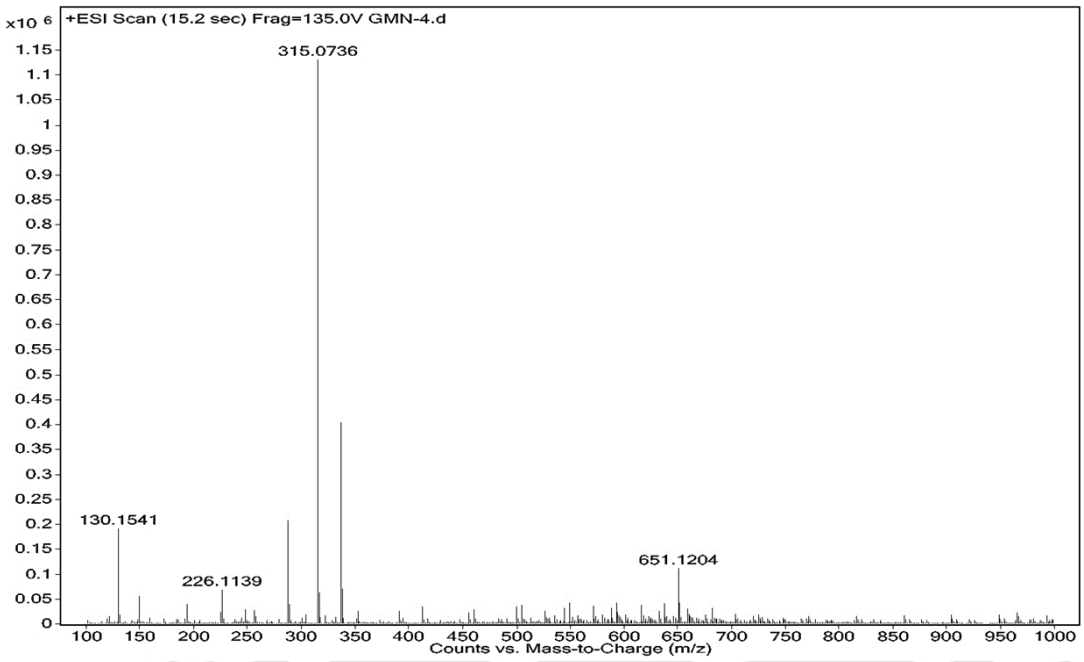

Fig. 4.3 HR-MS spectra of purified compound, displaying the molecular ion $[M+H]^+$ peak at m/z 315.0736.

4.3.3 Fourier transform infrared spectroscopy

Infrared (IR) spectroscopy is most useful in providing information about the presence or absence of specific functional groups (Márquez et al. 2018). As seen in **Fig. 4.4A**, the characteristic C=O stretching vibration of aldehyde appeared as a prominent band at ~1648.86 cm^{-1}. The peak at ~1596.29 cm^{-1} displayed the presence of alkenyl C=C (aromatic) in the compound, in conjugation with –CH group on *cis* position displayed at ~830.73 cm^{-1}. A peak confirmed the presence of the asymmetric C–H stretch of the CH_3 group at ~2937.39 cm^{-1} in the FTIR spectrum. Moreover, The FTIR spectra showed prominent functional group signatures at 3313.05 cm^{-1}, 1648.86 cm^{-1}, 1596.29 cm^{-1}, and 1159.93 cm^{-1} corresponding to hydroxyl, carbonyl group,

C=C (Aromatic), C-O (Stretch), respectively. The characteristic of C=C conjugation with –CH group on *cis* position was displayed at ~830.73 cm^{-1}. The asymmetric C–H, a distinct peak at ~2937.39 cm^{-1}confirmed H stretch of CH_3 group (**Fig. 4.4A**).

4.3.4 Raman spectroscopy

The Raman spectrum of crystalized compound was recorded at excitation wavelengths of 514 nm. The most intense bands were observed as ~791.48 cm^{-1}, ~1182.83 cm^{-1}, and ~1625.32 cm^{-1}, as shown (**Fig. 4.4B**). The first two peaks corresponded to the bending vibrations of C–H bonds, C-O stretch, respectively, while the third peak was an outcome of the stretching of C=O bond. The functional groups were validated by Raman shift at 1625.32 cm^{-1} for the conjugated carbonyl group and 1182.32 cm^{-1} for C=O stretch.

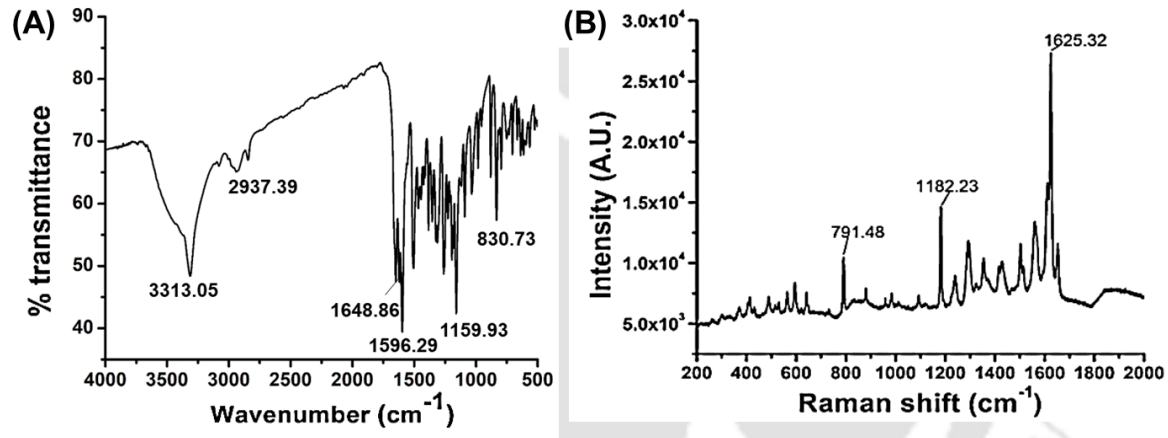

Fig. 4.4 (A) FTIR spectra of the purified compound showing prominent functional group C=C (aromatic) at 1596.29 cm^{-1}. (B) Raman spectra of the crystalized compound at λ_{514} nm displaying a peak at ~1625.32 cm^{-1}, indicating C=O bond stretch.

4.3.5 Nuclear magnetic resonance

The ^{1}H NMR spectra of the isolated compound showed four peaks at δ (ppm) = 6.40 (1H, d, J=1.8), 6.51 (1H, d, J=1.8), and 6.62 (1H, s), 11.76 (1H, s). Two doublets at δ = 7.07 (2H, d, J=9 Hz) and δ = 8.19 (2H, d, J=9 Hz) represent the four hydrogens (C2'-H, C6'-H, and C3'-H, C5'-H) associated with a benzene ring (**Fig. 4.5A**). Two singlets peaks at δ = 3.91 (3H, s) and δ = 3.92 (3H, s) represent the two $–OCH_3$ groups.

The ^{13}C NMR spectrum showed the presence of 17 carbons, indicating the presence of –CH, $-OCH_3$, and quaternary carbons. Two peaks at δ (ppm) = 55.43 and 55.85 indicated carbons

linked to an oxygen atom in –OCH_3 group. The –C=C was confirmed by the signal at δ (ppm) = 156.71 and δ (ppm)= 160.72. The presence of other carbon peaks was ascertained by the signals at δ (ppm) 92.21, 97.90, 114.09, 123.19, 129.39, 135.66, 145.71, 161.05, 165.70, 175.18 (**Fig. 4.5B**).

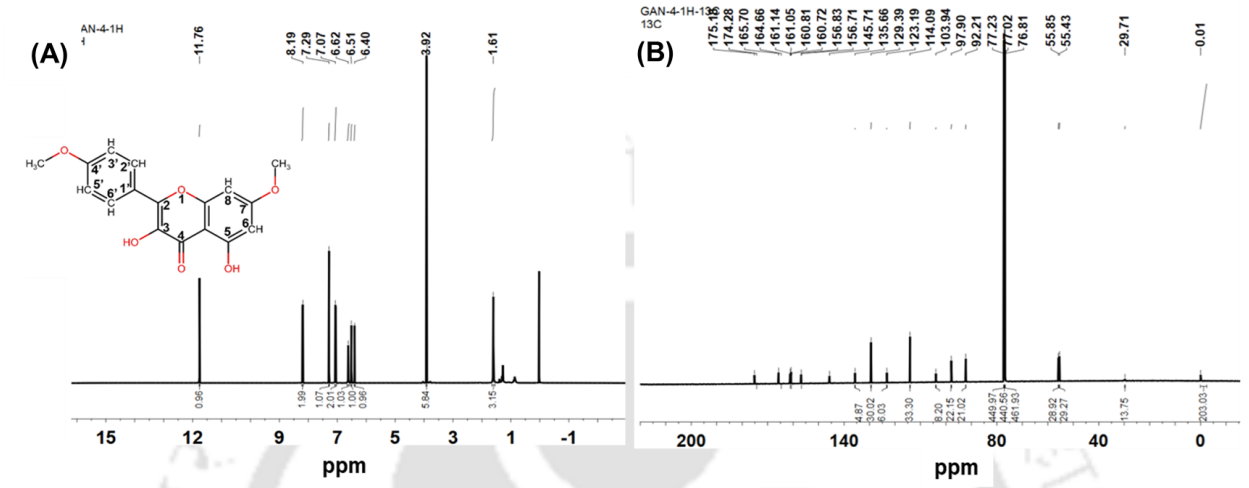

Fig. 4.5 (A) ^{1}H NMR spectra of purified compound (B) ^{13}C NMR spectra of purified compound

DEPT experiments were used for CHn multiplicity determination by variation of the selection angle parameter (the tip angle of the final ^{1}H pulse). Angle 135° displayed all -CH and -CH_3 group in a phase opposite to -CH_2 group. Consequently, the DEPT 135 spectra (**Fig. 4.6A**) demonstrated the presence of two –CH_3 and six –CH groups.

The HSQC spectrum exhibited the interactions between the protons and carbons (**Fig. 4.6B**). Two hydrogen at δ = 6.39 (C8-H) and 6.51 (C6-H) correlated with carbon peak at δ = 97.84 and δ= 92.15. This along with singlet peak at δ = 3.93 (4'-OCH_3, 7-OCH_3) and two doublet peaks at δ =7.02 (C2'-H, C6'-H), δ = 8.19 (C3'-H, C5'-H) correlated with one carbon peak at δ = 55.32 and two carbon peaks at δ= 114.07, δ=129.40 signifying the dimethoxy and –CH groups, respectively.

Furthermore, the ^{1}H and ^{13}C NMR data tabulated in **table 4.1,** correlated well with a previously published report (Hsiang and Yusoff 2012). The compound "3,5-dihydroxy-4′,7-dimethoxyflavone (synonim kaempferol 7,4′-dimethyl ether)" is a well-known compound (**Fig. 4.7**).

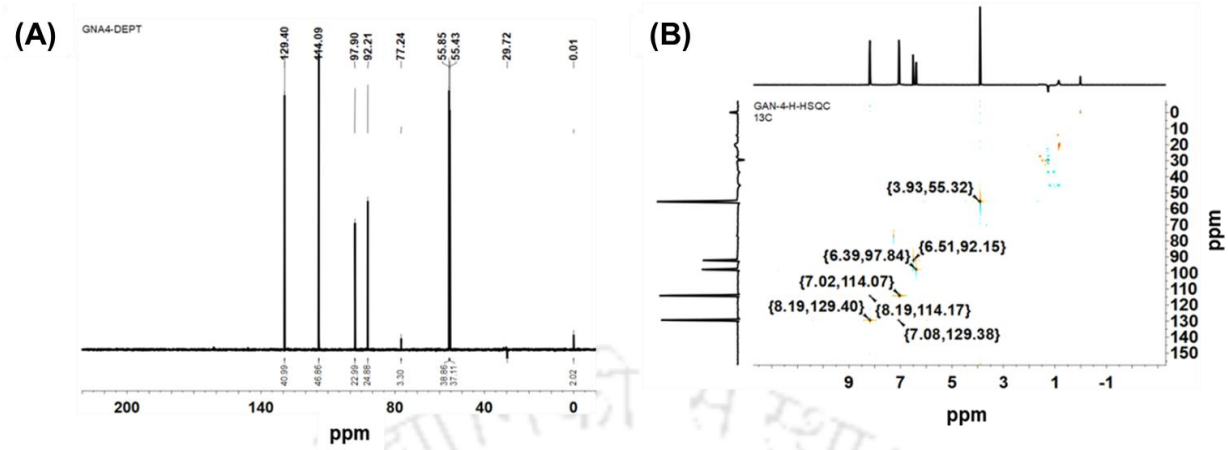

Fig. 4.6 (A) DEPT-135 NMR spectra of isolated compound, displaying CH and CH_3 group (B) HSQC, 2D NMR spectra of compound, showing proton-carbon single bond correlation.

Table 4.1. ^{1}H and ^{13}C NMR of 3,5-dihydroxy-4',7-dimethoxyflavone (DHDM). δ and J denotes chemical shift and coupling constant, respectively. Coupling constant (J) unit displayed in Hz.

Position	**δ_H (J Hz)**	**δ_C**
1′		123.19
2		145.71
2'6'	7.07,d, (2H, *J* =9Hz)	129.39
3	6.62, s, (1H)	135.66
3'5'	8.19, d, (2H, *J* = 9Hz)	114.09
4		175.18
4'		160.72
4a		103.94
5	11.76, s, (1H)	161.05
6	6.51, d, (1H, *J* =1.8 Hz)	97.90
7		165.70
8	6.40, d, (1H, *J* = 1.8Hz)	92.21
8a		156.71
OCH_3-4'	3.91, s, (3H)	55.43
OCH_3-7	3.92, s, (3H)	55.85

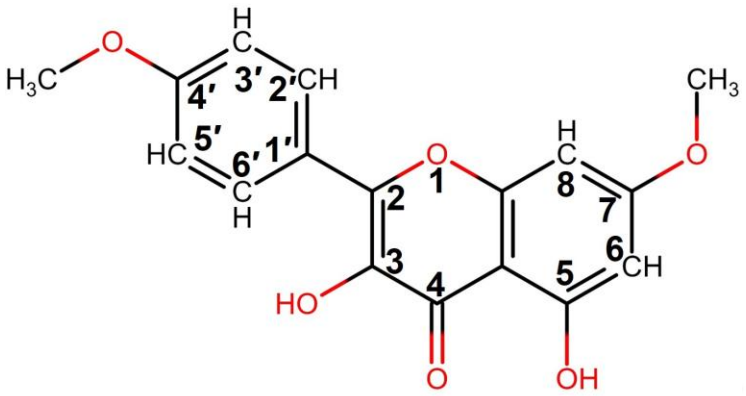

Fig. 4.7 Chemical structure of 3,5-dihydroxy-4′,7-dimethoxyflavone (DHDM).

4.3.6 Field emission scanning electron microscopy

The compound obtained in the form of yellow powder was crystallized using slow evaporation method at room temperature and analyzed by FESEM. FESEM image of the compound confirmed that it has a needle-shaped crystal having sharp edges. The crystal size obtained after purification and crystallization is in the range of 0.1-0.5 mm. FESEM images also showed a size of crystal height 19.90 µM, width 16.75 µM (**Fig. 4.8A**).

4.3.7 Single crystal X-ray diffraction (SC-XRD)

The SC-XRD pattern of the compound was acquired, and the crystal unit cell of the compound was found to be monoclinic; the molecular formula was $C_{17}H_{14}0_6$, cell length a= 28.3706Å, b=4.7989Å, c= 21.3039Å, cell angle alpha=90.0° beta=97.05° gamma=90.0° cell volume= 2878.5. SC-XRD determines atom position in three-dimensional space. Various chemical and physical properties of the compound crystal are listed in **table. 4.2**. Chemical structure, ball-stick model, crystal packing, and ellipsoid plot of the molecular structure of compound as obtained from X-ray diffraction technique and mercury software respectively is shown in **figure 4.8 B,C**. There is no formation of hydrogen bond within the crystal unit cell. The ground state optimized geometry was found to be nonplanar. The X-ray diffraction data of refined structure was submitted in Cambridge crystallographic data center (CCDC No. 1956166).

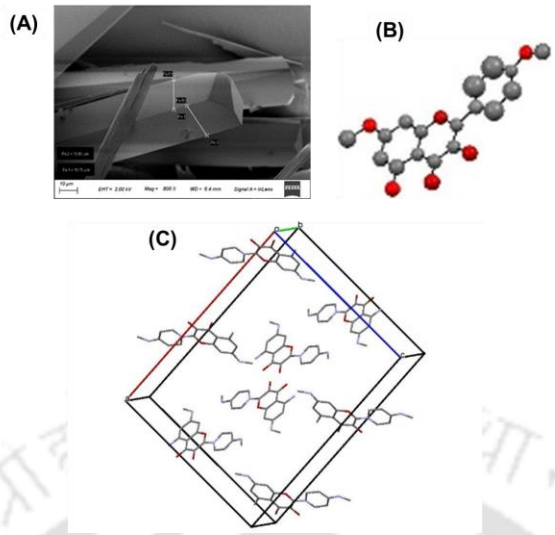

Fig. 4.8. Characterization of DHDM. (A) FESEM image showing the crystal structure of the compound. (B) Ball-stick model of compound, (C) crystal packing in a unit cell.

Table 4.2. Single crystal X-ray Diffraction (SC-XRD) data of 3,5-dihydroxy-4',7-dimethoxyflavone (DHDM).

SC-XRD data of 3,5-dihydroxy-4',7-dimethoxyflavone	
Empirical formula	$C_{17}H_{14}O_6$
Formula weight	314.29
Crystal color	Yellow
Crystal system	Monoclinic
Space group	C12/c1
Bond length a (Å)	28.3706
b (Å)	4.7989
c (Å)	21.3039
Bond angle α (deg)	90.0
β (deg)	97.056
γ (deg)	90.0
Volume (Å3)	2878.5
Temperature	293 (2) K

4.4 Conclusion

In the current work, 3,5-dihydroxy-4',7-dimethoxyflavone (DHDM), a flavone was isolated from leaves of *Alpinia nigra* (family Zingiberaceae). The compound was purified, crystallized and structural characterization was performed using spectroscopic techniques that include HRMS, FTIR, Raman, 1D NMR, and 2D NMR. The crystal is monoclinic as determined by SC-XRD pattern and crystal data was submitted to Cambridge crystallographic data center (CCDC No. 1956166).

Antioxidant, anti-tyrosinase and anti-inflammatory activities of 3, 5-dihydroxy-4', 7-dimethoxyflavone isolated from the leaves of *Alpinia nigra*

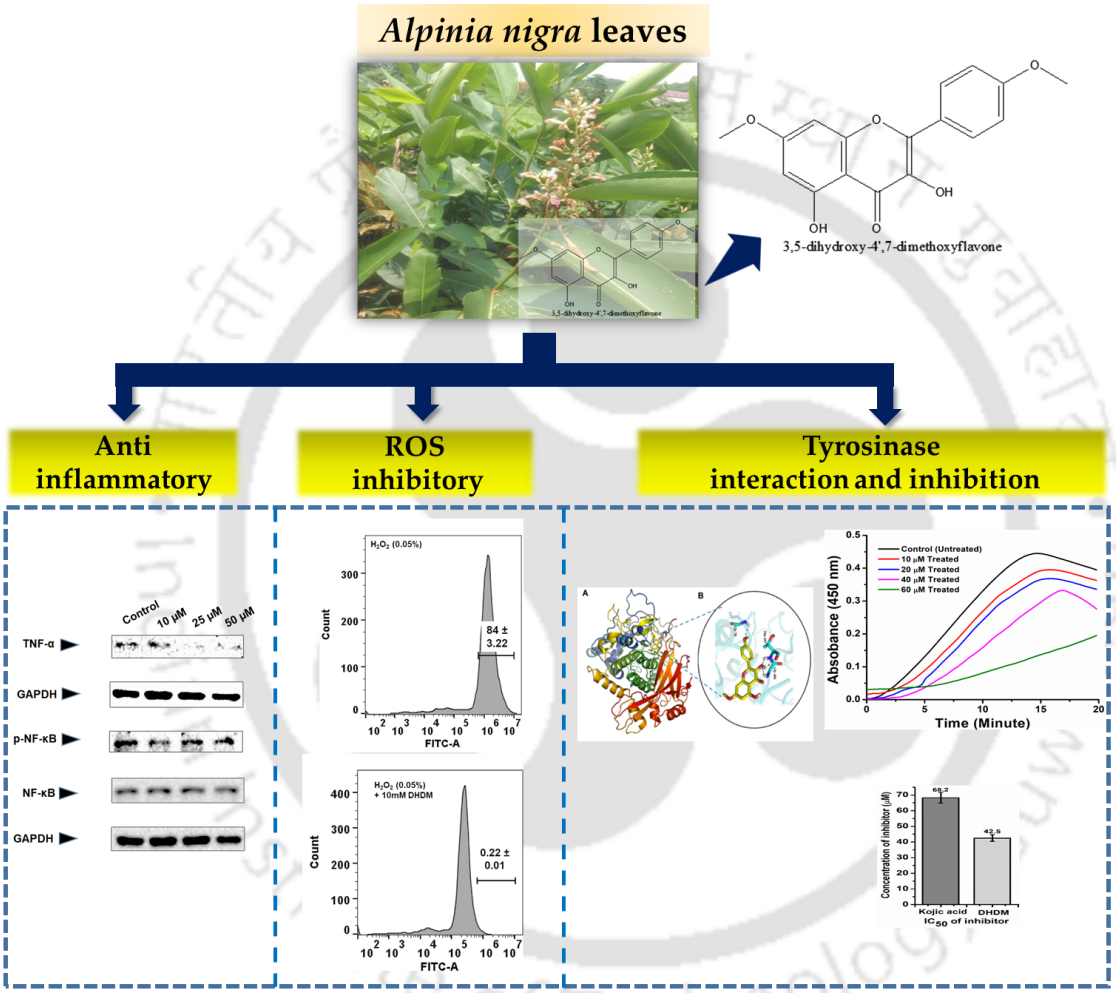

Overexposure to sunlight and high UV radiation leads to uncontrolled melanin production in the skin, leading to hyperpigmentation and inflammatory diseases. Therefore, in this chapter Antioxidant, anti-tyrosinase and anti-inflammatory activities of 3,5-dihydroxy-4',7-dimethoxyflavone was investigated.

Chapter 5

Antioxidant, anti-tyrosinase and anti-inflammatory activities of 3,5-dihydroxy-4',7-dimethoxyflavone isolated from the leaves of *Alpinia nigra*

5.1 Introduction

There is a tremendous increase in the rate of skin diseases due to excess exposure to ultraviolet (UV) radiation. UV radiation also causes overexpression of tyrosinase leading to uncontrolled melanin synthesis. Melanin is helpful in phenotypic appearance and protects human skin from UV radiation. On the other hand, overexposure to sunlight and high UV radiation leads to uncontrolled melanin production in the skin leading to some of the hyperpigmentation diseases like melasma, freckles, melanoma, and age spots. UV rays penetrate deep into the skin and reach the basal layer of the epidermis, thereby contributing to photoaging (Tyrrell and Keyse 1990).

Tyrosinase (EC 1.14.18.1), an effective multifunctional enzyme plays an important role in pigmentation of fruits, melanin formation in mammals and is widely distributed in melanosomes of bacteria, fungi, plant, and mammals (Kim et al. 2017). In mammalian cells, tyrosinase is involved in melanin synthesis through melanogenesis pathway. It is regulated by oxidation of tyrosine to dopaquenone in the first step, after which dopaquinone is converted into dopachrome through autoxidation (Hridya et al. 2015). Extensive research is being carried out on tyrosinase inhibitor, due to its medicinal importance in curing hyperpigmentation disorder and also for other applications like cosmetics, food, and pharmaceutical industries.

Many tyrosinase inhibitors, either from a synthetic or natural source, have been reported to prevent the hyper production of melanin in the epidermal layer. However, the use of synthetic drugs is not preferable due to their adverse side effects (Sahoo et al. 2018). Kojic acid is a well-known tyrosinase inhibitor but exhibits cellular toxicity (Saeedi et al. 2019). Plant secondary metabolites such as alkaloids and flavonoids are reported as protectors against free radicals and high UV radiation (Das and Biswas, 2012). Flavonoids are polyphenolic compounds widely present in various plant parts like seeds, bark, flower and leaves (Swargiary and Roy, 2015; Harborne and Williams 2000). Due to the presence of the hydroxyl group, polyphenols are considered as the largest group of tyrosinase inhibitor (Kubo et al. 2000).

Since plants are rich source of chemical constituents, there is a need to explore and isolate bioactive components from *A. nigra* that possess the therapeutic potential for treating hyperpigmentation (Batubara et al., 2016). For example, some flavonoids such as resveratrol and quercetin possess pharmacological potency as cure for hyperpigmentation (Fan et al. 2017; Zimmermann Franco et al. 2012). The present study was focused on the antioxidant, anti-tyrosinase and anti-inflammatory activities of a flavone, 3,5-dihydroxy-4',7-dimethoxyflavone (DHDM) isolated from ethyl acetate leaf extract of *A. nigra* (Ghosh et al. 2013; Das et al. 2014).

5.2 Materials and methods

5.2.1 Chemicals and cell culture

Tyrosinase (T3824), dimethyl-sulfoxide (DMSO), kojic acid, L-tyrosine, ethyl acetate, hexane, methanol, acetonitrile and chloroform-d1 were purchased from Sigma Aldrich (St. Louis, Missouri, United States). Silica gel 60-120 mesh was procured from Sisco Research Laboratories Pvt. Ltd (Kolkata, India) and MTT (3(4,5- dimethylthiazol-2-yl)-2,5-diphenyl tetrazolium bromide) was obtained from Himedia (Mumbai, India). The THP-1 (human macrophage cell line) and HaCaT cells (non-cancerous human keratinocyte cell line) were procured from National Centre for Cell Sciences (NCCS) (Pune, India) and cultured in RPMI-1640 and DMEM (Gibco™; Life Technologies, NY, USA) media respectively, supplemented with 10% fetal bovine serum (FBS; Gibco®, Grand Island, NY, USA) and 1% PenStrep (Invitrogen, Carlsbad, CA, USA). The cells were maintained at 37°C in 5% CO_2 and 95% humidity in a CO_2-regulated incubator.

5.2.2 MTT assay

Cell cytotoxicity was performed using the 3 (4,5- dimethylthiazol-2-yl)-2,5-diphenyl tetrazolium bromide (MTT) assay. THP-1 (2,000) cells were seeded in 96-well plates and subsequently these cells were treated with a varying concentrations of DHDM (10 µM to 200 µM). Further, it was incubated for 24 h in the CO_2 incubator (5% CO_2, 37°C). The cells were centrifuged at 200 g for 15 min and the pellet obtained was suspended in MTT solution (working concentartion~0.5 mg/mL). The samples were incubated at 37°C for 3 h, after which the cells were re-centrifuged at

200 g for 15 min. The formazan crystals so formed were dissolved in 200 µl dimethyl sulfoxide (DMSO). Finally, the absorbance was recorded at 570 nm.

Similarly, the effect of DHDM on the viability of HaCaT cells was also determined by MTT assay. Briefly, 2000 cells were seeded in 96 well plates and incubated for 24 h at 37°C, treated with different concentrations of DHDM (10, 20, 40, 60 and 80 µM) and incubated for 72 h. After incubation, 10 µl of 5 mg/mL of MTT solution was added to each well and further incubated for 2 h and formazan crystals thus formed were dissolved in DMSO. The absorbance was measured with a microplate reader (Molecular Devices, Spectramax iD3) at 570 nm (Monisha et al. 2018; Bordoloi et al. 2019).

5.2.3 DPPH free radical scavenging assay

Free radical scavenging was conducted through 2,2-Diphenyl-1-picrylhydrazyl (DPPH) assay. To perform this assay, 0.1 mM of DPPH solution was prepared in methanol. About 200 µl of prepared DPPH solution was added to different concentrations of DHDM (5, 10, 20, 30, 40 and 50 µM). Ascorbic acid was used as a positive control. Sample was incubated at room temperature for 30 min. After incubation, the absorbance was taken at 517 nm. The capability to scavenge DPPH free radicals was calculated using the equation 1. The graph was plotted as the % of DPPH radical scavenging vs. concentration of tested sample.

$$\text{Radical scavenging } (\%) = \left(\frac{\text{OD of Control} - \text{OD of Sample}}{\text{OD of Control}}\right) \times 100 \qquad \text{(Equ.1)}$$

5.2.4 ROS inhibitory activity

Briefly, 1 X 10^6 HaCaT cells were seeded in a 6-well plate and treated with 0.05% of hydrogen peroxide (H_2O_2) in each well for studying the levels of reactive oxygen species (ROS). It has been reported that endogenous ROS can be generated by addition of H_2O_2 and thus can be used as a control (Bae et al. 2014; Warinhomhoun et al. 2021). Further, the cells were treated with different concentrations of DHDM (10, 20, 40, 60 and 80 µM) and incubated in 5% CO_2 incubator at 37°C for 24 h. Additionally, ascorbic acid (50 µM) was used as positive control. Cells were pelleted and washed with 1% phosphate buffer saline (PBS, pH 7.4). Furthermore, cells were suspended in 500 µl of 1% PBS and incubated with 10 µM 2′,7′-dichlorodihydrofluorescin diacetate (H_2DCF-DA) for 30 min at 37°C. For quantitative

assessment, the cells were analyzed using flow cytometry (BC, CytoFlex S Analyser). The data was further analyzed with help of FlowJo software (Ashland, Oregon, United States).

5.2.5 Docking of DHDM with tyrosinase

Docking was performed using AutoDock Tools (ADT) which provides a graphical interface to dock ligand, especially against the protein (Morris et al. 2008b). For tyrosinase (5M6B), the .pdb file was downloaded from protein database (PDB), and unessential residues of the proteins were removed by PYMOL molecular visualization software. These .pdb files (tyrosinase and inhibitor) were uploaded in AutoDock Tools (ADT) to generate .pdbqt files. Finally, these files were uploaded in raccoon virtual screening software to dock the inhibitor against the tyrosinase. The docked structure with lowest binding energy was used to analyze the hydrogen bond interactions.

5.2.6 Fluorescence spectral studies of tyrosinase upon the interaction with DHDM

Fluorescence quenching of tyrosinase upon addition of DHDM was performed using earlier defined protocol with some modifications (Kim et al. 2006a). Briefly, emission fluorescence spectra were recorded in the range of 320-450 nm at the excitation wavelength of 290 nm (λ_{ex}). Enzyme tyrosinase (125 U/mL) in 50 mM potassium phosphate buffer (pH 6.8) was treated with a range of DHDM concentrations (10-60 µM) for 15 min at 4°C. Finally, the change in fluorescence spectral pattern was recorded, and fluorescence quenching constant (Stern–Volmer quenching constant) was calculated using the following equation.

$$Fo/F = 1 + kq\,\tau o[Q] = 1 + Ksv[Q] \quad \text{(Equ.2)}$$

Where, Fo is the fluorescence intensity of enzyme alone, F is the intensity of fluorescence on addition of the DHDM, τo is a fluorophore lifetime, [Q] is the concentration of the quencher, K_{SV} and kq are the Stern–Volmer quenching and bimolecular quenching constant, respectively. Hence, K_{SV} was calculated from Fo/F vs. [Q] plot using equation 2.

5.2.7 Tyrosinase inhibitory activity of DHDM

The inhibitory effects of DHDM on tyrosinase enzyme were explored by spectroscopic studies as reported earlier (Chan et al. 2011). The reaction mixture of tyrosinase (300 U/mL) with varying concentrations of the compound (10-60 µM) in 50 mM potassium phosphate buffer (pH 6.8) was

incubated at 4°C for 5 min. After incubation, a fixed concentration of L-tyrosine (500 µM) was added, followed by incubation for 15 min at room temperature. Finally, product formation (dopachrome) was determined by measuring the absorbance at 450 nm. Kojic acid was used as a positive control. Percentage inhibition of tyrosinase was calculated by using the following equation.

$$\text{Inhibition } (\%) = (A - B)/(C - D) \times 100 \quad \text{(Equ.3)}$$

Where A and B are the absorbance of the test and control sample; C and D are the absorbance of tyrosinase and L-tyrosine, respectively. The inhibitory concentration (IC_{50}) of the compound was calculated

5.2.8 Kinetic analysis

The absorbance of the reaction mixture containing L-tyrosine (500 µM) with tyrosinase (300 U/mL) supplemented with varying concentrations of DHDM (10-60 µM) in 50 mM potassium phosphate buffer (pH 6.8) was measured at different time intervals. The change in the absorbance of the reaction mixture treated with different DHDM concentrations was measured and interpreted in terms of inhibition of enzymatic activity.

5.2.9 Western blot analysis

To determine the effect of DHDM on the inflammatory proteins, whole cell extracts were prepared by subjecting DHDM-treated cells to lysis in lysis buffer (20 mM HEPES, 2 mM EDTA, 250 mM NaCl, 0.1% NP40) in the presence of protease inhibitors (2 µg/mL aprotinin, 2 µg/mL leupeptin hemisulfate, 1mM DTT, and 1 mM PMSF). The lysates were centrifuged at 13,000 g for 10 min to remove insoluble material. Supernatants were collected and stored at -80°C. The lysates were resolved using sodium dodecyl sulfate polyacrylamide gel electrophoresis (SDS-PAGE). Following electrophoresis, the proteins were electro transferred to nitrocellulose membranes, blotted with the relevant antibodies. The bands representing different proteins were visualized using Clarity Western ECL Substrate (Bio-Rad, Hercules, CA, USA) in a ChemiDoc™ XRS System (Bio-Rad). The housekeeping gene glyceraldehyde 3-phosphate dehydrogenase (GAPDH) was used as the loading control.

5.2.10 Statistical analysis

All experiments were performed in triplicate. The statistical analysis was executed using OriginPro 8.5 software. Analyzed data were expressed as mean ± standard deviation (SD), and $p< 0.05$ revealed statistical significance.

5.3 Results and discussion

5.3.1 DHDM is not toxic to normal cells

On assessment of possible cytotoxicity of DHDM towards the THP-1 cell lines, there was no significant reduction in the number of viable cell as compared to the untreated control (**Fig. 5.1A**). Hence, the result suggested non-toxic nature of DHDM even at a higher concentration (200 µM) upon 24 h of exposure. THP-1 cells are macrophages previously used as a model for immune stimulation (Chanput et al. 2014). Similar report exists about the toxicity of plant extracts on THP-1 cells. The finding also showed the efficacy of plant extract against tyrosinase for the development of new drug entities to cure hyperpigmentation (Lee et al. 2015).

Furthermore, we examined the effect of DHDM in human keratinocytes, HaCaT cells by MTT assay. It was observed that the treatment with different concentrations of DHDM did not reduce the viability of HaCaT cells (**Fig. 5.1B**). The non-cytotoxic effect of DHDM in HaCaT cells was observed up to 80 µM. Thus, the non-toxic effect of DHDM suggests its safe behavior towards human skin cells and could be effectively employed as regimen for skin problems.

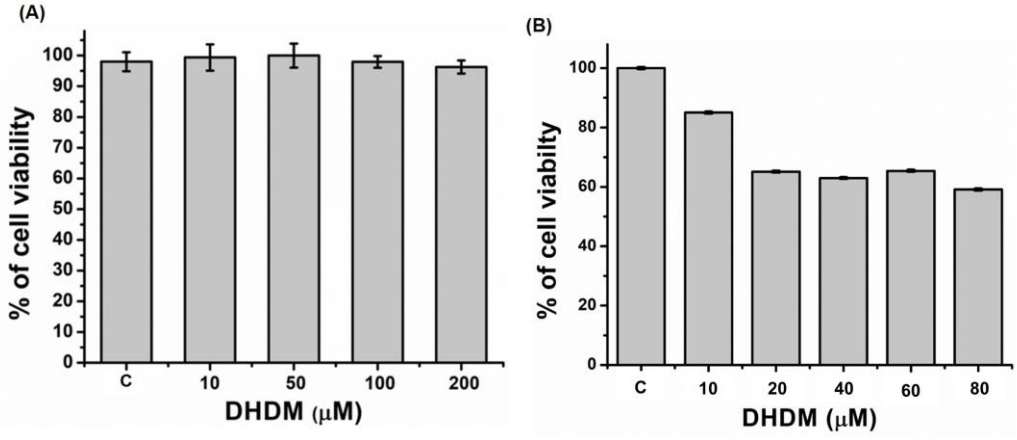

Fig. 5.1 Cell viability assay at varied concentrations of DHDM. (A) On human macrophage THP-1 cell lines; (B) Human keratinocyte HaCaT cell lines. Values are means ± SD for triplicate assay.

5.3.2 DPPH scavenging activities of DHDM

The beneficial health effects of flavonoids are primarily attributed to their antioxidant property. The antioxidant activity of DHDM was tested by DPPH radical scavenging assay. The DPPH assay is a non-enzymatic method mainly used to deliver basic information on the reactivity of the compounds to scavenge free radicals (Haida and Hakiman 2019). The lower absorbance of the reaction mixture (DPPH and tested sample) indicates a higher free radical scavenging activity. Here, the anti-oxidative potential of isolated compound, DHDM and ascorbic acid (positive control) was investigated. The different concentrations of DHDM displayed potent antioxidant behavior similar to ascorbic acid (**Fig. 5.2**). Recent studies have demonstrated that the skin retains antioxidant defense mechanism to deal with UV-induced oxidative stress and prevents skin disease by combating with over production of tyrosinase. Conversely, unwarranted chronic exposure to UV radiation can devastate the cutaneous antioxidant capacity, leading to oxidative stress and oxidative damage. This may result in inflammation leading to diverse skin disorders and premature aging of the skin (Nichols and Katiyar 2010). Some plant flavonoids for instance, quercetin has shown immense potential as antioxidant, anti-tyrosinase, and anti-inflammatory agents that reduce the oxidative stress and prevents the damage of the skin keratinocytes cells (Xu et al. 2019). In line with this study, our present finding reveales that DHDM possesses strong antioxidant activity.

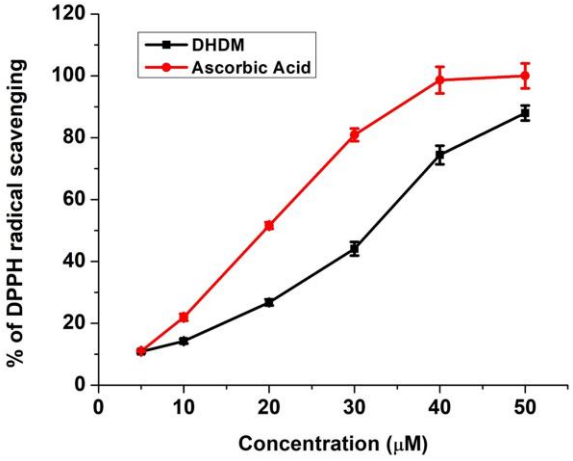

Fig. 5.2 DPPH radical scavenging activity of ascorbic acid and DHDM. Values are means ± SD for triplicate assay.

5.3.3 ROS inhibitory activity

ROS are byproducts of cellular metabolism, which are generally produced in the mitochondria. ROS are normally generated in different cell types that primarily helps in cell signaling and provides protection against the pathogens (Alfadda and Sallam 2012). However, intense sunlight, chemical and UV radiation causes high ROS production in cells. Excessive generation of ROS act as toxicants which leads to cellular damage (Nichols and Katiyar 2010). Redox imbalance occurs with increasing age, which alters the oxidative level (Liguori et al. 2018). Hence, we examined and determined the ROS inhibitory activity in the keratinocyte cells after administrating with H_2O_2 and DHDM. The H_2O_2 induced ROS level was reduced by 84 ± 3.22% to 0.62 ± 0.03% with increasing concentration of DHDM (10, 20, 40, 60, and 80 µM) respectively **(Fig. 5.3**). This result was consistent with previous studies, in which polyphenolic compound inhibited ROS *in vitro* (Profumo et al., 2016). Furthermore, DHDM was demonstrated to possess strong anti-oxidative activity, which was mediated through scavenging and neutralizing free radicals *in vitro* at various concentrations. Many studies have shown that the ROS inhibitory compound possesses anti-inflammatory activities too (Sudsai et al., 2016; Syahida et al., 2006). Therefore, we anticipate that the compound DHDM might exhibit anti-inflammatory properties as well through the inhibition of ROS accumulation in keratinocyte cells.

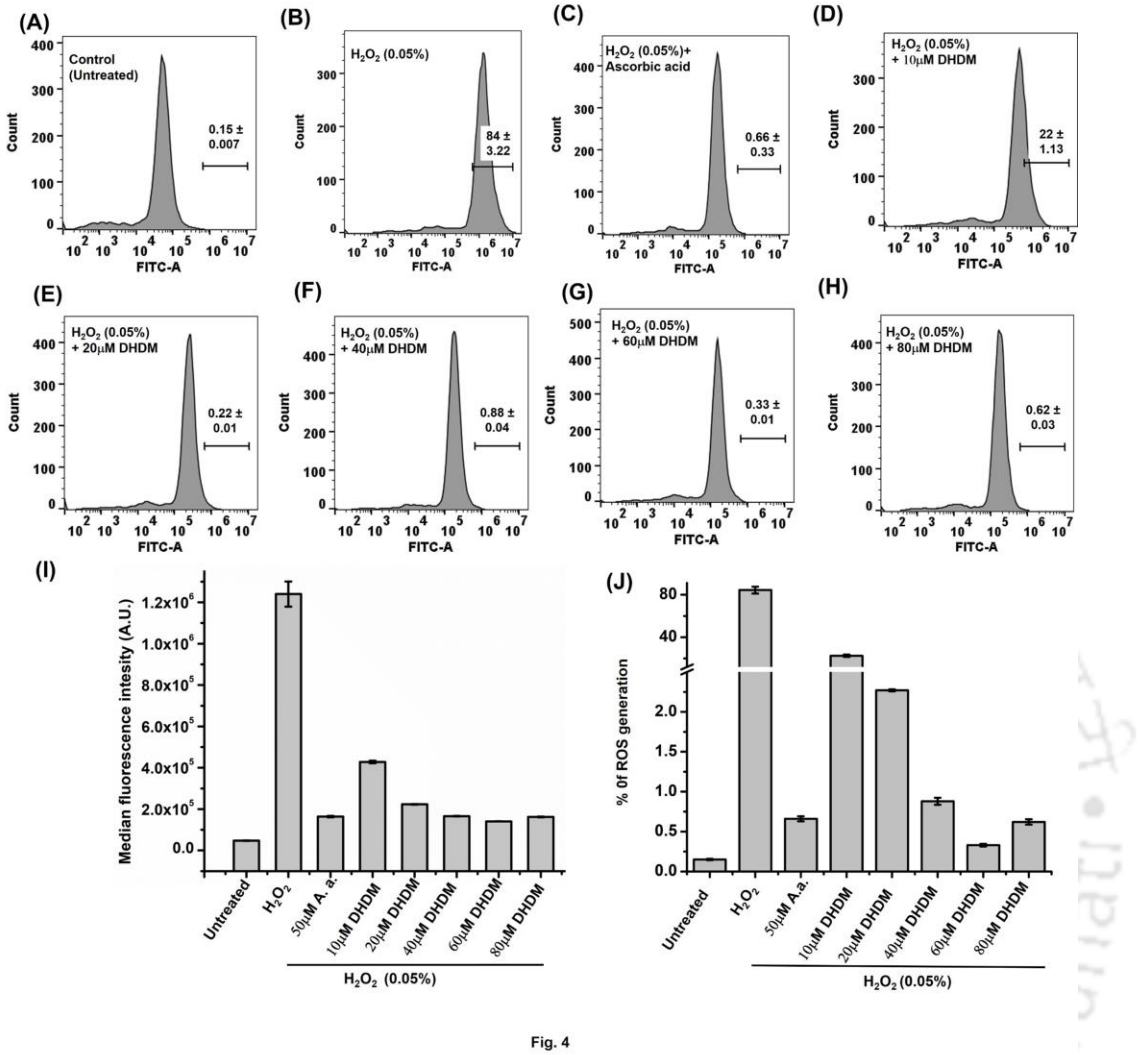

Fig. 4

Fig. 5.3 Flow cytometry analysis of HaCaT cells using D_2DCF-DA for cellular ROS determination. (A) Control; (B) 0.05% H_2O_2; (C) 0.05% H_2O_2 + Ascorbic acid (A.a); (D) 10 µM DHDM + 0.05% H_2O_2; (E) 20 µM DHDM + 0.05% H_2O_2; (F) 40 µM DHDM + 0.05% H_2O_2; (G) 60 µM DHDM + 0.05% H_2O_2; (H) 80 µM DHDM + 0.05% H_2O_2; (I) Median fluorescence intensity (MFI) reduction; (J) % of ROS with increasing concentration of DHDM. Values are means ± SD for triplicate assay.

5.3.4 Analysis of interaction between DHDM and tyrosinase

On docking DHDM against the target protein, tyrosinase, a total of 10 structures was obtained. Out of 10-docked structure, the lowest energy structure was taken for interaction studies. DHDM bound at a different site in the enzyme and not on catalytic center, which suggests the allosteric

nature of the tyrosinase enzyme. The DHDM interacted with mainly three amino acid residues viz., Gly78, Gly456, and Thr457 (**Fig. 5.4**). It was observed that DHDM binds to the protein/enzyme by hydrogen binding in the inner grooves. However, after binding with DHDM, the protein undergoes changes that lead to change of affinity of the substrate to the protein. The binding energy of the best-docked structure was found to be -4.21 Kcal/mol. The low binding score corresponds to the strong interaction of the inhibitor with the allosteric site of the enzyme (Ghosh et al. 2013a). This correlated with earlier studies where in 3', 4' dihydroxy groups in C ring of quercetin interacted with amino acid residues such as Gly281 and Ser282 (Fan et al. 2017). Moreover, earlier published data has shown that kojic acid binds with His63 and Ser206 which subsequently resulted in inhibition of enzyme activity (Bochot et al. 2014). However, the interaction between DHDM and tyrosinase may lead to conformational changes, thereby preventing the substrate L-tyrosine to react with the enzyme.

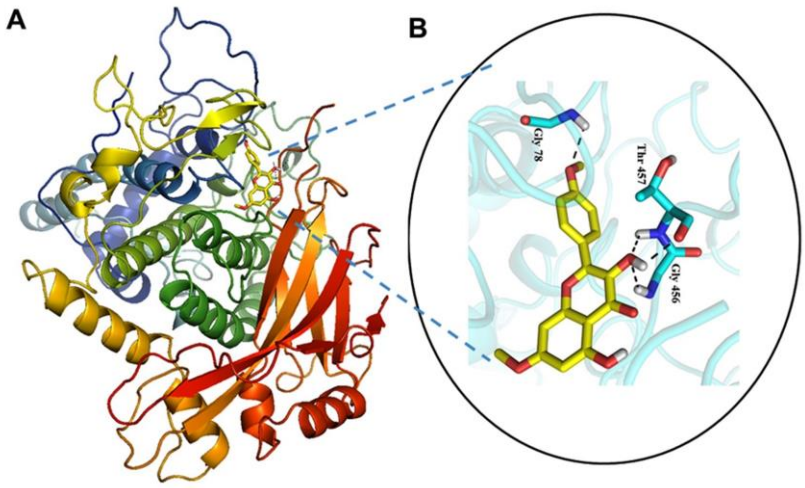

Fig. 5.4 Predicted docked conformation of DHDM against tyrosinase. (A) The overall structure of tyrosinase with inhibitor. Protein has been represented in rainbow color; (B) Docked ligand site of tyrosinase. All the interactions of inhibitor with the protein are represented in a black dashed line. Amino acid Gly-78, Gly-456, and Thr-457 of protein showed interaction with the inhibitor.

5.3.5 Analysis of intrinsic fluorescent quenching

To validate the interaction of isolated compound (DHDM) with tyrosinase, the intrinsic fluorescence study of the enzyme was evaluated. The fluorescence study of tyrosinase was

accomplished by keeping the concentration of tyrosinase fixed (125 U/mL) and varying the concentration of the compound (10-60 µM). The emission maxima of fluorescence spectra were acquired at 341 nm. The emission intensity of tyrosinase decreased gradually with corresponding increase in the concentrations of DHDM (10-60 µM) (**Fig. 5.5A**). Additionally, the binding efficacy of DHDM on tyrosinase was also evaluated by quenching studies. The fluorescence quenching was determined by the Stern-Volmer plot at various concentrations of DHDM through which the K_{sv} of 2.4 × 10^{-3} µM obtained (**Fig. 5.5B**). Consequently, this linearity of Stern-Volmer plot indicated the interaction of DHDM with tyrosinase in dose dependent manner. However, the interaction between DHDM and tyrosinase may lead to conformational changes, thereby preventing the substrate L-tyrosine to react with the enzyme. In support of the conformational change after binding of DHDM with tyrosinase, intrinsic fluorescence study was performed. Similar studies has been carried out on Apigenin with tyrosinase earlier (Xiong et al. 2016). Therefore, by intrinsic fluorescence experiment, conformational change of tyrosinase upon interaction with DHDM was observed. Binding of DHDM may attribute to unfolding of the enzyme, which eventually leads to decrease in fluorescence intensity.

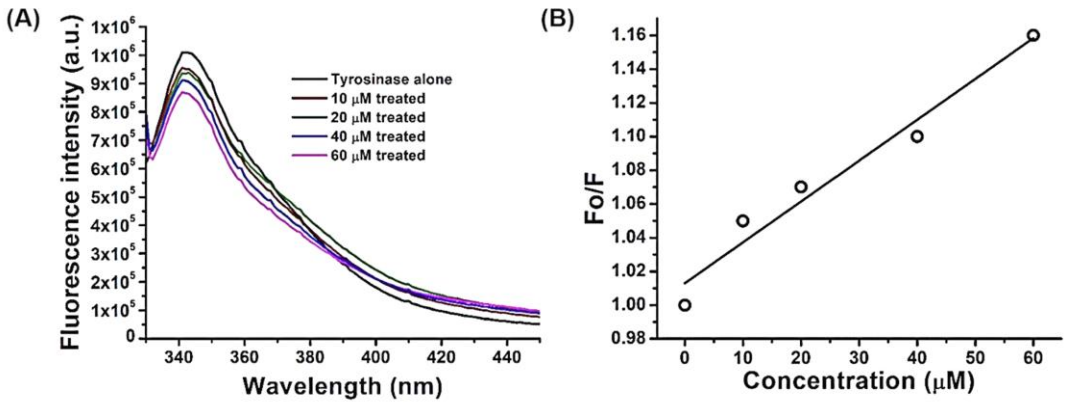

Fig. 5.5. Intrinsic fluorescence study of tyrosinase. (A) Varying concentrations of test sample (tyrosinase + DHDM) wherein DHDM showed quenching of fluorescence intensity of tyrosinase in a dose dependent manner. (B) The linear plot by Stern-Volmer equation where F_O and F are the fluorescence intensities of tyrosinase before and after the addition of the DHDM.

5.3.6 Inhibitory activity of DHDM towards tyrosinase

Time dependent enzyme kinetics was performed with fixed concentration of L-tyrosine and tyrosinase at a DHDM concentrations ranging from 10-60 µM (**Fig. 5.6A**). A gradual reduction

of tyrosinase activity with increasing DHDM concentration was observed. The maximum inhibition was recorded at 60 µM of DHDM concentration. The inhibition of tyrosinase activity by DHDM was comparatively analyzed with the well-known tyrosinase inhibitor, kojic acid (Choi et al. 2012). The formation of product (dopachrome) was monitored after 20 min of incubation. A significant decrease in tyrosinase activity (~16% to ~36%) was observed upon application of increasing concentration (20 µM) of DHDM. However, the decrease in tyrosinase activity can be related to anti-phenolase effect against melanin synthesis (Pillaiyar et al., 2017). Maximum inhibition (68.7%) was observed at 60µM concentration of DHDM and 50% inhibition (IC_{50}) at 42.5 µM (**Fig. 5.6B**). Similarly, the effect of kojic acid on tyrosinase activity was also measured (**Fig. 5.6C**). Maximum inhibition by kojic acid was observed at 80 µM concentration and 50% inhibition at 68.2 µM. However, IC_{50} value of DHDM was found to be 42.5 µM, which is less than the IC_{50} of kojic acid (**Fig. 5.6D**). The possible cause of such high inhibitory action of DHDM may be due to the 2, 4-hydroxyphenyl moiety (Chen and Kubo 2002). This study revealed that the formation of dopachrome gradually decreases in the presence of increasing concentration of DHDM. Since, dopachrome formation is the initial and rate-limiting step during melanin synthesis, DHDM prevents dopachrome formation by inhibiting the tyrosinase activity. Moreover, at a concentration of 42.5 µM, DHDM showed higher inhibitory potency than kojic acid, which may be due to the structural analogy with quercetin, a potent inhibitor and the presence of 2,4 hydroxyphenyl moiety as the main functional group responsible for higher inhibitory activity (Han et al. 2012).

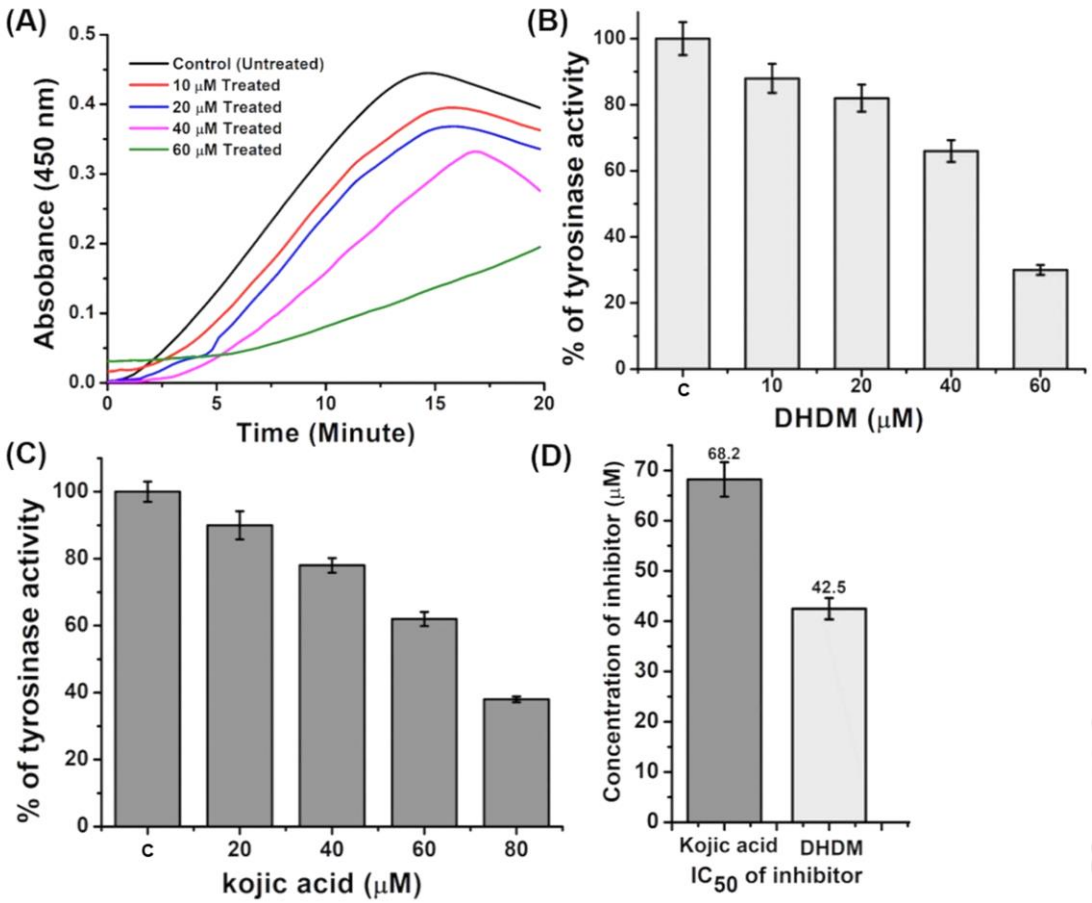

Fig. 5.6 Effect of DHDM on tyrosinase enzyme. (A) Kinetics of tyrosinase at different DHDM concentrations with respect to time; (B) % inhibitory effect of DHDM on tyrosinase activity; (C) % inhibitory effect of kojic acid on tyrosinase activity; (D) Inhibition of mushroom tyrosinase by kojic acid and DHDM. Assays were carried out as described in the experimental section. Values are means ± SD for triplicate assay.

5.3.7 DHDM shows strong anti-inflammatory activity

In the present study we have evaluated the potential of DHDM in suppressing inflammatory mediators *in vitro*. GAPDH was used as positive control. Our results demonstrated that DHDM inhibited the expression of TNF-α and the activation of NF-κB in dose dependent manner in human keratinocytes cell line HaCaT (**Fig. 5.7**). TNF-α stimulates epidermal keratinocytes that trigger the activation of signaling pathways involved in pro-inflammatory responses. NF-κB is an extensively expressed transcription factor, which is regulated through inflammatory mediator (TNF-α) and also through UVB exposure causing oxidative stress. The phosphorylation-

triggered degradation through phosphorylation at serine-32 of inhibitor kappa B-alpha (IκB-α), is a major mechanism of NF-κB activation (Desai et al. 2018). The phosphorylation of IκB leads to its ubiquitination and ultimate degradation by the proteasome, allowing NF-κB to translocate to the nucleus where it activates the expression of its target genes. Activation of the NF-κB/Rel family of transcription factors regulates the expression of genes that participate in different pathways involved in inflammation, cell proliferation, and cell survival (Kunnumakkara et al. 2020). However, our study suggests that there is a significant decrease in the level of NF-κB-p65 after the treatment with DHDM. Therefore, these results suggest that DHDM could have high potential in the prevention and treatment of inflammatory disorders. However, further studies on *in vivo* inflammatory models are required to validate these results.

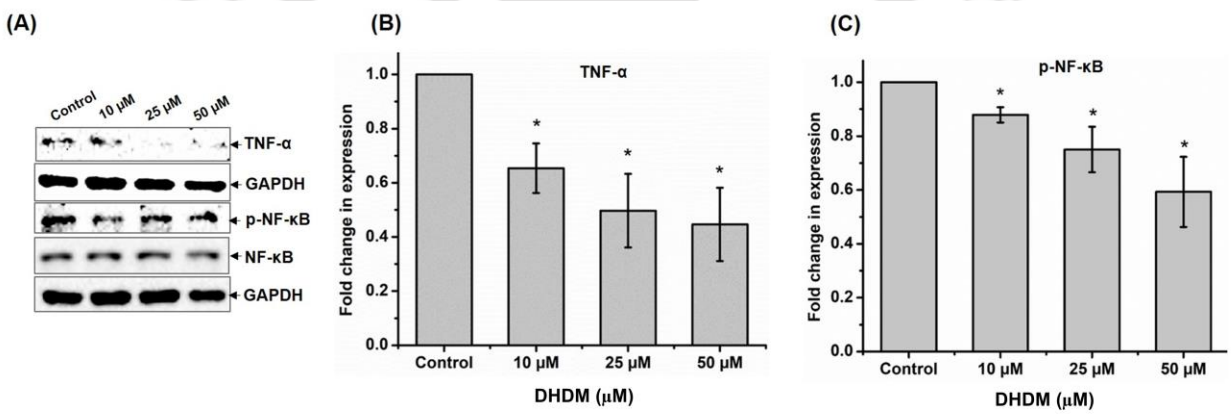

Fig. 5.7 The effect of DHDM on the expression of inflammatory proteins TNF-α, NF-κB and p-NF-κB in HaCaT cells. (A) Representative western blots showing the effect of varied concentrations of DHDM on TNF-α (26 kDa), p-NF-κB (65 kDa) and NF-κB (65 kDa). Constitutive protein GAPDH (37 kDa) was used as an internal control. The densitometry analysis of TNF-α (B) and p-NF-Kb (C) revealed its inhibition with the treatment of DHDM in HaCaT cells. Data are expressed as mean ± SD (n=3), * denotes $p<0.05$ vs. Control.

5.4 Conclusion

Excessive sunlight and over exposure to UV radiation leads to abnormal melanin production in the skin triggering hyperpigmentation. Medicinal plants are considered as a rich source of bioactive compounds, which possess not only nutritional value but also pharmacological potency

as cure for hyperpigmentation and prevent damage caused due to UV radiation. Therefore, the effect of DHDM on the cell viability was examined on THP-1 and HaCaT cell lines and it was concluded that the treatment of DHDM did not induce any cellular cytotoxicity. The antioxidant and ROS inhibitory activity revealed that DHDM possesses high ability to scavenge free radicals and reduce excessive ROS similar to the known potent agent, ascorbic acid. Further, the inhibition of tyrosinase activity by DHDM was investigated through spectroscopic techniques and molecular docking simulation. The molecular docking studies proved that -OH and -OCH_3 group of DHDM interacts with the Gly-78, Gly-456, and Thr-457 amino acid residue of tyrosinase leading to conformational changes of catalytic site, thereby preventing the substrate L-tyrosine to react with the enzyme. Subsequently, intrinsic fluorescence study of tyrosinase was performed in the presence of various concentrations of DHDM (10-60 µM). The Ksv value (Ksv=2.4x 10^{-3} µM) indicated that the compound binds to tyrosinase. Further, the effect of DHDM on melanin synthesis was analyzed through enzyme kinetic studies by phenolase activity. Furthermore, anti-inflammatory activity was also investigated and confirms that DHDM suppressed the expression of TNF-α and p-NF-κB in HaCaT cells. Based on our results we conclude that the compound DHDM acts as a potential inhibitor of tyrosinase, and scavenge free radicals. Therefore, this natural compound might be explored further for the development of a new drug for the cure of hyperpigmentation and skin disorder.

Synthesis and characterization of zinc derivatized 3, 5-dihydroxy 4′, 7-dimethoxyflavone and its anti leishmaniasis activity against *Leishmania donovani*

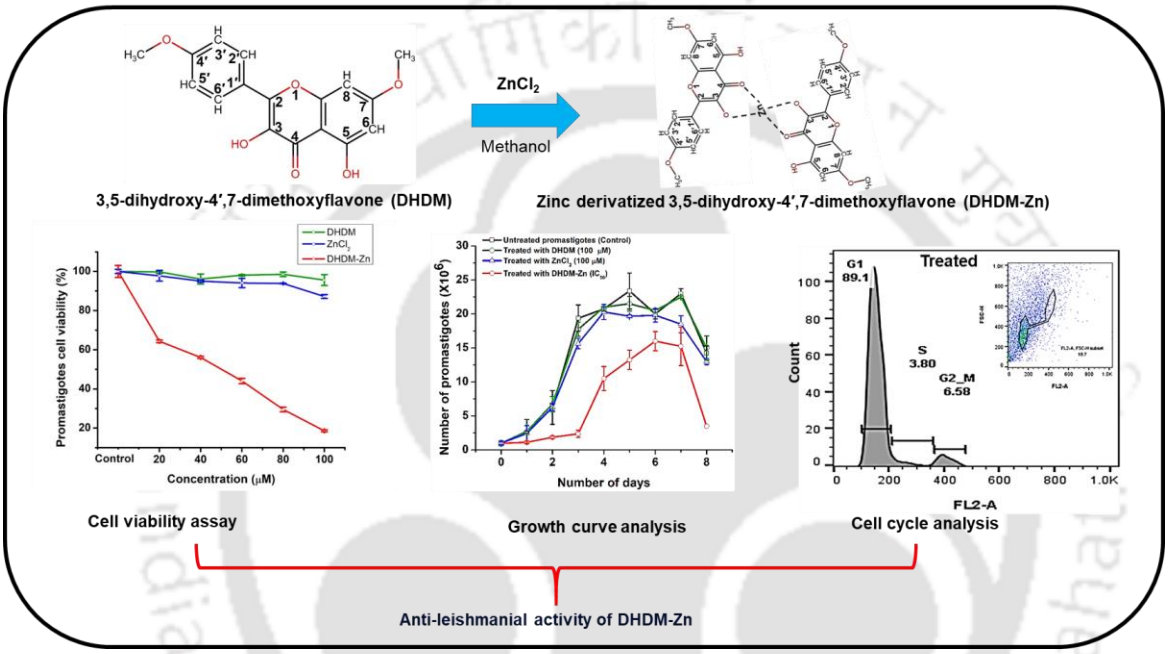

Leishmania donovani is the main causative agent of visceral leishmaniasis that affects millions of people worldwide. This study reports the synthesis and characterization of zinc derivatized 3,5-dihydroxy 4′, 7- dimethoxyflavone (DHDM-Zn) compound for the development of new antileishmanial agents.

Chapter 6

Synthesis and characterization of zinc derivatized 3, 5-dihydroxy 4′, 7-dimethoxyflavone and its anti leishmaniasis activity against *Leishmania donovani*

6.1 Introduction

Leishmaniasis is a neglected infectious disease that affects millions of people worldwide. The disease is more pronounced in tropical and subtropical regions, including the eastern part of India. A recent report suggested that visceral leishmaniasis (VL) accounts for 50000 to 90000 new cases worldwide annually (WHO report 2019). *Leishmania donovani* is the main causative agent of VL, transmitted by the bite of the female sand-fly (*Phlebotomus*). In India, this disease is commonly known as kala-azar. The digenetic life cycle of the parasite is completed in two different stages (flagellated promastigote and aflagellated amastigote) (Van et al. 2020). The spindle shape promastigote form resides in the mid-gut of sand-fly and is subsequently transferred into the human blood by the bite of the carrier. The other oval aflagellated form infests human immune cells such as macrophage and dendritic cells (Prakash et al. 2019). VL is a lethal form of the disease leishmaniasis that mostly targets visceral organs like liver, spleen, and bone marrow (Mansuri et al. 2020). Current therapies for leishmaniasis are limited due to their low availability, high cost, and toxicity. Besides, the development of drug resistance by the pathogen is a key problem in the treatment of VL in endemic areas. Hence, it is vital to develop a new, improved drug for the treatment of this lethal disease.

Plant-derived products are used traditionally for the cure of parasitic infections due to lower toxicity and adequate availability. For instance, Artemisinin isolated from *Artemisia annua* is recognized as an antimalarial drug and with proven efficacy against cutaneous leishmaniasis (CL) (Sen et al. 2007). Essential micronutrient derived from plant products have already been explored for effective anti-leishmanial activity. Recently, zinc fabricated plant polyphenolic compound, quercetin, was reported for its anti-leishmanial effect (Da Silva et al. 2012; Saini et al. 2017).

Zinc is an essential micronutrient in all life forms, including prokaryotes and eukaryotes (Bonaventura et al. 2015). Zinc ions are used for various metabolic processes and work as

essential cofactors of enzymes associated with cellular processes. It exhibits an imperative role in cell growth and maintaining cellular homeostasis (Beyersmann and Haase 2001). Plant phenolic compounds like flavonoids have been widely reported as an effective chelator for essential metal ions like zinc, iron, copper, platinum, and palladium (Perez et al. 2009). Flavonoid-metal complexes have been shown to retain better anticancer activity on cancer cells as compared to their free flavonoid counterpart (Lee and Tuyet 2019). Remarkably, zinc scripts a significant role in the virulence of *L. donovani,* aided by high quantity of glycoprotein 63 (GP63) protease (Zn containing metalloenzyme) (Yang et al. 1993). Some studies reported metalloproteinase (GP63) in *Leishmania major* as the specific function of zinc in the cellular processes of the parasite (Macdonald et al. 1995). Recently many papers documented the metal ion complex of flavonoids with metal ions like iron, zinc, and copper for their antioxidant activity (Jeslin Kanaga Inba et al. 2013). However, the effect of zinc complexed drugs on the survival of *L. donovani* has not been explored to date.

In the current study, we report the synthesis and structural analysis of the Zn(II) complex of 3,5-dihydroxy 4′, 7-dimethoxy (DHDM) isolated from leaf of *Alpinia nigra* L. and its effects against *L. donovani*.

6.2 Materials and methods

6.2.1 Materials and parasite culture

Zinc chloride ($ZnCl_2$), M199 media, and RPMI media were purchased from Himedia. Methanol (HPLC grade) and dimethyl sulfoxide (DMSO) were purchased from Merck. Propidium iodide (PI) and DMSO (cell grade) were purchased from Sigma. *L. donovani* strain (BHU 1081) was provided by Prof. Shyam Sundar, Banaras Hindu University. The parasite was cultured at 25°C to 28°C and maintained in M199 media (Gibco, Grand Island, NY; 0.12 mM adenine, 0.0005% hemin, 10% fetal bovine serum) with the addition of the selective antibiotic Geneticin (10 µg/mL, G418; Gibco). The stock concentration (60 mM) of DHDM, $ZnCl_2$ and derivatized compound DHDM-Zn were prepared by dissolving in DMSO. Further, working concentration were made by diluting the stock in 1% PBS (pH 7.4), such that the DMSO concentration was ≤ 0.2%.

6.2.2 Synthesis of Zn^{2+} complex of DHDM (DHDM-Zn)

The synthesis of the DHDM-Zn complex was based on an earlier reported protocol with some modifications (Tan et al. 2009). DHDM ($C_{17}H_{14}O_6$) was isolated from the leaves of *A. nigra* following our earlier report (Gupta et al. 2021). The compound, DHDM (0.014 g, 0.045 mmol) was mixed with $ZnCl_2$ (0.003 g, 0.022 mmol) in 15 mL of methanol and incubated for 1 h 50 minutes at room temperature, subsequently; 30 mL of 1% PBS buffer (pH = 7.5) was added. The mixture was continuously stirred at 37°C and further incubated at 4°C for 4 h. The yellow colored precipitate formed was centrifuged at 5000 rpm for 5 min, and rinsed thrice with deionized water to remove the unreacted chemicals. The complex, $[Zn(DHDM)_2]$ obtained in the form of a pellet was lyophilized and stored at 4°C for further structural examination. Yield of the product: 0.026 g. FTIR (ATR, cm^{-1}): 1651, 1003, 563. Λ_M: 27.30 µS/cm (MeOH).

6.2.3 UV–Visible spectrophotometric studies

In brief, the interaction study between DHDM with Zn^{+2} was analyzed by mixing DHDM with $ZnCl_2$ (mole ratio = 2:1) in methanol and the absorbance was recorded in the wavelength range of 290-500 nm.

6.2.4 Fluorescence studies

The DHDM-Zn solution was prepared by dissolving a suitable amount of derivatized compound in methanol (HPLC grade). For understanding the interaction of DHDM with Zn^{+2}, initially, DHDM (2 µM) was dissolved in methanol and supplemented with 1 µM methanolic solution of $ZnCl_2$. Fluorescence spectra were analyzed in the emission range of 400-700 nm.

6.2.5 Fourier transform infrared spectroscopy

The small amount of crystalline DHDM and derivatized DHDM-Zn compound were placed on the attenuated total reflection (ATR) region of FTIR. The spectra recorded were in the range of 400-4000 cm^{-1}.

6.2.6 Raman spectroscopy studies

The crystals of both DHDM and DHDM-Zn were kept on a glass slide and loaded in the Raman spectrophotometer at 514 nm of an argon-ion laser. The spectra were examined in the range of 200-2000 cm^{-1}.

6.2.7 Conductivity measurements

The conductivity of the complex compound (DHDM-Zn) was determined by a previously described method (Ozturk et al. 2007). Briefly, constant concentration of $ZnCl_2$ (100 µM) was titrated with different concentrations of DHDM (100–300 µM) with respect to time to know the complexity and conductivity change during complex formation (DHDM-Zn). Titrations were performed in methanol solution at 25°C using VSI-04 deluxe conductivity meter.

6.2.8 Mass determination

High-resolution mass spectrometry (HRMS) of derivatized compound (DHDM-Zn) was analyzed using Agilent QTOF 6520 with electron spray ionization (ESI) technique. Mass spectrometric experiment was operated in positive mode. The data was acquired with parameters with spray voltage of 5 kV and temperature of 350°C. Typically, the sample was prepared by dissolving the derivatized compound (DHDM-Zn complex) in methanol solvent (1 mg/mL) and then again diluted to 1.5 mL with methanol. The mass spectra were recorded in the range 0-1000 m/z ratios, in positive ESI mode.

6.2.9 Nuclear magnetic resonance

Nuclear magnetic resonance (NMR) analysis was performed by dissolving the DHDM compound and derivatized compound (DHDM-Zn) in 600 µL of DMSO-d_6. Proton and ^{13}C NMR was analyzed on a Bruker 600 MHz instrument. The peaks for DMSO- d_6 appeared at δ (ppm) = 2.25. The peak for water was removed manually. The Top Spin 2.1 was performed for NMR acquisition, and Mestrenova 8.0 software was used for NMR spectra analysis.

6.2.10 SEM with EDX studies

Morphological and elemental composition analysis of the synthesized complex was performed using scanning electron microscopy (SEM) equipped with energy dispersive X-Ray analyzer

(EDX). The crystallized samples were mounted on the copper grid, and the gold coating was done before analysis.

6.2.11 Stability of DHDM-Zn in the biological media

The stability of the Zn complex in the media used for the biological evaluations was examined by UV-Visible spectroscopic technique (Basu et al. 2019; Kettle 1996). The complex compound in DMSO was added to M199 and RPMI media to get the working concentration of 100 µM and its spectra checked at different time intervals (0 h, 24 h, and 48 h).

6.2.12 Cytotoxicity assays on THP-1 cell lines

The cytotoxicity effect of the DHDM, $ZnCl_2$ and synthesized complex (DHDM-Zn) on THP-1 cell lines (Human macrophage cell) was examined by the 3-(4, 5-dimethylthiazol-2-yl)-2,5-diphenyltetrazolium bromide (MTT) assay. Briefly, 10000 cells of THP-1 were seeded in a sterile 96-well culture plate. Subsequently, these cells were treated with DHDM, $ZnCl_2$ and DHDM-Zn compound at concentrations that ranged from 50 µM to 200 µM. Cells were incubated for 24 h at 37°C in 5% CO_2 incubator. After that the cells were centrifuged at 2500 rpm for 15 min. Pelleted cells were suspended in MTT (working concentration~0.5 mg/mL), which was further incubated at 37°C for 3 h. After incubation, the cells were again centrifuged at 4500 rpm for 45 min. The formazan crystals thus formed were dissolved in DMSO (200 µL), and the absorbance was recorded at 570 nm. All experiments were performed in triplicate.

6.2.13 Anti-leishmanial activity

The effect of the DHDM, $ZnCl_2$ and synthesized complex (DHDM-Zn) on *L. donovani* promastigotes (parasite) was executed through the MTT assay as documented earlier, with some modification (Kumar et al. 2017). In brief, one million (1×10^6 parasites/mL) cells of *L. donovani* cells were seeded in a sterile 96-well plate. Consequently, these cells were treated with DHDM, $ZnCl_2$ and DHDM-Zn at a varying concentrations from 20 µM to 100 µM. Cells were incubated for 24 h at 25°C, pelleted at 4500 rpm for 45 min. Pelleted cells thus obtained were suspended in MTT solution (working concentration~0.5 mg/mL). The samples were further incubated at 25°C for 3 h. After which the cells were re-centrifuged at 4500 rpm for 45 min and formazan crystals formed were dissolved in DMSO (200 µL). The absorbance was measured at 570 nm. As a

negative control, 0.2% DMSO was taken, whereas miltefosine (IC_{50}, 20 µM) was kept as a positive control. The concentration of the DHDM-Zn at which 50% inhibition was achieved was taken as IC_{50} value. All experiments were performed in triplicate.

6.2.14 Promastigote growth analysis

The growth curve study of *L. donovani* promastigote cells was analyzed in the presence and absence of the DHDM-Zn complex. In addition, we also examined the effect of DHDM (100 µM) and $ZnCl_2$ (100 µM) on the growth of *L. donovani* promastigotes. In brief, $1x10^5$ cells/mL were inoculated in 5 mL M199 media, in triplicates. Counting the cells at every 24 h interval by the aid of hemocytometer monitored cell growth.

6.2.15 Cell cycle analysis

The cell cycle was analyzed using flow cytometry methods following the method described earlier with some modifications (Wheeler et al. 2011). In brief, $2×10^5$ *L. donovani* promastigote cells were treated with IC_{50} (63.7 µM) of DHDM-Zn for 24 h at 25°C. Cells were centrifuged at 2500 rpm for 7 min to remove dead cell debris and washed thrice with pre-chilled phosphate buffer saline (pH=7.5). Subsequently, the promastigote cells were fixed with 70% methanol (pre-chilled) and incubated for 18 h at -20°C. The cells were centrifuged at 4500 rpm, washed thrice with PBS (chilled), and then incubated with RNase A (200 µg/mL) for 30 min at 37°C. Afterwards, the cells were treated with PI (20 µg/mL), incubated at 37°C for 30 min in the dark. Data were acquired in BD flow Cytometer and analyzed using FlowJo_V10 software. Untreated promastigote cells were analyzed as a negative control, and unstained parasite promastigote cells were used to set background fluorescence.

6.2.16 DNA content

The total genomic DNA content of promastigote cells of the untreated and treated samples for 24 h with IC_{50} of the derivatized compound (63.7 µM) and IC_{50} of miltefosine (20 µM) was quantified at 260/280 nm by spectrophotometer (Saudagar and Dubey 2014). Briefly, $1×10^8$ promastigotes cells were pelleted down and dissolved in lysis buffer (500 µL). The lysis buffer was prepared using 10 mM EDTA, 50 mM Tris-HCl and 0.5% SDS; pH 7.5. Afterwards, 100 µg/mL of proteinase K was added to the mixture, vortexed thoroughly, and kept at 37°C for 1 h.

Subsequently, 25:24:1 ratio of phenol-chloroform-isoamylalcohol (500 µL) was added and centrifuged at 15000 rpm for 15 min. The upper phase was collected to which 2 volumes of 100% ethanol and 1/10th volume of 3 M sodium acetate were added and incubated at -20°C for 24 h. The DNA sample was centrifuged for 20 min at 15000 rpm and washed twice with 70% ethanol (800 µL). The pellet containing DNA was dissolved in TE buffer and quantified.

6.3 Result and discussion

6.3.1 Derivatization and characterization of DHDM- zinc complex

The complex was synthesized by mixing the ligand, DHDM, and Zn^{2+} in 2:1 ratio in methanol (Scheme 1). The complex was obtained as crystalline yellow solid. Characterization of the compound was performed with spectroscopic techniques such as UV-visible, EDX, FTIR, Raman, HRMS, and NMR (^{13}C, ^{1}H) spectroscopy.

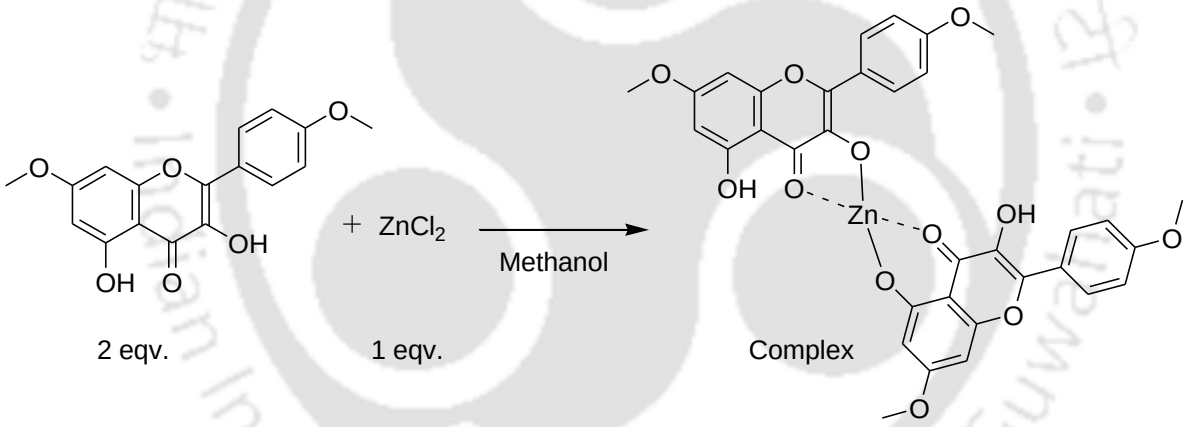

Scheme 1. Reaction scheme of the complexation of DHDM with Zn^{2+}

6.3.2 UV spectroscopic

The interaction study of Zn with DHDM was analyzed through UV spectroscopic technique. The UV–vis absorbance spectra of the derivatized product and the isolated DHDM was in the range of 200 to 500 nm **(Fig. 6.1A)**. The isolated compound (DHDM) displayed two major peaks; 263 nm (band II) and 367 nm (band I), while the complex (DHDM-Zn complex) showed absorption at 267 nm (band II) and 421 nm (band I). Benzoyl system absorption was associated with band II, while cinnamoyl system absorption corresponded to band I (Lee and Tuyet 2019). The bands may be attributed to HOMO–LUMO energy gaps. The first absorption band has $\pi \rightarrow \pi^*$

character. After coordination with Zn^{2+}, the UV spectra of DHDM showed a bathochromic (red) shift. This bathochromic shift is caused by a strong charge transfer from the flavonoid to the metallic center, while others attribute the shift to a decrease in the HOMO–LUMO gap in the flavonoid molecule, rather than to an ligand to metal charge transfer (LMCT) transition. In contrast, a notable band I shifted after complexation with zinc metal. The minor shifting of the band II in the complex indicated that C5-OH was not directly involved in the interaction with the metal ion. This assumption could be inferred due to less steric hindrance of C5-OH, as described in the earlier reports as well (De Souza and De Giovani 2004; Tu et al. 2016).

6.3.3 Fluorescence studies

The fluorescence study of DHDM and derivatized compound DHDM-Zn was carried out in the range of 400-700 nm. The emission maxima of fluorescence spectra were acquired at 505 nm for the derivatized compound, whereas DHDM did not show significant emission intensity (**Fig. 6.1B**). As displayed in figure 1B, the emission intensity of the derivatized compound was significantly higher as compared to the isolated compound DHDM. Additionally, the binding efficacy of Zn on DHDM was also evaluated from the primary finding of UV spectral analysis. Such interaction was also validated in an earlier report performed using kaempferol-Zn complex (Tu et al. 2016). The result suggested that flavones can be conjugated with zinc metal ion by the interaction of metal ion through π electrons or carbonyl group of flavones (Uivarosi and Munteanu 2017), thereby promoting the zinc metal ion binding and stabilizing the complex. This finding revealed that the complex formation enhances the coplanarity of the derivatized compound.

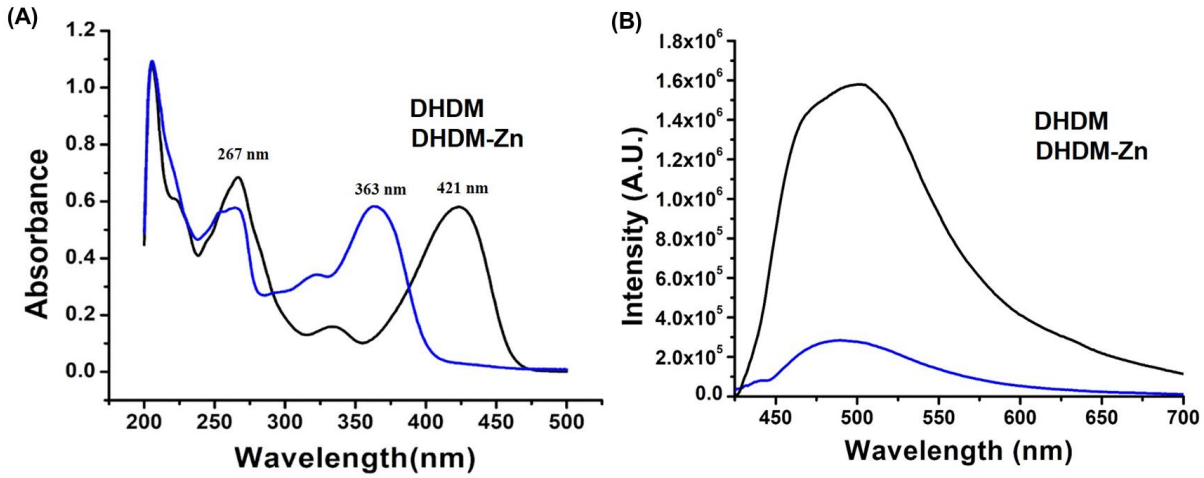

Fig. 6.1 (A) UV visible spectra of DHDM and DHDM-Zn complex, showing a notable band I shift after complexation with zinc metal. (B) Emission spectra of DHDM and DHDM-Zn showing peak at λ421.

6.3.4 FTIR analysis

The broad peak in 3100-3400 cm^{-1} regions confirmed the presence of hydroxyl group in the compound, DHDM, and derivatized DHDM-Zn complex. An earlier report on the FTIR spectral analysis of DHDM showed some of the characteristic stretching's of DHDM at 3313 cm^{-1}, 1648 cm^{-1}, 1596 cm^{-1}, and 1159 cm^{-1}, corresponding to the presence of hydroxyl (O-H), carbonyl group (C=O), C=C (aromatic), C-O (stretch), respectively (Gupta et al. 2021). The shift in the CO stretches of DHDM was observed in the complex (Fig. 2a). The zinc ion perhaps coordinated between the hydroxyl oxygen atoms (C3-OH) and the carbonyl oxygen atoms (C4=O). Maximum shift observed for the C-O stretch from 1159 to 1003 cm^{-1}. Moreover, a peak at 563 cm^{-1} revealed Zn-O bond stretching present in the DHDM-Zn complex. The peak was absent in the DHDM spectrum**.** This confirmed the formation of the zinc metal complex (**Fig. 6.2A**).

6.3.5 Raman spectroscopy

The Raman spectrum of isolated and derivatized compounds was performed at 514 nm excitation wavelengths. The most prominent bands were obtained at ~791.48, ~1182.83, and ~1625.32 cm^{-1}, as shown for the DHDM compound (**Fig. 6.2B**). The first two bands were associated with bending vibrations of C–H bonds and C-O stretch in both molecules, whereas the third band was obtained due to stretching of C=O bond. However, for the synthesized compound (DHDM-Zn),

the relative intensity of the Raman band at 433.26 cm^{-1} represented the characteristic absorption of the Zn-O stretched bond. Other peaks were comparatively similar to the DHDM compound. The data obtained were validated against previously reported findings (Bhunia et al. 2016).

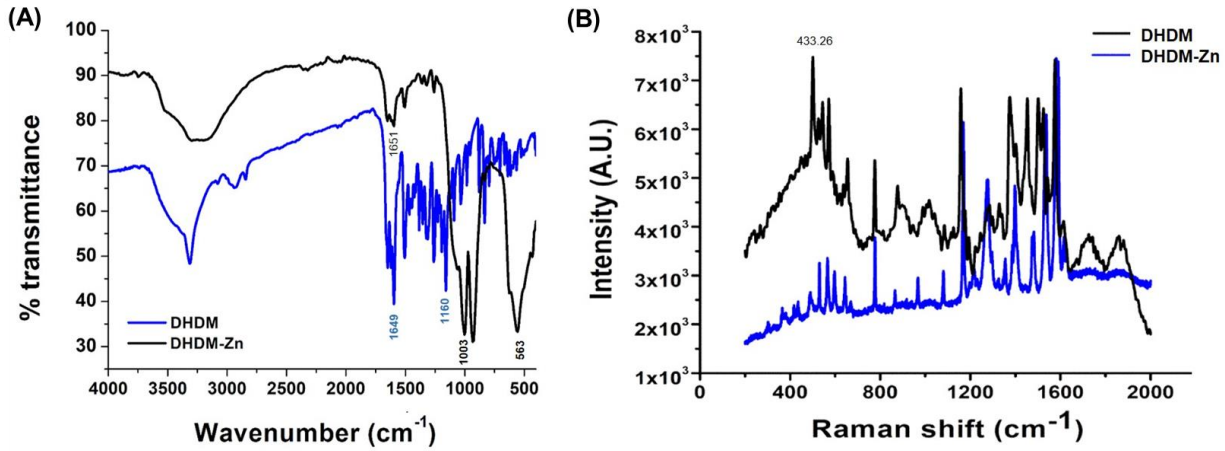

Fig. 6.2 Comparison of (A) FTIR spectra and (B) Raman spectra of DHDM and DHDM-Zn derivatized compound.

6.3.6 Conductivity measurements

Molecular composition and electrolytic nature of complex can be studied by conductivity measurements (Robert et al. 1975). Molar conductance depends on the solvent system used (Ozturk et al. 2007). To understand the composition of the complex formation of DHDM-Zn, we performed conductivity titration of DHDM by $ZnCl_2$ in methanol solution at different time points. At baseline $ZnCl_2$ concentration, DHDM has shown a conductivity of ~4.48 µS/cm in methanol solution. The conductivity increases to a value ~27.30 µS/cm when the [$ZnCl_2$]/[DHDM] ratio is increased to 1:2 (molar ratio) (**Fig. 6.3**). This can be attributed to the formation of a non-electrolytic complex in methanol. The [$ZnCl_2$]/[DHDM] ratio 1:2 showed the maximum change in conductivity, indicating that two molecules of DHDM bind with one molecule of zinc. Conductance value of ~27.30 µS/cm in methanol of the complex is due to the partial ionization due to hydrogen bonding in methanol which is a protic solvent capable of forming hydrogen bonding. Comparison with the literature confirmed the partial ionization due to hydrogen bonding (Sahoo and Ray 2010; Geary 1971). The ^1H NMR and ESI mass data confirmed the non-electrolytic behavior of the complex. The phenolic OH groups are acidic in

nature, and get deprotonated in presence of Zn^{2+} to give mono-negative ligand, thereby forming neutral [$Zn(DHDM)_2$] complex.

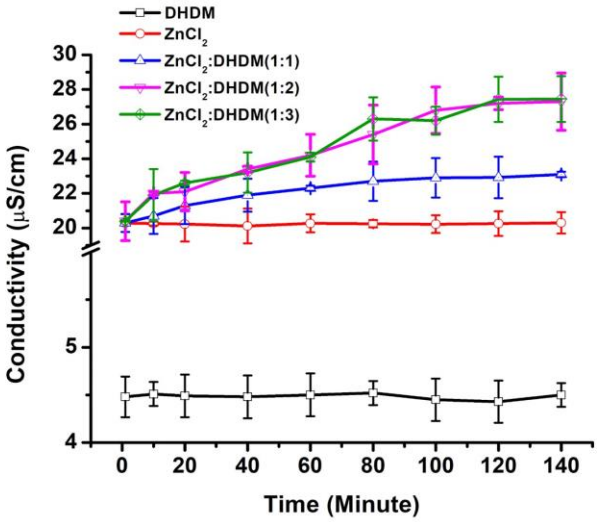

Fig. 6.3 Conductivity titrations of $ZnCl_2$ (100 µM) with varying concentrations of DHDM (100-300 µM) in methanol at 25°C showing DHDM-Zn complex formation.

6.3.7 Mass spectrometric analysis

High-resolution mass spectrometric (HRMS) was executed to know the mass and compound metal interaction in positive and negative ion mode. Earlier report suggests positive ion mode of electrospray ionization mass spectrometry (ESI-MS) to detect and study metal-protein interaction (Guo et al. 2019). Here in, positive ion mode of ESI-MS has been applied to detect and study compound-metal interaction. The pattern of the complex in the presence of methanol is shown (**Fig. 6.4A**). The prominent peaks found at m/z 315.0736, 377.0653, 691.9404. These peaks are assigned to $[DHDM+H]^+$, $[Zn(DHDM –H)]^+$, $[Zn(DHDM\text{-}H)_2+H]^+$ respectively (**Table 6.1**). It indicated coordination of Zn(II) to DHDM. The interaction could be through the C3-OH and C4=O groups of the DHDM molecule. Generally, ESI-MS generates an isotopic spectral pattern of charged metal-ligands that is primarily identified by the relative abundance of isotopic spectra. These spectra are known as metal-specific isotopic patterns (Tsednee et al. 2016). The data implies that each DHDM combines one Zn(II) ion to form a conjugate ring. The mass spectra data confirmed the formation of DHDM bis complex of Zn^{2+}. The proposed structure of complex is shown (**Fig. 6.4B**).

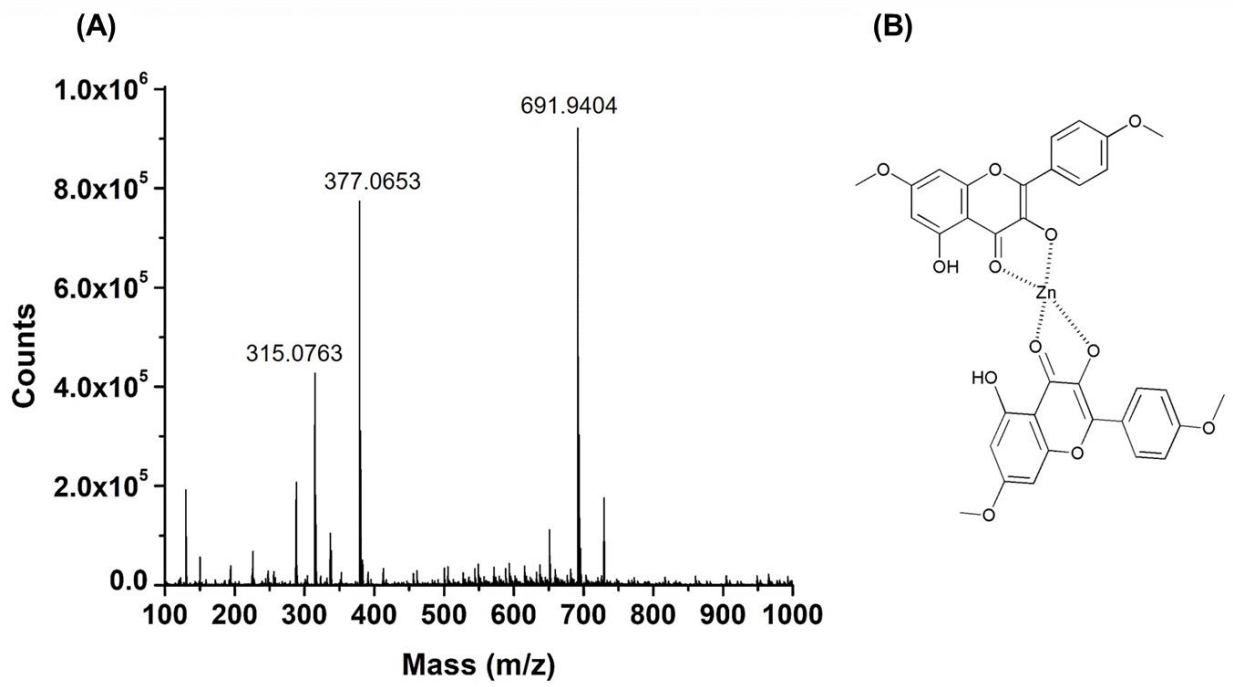

Fig. 6.4 (A) HRMS spectra of DHDM-Zn complex in methanol displaying the molecular ion $[M+H]^+$ peak at m/z 377.0653 and at m/z 691.9404 (B) The predicated structure of the $[Zn(DHDM)_2]$ complex.

Table 6.1 The mass (m/z) data of DHDM-Zn complex.

Structure	**Calculated**	**Found**
$[DHDM+H]^+$	315.0863	315.0736
$[Zn(DHDM –H)]^+$	377.0003	377.0653
$[Zn(DHDM-H)_2+H]^+$	691.0788	691.9404

6.3.8 NMR spectroscopy

The ^{13}C NMR of DHDM and complex DHDM-Zn were analyzed for the confirmation of carbon position and number in complex compound. The ^{13}C NMR spectrum of compound (DHDM) showed the presence of 17 carbon atoms, indicating the presence of aromatic carbon, -OCH_3 and quaternary carbons. Two peaks at δ (ppm) = 55.43 and 55.77 indicated carbons linked to an oxygen atom in –OCH_3 group. The –C=C was confirmed by the signal at δ (ppm) = 156.57 and δ = 160.73. The presence of other carbon peaks was ascertained by the signals at δ 92.43, 97.93, 114.71, 123.44, 130.13, 136.92, 147.20, 161.36, 165.52, 176.45 (**Fig. 6.5A**). However, the ^{13}C

NMR spectrum for the synthesized compound (DHDM-Zn) showed the presence of 17 carbons and represented chemical shifting **(Fig. 6.5B**). The chemical shift changes due to complex formation are most noticeable for carbon position at C3, C4, and C5. The chemical shifts are represented in **Table 6.2**, supporting a direct comparison between the chemical shifts of the ligand (DHDM) and the metal complex (DHDM-Zn). The signals for C3 and C5 from DHDM-Zn showed downfield shifts whereas C4 showed an upfield shifts as a result of the coordination to the metal ion (Ahmedova et al. 2012). Maximum shift in δ value observed for C5 position (161.36-160.66) although the changes in chemical shift values of these carbon atoms in ^{13}C NMR was less in comparison with that observed for the respective protons. This might be due to very less sensitivity of ^{13}C NMR. The ^{1}H NMR (highly sensitive) spectra clearly showed significant changes of hydrogen peak of (C3-OH) after complexation. It is absent after complexation. The spectra were taken in DMSO where proton exchange is minimum. It confirmed the zinc metal ion complexation with DHDM.

The synthesized DHDM-Zn complexed compound was further characterized using the ^{1}H- NMR spectrometry. The peaks at δ (ppm) = 6.62 (C3-OH), 6.40 (C6-H), 6.51 (C8-H), 7.05 (3′, 5′-H), 8.20 (2′, 6′-H) and 11.80 (C5-OH) appeared in isolated DHDM, while the derivatized compound (i.e., DHDM-Zn) showed peaks at δ (ppm) = 6.35 (C6-H), 6.75 (C8-H), 7.18 (3′, 5′-H), 8.18 (2′, 6′-H) and 12.41 (C5-OH). ^{1}H-NMR peak exhibited one major peak at δ 6.62 (C3-OH), which was present in DHDM (**Fig. 6.5C**). In contrast, this major peak was absent in the derivatized compound (DHDM-Zn), because it was involved in zinc chelation during conjugation (**Fig. 6.5D)**. Besides, the peak at δ (ppm) = 11.80 in the DHDM shifted towards δ (ppm) = 12.41 in case of DHDM-Zn. The ^{1}H-NMR data indicated a strong intramolecular hydrogen bond made by C5-OH proton and a carbonyl oxygen atom (C4=O) (Primikyri et al. 2015).

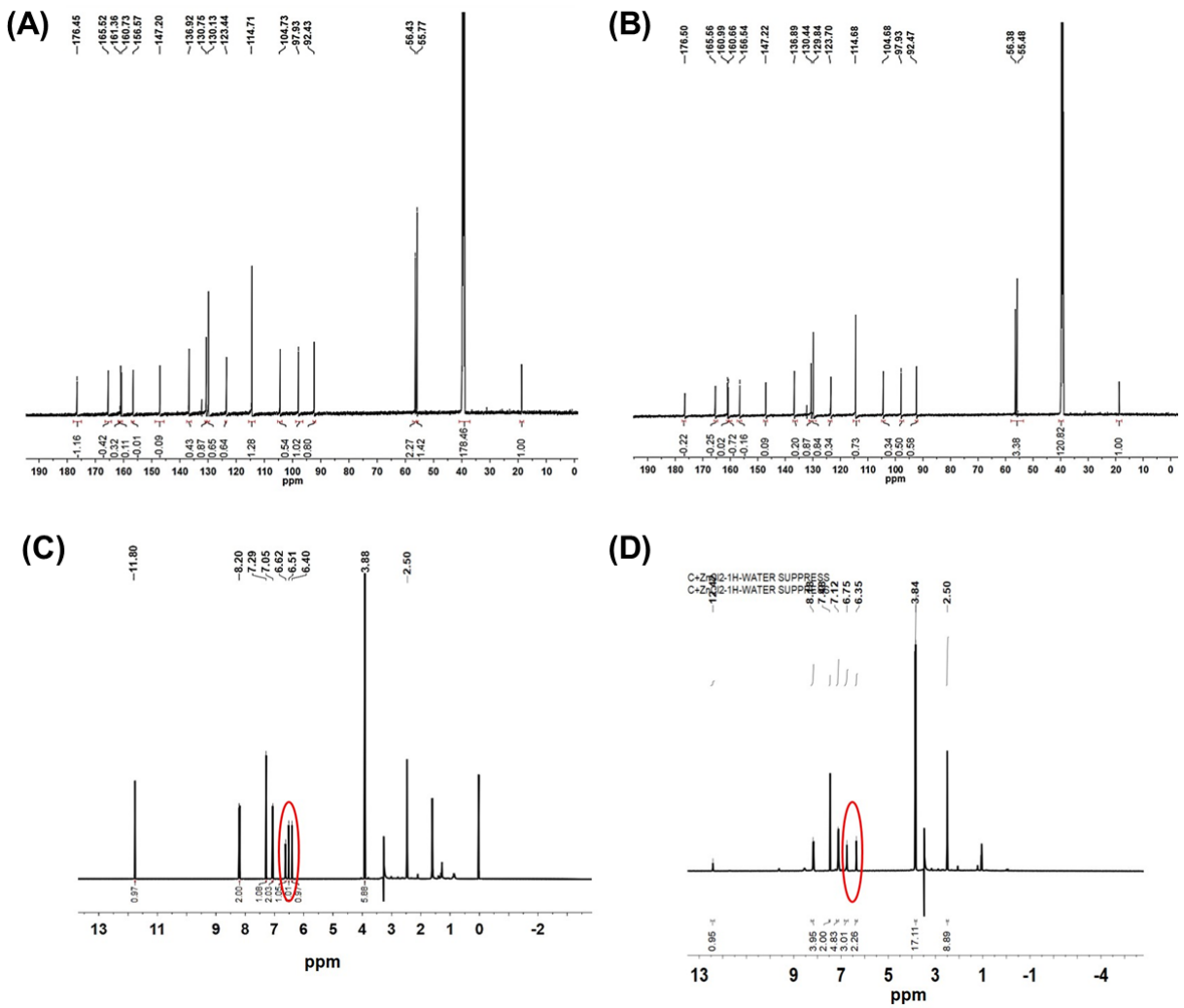

Fig. 6.5 Comparison of ^{13}C NMR spectra of DHDM (A) and its Zn^{2+} complex (B); and ^{1}H NMR spectra of DHDM (C) and its Zn^{2+} complex (D).

Table 6.2 ^{13}C and ^{1}H-NMR of 3,5-dihydroxy-4',7-dimethoxyflavone (DHDM) and complex compound (DHDM-Zn). δ and J denotes chemical shift and coupling constant respectively.

Position	(DHDM) δ_C	(DHDM-Zn) δ_C	(DHDM) δ_H (J Hz)	(DHDM-Zn) δ_H (J Hz)
1′	123.44	123.70		
2	147.20	147.22		
2'6'	130.13	129.84	8.20, d, (2H, J =9 Hz)	8.18,d, (2H, J =9 Hz)
3	136.92	136.89	6.62, s, (1H)	
3'5'	114.71	114.68	7.05, d, (2H, J = 9 Hz)	7.18, d, (2H, J = 9 Hz)
4	176.45	176.50		
4'	160.73	160.99		
4a	104.73	104.68		
5	161.36	160.66	11.80, s, (1H)	12.41, s, (1H)
6	97.93	97.93	6.40, d, (1H, J =1.8 Hz)	6.35, d, (1H, J =1.8 Hz)
7	165.52	165.56		
8	92.43	92.47	6.51, d, (1H, J= 1.8 Hz)	6.75, d, (1H, J = 1.8 Hz)
8a	156.57	156.54		
OCH_3-4'	55.43	55.38	3.88, s, (3H)	3.84, s, (3H)
OCH_3-7	55.77	55.48	3.88, s, (3H)	3.84, s, (3H)

6.3.9 FESEM-EDX analysis

Elemental analysis of the derivatized compound was examined by energy dispersive X-Ray analysis (EDX). EDX is an X-Ray based technique used to identify and confirming the elemental composition of materials (Scimeca et al. 2018). The data produced by EDX analysis consist of spectra showing peaks corresponding to the elements making up the true composition of the materials. SEM is helpful in analyzing the morphology of the sample and provides topographical information. The surface morphology of the derivatized DHDM-Zn was mostly rod shaped. The complex displayed aggregation of the derivatized product (**Fig. 6.6A**), and it provided clear information on DHDM-Zn conjugation. The size of DHDM-Zn was distributed in the range of 70-90 nm **(Fig. 6.6B**). In EDX, the characteristic X-ray emission corresponded to a specific atom

(Selvarajan and Mohanasrinivasan 2013; Dobrucka and Długaszewska 2016). EDX spectrum displayed elemental peaks, which were identified as carbon, zinc, and oxygen. The weight % values of carbon, oxygen, and zinc were obtained at 62.1, 29.2, and 8.8, respectively, from the EDX spectrum (**Fig. 6.7B**). SEM elemental mapping of synthesized compound was analyzed and displayed as oxygen, carbon, and zinc element, respectively (**Fig. 6.7D-F**). This FESEM-EDX analysis was performed for the Zn metal confirmation in the complex compound. Fundamentally the elemental percentage values obtained from FESEM-EDX analysis are less sensitive and qualitative (Atkins and Overton 2010). We did not calculate and report the atomic mol ratio from the EDX result.

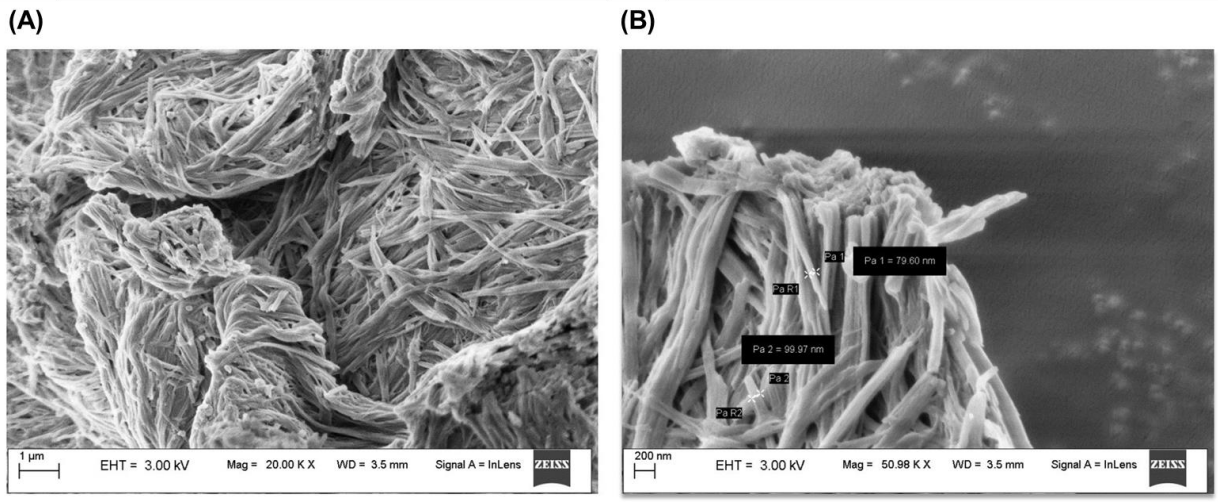

Fig. 6.6 FESEM image of the synthesized DHDM-Zn complex. (A) Shape: Cluster of rod shaped DHDM-Zn complex. (B) Size: 79-99 nm.

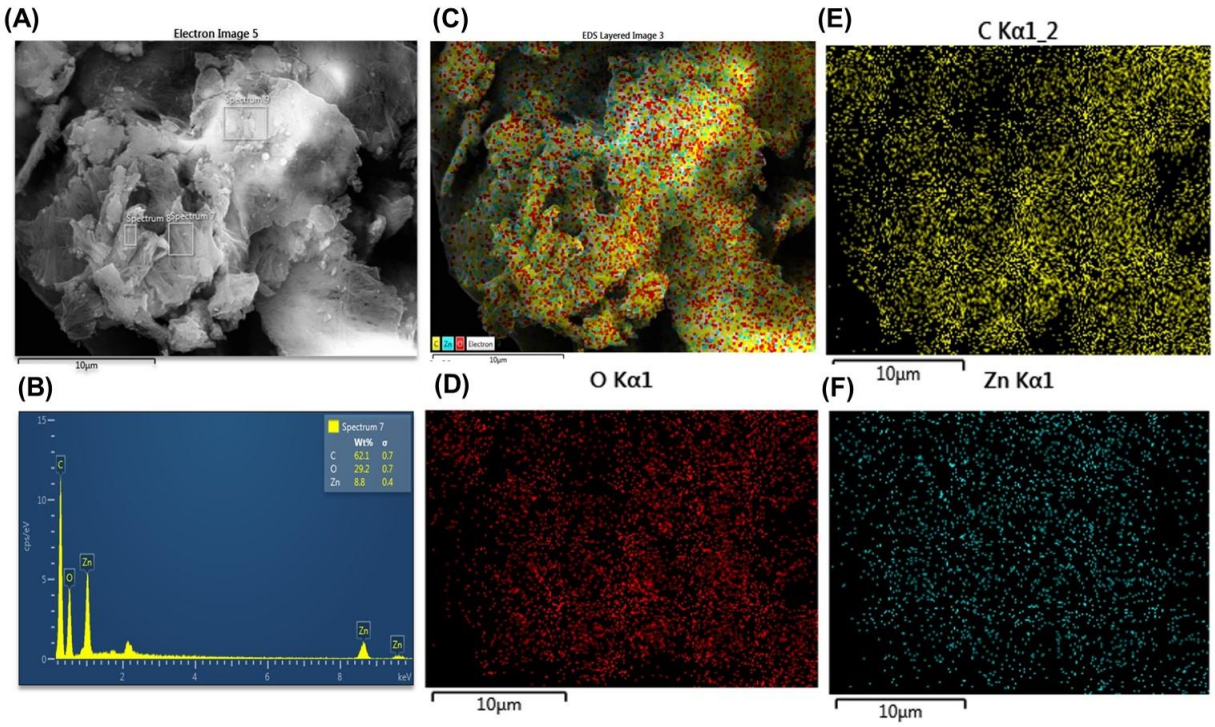

Fig. 6.7 (A) FESEM-EDX image of the DHDM-Zn complex. (B) EDX spectrum of DHDM-Zn complex showing 62.1% of carbon, 29.2% of oxygen, and 8.8% of Zn elements (C) SEM elemental mapping image of DHDM-Zn complex showing Oxygen (D), Carbon (E), and Zinc (F) elements.

6.3.10 Stability of DHDM-Zn in the biological media

The stability of a compound is an important parameter to study its use as a biologically active compound in biological medium; hence stability of DHDM-Zn has been thoroughly investigated in this study. The complex stability was examined in the biological media (M199 and RPMI media) at different times using UV-visible spectroscopy. The UV-vis absorption band was observed at 380 nm and 420 nm in M199 media and 391 nm and 420 nm in RPMI media. The absorption band was prominent at each time intervals (**Fig. 6.8**), affirming that the complex was stable in biological media.

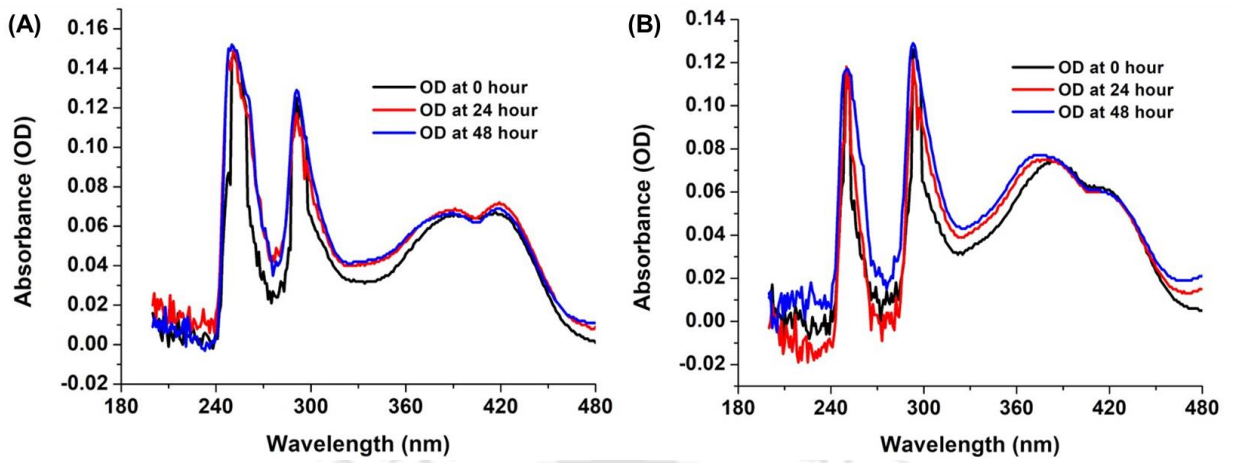

Fig. 6.8 UV-vis spectra of DHDM-Zn complex for stability determination in biological media (A) In RPMI media (B) In M199, at the different times (0 h, 24 h, 48 h).

6.3.11 Cytotoxicity assays on THP-1 cell lines

Cytotoxicity studies are essential for the development of therapeutic medicine (Lue et al. 2017). The possible cytotoxicity of DHDM, $ZnCl_2$ and complex (DHDM-Zn) towards the THP-1 cell (a human monocytes cell line) was executed. While, the compound DHDM and DHDM-Zn represented no significant toxicity on THP-1 cells, $ZnCl_2$ showed toxicity at the higher concentrations (100-200 μM) (**Fig. 6.9**). Hence, the result suggested that derivatized compound (DHDM-Zn) of non-toxic in nature even at a 200-μM concentration after 24 h of exposure. THP-1 cells are human macrophages earlier used as a studied model for human monocytes (Bosshart et al. 2016). Macrophages and monocytes belong to the innate immune system, in which their key roles are recognition and to eliminate foreign pathogens such as viruses, fungi, bacteria, and parasite. Macrophages also play a role in proliferation to increase the amount of cells that are able to engulf and digest pathogens (Das et al. 2003). Our current finding corroborates with earlier similar work and showed the efficacy of zinc complex (DHDM-Zn) against *L. donovani* for the development of new drug entities to cure parasitic disease.

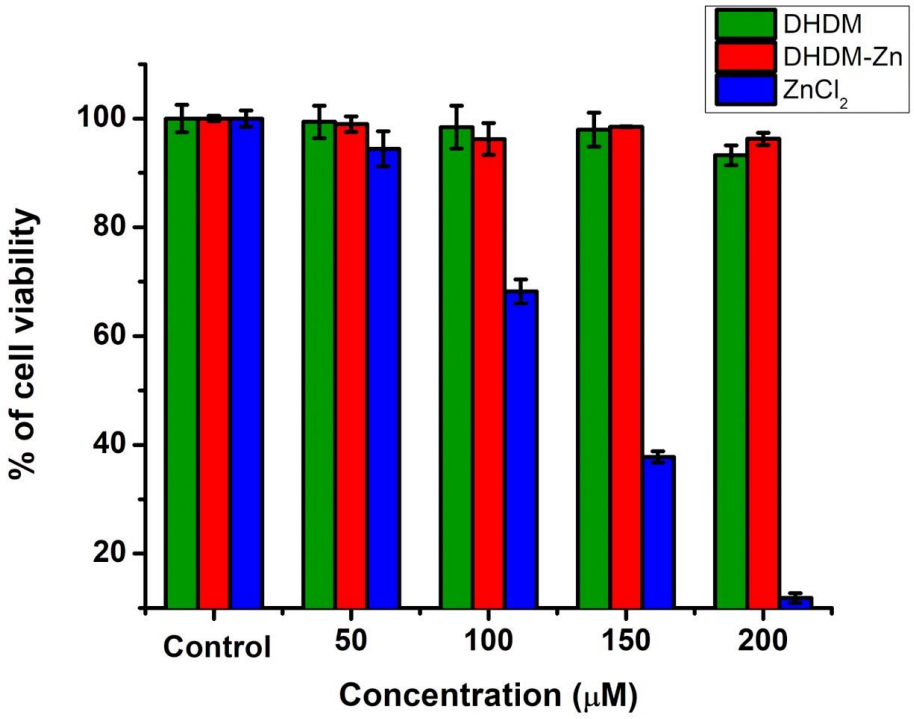

Fig. 6.9 Cytotoxicity effect of the DHDM, $ZnCl_2$ and DHDM-Zn on THP-1 cell line (Human macrophage cell). The effect of compound analyzed in THP-1 cell line through MTT assay demonstrated that only $ZnCl_2$ displayed toxicity when concentration reached more than 100 µM whereas compounds DHDM and DHDM-Zn are not cytotoxic to the normal THP-1 cells up to 200 µM.

6.3.12 Anti-leishmanial effect of DHDM-Zn

L. donovani promastigote cells (1×10^6 cells/mL) were exposed to varying doses (20 µM to 100 µM) of DHDM, $ZnCl_2$ and derivatized DHDM-Zn for 24 h to examine its role as an anti-leishmanial compound. DHDM-Zn displayed considerable leishmanicidal activity with IC_{50} value of 63±0.73 µM (**Fig. 6.10**). Meanwhile, the compound DHDM showed no significant effect but $ZnCl_2$ showed ~10% inhibition of *L. donovani* promastigote cells at higher concentration (100 µM). Interestingly, beyond the concentration of 100 µM of the DHDM-Zn, the promastigote cells showed baseline absorbance. During the anti-leishmanial study, DMSO (0.2%) treated promastigote cells were used as a negative control, which showed no observable incidence of death. Besides, cells treated with miltefosine were taken as a positive control. This study is important as many aspects of the derivatized compound activity on *Leishmania* species,

are executed on promastigote cells. Promastigotes and amastigotes are parasitic forms; evaluations through these promastigote forms of *L. donovani* are relevant and reveal the possible leishmanicidal activity (Araújo et al. 2019).

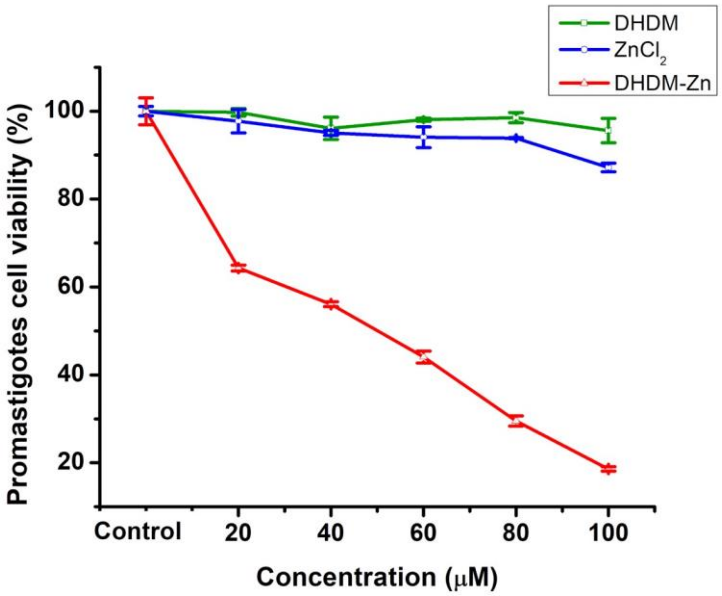

Fig. 6.10 The anti-leishmanial activity of the DHDM, $ZnCl_2$ and DHDM-Zn synthesized compound on *Leishmania donovani* promastigotes showing decreasing % of cell viability of promastigotes (parasite) on exposure to increasing concentration of the synthesized complex (DHDM-Zn) upon 24 h treatment.

6.3.13 Growth curve analysis

Comparative study of promastigote growth curves of the treated and control cells of *Leishmania* revealed that the cells entered the logarithmic growth phase after two days in the culture (**Fig. 6.11A**). The stationary phase was obtained after an average of 4 or 5 days. Significant growth inhibition in the cells was observed on the 3rd day in treated promastigote upon treatment with DHDM-Zn (IC_{50}). The difference in the number of cells in the treated and untreated samples on 3rd day was also observed (**Fig. 6.11B**), confirming the reliability of growth curve data. No significant growth inhibition was observed in case of DHDM (100 µM) and $ZnCl_2$ (100 µM) treated sample. The rate of growth was significantly slow compared to untreated cells. Since infectivity is related to the metacyclogenesis of both strains (wild type and resistance), host cell infectivity of stationary-phase of parasite promastigotes was specifically examined (Borrell and Gagneux 2009; Hendrickx et al. 2015). Although treating with the derivatized compound

inhibited cell growth of promastigote form of *L. donovani* parasite, this finding could have an impact on inhibition of the infectivity of promastigote.

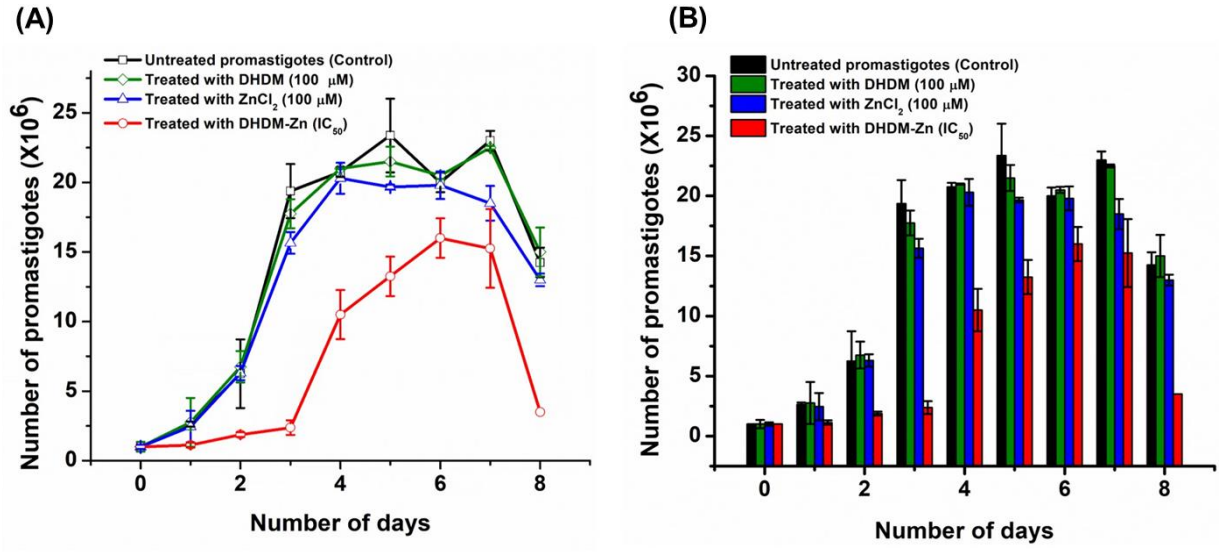

Fig. 6.11 Comparative growth curve analysis of *Leishmania* promastigote cells for untreated (control) and treated with DHDM, $ZnCl_2$ and DHDM-Zn complex showing significant difference in the promastigote counts. (A) The tested cells entered the logarithmic growth phase after 2 days in culture and the stationary phase was achieved after an average of 4 to 5 days for the untreated cells (B) The Bar graph shows that compared to the untreated cells, DHDM-Zn treated cells has a significantly lower growth rate.

6.3.14 Cell cycle analysis

Growth inhibition of promastigotes in a particular stage of the cell cycle was examined through flow cytometry. The emitted fluorescence intensity of bound PI associated with the quantity of DNA percentage of G1 peak corresponded to the cell arrests in the phase. Only 73.6% of promastigote of the control cells (0.2% DMSO treated) were arrested in the G1 region (**Fig. 6.12A**) while promastigote cells treated with IC_{50} of DHDM-Zn for 24 h resulted in 89.1% of cell arrest in the G1 region (**Fig. 6.12B**). These data suggested that there was the augmentation of cells in the G1 region by extending the G1 phase, due to the arrest of the cell cycle through the G1/S checkpoint and DNA arrest prevents the initiation of nuclear division in the targeted parasite. A similar study described the initiation of arrest in the G0/G1 phase by leishmanicidal compounds, dibenzalacetone. This compound was reported earlier to possess anti-leishmanial activity by changing the cell cycle profile by a rise in the G0/G1 phase, which is correlated with

the decrease in the DNA content in the S phase and G2/M phases of the parasite promastigotes (Chauhan et al. 2018). This study reveals for the first time, the anti-proliferative effect of DHDM analog (DHDM-Zn) in the extracellular promastigotes of *L. donovani*. The anti-proliferative effects observed represented a more prominent effect of DHDM-Zn against extracellular promastigotes.

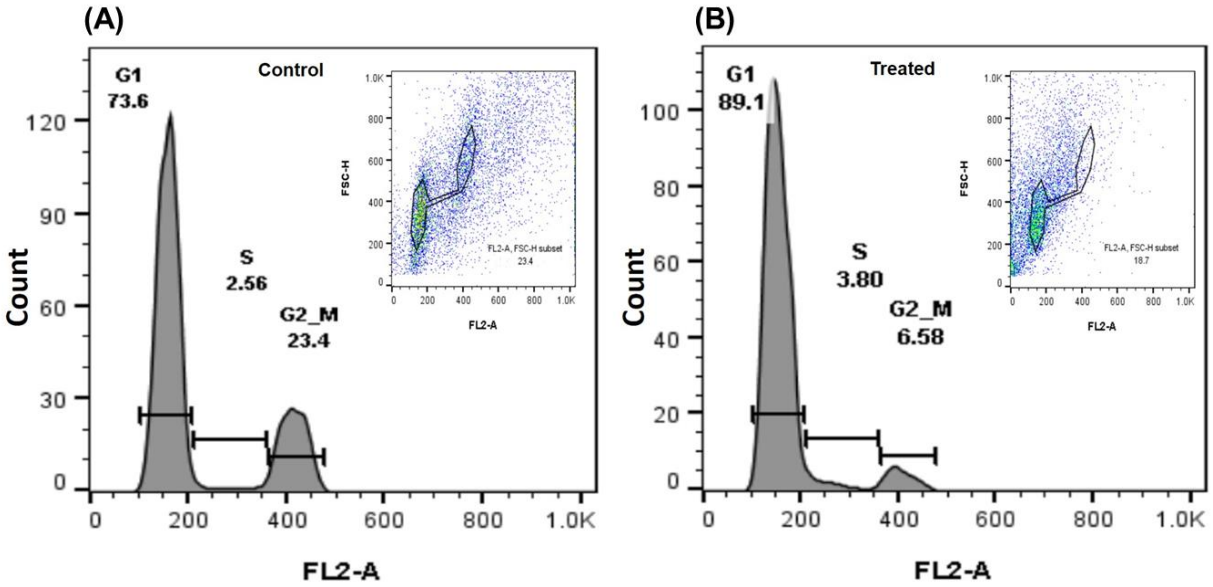

Fig. 6.12 The DNA content analysis using flow cytometry after 24 h treatment of *Leishmania donovani* promastigotes cells. (A) The control cells (promastigote cells treated with 0.2% DMSO) were found 73.6% in the G1 region, 2.56% in the S phase, and 23.4% in the G2/M phase. (B) Leishmanial cells treated with IC_{50} of DHDM-Zn resulted in 89.1% cells in the G1 region, 3.8% in the S phase and 6.58% in G2/M phase.

6.3.15 DNA content determination

DNA content analysis of *Leishmania* promastigotes was used to estimate the amount of DNA on treatment with IC_{50} value of the positive control (miltefosine) and derivatized compound for 24 h. The DNA content was quantified to be 283±0.81 ng/µL in the untreated sample, whereas *Leishmania* cell treated with IC_{50} of positive control for 24 h resulted in 50±0.53 ng/µL and 65.5±0.36 ng/µL for DHDM-Zn **(Fig. 6.13**). Thus, suggesting that DNA content may be lower due to inhibition in the initiation of nuclear division in *L. donovani*. A similar experiment was performed where it was shown that some flavonoids tend to bind with topoisomerase 1 and prevent nuclear division in *Leishmania* cells (Singh and Dey 2007). In comparison with the

potent drug miltefosine, which is used clinically for curing leishmanial diseases, DHDM-Zn exhibited closer efficacy to that of reported positive control.

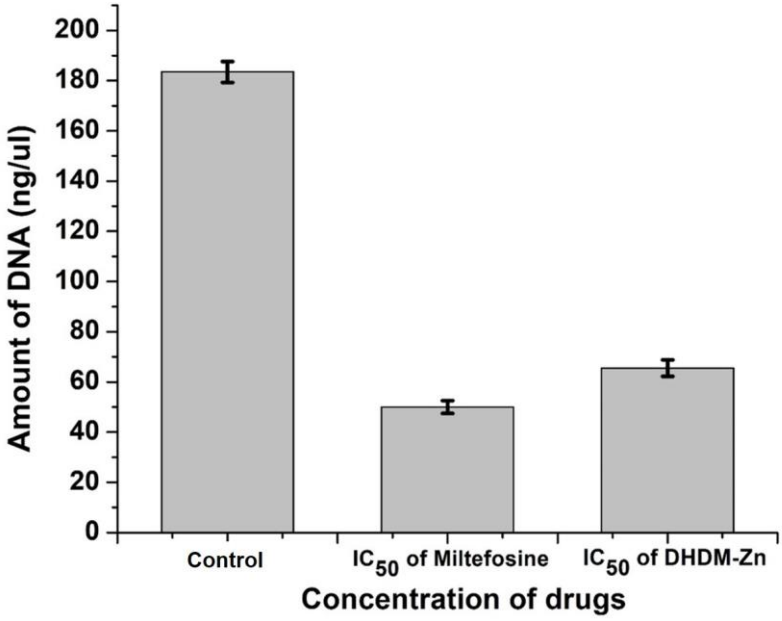

Fig. 6.13 DNA content determination of promastigote cells of *L. donovani* through IC_{50} value of potent drug (miltefosine) and newly derivatized compound (DHDM-Zn) after 24 h treatment.

6.4 Conclusions

In the current work, we used Zn^{2+} complex of DHDM to enhance their anti-leishmanial effect. The complex, $[Zn(DHDM)_2]$ was characterized using UV-vis spectroscopy, HRMS, NMR, Raman, and FESEM- EDX. The complex compound showed two major peaks in UV-visible spectra; band I shift was attributed to C3-OH interaction with the metal ion. Further, the shifting of band I was confirmed by emission maxima of fluorescence spectra. In the Raman and FT-IR spectrum of Zinc(II) complex compound, the most intense peak revealed the vibration signal of Zn-O existing in the DHDM-Zn complex. ^1H NMR confirmed the coordination of Zn^{2+} with the C3-OH and C4=O group of DHDM. The ESI mass spectra confirmed the formation of bis complex, $[Zn(DHDM)_2]$.

In vitro cytotoxic activity of DHDM, $ZnCl_2$ and DHDM-Zn complex was examined for THP-1 cell line (macrophage cell) at concentrations ranging from 20 to 200 µM. $ZnCl_2$ showed

toxicity at concentration range of 100 to 200 µM but DHDM and derivatized compound (DHDM-Zn) showed no toxicity. Meanwhile, DHDM-Zn displayed considerable leishmanicidal activity (~63±0.73 µM). Interestingly, we observed that beyond the concentration of 100 µM of the conjugated compound, the promastigote cells showed only baseline absorbance. In contrast, the compound represented no significant toxicity on healthy THP-1 cells, a vital and key prerequisite of any drug candidate. Significant growth inhibition in the promastigote cells was observed upon DHDM-Zn (IC_{50}) treatment. Promastigote cells were arrested at the G1 phase as confirmed through cell cycle analysis. Further, DHDM-Zn showed a similar reduction of DNA content of promastigote cells as miltefosine. Our study suggested that metal derivative compound could have better anti-leishmanial activity.

Proposed application of 3, 5-dihydroxy 4′, 7-dimethoxyflavone as a DNA binding dye

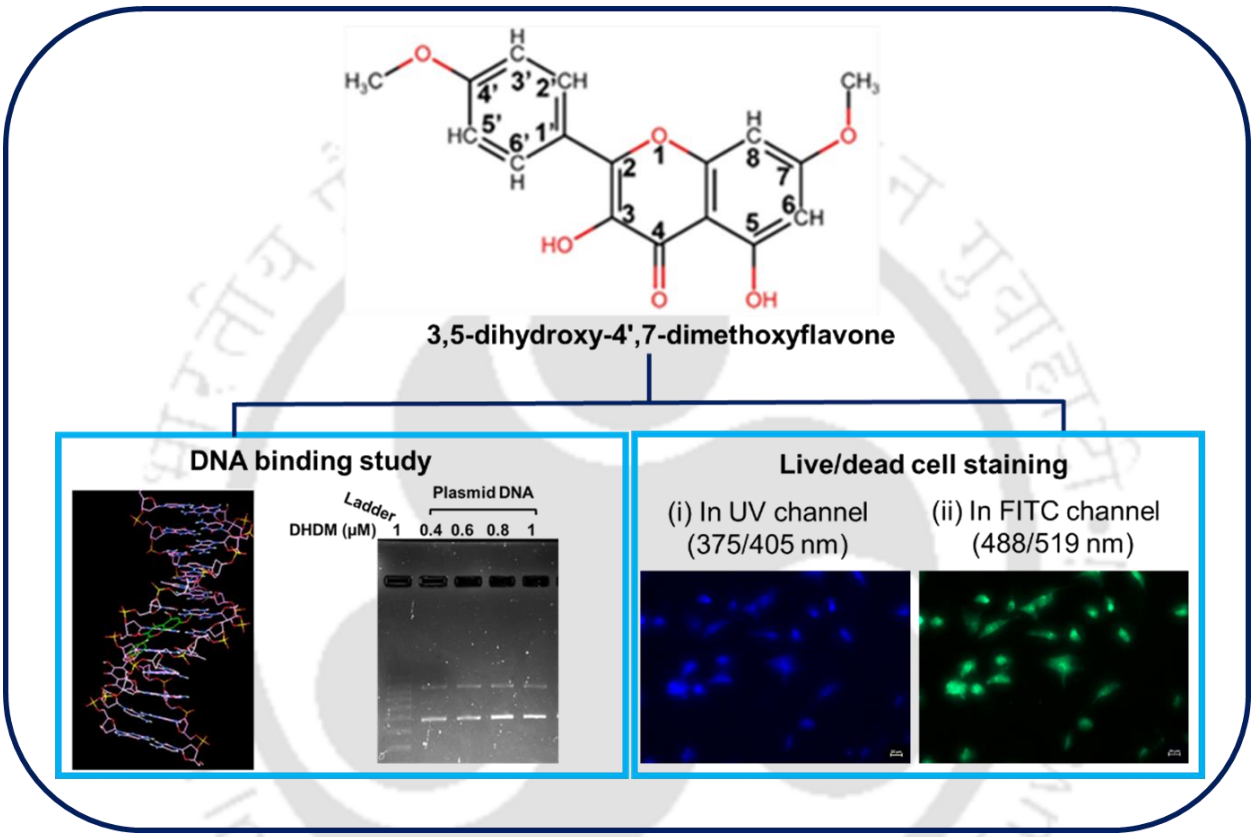

In this study, we have investigated the interaction of DHDM with plasmid DNA using UV/vis spectroscopy and ITC to get an insight and better understanding of the interaction mechanism. Further, the study to confirm the live/dead cell through fluorescence microscopy was carried out.

Chapter 7

Proposed application of 3, 5-dihydroxy 4′, 7-dimethoxyflavone as a DNA binding dye

7.1 Introduction

Staining is a key technique for labeling, detection, visualization, targeting, and identification of biological samples. In biology, chemistry, and medicine, stains and dyes are commonly employed to detect nucleic acids, proteins, and other biological components (Mehnert et al. 2018). Stains are chemical compounds that produce a measurable effect when they bind with a specific target. A stain does not exhibit the detectable response in the absence of the target. These characteristics make stains useful for detecting the presence or absence of a specific target in a sample. The observable response can be qualitative or quantitative, depending on the target, and test conditions (Pilling and Gardner 2016).

In biotechnological research, detecting and quantifying nucleic acids, particularly DNA, dsDNA, ssDNA and plasmid DNA is a common task (Wang et al. 2017). The nucleic acid screening applications use currently available hazardous and mutagenic fluorescent stains such as propidium iodide (PI), ethidium bromide (EtBr), and syber green. EtBr has been the most widely used dye because of its low cost and high sensitivity for nucleic acid screening in agarose gels for decades. However, the costs of detoxification and waste management could make the dye expensive and hazardous to researchers and the environment (O'Neil et al. 2018). To the best of our knowledge, earlier studies have discussed the antioxidant property and DNA-binding capabilities of class of flavonoids. Quercetin and rutin have been reported as DNA binding properties using spectroscopy (Janjua et al. 2009). Furthermore, the karanjin isolated from the karanj plant exhibited DNA binding, which was confirmed using an agarose-gel experiment (Arshad et al. 2013). Herein, the isolated compound a flavonoid, DHDM from *A. nigra* leaves was investigated for DNA binding using spectroscopic and calorimetric techniques. The confirmatory test of DNA binding property was exhibited by studying the binding affinity of DHDM-DNA using an agarose-gel. The novelty of this study is that it highlights the development of EtBr alternative dye for staining nucleic acids primarly ds DNA. Furthermore, this research study also highlights the application of DHDM as a new dye for microscopic differentiation of live and dead cells.

7.2 Material and methods

7.2.1 Cell culture

Baby hamster kidney fibroblasts cells (BHK-21) were cultured in DMEM medium. *Escherichia coli* and *Saccharomyces cerevisiae* were cultured in nutrient broth/agar medium, and yeast extract–peptone–dextrose (YPD) medium and culture was maintained at 37°C and 30°C, respectively.

7.2.2 Docking of DHDM with DNA

The protein data bank (PDB) was used to obtain the native structure of DNA (PDB ID:1BNA). The AutoDock 4.2 was used for docking studies (Morris et al. 2008b). The size of the grid box was set to 40, 40, and 40 for X, Y, and Z, correspondingly, with a spacing of 0.375. A total of 1000 docking simulations were run with the target DNA (rigid) and the ligand (DHDM) as flexible. The binding affinity of the ligand was calculated as a negative score in kcal/mol units. The interactions between the DHDM and DNA were examined using the PyMOL.

7.2.3 UV–vis spectrophotometric study

The spectrophotometric investigations of DHDM-DNA binding were carried out using a UV–vis spectrophotometer. The UV–vis spectra of DHDM and the DNA-DHDM complex were studied in the wavelength range 200–550 nm. The experiment was carried out with a constant concentration of DHDM (5 µM) and a titration of various plasmid DNA concentrations (10–90 ng). The nucleus-free water (0.01% DMSO) was used for baseline correction (blank).

7.2.4 Isothermal titration calorimetry (ITC) study

The thermodynamic parameter measurement of DHDM-DNA binding was performed using MicroCal ITC200 (GE Healthcare, Chicago, IL, USA). The DNA and ligand (DHDM) were dialyzed in the same buffer (a nucleus free water containing 0.01% DMSO) to reduce the heat of dilution of the experiment. The prepared DNA and DHDM samples were injected into cells and syringe with a concentration of 10 µM and 100 µM, respectively. Titrations was done at 25°C with a stirring speed of 500 rpm. The preinjection volume was kept 0.4 µL followed by 2.4 µL of

20 injections at every 180 s for each titration. Heat fluctuations due to ligand (DHDM) dilution in the buffer were also taken into account and subtracted from the heat of reactions to obtain the accurate heat associated with DNA-DHDM binding. The data were analyzed using the program ORIGIN version 7 embedded in MicroCal (GE Healthcare). The thermodynamic parameters such as enthalpy change (H), stoichiometry ratio (n), and association constant (Ka) were calculated after all the integrated data were fitted using a one-site binding model. The equation $\Delta G = \Delta H - T\Delta S$ was used to determine other thermodynamic parameters, such as a change in Gibbsfree energy (ΔG) and entropy change (ΔS).

7.2.5 Visualization of DNA band in gel electrophoresis

7.2.5.1 DHDM concentration dependent

Staining and nucleic acid binding properties of DHDM were tested using agarose-gel electrophoresis. The DNA concentration (70 ng) was kept constant and incubated with DHDM (0.04 -40 µM) for 1 minute. Loading dye (bromphenol blue and xylene cyanol) was loaded into separate wells for tracking. Gel electrophoresis was run for 30 minutes (90 V). Finally, DNA staining was observed using a UV transilluminator. Intensity of DNA bands calculated by imagej software.

7.2.5.2 Ethidium bromide and DHDM staining comparison

An agarose gel-based experiment was used to compare the DNA staining of EtBr and DHDM. EtBr (1 µM) was added in agarose gel, and wells were loaded with varying concentrations of DNA (5-70 ng). Comparatively, an agarose gel-based experiment was used to investigate the effect of DHDM on DNA binding and staining. Briefly, similar concentrations of DNA (5-70ng) were mixed with DHDM (1 µM) and incubated for 1 minute at room temperature (37°C). DNA-DHDM was loaded in agarose gel well. The electrophoresis apparatus was run for 30 minutes (90 V). Finally, DNA staining was observed using a UV transilluminator device. Intensity of DNA bands calculated by imagej software.

7.2.5.3 Staining of genomic DNA

Genomic DNA was extracted from mammalian cell (BHK-21) by the earlier described method (Koh 2013). Further, 120 ng of DNA was incubated with DHDM (1 µM) for 1 minute, and gel electrophoresis experiment was conducted as described in section (7.2.5.2**)**.

7.2.5.4 Staining of ds-linear DNA

PCR product (1.1 Kb) was used as ds-linear DNA for studying the binding and staining properties of DHDM with concentration 1 µM, using agarose gel-based experiment.

7.2.5.5 Staining of RNA

Overnight mammalian cell (BHK) culture was inoculated into fresh DMEM medium. Mammalian cells were grown at 37°C at 5% CO_2 for 24 h. Total RNA was extracted and purified using the trizol method. The concentration and purity of extracted total RNA was determined by ultraviolet absorption (260/280 nm) using a NanoDrop (ND-1000 spectrophotometer). About 100 ng of RNA was incubated with DHDM (1 µM) for 1 minute, and gel electrophoresis experiment was conducted.

7.2.5.6 Staining of single standard- linear DNA (ss-Linear DNA)

The single standard DNA from salmon testes (D 7656) was purchased from Sigma Aldrich (St. Louis, MO, USA). The stock concentration (200 ng) of DNA was prepared by dissolving in nucleus-free water. The concentration and purity of DNA was determined by ultraviolet absorption (260/280 nm) using a NanoDrop (ND-1000 spectrophotometer). Further, working concertation (70 ng) was made by diluting the stock in nucleus-free water. The working concentration of DHDM (1 µM) was added and incubated at room temperature (37°C) for 1 minute. Further, staining was determined using agarose gel-based experiment.

7.2.6 Live and dead cell differentiation using fluorescence microscopy

7.2.6.1 Mammalian cells staining

The live and dead cell differentiation properties of DHDM were analyzed using baby hamster kidney fibroblasts cells (BHK-21) by fluorescence microscope (Zeiss microscope, Zeiss, Germany) at 20X magnification (Song et al. 2017). For live-cell staining, 1,000 cells were

seeded in 6-well plates and incubated for 24 h at 37°C in CO_2 incubator. Then, the cells were treated with DHDM (50, and 60 µM) and incubated for 12 h. For dead cell staining, cells were incubated in 70% ethanol for 30 minutes. Further, cells were washed thoroughly with 1X PBS and again incubated with different concentrations of DHDM (30, 40, 50, and 60 µM) for 1 minute. Cells were washed again with 1X PBS to reduce extra stain. The staining properties of DHDM was examined in UV (375/405 nm) and FITC (488/519 nm) channel of fluorescence microscope. The staining affinity of DHDM was determined by analyzing the data with imagej software.

7.2.7 Positive control for confirming nucleus staining

Dead cell was prepared as described in section 7.2.6.1. The cells were incubated with fluorescent stain, 4′,6-diamidino-2-phenylindole (DAPI) (1% v/v) for 3 minutes, at room temperature (37°C) in dark for staining of nucleus and analyzed in UV (375/405 nm) channel. Similarly, another positive control, acridine orange (0.2% v/v) was added to the cells for 5 minutes at room temperature (37°C) in dark and analyzed in FITC (488/519 nm) channel. Staining of cells were examined in UV (375/405 nm) and FITC (488/519 nm) channel of fluorescence microscope at 20X magnification, respectively.

7.2.8 Yeast cells (*S. cerevisiae*) and bacterial cells (*E. coli*) dead cell staining

S. cerevisiae culture (OD600 0.6) was incubated with 70% ethanol for 30 minutes and washed two times with 1X PBS. After washing, smear was made on a glass slide and fixed by heat cell fixing method. Further, fixed cells were stained with concentration of DHDM (50 µM) for 1 minute. Similarly, *E. coli* (OD600 0.6), bacterial dead cells were prepared as described above. Cells were washed thoroughly with 1X PBS, and staining was analyzed in UV (375/405 nm) and FITC (488/519 nm) channel of fluorescence microscope at 20X magnification.

7.3 Result and discussion

7.3.1 Molecular docking

Molecular docking gives a detailed understanding of the ligand receptor interaction, which may help to validate the experimental findings. This approach provides sufficient knowledge on drug-

DNA interactions, which contributes in rational drug design and discovery (Pinzi and Rastelli 2019). The docked structure of DHDM to DNA produced by AutoDock-vina is shown in **Fig. 7.1** The molecular pose with the lowest binding energy was identified as DHDM bound in the minor groove of the DNA. Minor groove targeting of DNA by a single ligand is thought to be a useful targeting method (Koonammackal et al. 2011). The DHDM shows non-covalent interaction in a GC-rich region of DNA. Hydrogen bonds formed with guanine stabilizes the DHDM-DNA complex (**Fig. 7.1 C**). The docked DHDM-DNA complex had minimum binding energy of -9.1 kcal/mol, which is close to ITC analysis results. The negative value of binding energy indicates that DHDM has a high binding potential with DNA. Thus, the reciprocal complementarity of multi-spectroscopic investigations and molecular docking data strengthens our experimental findings that DHDM binds to a minor groove of DNA.

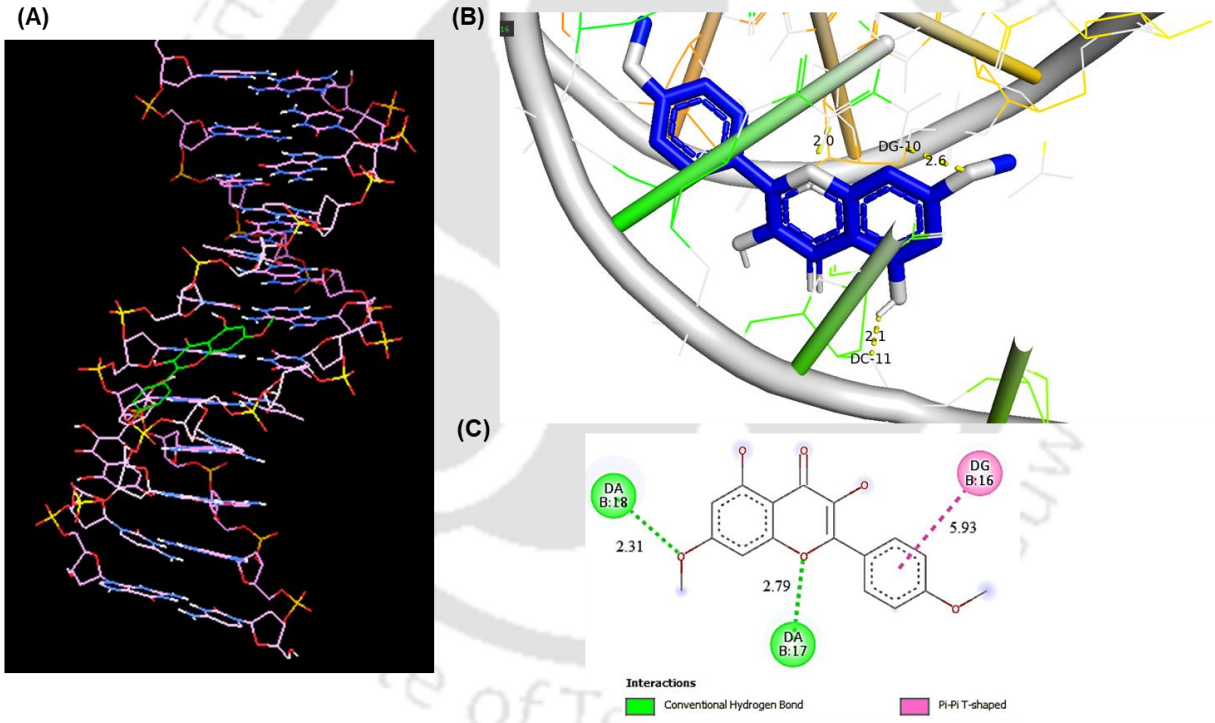

Fig. 7.1 DHDM bind with the minor groove of DNA: (A & B) DHDM intercalate with DNA. (C) Showing hydrogen binding with A and G bases of DNA.

7.3.2 UV–vis absorption studies for binding of DHDM-DNA

The interaction of DHDM-DNA was studied in UV–vis absorption spectroscopy. The study suggests that the DHDM may have intercalated between the two strands of DNA, resulting in increased absorbance value due to the unravelling of the DNA double-helix as aromatic bases are

more exposed to UV rays. Furthermore, the intercalative form of binding was shown by a hyperchromic shift in the absorption maximum of DHDM. The absorption profile of DHDM showed absorption maxima at 267 nm (band II), 320 nm and 370 nm (band I) (**Fig. 7.2 A,B**). The light absorption of the cinnamoyl system (B + C ring) is assigned to band I, which is located in the wavelength range of 300–400 nm, while the absorption of the benzoyl system (A + C ring) is attributed to band II, which is located in the wavelength range of 240–300 nm. When DNA is added to a DHDM solution in aqueous buffer, the absorption spectra of DHDM show an increase in absorbance (hyperchromism) of the absorption maximum, indicating that DHDM detects a hydrophobic environment within the DNA matrix that protects it from the polar aqueous environment (Rahman et al. 2019). Depending on the DNA structure, the level of hyperchromism varies greatly. As a result, our findings suggest that DHDM and DNA structures have an exterior binding mechanism. Additionally, this finding also suggests that throughout the binding process, multiple types of interactions may be present.

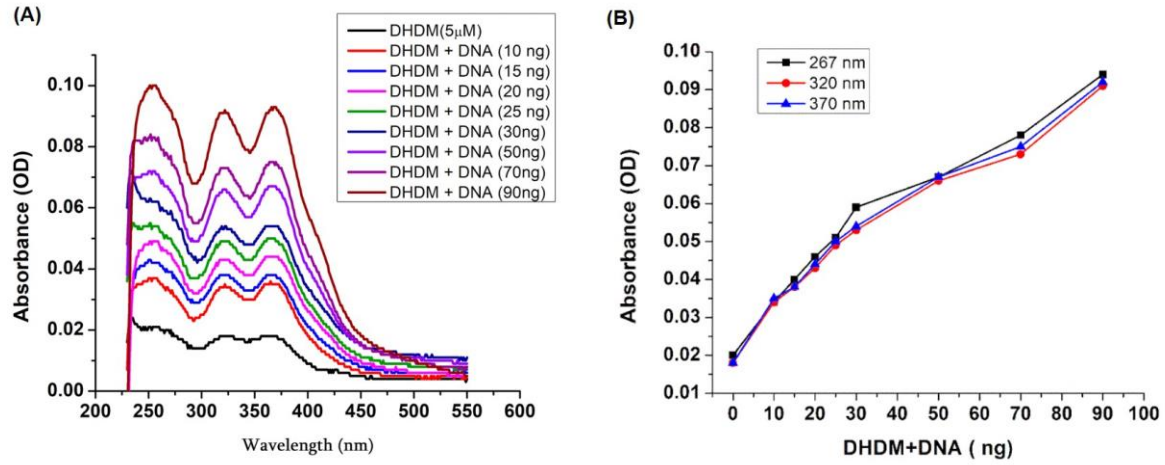

Fig. 7.2 (A) UV–vis absorption spectra of DHDM with varying concentrations of DNA and (B) Plot of absorbance (267 nm, 320 nm and 370 nm) vs concentration of DNA.

7.3.3 Isothermal titration calorimetry analysis of DHDM-DNA binding

Isothermal titration calorimetry (ITC) was used to investigate the energetics of DHDM-DNA binding. The thermodynamic properties of the DHDM-DNA binding were determined by fitting the integrated temperatures to the one binding site model (**Fig. 7.3**). The ITC thermogram's negative value indicates that the binding reaction is exothermic. The enthalpy (ΔH = −39.92 kcal mol−1) changes for the association process is greater than the entropy change (TΔS = −0.111

kcal mol−1), showing that the binding process is enthalpy driven. The Gibbs free energy change is also negative ($\Delta G = -39.809$ kcal mol^{-1}), showing that the binding reaction is spontaneous. The Ka value (1.24×10^5 M^{-1}) was calculated from the ITC data of DHDM-DNA complexation. The binding of DHDM to DNA resulted in negative enthalpy changes, indicating an exothermic binding process involving electrostatic interactions. Furthermore, both enthalpy and entropy have negative values for DHDM–DNA complexes, implying that hydrogen bonding and van der Waals forces play an important role in DHDM–DNA binding (Haris et al. 2017). Higher negative ΔG° values throughout the interaction process suggest that DHDM–DNA complex formation will be considerably spontaneous in nature. However, the previous reports also reveals ITC values which confirms the binding of flavonoid with DNA (Mary et al. 2017).

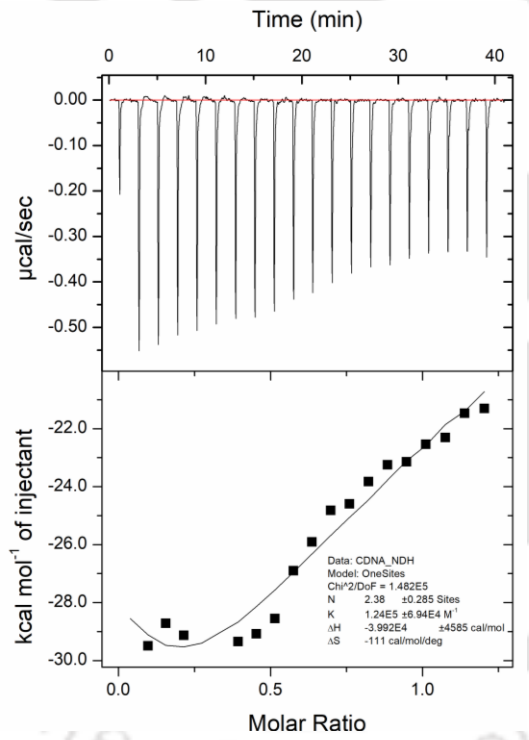

Fig. 7.3 ITC profile for the titration of DHDM into the solution of DNA. In the top panel the heat burst curves are the result of successive injection of aliquots of DHDM into DNA. The bottom panel represents the corresponding normalized heat signals versus molar ratio.

7.3.4 Visualization of DNA band

Gel electrophoresis technique was applied for separation of DNA fragments according to their size. This experiment also helps in knowing the binding of DHDM to DNA. EtBr, a well known

dye intercalates with the DNA by major groove (Saeidnia and Abdollahi 2013). EtBr help to distinguish the fragment of DNA due to its fluorescence property upon DNA binding (Vardevanyan et al. 2003). DHDM also bind to the DNA with the minor groove and intercalates between the two strands of DNA (proved by *Insilco* study section 7.3.1). Since the DHDM excites at 320 nm and 370 nm, the experiment was performed to know whether the DNA visualization in UV light could be done by adding the DHDM with DNA sample instead of using EtBr.

7.3.4.1 DHDM concentration dependent staining

To investigate the staining and binding capabilities of DHDM, DNA samples were loaded into wells. DNA binding effectiveness was demonstrated using varied concentrations of DHDM (0.04 - 40 µM) **(Fig. 7.4A**). DNA staining with DHDM was shown to be concentration dependent, with increasing DHDM concentration resulting in a progressive increase in DNA band intensity **(Fig. 7.4B**). At a concentration of 40 µM DHDM, the highest DNA band intensity was recorded, while 70 ng of DNA stained significantly with a 1 µM dose of DHDM. The DHDM stained DNA band intensity was compared to that of EtBr, a well-known DNA intercalating dye (Bonasera et al. 2007; Li et al. 2020).

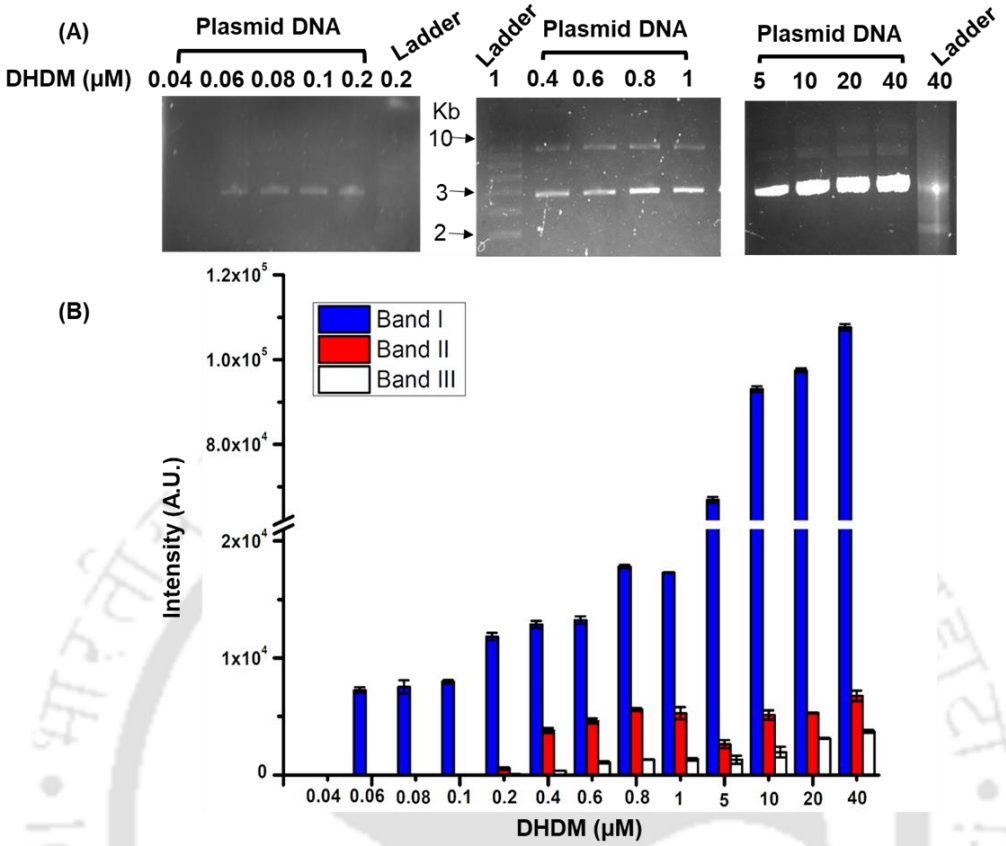

Fig. 7.4. (A) Concentration-dependent staining of DNA (70 ng) added with DHDM concentration ranging from 0.04-40 µM. (B) fluorescence intensity of DHDM bound to DNA.

7.3.4.2 Comparative staining of EtBr and DHDM

The DNA staining with DHDM and the well-known EtBr was compared using a fixed concentration of DHDM and EtBr and varied DNA amounts ranging from 5-70 ng. This was done to determine the sensitivity of DHDM for DNA staining properties. With DHDM, the maximal band intensity was 50 ng of DNA while with EtBr, it was 30 ng **(Fig. 7.5)**. In a prior investigation, 30 ng of DNA was found to be capable of staining with EtBr (O'Neil et al. 2019). The current finding revealed DHDM to be promising DNA staining dye upto 50 ng of DNA, which was less sensitive to EtBr.

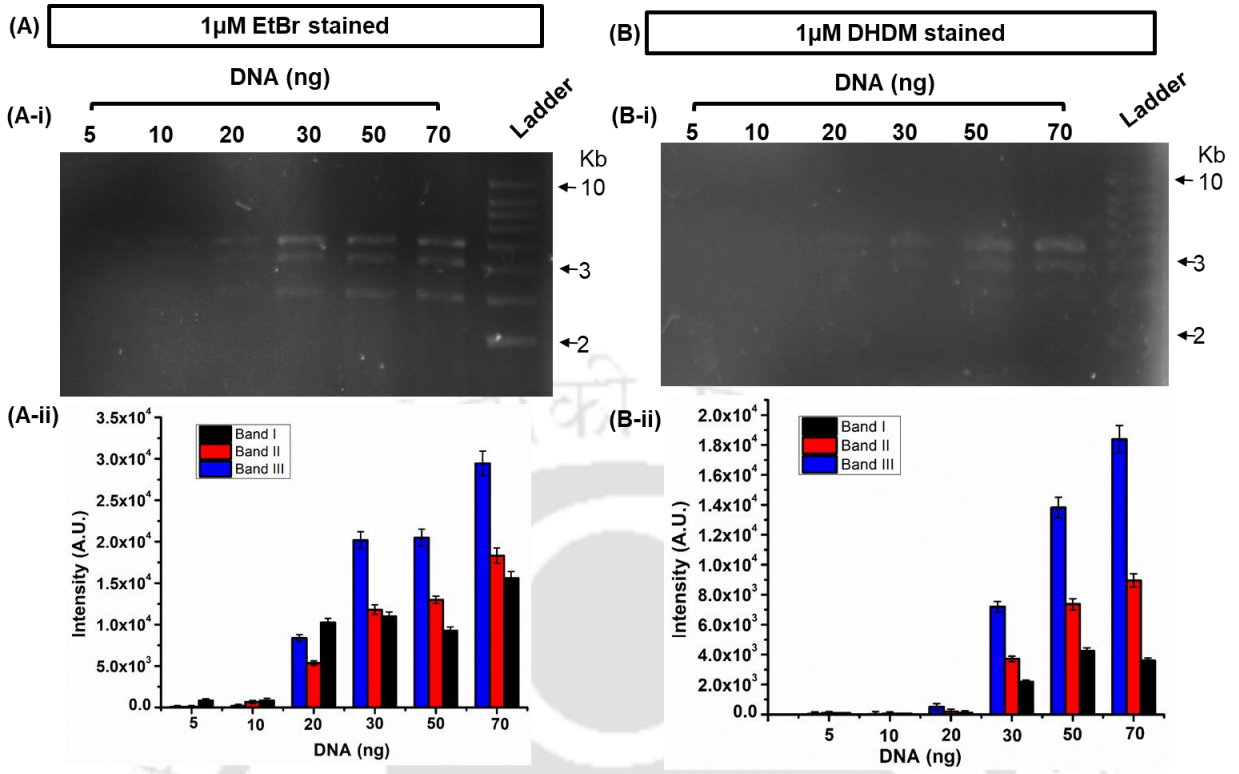

Fig. 7.5 The comparative staining of (A) EtBr (1 µM), (B) DHDM (1 µM) at various concentrations of DNA (5 -70 ng). (A-ii) and (B-ii) fluorescence intensity of DNA bound EtBr and DHDM, respectively.

7.3.4.3 Staining of genomic DNA

The staining of genomic DNA with DHDM were analyzed for the confirmation of DNA binding using agarose gel-based assay. The agarose gel-based study showed that DHDM was able to stain genomic DNA. The significant staining was observed in the DHDM in comparison to EtBr (**Fig. 7.6A**). Genomic DNA staining is a prime technique for drug development. However, through genomic DNA staining, apoptosis of cells has been studied (Chanput et al., 2014). A similar report exists about the development of new drug mechanisms on cancer and parasitic disease treatment with the help of genomic DNA staining (Marinho et al. 2014; Yaorong and Xiaoling 2019). The present finding has also showed the efficacy of natural compound towards the development of new dye for DNA. Apigenin intercalation with DNA duplex has been recently reported (Nafisi et al. 2008). Hence, flavonoids may intercalate or participate in the formation of hydrogen bonds with the stacking of nucleic acid bases.

7.3.4.4 Staining of RNA

The staining study of RNA with DHDM was carried out using agarose gel–based technique. The binding and staining were analyzed at 1 µm of DHDM.DHDM did not show significant staining activity (**Fig. 7.6B**). As displayed in figure 6B, the staining of the RNA was significantly with EtBr. Such staining was also validated in an earlier reports performed using EtBr as RNA staining dye (Tu et al. 2016). RNA are versatile molecules that play essential role in many biological processes and subsequently helps in drug targeting (Tajmir-Riahi et al. 2007). The result suggested that DHDM could not bind with RNA. Meanwhile, flavonoids such as morin, apigenin, and naringin showed binding with yeast RNA at physiological conditions in aqueous solution as detected using FTIR, UV–visible spectroscopic methods (Nafisi et al. 2009). The binding constants of other flavonoids: delphinidin, kaempferol, and quercetin, with RNA has been measured before (Kanakis et al. 2007).

7.3.4.5 Staining of ds-linear DNA

In the present study, we evaluated in more detail the effects DHDM for staining of ds-linear DNA. The agarose gel based assay confirmed significant binding of ds-linear DNA with DHDM (**Fig 7.6 C)**. Further, compared to the staining of EtBr, it was observed that it binds with ds-linear DNA more intensively in comparison to DHDM. Previous studies showed various dyes such as Mayer's hematoxylin, eosin Y, methyl green, and MayGrunwald solution used for staining of ds-linear DNA (Murase et al. 2000). Some studies reported hematoxylin and eosin–stained including Wright's solution instead of hematoxylin, that have been used for this purpose (Ramesh et al. 2019). To our knowledge, this study might be helpful in semi-PCR analysis.

7.3.4.6 Staining of ss-linear DNA

Agarose-gel based assay was carried out to investigate the binding of DHDM to ssDNA. The result indicated that DHDM did not stain ss-linear DNA (**Fig. 7.6 D**). However, in the presence of EtBr, ssDNA staining was observed. The previous result revealed that flavonoids have properties to bound with ssDNA (Bi et al. 2006). However, this current finding could not find any observable binding of DHDM with ss-linear DNA.

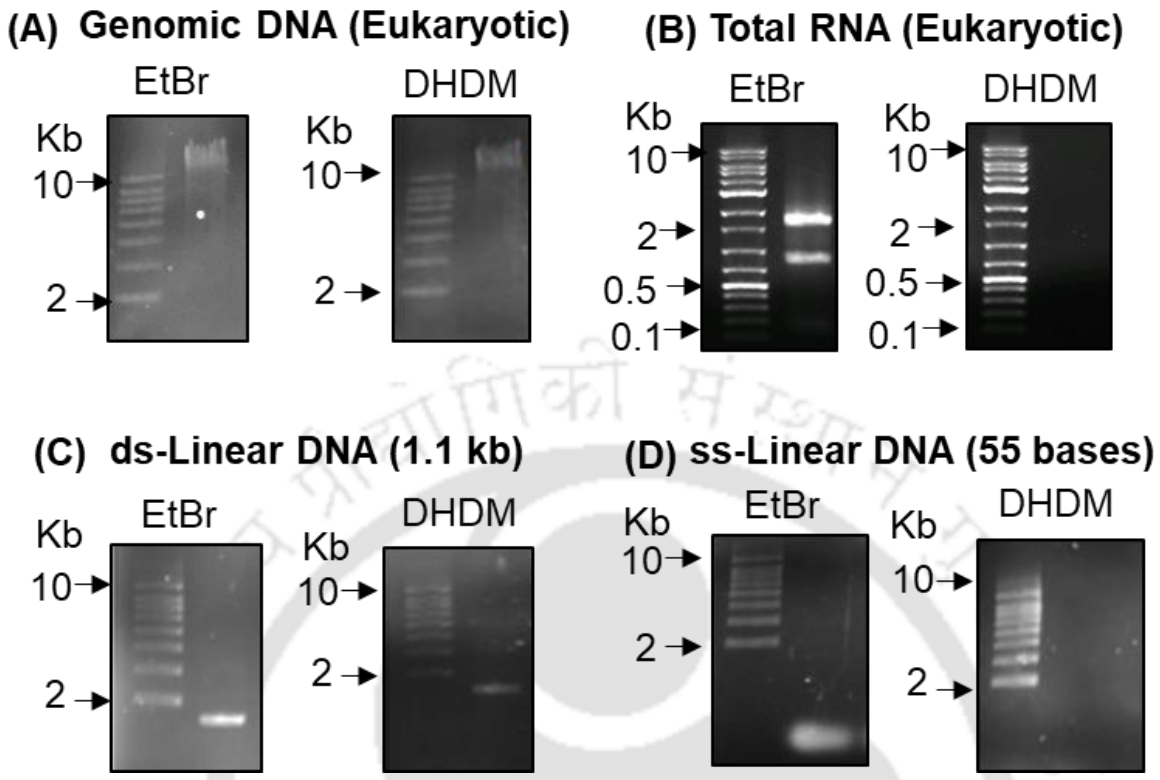

Fig. 7.6 DHDM staining properties (A) Staining of genomic DNA, (B) Total RNA, (C) ds-linear DNA and (D) ss-linear DNA by DHDM.

7.3.5 Live and dead cell differentiation

Staining is a technique used to enhance contrast in samples, usually at the microscopic level (Gnerucci et al. 2019). In this study, we aimed to understand the effect of DHDM treatment on mammalian, yeast, and bacterial cells and develop a simple approach for live/dead cell differentiation. A pilot experiment was initially performed with baby hamster kidney fibroblasts cells (BHK-21)

7.3.5.1 Mammalian cells staining

Mammalian live cell staining: BHK-21 live cells were grown in culture medium (6 well plate) followed by DHDM treatment. Treated cells were analyzed in UV and FITC channel. Cells were not visualized in both channels with 60 µM and 50 µM of DHDM (**Fig. 7.7**). It indicated that DHDM did not penetrate the live cell. Previous reports also showed similar results for PI stain

(Collins and Donoghue 1999; Jones et al. 2016). Therefore, this finding reveals that DHDM could not be used for live-cell staining.

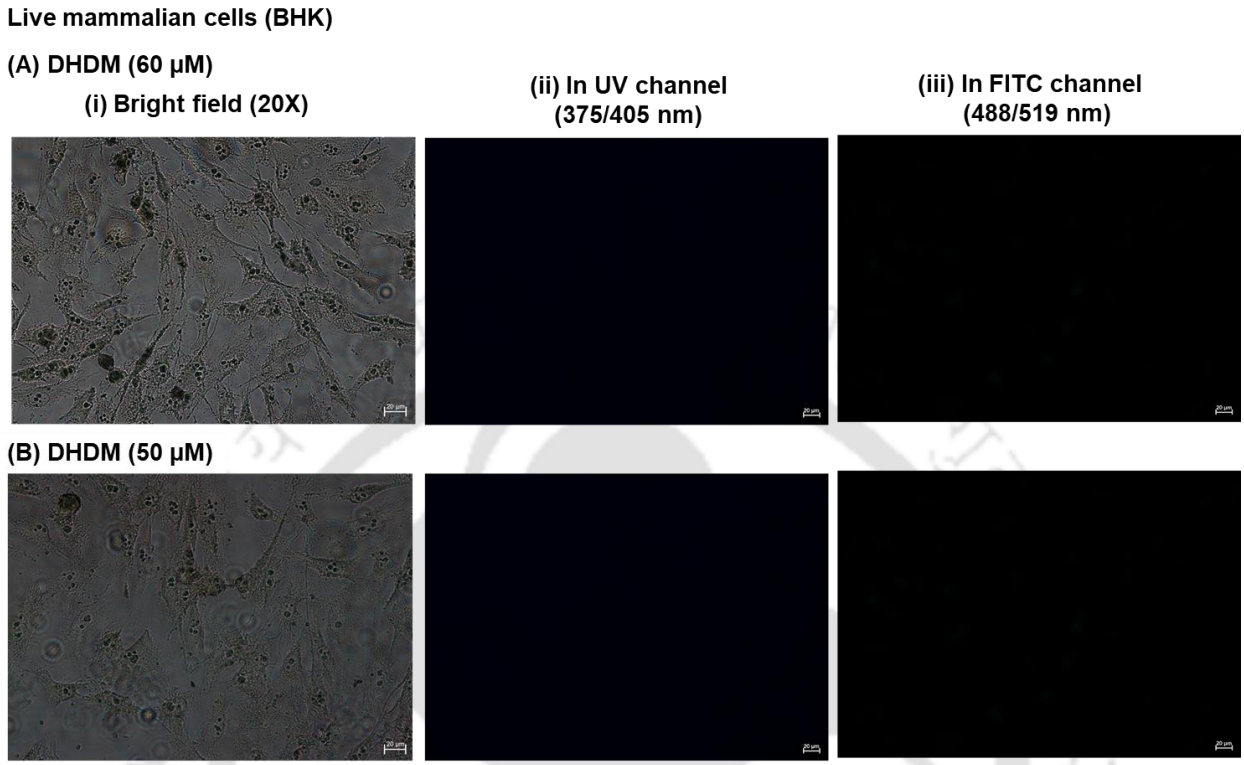

Fig. 7.7 Staining of live BHK 21 cells by 3, 5-dihydroxy 4′, 7-dimethoxyflavone at (A) 60 µM, (B) 50 µM in UV and FITC channel of fluorescence microscopy.

Mammalian dead cell staining: We next re-examined the effect of DHDM on the dead cell of BHK-21 cells using the concentrations (30-60 µM). After DHDM treatment and incubation for 1 minute, cells were washed, analyzed and imaged under UV and FITC channel of fluorescence microscope. It shows that dead cells were stained and visualized with DHDM under UV and FITC channel (**Fig. 7.8)**. The stained cells were then analyzed and validated for the optimal concentration of dead cell staining in both channels. The stained cells were then subjected to statistical analysis. It showed concentration dependent staining (**Fig. 7.8iv**). The fluorescence intensity data showed that the staining of cells treated at 50 µM was significantly better in comparision with that of 40 µM and 30 µM, indicating optimal concentration. Relatively nucleus region was prominently stained, which indicates that DHDM binds with nucleus. Therefore, this study further confirmed the DHDM interaction with DNA. However the previous study showed that kaempferol (50 µM) stains the nucleus of mouse Hepa-1c1c7 cells due to the formation of

flavone-macromolecule complex and staining was observed in FITC channel of microscope (Mukai et al. 2009).

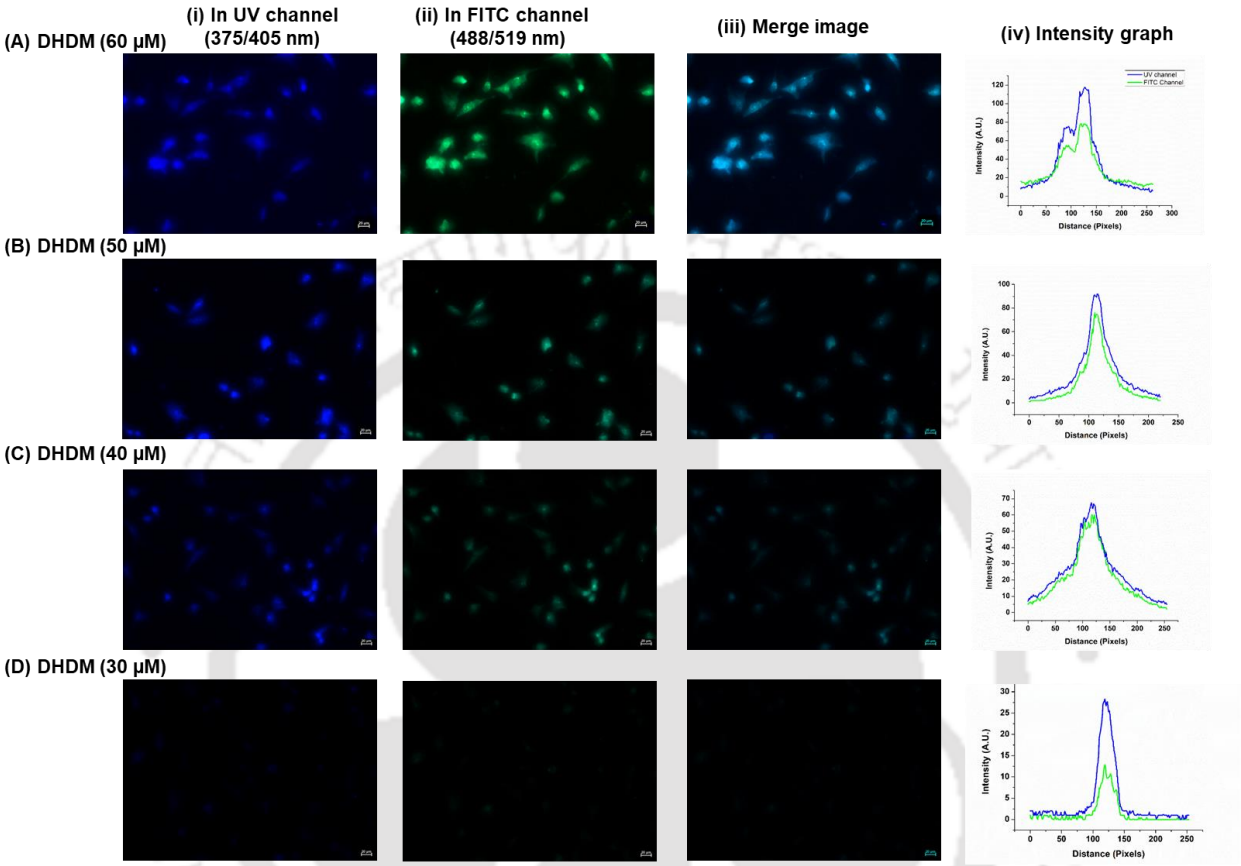

Fig. 7.8 Staining of dead BHK-21 cell by 3, 5-dihydroxy 4′, 7-dimethoxyflavone at (a) 60 µM (b) 50 µM (c) 40 µM (D) 30 µM, in UV and FITC channel of fluorescence microscope (8-iv) The intensity graph of DHDM fluorescence.

7.3.6 Positive control for confirming nucleus staining

For confirmation of nucleus staining properties, DAPI (Coleman et al. 1981) and acridine orange (Arnoczky et al. 2002) was used to investigate in UV and FITC channel. DAPI binds with nucleus and fluorescence in the UV channel (**Fig. 7.9 A**). DAPI is specifically binds to the DNA minor groove with ATT base pairs and is used as a fluorescent probe for screening of nucleus as reported by Li et al. (2015). Furthermore. acridine orange was investigated for confirmation of nucleus staining in the FITC channel (**Fig. 7.9 B**). The results confirmed the nucleus cell staining thorough DAPI and acridine orange.

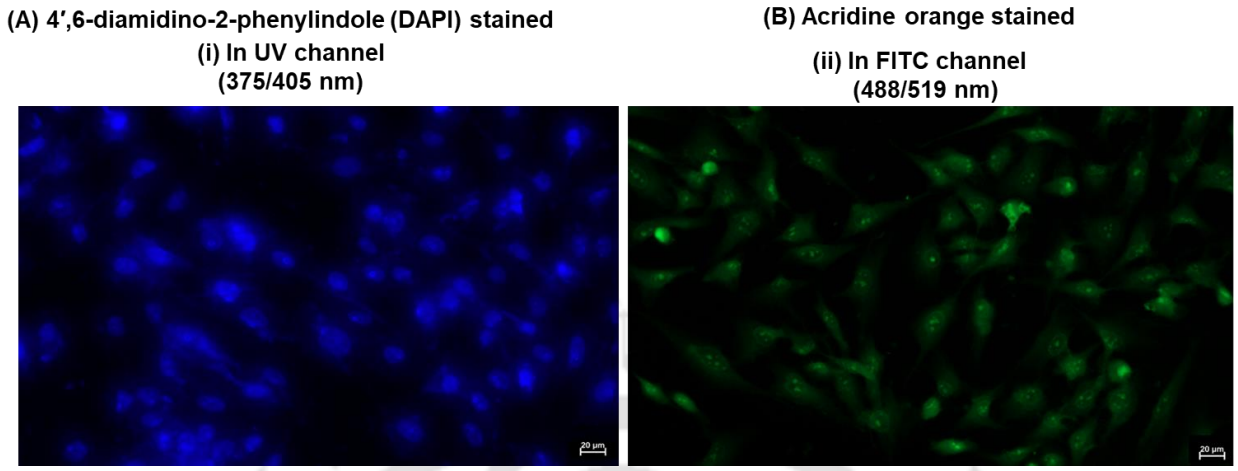

Fig. 7.9 Staining of dead BHK-21 cells (A) DAPI (1% v/v) and (B) Acridine orange (0.2% v/v) in UV and FITC channel of fluorescence microscope.

7.3.7 Yeast cells (*S. cerevisiae*) and bacterial cells (*E. coli*) dead cells staining

DHDM (50 µM) was investigated for nucleus staining of yeast (*S. cerevisiae*) dead cells. The result indicates that DHDM is suitable for dead cells staining of *S. cerevisiae*. The dead cell staining was observed in UV and FITC channel (**Fig. 7.10A**). Similarly, dead cell staining of *E. coli* with DHDM (50 µM) was investigated. The result indicated that similar to *S. cerevisiae* and BHK 21, it stained dead *E. coli* cells in UV and FITC channel (**Fig. 7.10B**). Hence, dead cells have permeable membranes, which allow staining chemicals to easily flow through and stain the inner cell portion (Kato et al. 1999). Therefore, this experiment revealed that DHDM stained the dead cells due to cell permeability. Bacterial live/dead cells differentiation is commonly used to evaluate antimicrobial characteristics, to test the survival of unculturable bacteria and to evaluate microbiological quality (Grégori et al. 2001). Nucleus staining has been used to assess the cell functions and examine the sensitivity of bacteria to biocides in fields like medicine, biotechnology, and the food industry.

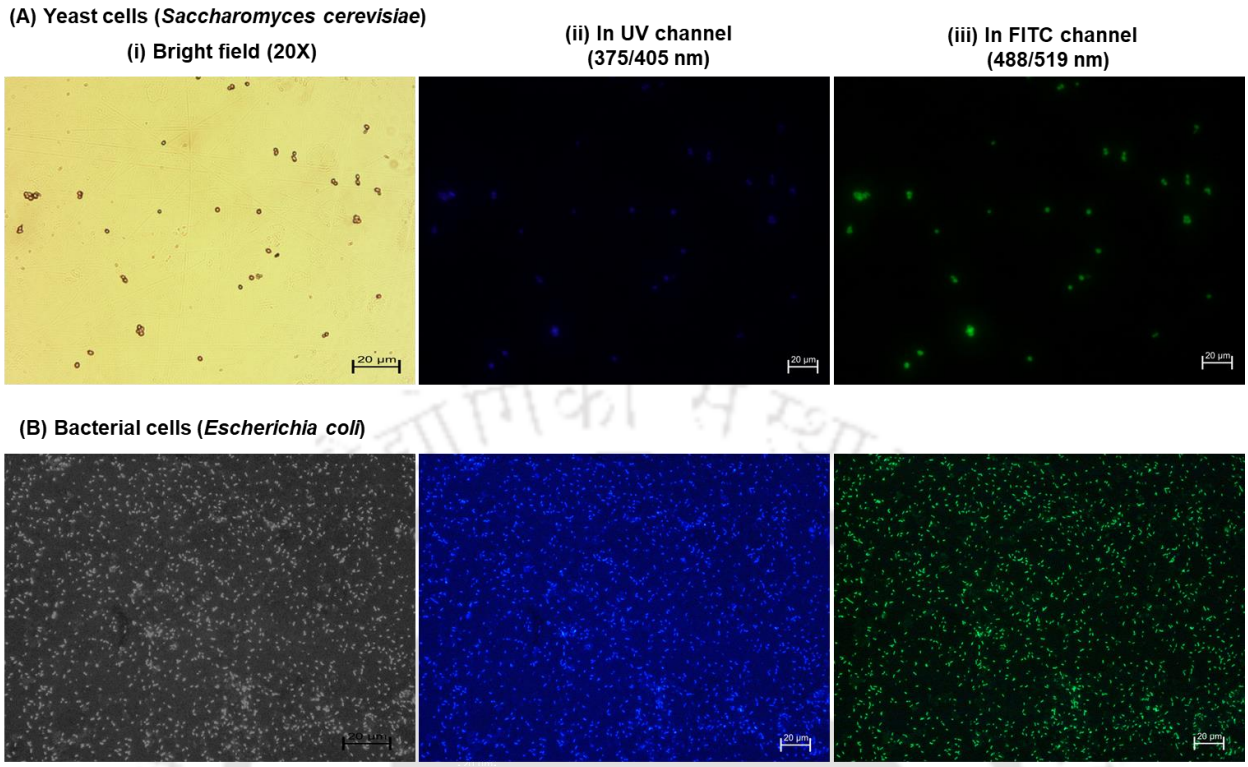

Fig. 7.10 The staining of dead cell (A) *S. cerevisiae* (B) *E. coli* by 3, 5-dihydroxy 4′, 7-dimethoxyflavone (50 µM), in UV and FITC channel of fluorescence microscopy.

7.4 Conclusion

Novel compound, 3,5-dihydroxy-4’,7-dimethoxyflavone (DHDM) was isolated and characterized from leaves of *A. nigra*. The interaction of DHDM with DNA was investigated through molecular docking simulation, ITC, and spectroscopic techniques. The OH and -OCH_3 groups of DHDM binds with the A and G bases of DNA, causing intercalation between two bases, as revealed by molecular docking studies. Following that, UV/vis spectroscopy was used to prove DHDM-DNA binding studies, which revealed hyperchromic shifting of DHDM absorbance as the concentration of DNA was increased. Furthermore, ITC data revealed that the binding reaction occurred spontaneously. Additionally, the binding and staining properties of DHDM were investigated using agarose gel-based assay, which revealed that as the concentration of DHDM increased, the intensity of the DNA band increased in a dose-dependent manner. Using a gel-based assay, it was found that a concentration of 1 µM DHDM was optimal for DNA (50 ng) staining. Furthermore, live and dead cell staining revealed that DHDM could

only bind and stain the dead cells. This study concludes that DHDM is a DNA binding and dead cell staining compound. Hence, this natural compound could be used for the development of a new stain for the visualization of DNA in agarose gel electrophoresis and the differentiation of live/dead cells using fluorescence microscopy.

Chapter 8

Summary and future perspective

This chapter summarizes the key research highlights of the present thesis work. This investigation has opened new avenues, some of which can be addressed as part of future research.

Chapter 8

Summary and future perspective

8.1 Summary

A. nigra has immense importance in terms of its medicinal properties. Researchers have studied and exploited different properties of this plant according to their specific study. Rhizome is mostly investigated for pharmacological efficacy followed by leaf while other vegetative and reproductive parts are used moderately. In the present study, 3,5-dihydroxy-4′,7-dimethoxyflavone (DHDM) was isolated and purified from leaves *of A. nigra*. Structure of the isolated compound was elucidated and characterized by various analytical and spectroscopic techniques. The compound "3,5-dihydroxy-4′,7-dimethoxyflavone (synonim kaempferol 7,4′-dimethyl ether)" is a well-known compound. Furthermore, certain modifications were made by conjugating the compound DHDM with metal complexation to enhance its anti-leishmanial effect. Overall, the thesis is divided into 7 chapters, and the key research findings of the chapters 3-7 are as follows:

Chapter 3. The phytochemical screening of leaf extract of *A. nigra* was evaluated for antibacterial, anti-biofilm activity towards *Pseudomonas aeruginosa*. Antibacterial activity and growth curve analysis of bacterial cells confirmed the significant bacterial cell death in L-EtAc treated sample. The qRT-PCR data revealed reduced *las*I, *las*R, *las*B, *rhl*I, *rhl*R and *rhl*A gene expression, which may be directly associated with biofilm and extracellular matrix formation.

Chapter 4. 3,5-dihydroxy-4′,7-dimethoxyflavone (DHDM), a flavone was isolated, characterized, and reported for the first time from leaves of *A. nigra* by spectroscopic techniques.

Chapter 5. The purified compound was evaluated for its antioxidant, anti-tyrosinase, and anti-inflammatory potential. The cytotoxicity of DHDM was evaluated on THP-1 and HaCaT cell lines suggesting its non-toxic nature. Moreover, DHDM inhibited the expression of inflammatory proteins like TNF-α and NF-κB. Thus, DHDM could be developed as a new drug or drug lead for treating hyperpigmentation and inflammatory-related diseases.

Chapter 6. A zinc metal derivative of DHDM was synthesized and characterized (DHDM-Zn). Characterization of the complex was further accomplished by multi-spectroscopic techniques such as FTIR, Raman, HRMS, NMR, FESEM-EDX. Further, it was demonstrated that DHDM-Zn exhibited an excellent *in vitro* antagonistic effect against the promastigote form

of *L. donovani*. In addition, the possible mechanisms of promastigote *L. donovani* cell death, by involvement of derivatized compound in arrest of the cell cycle in the G1 phase and residual cell count reduction were investigated. Promastigote growth kinetics performed in the presence of the derivatized compound revealed a slow growth rate. The combination of growth kinetics and cell cycle analysis made it possible to interpret and classify the cause of leishmanial cell death accurately. These results support that zinc derivatized complex (DHDM-Zn) might work as a lead compound for designing and developing a new anti-leishmanial drug.

Chapter 7. The application of a DHDM was investigated for nucleic acid staining and differential live/dead cell staining. DHDM was found to interact with nucleic acid and form complex which was investigated for various applications. The molecular docking study showed that DHDM bound in the minor groove of DNA based on the lowest binding energy. It was successfully utilized for visualizing plasmid DNA, genomic DNA, ss-linear DNA, and ds-linear DNA in agarose gel electrophoresis without affecting the DNA mobility in the gel. Extended application was also studied in fluorescence microscopy, where it stained the dead cells and differentiated them from live cells in different cells like bacteria, yeast, and mammalian cells. Most widely, dyes like Ethidium bromide, Propidium iodide are carcinogens and environmental pollutants. DHDM being a natural compound is a major benefit and thus can serve as an alternative for the above mention dyes.

8.2 Future perspective

The present study has enabled the identification and characterization of compounds from leaves of *A. nigra*. It has also addressed the biological activity of the isolated compound. This investigation has opened new avenues, some of which are listed below that can be addressed as part of future research:

- The L-EtAc extract showed antibacterial, antibiofilm, and antiquarun sensing activity. Hence, further research can be done on the compounds of L-EtAc extract to design and develop a new drug to cure chronic disease associated with the biofilm-forming pathogen.
- Bioactive compounds profiling from *A. nigra* may establish medicinal property profiling of *A. nigra* varieties of NE India.

- 3,5-dihydroxy-4′,7-dimethoxyflavone (DHDM) has a strong antioxidant and ROS inhibitory activity. Hence, this compound can be developed has a potential and effective anticancer agent.
- Studies can be carried out on how 3,5-dihydroxy-4′,7-dimethoxyflavone (DHDM) produces its potential anti-tyrosinase activity and whether it would be effective against skin related diseases.
- Our study suggests a significant decrease in the level of NF-κB-p65 after the treatment with DHDM. Therefore, further studies on *in vivo* disease models can be explored.
- Flavonoid-metal complexes (DHDM-Zn) showed better anti-leishmanial activity. Hence, our study suggested that metal derivative compound can be explored for development new drug to cure parasitic diseases.
- 3,5-dihydroxy-4′,7-dimethoxyflavone (DHDM) can be explored in the field of synthetic chemistry for preparation of biologically effective analogues.

References

Abinaya M, Gayathri M (2019) Inhibition of biofilm formation, quorum sensing activity and molecular docking study of isolated 3, 5, 7-Trihydroxyflavone from *Alstonia scholaris* leaf against P.aeruginosa. Bioorg Chem 87:291–301.

Aboul-Enein HY, Berczyńsk P, Kruk I (2013) Phenolic compounds: The role of redox regulation in neurodegenerative disease and cancer. Mini Rev Med Chem 13:385–98.

Abu Ahmed AM, Sharmen F, Mannan A, Rahman MA (2015) Phytochemical, analgesic, antibacterial, and cytotoxic effects of *Alpinia nigra* (Gaertn.) Burtt leaf extract. J Tradit Complement Med 5:248-452.

Abu Khalaf R, Alhusban AA, Al-Shalabi E (2019) Isolation and structure elucidation of bioactive polyphenols. Studies in Natural Products Chemistry 63:267–337

Ademiluyi AO, Oboh G (2013) Soybean phenolic-rich extracts inhibit key-enzymes linked to type 2 diabetes (α-amylase and α-glucosidase) and hypertension (angiotensin I converting enzyme) in vitro. Exp Toxicol Pathol 65:305–9.

Aghajanian C, Filiaci V, Dizon DS (2018) A phase II study of frontline paclitaxel/carboplatin/bevacizumab, paclitaxel/carboplatin/temsirolimus, or ixabepilone/carboplatin/bevacizumab in advanced/recurrent endometrial cancer. Gynecol Oncol 150:274–281.

Ahmad Khan MS, Ahmad I (2019) Herbal medicine. New Look to Phytomedicine 1:3–13.

Ahmedova A, Paradowska K, Wawer I (2012) ^{1}H, ^{13}C MAS NMR and DFT GIAO study of quercetin and its complex with Al(III) in solid state. J Inorg Biochem 110:27-35.

Ajiboye BO, Ojo OA, Okesola MA (2018) In vitro antioxidant activities and inhibitory effects of phenolic extract of *Senecio biafrae* (Oliv and Hiern) against key enzymes linked with type II diabetes mellitus and Alzheimer's disease. Food Sci Nutr 6:1803–1810.

Alfadda AA, Sallam RM (2012) Reactive oxygen species in health and disease. J Biomed Biotechnol 2012:936486.

Alvar J, Vélez ID, Bern C (2012) Leishmaniasis worldwide and global estimates of its incidence. PLoS One 7:e35671.

Amparo TR, Seibert JB, Vieira PM de A (2020) Herbal medicines to the treatment of skin and soft tissue infections: Advantages of the multi-targets action. Phytother Res 34:94–103.

An N, Zou Z, Tian Z (2008) Diarylheptanoids from the rhizomes of *Alpinia officinarum* and their

anticancer activity. Fitoterapia 79:27–31.

Araújo M V, Queiroz AC, Silva JFM (2019) Flavonoids induce cell death in *Leishmania amazonensis* : In vitro characterization by flow cytometry and Raman spectroscopy. Analyst 144:5232–5244.

Arfaoui L (2021) Dietary plant polyphenols: effects of food processing on their content and bioavailability. Molecules 26:2959

Arnoczky SP, Lavagnino M, Whallon JH, Hoonjan A (2002) In situ cell nucleus deformation in tendons under tensile load; a morphological analysis using confocal laser microscopy. J Orthop Res 20:29–35.

Arshad N, Rashid N, Absar S (2013) UV-absorption studies of interaction of karanjin and karanjachromene with ds. DNA: Evaluation of binding and antioxidant activity. Open Chem 11:2040–2047.

Artés F, Castañer M, Gil MI (1998) Revisión: El pardeamiento enzimático en frutas y hortalizas mínimamente procesadas Review: Enzymatic browning in minimally processed fruit and vegetables. Food Sci Technol Int 4:377–389.

Atanasov AG, Waltenberger B, Pferschy-Wenzig E-M (2015a) Discovery and resupply of pharmacologically active plant-derived natural products: A review. Biotechnol Adv 33:1582–1614.

Atanasov AG, Waltenberger B, Pferschy-Wenzig E-M (2015b) Discovery and resupply of pharmacologically active plant-derived natural products: A review. Biotechnol Adv 33:1582–1614.

Awang K, Ibrahim H, Rosmy Syamsir D (2011) Chemical constituents and antimicrobial activity of the leaf and rhizome oils of *Alpinia pahangensis* Ridl., An endemic wild ginger from peninsular Malaysia. Chem Biodivers 8:668–673.

Badr JM, Hadad GM, Nahriry K, Hassanean HA (2015) Validated HPLC method for simultaneous estimation of khellol glucoside, khellin and visnagin in *Ammi visnaga* L. fruits and pharmaceutical preparations. Nat Prod Res 29:593–601.

Bae S, Lee EJ, Lee JH (2014) Oridonin protects HaCaT keratinocytes against hydrogen peroxide-induced oxidative stress by altering microRNA expression. Int J Mol Med. 33:185-93

Balabanova L, Shkryl Y, Slepchenko L (2020) Genomic features of a food-derived *Pseudomonas*

aeruginosa Strain PAEM and biofilm-associated gene expression under a marine bacterial α-galactosidase. Int J Mol Sci 21:7666.

Banjarnahor SDS, Artanti N (2015) Antioxidant properties of flavonoids. Med J Indones 23:239–44.

Basu U, Karges J, Chotard F, et al (2019) Investigation of photo-activation on ruthenium(II)–arene complexes for the discovery of potential selective cytotoxic agents. Polyhedron 172:22–27.

Batra P, Sharma AK (2013) Anti-cancer potential of flavonoids: recent trends and future perspectives. 3 Biotech 3:439–459.

Bernatova I (2018) Biological activities of (−)-epicatechin and (−)-epicatechin-containing foods: Focus on cardiovascular and neuropsychological health. Biotechnol Adv 36:666–681.

Beyersmann D, Haase H (2001) Functions of zinc in signaling, proliferation and differentiation of mammalian cells. Biometals 14:331–41.

Bhunia A K, Jha P K, Rout SS D (2016) Morphological properties and raman spectroscopy of ZnO nanorods. J Phys Sci 21:111-118.

Bi S, Qiao C, Song D (2006) Study of interactions of flavonoids with DNA using acridine orange as a fluorescence probe. Sensors Actuators B Chem 119:199–208.

Bian Y, Wei J, Zhao C, Li G (2020) Natural polyphenols targeting senescence: A novel prevention and therapy strategy for cancer. Int. J. Mol. Sci. 21:684

Birks JS (2006) Cholinesterase inhibitors for Alzheimer's disease. Cochrane Database of Systematic Review 1: CD005593.

Bochot C, Gouron A, Bubacco L (2014) Probing kojic acid binding to tyrosinase enzyme: insights from a model complex and QM/MM calculations. Chem Commun 50:308–310.

Bonasera V, Alberti S, Sacchetti A (2007) Protocol for high-sensitivity/long linear-range spectrofluorimetric DNA quantification using ethidium bromide. Biotechniques 43:173–176.

Bonaventura P, Benedetti G, Albarède F, Miossec P (2015) Zinc and its role in immunity and inflammation. Autoimmun. Rev. 14:277-85.

Bordoloi D, monisha J, roy NK (2019) an investigation on the therapeutic potential of butein, a tretrahydroxychalcone against human oral squamous cell carcinoma. Asian Pacific J Cancer Prev 20:3437–3446.

Borrell S, Gagneux S (2009) Infectiousness, reproductive fitness and evolution of drug-resistant Mycobacterium tuberculosis. Int J Tuberc Lung Dis 13:1456–66.

Bosshart H, Heinzelmann M (2016) THP-1 cells as a model for human monocytes. Ann Transl Med. 4:438.

Broadley MR, White PJ, Hammond JP (2007) Zinc in plants. New Phytol 173:677–702.

Brown ED, Wright GD (2016) Antibacterial drug discovery in the resistance era. Nature 529:336–43.

Bruker (2009) APEX2, SAINT and SADABS. APEX II, Bruker AXS Inc., Madison, Wisconsin, USA.

Cabanes J, Chazarra S, Garcia-carmona F (1994) Kojic acid, a cosmetic skin whitening agent, is a slow-binding inhibitor of catecholase activity of tyrosinase. J Pharm Pharmacol 46:982–985.

Cauz ACG, Carretero GPB, Saraiva GK V (2019) Violacein targets the cytoplasmic membrane of bacteria. ACS Infect Dis 5:539–549.

Cerqueira APM, Santana IB, Araújo JSC (2021) Homology modeling, docking, molecular dynamics and in vitro studies to identify *Rhipicephalus microplus* acetylcholinesterase inhibitors. J Biomol Struct Dyn 1:1–11.

Chakrabartty I, Vijayasekhar A, Rangan L (2021) Therapeutic potential of labdane diterpene isolated from Alpinia nigra : detailed hemato-compatibility and antimicrobial studies. Nat Prod Res 35:1000–1004.

Chan YY, Kim KH, Cheah SH (2011) Inhibitory effects of *Sargassum polycystum* on tyrosinase activity and melanin formation in B16F10 murine melanoma cells. J Ethnopharmacol 137:1183–1188.

Chanput W, Mes JJ, Wichers HJ (2014) THP-1 cell line: An in vitro cell model for immune modulation approach. Int Immunopharmacol 23:37–45.

Chauhan IS, Rao GS, Shankar J (2018) Chemoprevention of Leishmaniasis: In-vitro antiparasitic activity of dibenzalacetone, a synthetic curcumin analog leads to apoptotic cell death in *Leishmania donovani*. Parasitol Int 67:627-636

Chen Q-X, Kubo I (2002) Kinetics of mushroom tyrosinase inhibition by quercetin. J Agric Food Chem 50:4108–4112.

Chen Z, Pan X, Sheng Z (2019) Baicalin suppresses the proliferation and migration of ox-LDL-

VSMCs in atherosclerosis through upregulating miR-126-5p. Biol Pharm Bull. 42:1517-1523

Cho NH, Shaw JE, Karuranga S (2018) IDF Diabetes Atlas: Global estimates of diabetes prevalence for 2017 and projections for 2045. Diabetes Res Clin Pract 138:271–281.

Choi H, Kim K, Han J (2012) Kojic acid-induced IL-6 production in human keratinocytes plays a role in its anti-melanogenic activity in skin. J Dermatol Sci 66:207–215.

Coleman AW, Maguire MJ, Coleman JR (1981) Mithramycin- and 4'-6-diamidino-2-phenylindole (DAPI)-DNA staining for fluorescence microspectrophotometric measurement of DNA in nuclei, plastids, and virus particles. J Histochem Cytochem 29:959–968.

Collins AM, Donoghue AM (1999) Viability assessment of honey bee, *Apis mellifera*, sperm using dual fluorescent staining. Theriogenology 51:1513–1523.

Cragg GM, Newman DJ (2013) Natural products: a continuing source of novel drug leads. Biochim Biophys Acta 1830:3670–3695.

D.J. S (2012) Cinchona alkaloids: Quinine and quinidine. Treat. Prev. Malar. Antimalar. Drug Chem. Action and Use 1:45-68.

Da Silva ER, Maquiaveli Cdo C, Magalhães PP (2012) The leishmanicidal flavonols quercetin and quercitrin target Leishmania (Leishmania) amazonensis arginase. Exp Parasitol. 130:183-8.

Dai J, Han R, Xu Y (2020) Recent progress of antibacterial natural products: Future antibiotics candidates. Bioorg Chem 101:103922.

Das GB, Roy CK, Ganguly S, Akbar MA, Das P, Roy S (2003) Infection of human mononuclear phagocytes and macrophage-like THP1 cells with *Leishmania donovani* results in modulation of expression of a subset of chemokines and a chemokine receptor. Scand J Immunol. 57:366-74.

Dash S, Panda MK, Singh MC (2020) Bioactive molecules from the *Alpinia* Genus: A comprehensive review. Curr Pharm Biotechnol 21:1412–1421.

De Oliveira C, Comunello L, Maciel É (2013) The inhibitory effects of phenolic and terpenoid compounds from *baccharis trimera* in SiHa cells: Differences in their activity and mechanism of action. Molecules 18:11022–11032.

De Paula R, Rabalski I, Messia MC (2017) Effect of processing on phenolic acids composition and radical scavenging capacity of barley pasta. Food Res Int 102:136–143.

De Souza RFV, De Giovani WF (2004) Antioxidant properties of complexes of flavonoids with metal ions. Redox Rep 9:97–104.

De Souza RF V, De Giovani WF (2005) Synthesis, spectral and electrochemical properties of Al(III) and Zn(II) complexes with flavonoids. Spectrochim Acta A Mol Biomol Spectrosc 61:1985–90.

Deb L, Laishram S, Khumukcham N (2015) Past, present and perspectives of Manipur traditional medicine: A major health care system available for rural population in the North-East India. J Ethnopharmacol 169:387–400.

Debnath B, Singh WS, Das M (2018) Role of plant alkaloids on human health: A review of biological activities. Mater Today Chem 9:56–72.

Demetzos C, Dimas KS (2001) Labdane-type diterpenes: Chemistry and biological activity. Studies in Natural Products Chemistry.25:235–292.

Desai SJ, Prickril B, Rasooly A (2018) Mechanisms of phytonutrient modulation of cyclooxygenase-2 (COX-2) and inflammation related to cancer. Nutr Cancer 70:350–375.

Desborough MJR, Keeling DM (2017) The aspirin story - from willow to wonder drug. Br J Haematol 177:674–683.

Ding Z, Dai Y, Hao H (2008) Anti-inflammatory effects of scopoletin and underlying mechanisms. Pharm Biol 46:854–860.

Djordjevic D, Wiedmann M, McLandsborough LA (2002) Microtiter plate assay for assessment of *Listeria* monocytogenes biofilm formation. Appl Environ Microbiol 68:2950–2958.

Dobrucka R, Długaszewska J (2016) Biosynthesis and antibacterial activity of ZnO nanoparticles using *Trifolium pratense* flower extract. Saudi J Biol Sci 23:517–523.

Dolomanov O V., Bourhis LJ, Gildea RJ (2009) OLEX2: A complete structure solution, refinement and analysis program. J Appl Crystallogr 42:339-341.

Dwiecki K, Neunert G, Polewski P, Polewski K (2009) Antioxidant activity of daidzein, a natural antioxidant, and its spectroscopic properties in organic solvents and phosphatidylcholine liposomes. J Photochem Photobiol B Biol 96:242–248.

Egbuna C, Kumar S, Ifemeje JC (2020) Phytochemicals as lead compounds for new drug discovery. Elsevier 1: 357-364.

El-Seedi HR, Yosri N, Khalifa SAM (2021) Exploring natural products-based cancer therapeutics derived from egyptian flora. J Ethnopharmacol 269:113626.

Ellen L Lagendijk SUP (2015) Antimicrobial effects of Indonesian medicinal plants extracts on planktonic and biofilm growth of *Pseudomonas aeruginosa* and S*taphylococcus aureus*. J Hortic 02:1

Eming SA, Krieg T, Davidson JM (2007) Inflammation in wound repair: Molecular and cellular mechanisms. J. Invest. Dermatol 127:514-525.

Empl MT, Albers M, Wang S, Steinberg P (2015) The resveratrol tetramer r-viniferin induces a cell cycle arrest followed by apoptosis in the prostate cancer cell line LNCaP. Phytother Res 29:1640–5.

Eram S, Mujahid M, Bagga P (2019) A review on phytopharmacological activity of *Alpinia galanga*. Int J Pharm Pharm Sci 6–11.

Fan M, Zhang G, Hu X, et al (2017) Quercetin as a tyrosinase inhibitor: Inhibitory activity, conformational change and mechanism. Food Res Int 100:226–233.

Farmer RL, Biddle MM, Nibbs AE (2010) Concise syntheses of the abyssinones and discovery of new inhibitors of prostate cancer and MMP-2 expression. ACS Med Chem Lett 1:400–405.

Filipský T, Mladěnka P, Macáková K (2012) In vitro characteristics of 1-phenyl-3-methyl-4-acylpyrazol-5-ones iron chelators. Biochimie 94:125–131.

Fischer J, Robin Ganellin C (2006) Analogue-based drug discovery. Wiley 32:12-15.

Funamoto M, Shimizu K, Sunagawa Y (2019) Effects of highly absorbable curcumin in patients with impaired glucose tolerance and non-insulin-dependent Diabetes Mellitus. J Diabetes Res 2019:8208237.

Ganguly K, Wu R, Ollivault-Shiflett M (2011) Design, synthesis, and a novel application of quorum-sensing agonists as potential drug-delivery vehicles. J Drug Target 19:528-539.

Gao M, Coggin A, Yagnik K, Teplitski M (2012) Role of specific quorum-sensing signals in the regulation of exopolysaccharide II production within *Sinorhizobium meliloti* spreading colonies. PLoS One 7:e42611.

Geary WJ (1971) The use of conductivity measurements in organic solvents for the characterisation of coordination compounds. Coord Chem Rev 7:81–122.

Ghosh P, Devi GP, Priya R (2013a) Spectroscopic and in silico evaluation of interaction of dna with six anthraquinone derivatives. Appl Biochem Biotechnol 170:1127–1137.

Ghosh S, Ozek T, Tabanca N (2014a) Chemical composition and bioactivity studies of *Alpinia*

nigra essential oils. Ind Crops Prod 53:111–119.

Ghosh S, Ozek T, Tabanca N, Ali A (2014b) Chemical composition and bioactivity studies of *Alpinia nigra* essential oils. Ind Crops Prod 53:111–119

Ghosh S, Padilla-González GF, Rangan L (2013b) *Alpinia nigra* seeds: A potential source of free radical scavenger and antibacterial agent. Ind Crops Prod 49:348–356.

Ghosh S, Rangan L (2013) *Alpinia*: the gold mine of future therapeutics. 3 Biotech 3:173–185.

Ghosh S, Rangan L (2014a) Molecular docking and inhibition studies of α-amylase activity by labdane diterpenes from *Alpinia nigra* seeds. Med Chem Res 23:4836–4852.

Ghosh S, Rangan L (2014b) Molecular docking and inhibition kinetics of ??-glucosidase activity by labdane diterpenes isolated from tora seeds (*Alpinia nigra* B.L. Burtt.). Appl Biochem Biotechnol 175:1477–1489.

Ghosh S, Singh R, Dubey V, Rangan L (2016a) Antileishmanial activity of labdane diterpenes isolated from *Alpinia nigra* seeds. Lett Drug Des Discov 14:119–124.

Ghosh S, Singh R, Dubey V, Rangan L (2016b) Antileishmanial activity of labdane diterpenes isolated from Alpinia nigra Seeds. Lett Drug Des Discov 14:119–124.

Ghosh S, Singh RK, Kumar Dubey V, Rangan L (2017) Antileishmanial activity of labdane diterpenes isolated from *Alpinia nigra* seeds. Lett Drug Des Discov 14:119–124.

Giangiacomo KM, Kamassah A, Harris G, McManus OB (1998) Mechanism of Maxi-K channel activation by dehydrosoyasaponin-I. J Gen Physiol 112:485–501.

Gnerucci A, Faraoni P, Romano G, Fusi F (2019) Unstained cell imaging: Morphological insights from coupled fixation and darkfield microscopy. Acta Histochem 121:248–252.

Grégori G, Citterio S, Ghiani A (2001) Resolution of viable and membrane-compromised bacteria in freshwater and marine waters based on analytical flow cytometry and nucleic acid double staining. Appl Environ Microbiol 67:4662–4670.

Griffin WJ, Lin GD (2000) Chemotaxonomy and geographical distribution of tropane alkaloids. Phytochemistry 53:623–637.

Gupta MK, Senthilkumar S, Chiranjivi AK (2021) Antioxidant, anti-tyrosinase and anti-inflammatory activities of 3,5-dihydroxy-4′,7-dimethoxyflavone isolated from the leaves of *Alpinia nigra*. Phytomedicine Plus 1:100097.

Gutiérrez-Grijalva EP, López-Martínez LX, Contreras-Angulo LA (2020) Plant alkaloids: structures and bioactive properties. Plant-derived bioactives. Springer 85–117.

Guo C, Cheng M, Gross ML (2019) Protein-metal-ion interactions studied by mass spectrometry-based footprinting with isotope-encoded benzhydrazide. Anal Chem. 91:1416-1423.

Haida Z, Hakiman M (2019) A comprehensive review on the determination of enzymatic assay and nonenzymatic antioxidant activities. Food Sci Nutr 7:1555–1563.

Han YK, Park YJ, Ha YM, et al (2012) Characterization of a novel tyrosinase inhibitor, (2RS,4R)-2-(2,4-dihydroxyphenyl)thiazolidine-4-carboxylic acid (MHY384). Biochim Biophys Acta - Gen Subj 1820:542–549.

Harborne JB, Williams CA (2000) Advances in flavonoid research since 1992. Phytochemistry 55:481–504.

Haris P, Mary V, Aparna P (2017) A comprehensive approach to ascertain the binding mode of curcumin with DNA. Spectrochim Acta Part A Mol Biomol Spectrosc 175:155–163.

Hasanpourghadi M, Karthikeyan C, Pandurangan AK (2016) Targeting of tubulin polymerization and induction of mitotic blockage by Methyl 2-(5-fluoro-2-hydroxyphenyl)-1H-benzo[d]imidazole-5-carboxylate (MBIC) in human cervical cancer HeLa cell. J Exp Clin Cancer Res 35:58.

Hayat S, Sabri AN, McHugh TD (2018) Chloroform extract of turmeric inhibits biofilm formation, EPS production and motility in antibiotic resistant bacteria. J Gen Appl Microbiol 63:325–338.

He, Hu, Li (2019) Recent advances in biotransformation of saponins. Molecules 24:2365.

Heim KE, Tagliaferro AR, Bobilya DJ (2002) Flavonoid antioxidants: chemistry, metabolism and structure-activity relationships. J Nutr Biochem 13:572–584.

Hendrickx S, Leemans A, Mondelaers A (2015) Comparative fitness of a parent *Leishmania donovani* clinical isolate and its experimentally derived paromomycin-resistant strain. PLoS One 10:e0140139.

Hole KL, Williams RJ (2021) Flavonoids as an intervention for alzheimer's disease: Progress and hurdles towards defining a mechanism of action. Brain Plast 6:167–192.

Hong H, Landauer MR, Foriska MA, Ledney GD (2006) Antibacterial activity of the soy isoflavone genistein. J Basic Microbiol 46:329–335.

Hridya H, Amrita A, Sankari M (2015) Inhibitory effect of brazilein on tyrosinase and melanin synthesis: Kinetics and in silico approach. Int J Biol Macromol 81:228–234.

Hsiang TW, Yusoff MM (2012) Chemical and biological studies of *Zingiber phillipseae* rhizomes extract. Int J Pharma Bio Sci 3:631–637

Hua S-Z, Luo J-G, Wang X-B (2009) Two novel monoterpene–chalcone conjugates isolated from the seeds of *Alpinia katsumadai*. Bioorg Med Chem Lett 19:2728–2730.

Hubbe M, Chandra R, Dogu D, van Velzen STJ (2019) Analytical staining of cellulosic materials: A review. BioResources 14:7387–7464.

Iacopini P, Baldi M, Storchi P, Sebastiani L (2008) Catechin, epicatechin, quercetin, rutin and resveratrol in red grape: Content, in vitro antioxidant activity and interactions. J Food Compos Anal 21:589–598.

Ibrahim H, Aziz AN, Syamsir DR (2009) Essential oils of *Alpinia conchigera* Griff. and their antimicrobial activities. Food Chem 113:575–577.

Imran M, Aslam Gondal T, Atif M (2020) Apigenin as an anticancer agent. Phyther Res 34:1812–1828.

Islam F, Islam S, Shahjahan M (2014) Chemical constituents of essential oil from the leaf of *Alpinia Nigra* of Bangladesh. Int Food Res J 21:161–164

Issac Abraham SVP, Palani A, Ramaswamy BR (2011) Antiquorum sensing and antibiofilm potential of *Capparis spinosa*. Arch Med Res 42:658–668.

Jain SK, Prakash V (1995) Zingiberaceae in India: Phytogeography and endemism. Rheedea 5:154-169

Janjua NK, Siddiqa A, Yaqub A (2009) Spectrophotometric analysis of flavonoid–DNA binding interactions at physiological conditions. Spectrochim Acta Part A Mol Biomol Spectrosc 74:1135–1137.

Janssen A, Scheffer J (1985) Acetoxychavicol acetate, an antifungal component of *Alpinia galanga* 1. Planta Med 51:507–511.

Jeslin Kanaga Inba P, Annaraj B, Thalamuthu S, Neelakantan MA (2013) Cu(II), Ni(II), and Zn(II) complexes of salan-type ligand containing ester groups: Synthesis, characterization, electrochemical properties, and in vitro biological activities. Bioinorg Chem Appl 2013:1–11.

Jones K, Kim DW, Park JS, Khang CH (2016) Live-cell fluorescence imaging to investigate the dynamics of plant cell death during infection by the rice blast fungus *Magnaporthe oryzae*. BMC Plant Biol 16:69.

Kalaskar MG, Surana SJ (2014) Ethnomedicinal plants used against liver diseases among the tribes of India: Review. J Biol Sci 14:154–168.

Kalinowska M, Świderski G, Matejczyk M, Lewandowski W (2016) Spectroscopic, thermogravimetric and biological studies of Na(I), Ni(II) and Zn(II) complexes of quercetin. J Therm Anal Calorim 126:141–148.

Kamali E, Jamali A, Ardebili A (2020) Evaluation of antimicrobial resistance, biofilm forming potential, and the presence of biofilm-related genes among clinical isolates of *Pseudomonas aeruginosa*. BMC Res Notes 13:27.

Kanakis CD, Tarantilis PA, Polissiou MG (2007) An overview of DNA and RNA bindings to antioxidant flavonoids. Cell Biochem Biophys 49:29–36.

Karacan P, Okay O (2013) Ethidium bromide binding to DNA cryogels. React Funct Polym 73:442–450.

Karamanou M, Tsoucalas G, Pantos K, Androutsos G (2018) Isolating colchicine in 19th century: An Old Drug Revisited. Curr Pharm Des 24:654–658.

Katiyar C, Gupta A, Kanjilal S, Katiyar S (2012) Drug discovery from plant sources: An integrated approach. Ayu 33:10–9.

Kato F, Tanaka M, Nakamura K (1999) Rapid fluorometric assay for cell viability and cell growth using nucleic acid staining and cell lysis agents. Toxicol Vitr 13:923–929.

Kaur A, Singh R, Dey CS (2010) Antileishmanial phenylpropanoids from *Alpinia galanga* (Linn.) Willd. Indian J Exp Biol 48:314-317.

Kaverimanian V, Heuertz R (2019a) Effect of *Azadirachtin* on bacterial biofilm formation. FASEB J 33: S1.

Kaverimanian V, Heuertz R (2019b) Effect of *Azadirachtin* on bacterial biofilm formation. FASEB J 33:.

Keglevich P, Hazai L, Kalaus G, Szántay C (2012) Modifications on the basic skeletons of vinblastine and vincristine. Molecules 17:5893–5914.

Kettle SFA (1996) Stability of coordination compounds. In: Physical Inorganic Chemistry. Springer Berlin Heidelberg, Berlin, Heidelberg, pp 73–94.

Khan MTH, Orhan I, Senol FS (2009a) Cholinesterase inhibitory activities of some flavonoid derivatives and chosen xanthone and their molecular docking studies. Chem Biol Interact 181:383–9.

Khan MTH, Orhan I, Şenol FS (2009b) Cholinesterase inhibitory activities of some flavonoid derivatives and chosen xanthone and their molecular docking studies. Chem Biol Interact 181:383–389.

Kim D, Park J, Kim J (2006a) Flavonoids as Mushroom Tyrosinase Inhibitors: A Fluorescence Quenching Study. J Agric Food Chem 54:935–941.

Kim DE, Min JS, Jang MS (2019) Natural bis-benzylisoquinoline alkaloids-tetrandrine, fangchinoline, and cepharanthine, inhibit human coronavirus oc43 infection of mrc-5 human lung cells. Biomolecules 9:696.

Kim DH, Kim SJ, Ullah S (2017) Design, synthesis, and antimelanogenic effects of (2-substituted phenyl-1,3-dithiolan-4-yl)methanol derivatives. Drug Des Devel Ther Volume11:827–836.

Kim HJ, Lee I-S, Kang SS (2006b) Cholesterol biosynthesis inhibitors of microbial origin. Studies in Natural Products Chemistry 751–784.

Kinch MS, Patridge E, Plummer M, Hoyer D (2014) An analysis of FDA-approved drugs for infectious disease: antibacterial agents. Drug Discov Today 19:1283–7.

Koh CM (2013) Isolation of genomic dna from mammalian cells. Methods in Enzymology 161–169

Koonammackal MV, Nellipparambil UVN, Sudarsanakumar C (2011) Molecular dynamics simulations and binding free energy analysis of DNA minor groove complexes of curcumin. J Mol Model 17:2805–2816.

Korkina LG, Afanas'ev IB (1997) Antioxidant and chelating properties of flavonoids. Adv Pharmacol 38:151–63.

Kress WJ, Liu A-Z, Newman M, Li Q-J (2005) The molecular phylogeny of *Alpinia* (Zingiberaceae): a complex and polyphyletic genus of gingers. Am J Bot 92:167–178.

Kubo I, Kinst-Hori I, Chaudhuri SK (2000) Flavonols from Heterotheca inuloides : Tyrosinase Inhibitory Activity and Structural Criteria. Bioorg Med Chem 8:1749–1755.

Kumar R, Tiwari K, Dubey VK (2017) Methionine aminopeptidase 2 is a key regulator of apoptotic like cell death in *Leishmania donovani*. Sci Rep 7:95.

Kunnumakkara AB, Shabnam B, Girisa S (2020) Inflammation, NF-κB, and chronic diseases: How are they linked? Crit Rev Immunol 40:1–39.

Lachenmeier DW, Sproll C, Musshoff F (2010) Poppy Seed foods and opiate drug testing-where

are we today? Ther Drug Monit 32:11–18.

Latha C, Shriram VD, Jahagirdar SS (2009) Antiplasmid activity of 1′-acetoxychavicol acetate from *Alpinia galanga* against multi-drug resistant bacteria. J Ethnopharmacol. 123:522-525

Leal-Cardoso JH, Moreira MR, da Cruz GMP (2004) Effects of essential oil of *Alpinia zerumbet* on the compound action potential of the rat sciatic nerve. Phytomedicine 11:549–53.

Lee C-C, Chen Y-T, Chiu C-C (2015) *Polygonum cuspidatum* extracts as bioactive antioxidaion, anti-tyrosinase, immune stimulation and anticancer agents. J Biosci Bioeng 119:464–469.

Lee J-H, Jung HS, Giang PM (2006) Blockade of nuclear factor-κB signaling pathway and anti-inflammatory activity of cardamomin, a chalcone analog from *Alpinia conchigera*. J Pharmacol Exp Ther 316:271–278.

Lee J, Attila C, Cirillo SLG (2009) Indole and 7-hydroxyindole diminish *Pseudomonas aeruginosa* virulence. Microb Biotechnol.

Lee Y-H, Tuyet P-T (2019) Synthesis and biological evaluation of quercetin–zinc (II) complex for anti-cancer and anti-metastasis of human bladder cancer cells. Vitr Cell Dev Biol - Anim 55:395–404.

Li J, Yang Y, Mao Z (2016) Enhanced resolution of DNA separation using agarose gel electrophoresis doped with graphene oxide. Nanoscale Res Lett 11:404

Li J, Yu K, Bai J (2014) Synthesis, characterization and free radical scavenging activity of apigenin with or without magnesium(II). Oxid Antioxid Med Sci 3:231.

Li S, Jiang H, Lin Z (2015) An on-line high-performance liquid chromatography diode-array detector multi-stage mass spectrometry deoxyribonucleic acid 4′,6-diamidino-2-phenylindole fluorescence detector system for screening the DNA binding active compounds in Fufang Banbianlian Inje. J Chromatogr A 1424:37–50.

Li Z, Chang P-H, Jiang W-T, Liu Y (2020) Enhanced removal of ethidium bromide (EtBr) from aqueous solution using rectorite. J Hazard Mater 384:121254.

Liguori I, Russo G, Curcio F (2018) Oxidative stress, aging, and diseases. Clin. Interv. Aging 13:757–772

Lin Y-P, Hsu F-L, Chen C-S (2007) Constituents from the Formosan apple reduce tyrosinase activity in human epidermal melanocytes. Phytochemistry 68:1189–1199.

Liu B, Karttunen M (2018) Lipopeptide daptomycin: Interactions with bacterial and phospholipid membranes, stability of membrane aggregates and micellation in solution.

Biochim Biophys Acta - Biomembr 1860:1949–1954.

Liu F, Sun Z, Wang F (2020) Inhibition of biofilm formation and exopolysaccharide synthesis of Enterococcus faecalis by phenyllactic acid. Food Microbiol 86:103344.

Liu G, Li Y, Yang L, et al (2017) Cytotoxicity study of polyethylene glycol derivatives. RSC Adv 7:18252-18259.

Lopez V (2011) Are traditional medicinal plants and ethnobotany still valuable approaches in pharmaceutical research? Bol Latinoam y del Caribe Plantas Med y Aromat 10:3-10.

López JG-E (2020) Flavonoids in Health and Disease. Curr Med Chem.26:6972-6975

Lu Y, Wang Z, Wei D, Xiang H (2007) Mechanism and inhibitory effect of galangin and its flavonoid mixture from *Alpinia officinarum* on mushroom tyrosinase and B16 murine melanoma cells. J Enzyme Inhib Med Chem 22:433–438.

Ma G, Bavadekar SA, Davis YM, et al (2007) Pharmacological Effects of Ephedrine Alkaloids on Human α 1 - and α 2 -Adrenergic Receptor Subtypes. J Pharmacol Exp Ther 322:214–221.

Macdonald MH, Morrison CJ, McMaster WR (1995) Analysis of the active site and activation mechanism of the *Leishmania* surface metalloproteinase GP63. Biochim Biophys Acta - Protein Struct Mol Enzymol 1253:199–207.

Magalingam KB, Radhakrishnan AK, Haleagrahara N (2015) protective mechanisms of flavonoids in Parkinson's disease. Oxid Med Cell Longev 2015:1–14.

Malek SNA, Phang CW, Ibrahim H (2011) Phytochemical and Cytotoxic Investigations of *Alpinia mutica* Rhizomes. Molecules 16:583–589.

Malesev D, Kuntic V (2007) Investigation of metal-flavonoid chelates and the determination of flavonoids via metal-flavonoid complexing reactions. J Serbian Chem Soc 72:921–939.

Manach C, Scalbert A, Morand C (2004) Polyphenols: food sources and bioavailability. Am J Clin Nutr 79:727–47.

Mansuri R, Singh J, Diwan A (2020) An insight into the current perspective and potential drug targets for visceral leishmaniasis (VL). Curr Drug Targets 21:1105-1129.

Mao F, Ni W, Xu X (2016) Chemical structure-related drug-like criteria of global approved drugs. Molecules 21:75

Marín C, Ramírez-Macías I, López-Céspedes A, et al (2011) *In vitro* and *in vivo* trypanocidal activity of flavonoids from *Delphinium staphisagria* against chagas disease. J Nat Prod. 74:

744-750.

Marinho FA, Gonçalves KCS, Oliveira SSC (2014) The calpain inhibitor MDL28170 induces the expression of apoptotic markers in *Leishmania amazonensis* promastigotes. PLoS One 9:e87659.

Márquez MJ, Romani D, Díaz SB, Brandán SA (2018) Structural and vibrational characterization of anhydrous and dihydrated species of trehalose based on the FTIR and FTRaman spectra and DFT calculations. J King Saud Univ - Sci 30:229–249.

Mary V, Haris P, Varghese MK (2017) Experimental probing and molecular dynamics simulation of the molecular recognition of DNA duplexes by the flavonoid Luteolin. J Chem Inf Model 57:2237–2249.

Mashhadi Akbar Boojar M (2019) An overview of the cellular mechanisms of flavonoids radioprotective effects. Adv Pharm Bull 10:13–19.

Masuda T, Mizuguchi S, Tanaka T (2000) Isolation and Structure determination of new antioxidative ferulic acid glucoside esters from the rhizome of *Alpinia speciosa* , a zingiberaceae plant used in Okinawan food culture. J Agric Food Chem 48:1479–1484.

Meetei PA, Singh P, Nongdam P (2012) NeMedPlant: a database of therapeutic applications and chemical constituents of medicinal plants from north-east region of India in genomic sequences. Bioinformation 8:209–211.

Mehnert AK, Simon CS, Guizetti J (2018) Immunofluorescence staining protocol for STED nanoscopy of *Plasmodium*-infected red blood cells. bioRxiv.

Merritt, JH., Ha, DG., Cowles, KN., Lu, W., Morales, DK., Rabinowitz, J., Gitai, Z., O'Toole, GA (2010). Specific control of *Pseudomonas aeruginosa* surface-associated behaviors by two c-di-GMP diguanylate cyclases. mBio, 1(4), e00183-10.

Miljanich GP (2004) Ziconotide: neuronal calcium channel blocker for treating severe chronic pain. Curr Med Chem 11:3029–40.

Mohammadi S, Jafari B, Asgharian P (2020) Medicinal plants used in the treatment of Malaria: A key emphasis to *Artemisia, Cinchona, Cryptolepis*, and *Tabebuia* genera. Phytother Res 34:1556–1569.

Monisha J, Roy N, Padmavathi G (2018) NGAL is downregulated in oral squamous cell carcinoma and leads to increased survival, proliferation, migration and chemoresistance. cancers (Basel) 10:228.

Monson R, Baldocchi D (2014) Fluxes of biogenic volatile compounds between plants and the atmosphere. Terrestrial Biosphere-Atmosphere Fluxes. Cambridge University Press, Cambridge, 395–414

Morris GM, Huey R, Olson AJ (2008a) Using autodock for ligand-receptor docking. Curr Protoc Bioinforma 24:Unit 8.14.

Morris GM, Huey R, Olson AJ (2008b) Using autodock for ligand-receptor docking. Curr Protoc Bioinforma 24:.

Mueller MS, Runyambo N, Wagner I (2004) Randomized controlled trial of a traditional preparation of *Artemisia annua* L. (annual wormwood) in the treatment of malaria. Trans R Soc Trop Med Hyg 98:318–321.

Mukai R, Shirai Y, Saito N (2009) Subcellular localization of flavonol aglycone in hepatocytes visualized by confocal laser scanning fluorescence microscope. Cytotechnology 59:177–182.

Murase T, Inagaki H, Eimoto T (2000) Influence of histochemical and immunohistochemical stains on polymerase chain reaction. Mod Pathol 13:147–151.

Musarra-Pizzo M, Pennisi R, Ben-Amor I (2021) Antiviral activity exerted by natural products against human viruses. Viruses 13:828

Nafisi S, Hashemi M, Rajabi M, Tajmir-Riahi HA (2008) DNA adducts with antioxidant flavonoids: morin, apigenin, and naringin. DNA Cell Biol 27:433–442.

Nafisi S, Shadaloi A, Feizbakhsh A, Tajmir-Riahi HA (2009) RNA binding to antioxidant flavonoids. J Photochem Photobiol B Biol 94:1–7.

Newman DJ, Cragg GM (2016) Natural products as sources of new drugs from 1981 to 2014. J Nat Prod 79:629–61.

Nichols JA, Katiyar SK (2010a) Skin photoprotection by natural polyphenols: anti-inflammatory, antioxidant and DNA repair mechanisms. Arch Dermatol Res 302:71–83.

Nichols JA, Katiyar SK (2010b) Skin photoprotection by natural polyphenols: anti-inflammatory, antioxidant and DNA repair mechanisms. Arch Dermatol Res 302:71–83.

Nigam M, Atanassova M, Mishra AP (2019) Bioactive compounds and health benefits of *Artemisia species*. Nat Prod Commun 14:1934578X1985035.

O'Neil CS, Beach JL, Gruber TD (2018) Thiazole orange as an everyday replacement for ethidium bromide and costly DNA dyes for electrophoresis. Electrophoresis 39:1474–1477.

O'Neil CS, Beach JL, Gruber TD (2019) DNA electrophoresis using thiazole orange instead of ethidium bromide or alternative dyes. J Vis Exp.145

Oonmetta-aree J, Suzuki T, Gasaluck P, Eumkeb G (2006) Antimicrobial properties and action of galangal (A*lpinia galanga* Linn.) on Staphylococcus aureus. LWT - Food Sci Technol 39:1214–1220.

Othman AFM, Rukayadi Y, Radu S (2019) Inhibition of *Pseudomonas aeruginosa* Quorum sensing by *Curcuma xanthorrhiza* Roxb. Extract. J Pure Appl Microbiol. 13:1335-1347.

Ozturk II, Hadjikakou SK, Hadjiliadis N, Kourkoumelis N, Kubicki M, Baril M, Butler IS, Balzarini J (2007) Synthesis, structural characterization, and biological studies of new antimony(III) complexes with thiones. The influence of the solvent on the geometry of the complexes. Inorg Chem. 46:8652-61.

Panche AN, Diwan AD, Chandra SR (2016) Flavonoids: an overview. J Nutr Sci 5:e47.

Papadopoulou A, Green RJ, Frazier RA (2005) Interaction of flavonoids with bovine serum albumin: a fluorescence quenching study. J Agric Food Chem 53:158–163.

Paredes A, Alzuru M, Mendez J, Rodríguez-Ortega M (2003) Anti-sindbis activity of flavanones hesperetin and naringenin. Biol Pharm Bull 26:108–109.

Patocka J, Nepovimova E, Wu W, Kuca K (2020) Digoxin: Pharmacology and toxicology—A review. Environ Toxicol Pharmacol 79:103400.

Patrono C (2019) Aspirin. In: Platelets. Elsevier,921–936

Perez-Llarena F, Bou G (2009) Lactamase Inhibitors: The Story so Far. Curr Med Chem.

Perez CA, Wei Y, Guo M (2009) Iron-binding and anti-Fenton properties of baicalein and baicalin. J Inorg Biochem 103:326–332.

Pham HNT, Vuong Q Van, Bowyer MC, Scarlett CJ (2020) Phytochemicals derived from *Catharanthus roseus* and their health benefits. Technologies 8:80.

Phitak T, Choocheep K, Pothacharoen P, et al (2009) The effects of p-hydroxycinnamaldehyde from *Alpinia galanga* extracts on human chondrocytes. Phytochemistry 70:237–243.

Pilling M, Gardner P (2016) Fundamental developments in infrared spectroscopic imaging for biomedical applications. Chem Soc Rev 45:1935–1957.

Pinzi L, Rastelli G (2019) Molecular docking: shifting paradigms in drug discovery. Int J Mol Sci 20:4331.

Prakash J, Yadav S, Saha G, et al (2019) Episomal expression of human glutathione reductase

(HuGR) in *Leishmania* sheds light on evolutionary pressure for unique redox metabolism pathway: Impaired stress tolerance ability of *Leishmania donovani*. Int J Biol Macromol 121:498–507.

Prasad AS (2008) Zinc in Human Health: Effect of zinc on immune cells. Mol Med 14:353–357.

Pratim Sarma M (2017) Phytochemical analysis of traditional medicinal plants and their antimicrobial activity: An experience from north east india. Open Access J Pharm Res 1:000104.

Primikyri A, Mazzone G, Lekka C, et al (2015) Understanding zinc(ii) chelation with quercetin and luteolin: A combined NMR and theoretical study. J Phys Chem B 119:83–95.

Profumo E, Buttari B, D'Arcangelo D, et al (2016) The nutraceutical dehydrozingerone and its dimer counteract inflammation- and oxidative stress-induced dysfunction of in vitro cultured human endothelial cells: A novel perspective for the prevention and therapy of atherosclerosis. Oxid Med Cell Longev 2016:1–12.

Puhs K, MG T, NS W (2020) Antibiofilm Activity of Galangal (*Alpinia galanga*) Against Staphylococcus aureus. Food Process Nutr Sci 1:123-131.

Qais FA, Ahmad I (2018) In vitro interaction of cefotaxime with calf thymus DNA: Insights from spectroscopic, calorimetric and molecular modelling studies. J Pharm Biomed Anal 149:193–205.

Qiao C, Han Q, Song J, et al (2007) HPLC determination of two bioactive flavone glycosides and GC-MS analysis of volatile oil constituents in *Alpinia nigra*. Medicine (Baltimore) 2:85-91

Qiao C, Wang Z, Dong H, et al (2000) The chemical constituents of Blackfruit Galangal (Alpinia nigra). Chinese Tradit Herbs Med 31:404–405

Rahman A, O'Sullivan P, Rozas I (2019) Recent developments in compounds acting in the DNA minor groove. Medchemcomm 10:26–40.

Ramesh PS, Madegowda V, Kumar S, et al (2019) DNA extraction from archived hematoxylin and eosin-stained tissue slides for downstream molecular analysis. World J Methodol 9:32–43.

Rana R AC, Gulliya B (2019) Chemistry and pharmacology of flavonoids- A review. Indian J Pharm Educ Res 53:8–20.

Rao K, Ch B, Narasu LM, Giri A (2010) Antibacterial activity of *Alpinia galanga* (L) willd

crude extracts. Appl Biochem Biotechnol 162:871–884.

Ray S, Sengupta C, Roy K (2007) QSAR modeling of antiradical and antioxidant activities of flavonoids using electrotopological state (E-State) atom parameters. Open Chem 5:1094–1113.

Richardson PM, Harborne JB (1985) Phytochemical methods. Brittonia 37:309.

Robert K, Boggess, David A, Zatko (1975) The use of conductivity data for the structure determination of metal complexes. J Chem Educ 52: 649.

Rosso AM (2010) Poppy and opium in ancient times : Remedy or Narcotic ? Biomed Int 1: 81-87

Roy B, Tandon V (1998) Flukicidal activity of *Alpinia nigra* (Zingibe-raceae) against Fasciolopsis buski. Parasitol Int 47:241.

Roy B, Tandon V (1999) Flukicidal activity of *Alpinia nigra* (Zingiberaceae) against the trematode, Fasciolopsis buski, in humans. Biomed Lett 60:23-29.

Ruyter C, Akram M, Illahi I, Stöckigt J (1991) Investigation of the alkaloid content of *Rauwolfia serpentina* roots from regenerated plants. Planta Med 57:328–330.

Ryder C, Byrd M, Wozniak DJ (2007) Role of polysaccharides in *Pseudomonas aeruginosa* biofilm development. Curr Opin Microbiol 10:644–8.

Saeedi M, Eslamifar M, Khezri K (2019) Kojic acid applications in cosmetic and pharmaceutical preparations. Biomed Pharmacother 110:582–593.

Saeidnia S, Abdollahi M (2013) Are other fluorescent tags used instead of ethidium bromide safer? DARU J Pharm Sci 21:71.

Saha K, Sinha RK, Sinha S (2020) Distribution, cytology, genetic diversity and molecular phylogeny of selected species of zingiberaceae - A Review. Feddes Repert 131:58–68.

Sahoo S, Ghosh G, Das D, Nayak S (2013) Phytochemical investigation and In vitro antioxidant activity of an indigenous medicinal plant *Alpinia nigra* B.L. Burtt. Asian Pac J Trop Biomed 3:871–876.

Sahoo S, Kar B, Sahoo A, Nayak S (2017) Phytoconstituents analysis and bioactivity study of *Alpinia nigra* (Gaertn.) Burtt. J Essent Oil Bear Plants 20:1461–1471.

Sahoo SC, Ray M (2010) Three point chiral recognition and resolution of amino alcohols through well-defined interaction inside a metallocavity. Chem – A Eur J 16:5004–5007.

Saini S, Bharati K, Shaha C, Mukhopadhyay CK (2017) Zinc depletion promotes apoptosis-like death in drug-sensitive and antimony-resistance *Leishmania donovani*. Sci Rep 7:10488.

Salerni BL, Bates DJ, Albershardt TC, et al (2010) Vinblastine Induces Acute, Cell Cycle Phase–Independent Apoptosis in Some Leukemias and Lymphomas and Can Induce Acute Apoptosis in Others when Mcl-1 Is Suppressed. Mol Cancer Ther 9:791–802.

Santos GKN, Dutra KA, Barros RA, et al (2012) Essential oils from *Alpinia purpurata* (Zingiberaceae): Chemical composition, oviposition deterrence, larvicidal and antibacterial activity. Ind Crops Prod 40:254–260.

Saudagar P, Dubey VK (2014) Molecular Mechanisms of *In vitro* betulin-induced apoptosis of *Leishmania donovani*. Am J Trop Med Hyg 90:354–360.

Saudagar P, Saha P, Saikia AK, Dubey VK (2013) Molecular mechanism underlying antileishmanial effect of oxabicyclo[3.3.1]nonanones: Inhibition of key redox enzymes of the pathogen. Eur J Pharm Biopharm 85:569–577.

Savić-Gajić IM, Savić IM (2020) Drug design strategies with metal-hydroxyquinoline complexes. Expert Opin. Drug Discov 15:383-390.

Saxena M, Dubey R (2019) Target Enzyme in Alzheimer's Disease: Acetylcholinesterase Inhibitors. Curr Top Med Chem 19:264–275.

Schallreuter KU, Kothari S, Chavan B, Spencer JD (2008) Regulation of melanogenesis - controversies and new concepts. Exp Dermatol 17:395–404.

Scimeca M, Bischetti S, Lamsira HK (2018) Energy Dispersive X-ray (EDX) microanalysis: A powerful tool in biomedical research and diagnosis. Eur J Histochem 62:2841

Selvarajan E, Mohanasrinivasan V (2013) Biosynthesis and characterization of ZnO nanoparticles using *Lactobacillus plantarum* VITES07. Mater Lett 112:180–182.

Semedo MG, Dias-Silva N, Miguéis J, Pita JR (2021) Quinine in otology and neurotology: Ototoxicity and historic role in therapy. Otol Neurotol 42:145-152.

Sen R, Bandyopadhyay S, Dutta A, et al (2007) Artemisinin triggers induction of cell-cycle arrest and apoptosis in *Leishmania donovani* promastigotes. J Med Microbiol 56:1213–1218.

Shah Z, Gohar UF, Jamshed I, et al (2021) Podophyllotoxin: history, recent advances and future prospects. Biomolecules 11:603.

Sheldrick GM (2008) SHELX 97-2014. Acta Crystallogr A 64:

Shen Y, Zhang J, Sheng R (2009) Synthesis and biological evaluation of novel flavonoid derivatives as dual binding acetylcholinesterase inhibitors. J Enzyme Inhib Med Chem

24:372–80.

Shimmyo Y, Kihara T, Akaike A, et al (2008) Flavonols and flavones as BACE-1 inhibitors: structure-activity relationship in cell-free, cell-based and in silico studies reveal novel pharmacophore features. Biochim Biophys Acta 1780:819–25.

Silva TM, Bolzan TCA, Zanini MS (2020) Development and evaluation of a novel oral mucoadhesive ointment containing pomegranate peel extract as an adjuvant for oral hygiene of dogs. J Vet Dent 37:133-140.

Sinclair SA, Krämer U (2012) The zinc homeostasis network of land plants. Biochim Biophys Acta - Mol Cell Res 1823:1553–1567.

Singh G, Dey CS (2007) Induction of apoptosis-like cell death by pentamidine and doxorubicin through differential inhibition of topoisomerase II in arsenite-resistant *L. donovani*. Acta Trop 103:172–185.

Sirat HM, Jani NA (2013) Chemical constituents of the leaf of *Alpinia mutica* Roxb. Nat Prod Res 27:1468–70.

Snow Setzer M, Sharifi-Rad J, Setzer W (2016) The search for herbal antibiotics: An In-Silico investigation of antibacterial phytochemicals. Antibiotics 5:30.

Soleimanpour M, Imani F, Safari S (2016) The role of non-steroidal anti-inflammatory drugs (NSAIDs) in the treatment of patients with hepatic disease: A Review Article. Anesthesiol Pain Med 6:e37822

Somani S (1990) Eseroline, a metabolite of physostigmine, induces neuronal cell death. Toxicol Appl Pharmacol 106:28–37.

Song J, Liao X, Hu X, Chen F (2017) Screening *In vitro* Model for acrylamide-induced cytotoxicity intervention by cyanidin-3-glucoside. J Chinese Inst Food Sci Technol 17:11–19.

Song YJ, Yu HH, Kim YJ, et al (2019) Anti-biofilm activity of grapefruit seed extract against *Staphylococcus aureus* and *Escherichia coli*. J Microbiol Biotechnol 29:1177–1183.

Srivastava M, Kesharwani S, Kesharwani R, et al (2021) A review on potential bioactive chemical from *Rauwolfia serpentina*: reserpine. Int J Res Ayurveda Pharm 12:106–109.

Suhitha S, Devi S, Gunasekaran K, et al (2015) Phytochemical analyses and activity of herbal medicinal plants of north- east india for anti-diabetic, anti-cancer and anti-tuberculosis and their docking studies. Curr Top Med Chem 15:21–36.

Sun H, Zhang P, Zhu Y, et al (2018) Antioxidant and prebiotic activity of five peonidin-based anthocyanins extracted from purple sweet potato (*Ipomoea batatas* (L.) Lam.). Sci Rep 8:5018.

Swargiary A (2015) Astragalin, the active component of *Alpinia nigra* and its effect on tegumental ultrastructure of fluke parasite, *Fasciolopsis buski*. Int J Pharma Bio Sci

Swargiary A, Roy B (2015) In vitro anthelmintic efficacy of *Alpinia nigra* and its bioactive compound, astragalin against *Fasciolopsis Buski*. Int J Pharm Pharm Sci 7:30–35

Tajmir-Riahi HA, Diamantoglou S, Kanakis CD, et al (2007) Flavonoids interactions with DNA and RNA: binding modes and antioxidative effects. Acta Hortic 744:195–204.

Tan J, Wang B, Zhu L (2009) DNA binding, cytotoxicity, apoptotic inducing activity, and molecular modeling study of quercetin zinc(II) complex. Bioorg Med Chem 17:614–620.

Tang Z, Sahu SN, Khadeer MA (2006) Overexpression of the ZIP1 zinc transporter induces an osteogenic phenotype in mesenchymal stem cells. Bone 38:181–198.

Tejada S, Pinya S, Martorell M, et al (2017) Potential anti-inflammatory effects of hesperidin from the Genus *Citrus*. Curr Med Chem 25: 4929-4945

Thi MTT, Wibowo D, Rehm BHA (2020) *Pseudomonas aeruginosa* Biofilms. Int J Mol Sci 21: 8671

Thomford NE, Senthebane DA, Rowe A (2018) Natural products for drug discovery in the 21st century: Innovations for Novel Drug Discovery. Int J Mol Sci 19:1578.

Tsednee M, Huang YC, Chen YR, Yeh KC (2016) Identification of metal species by ESI-MS/MS through release of free metals from the corresponding metal-ligand complexes. Sci Rep. 6:26785.

Tu L-Y, Pi J, Jin H (2016) Synthesis, characterization and anticancer activity of kaempferol-zinc(II) complex. Bioorg Med Chem Lett 26:2730–2734.

Tushar, Basak S, Sarma GC, Rangan L (2010a) Ethnomedical uses of Zingiberaceous plants of Northeast India. J Ethnopharmacol 132:286–96.

Tushar, Basak S, Sarma GC, Rangan L (2010b) Ethnomedical uses of Zingiberaceous plants of Northeast India. J Ethnopharmacol 132:286–296.

Tyrrell RM, Keyse SM (1990) New trends in photobiology the interaction of UVA radiation with cultured cells. J Photochem Photobiol B Biol 4:349–361.

Uivarosi V, Munteanu A (2017) Flavonoid complexes as promising anticancer metallodrugs. in:

Flavonoids - From Biosynthesis to Human Health. InTech 14: 305-333.

Ullah A, Munir S, Badshah SL, et al (2020) Important flavonoids and their role as a therapeutic agent. Molecules 25:5243.

Unni BG, Borah A, Wann SB, et al (2009) Phytochemical and antibacterial study of traditional medicinal plants of North East India on *Escherichia coli*. Asian J Exp Sci 23:103-108

Upadhyay A, Chompoo J, Kishimoto W, et al (2011) HIV-1 integrase and neuraminidase inhibitors from Alpinia zerumbet. J Agric Food Chem 59:2857–2862.

Uz E, Karatas OF, Mete E, et al (2009) The effect of dietary ginger (*Zingiber officinals* Rosc) on renal ischemia/reperfusion injury in rat kidneys. Ren Fail 31:251–60.

Van BL, Hendrickx S, Maes L, Caljon G (2020) Sand fly studies predict transmission potential of drug-resistant Leishmania. Trends Parasitol. 36:785-795.

Vardevanyan PO, Antonyan AP, Parsadanyan MA (2003) The binding of ethidium bromide with DNA: interaction with single and double-stranded structures. Exp Mol Med 35:527–533.

Vasavi HS, Arun AB, Rekha PD (2016) Anti-quorum sensing activity of flavonoid-rich fraction from *Centella asiatica* L. against *Pseudomonas aeruginosa* PAO1. J Microbiol Immunol Infect 49:8–15.

Vellosa JCR, Regasini LO, Khalil NM (2011) Antioxidant and cytotoxic studies for kaempferol, quercetin and isoquercitrin. Eclética Química 36:07–20.

Vlachojannis J, Magora F, Chrubasik S (2011) Willow Species and Aspirin: Different Mechanism of Actions. Phyther Res 25:1102–1104.

Wang T, Li Q, Bi K (2018) Bioactive flavonoids in medicinal plants: Structure, activity and biological fate. Asian J Pharm Sci 13:12–23.

Wang YC, Huang TL (2005) Screening of anti- *Helicobacter pylori* herbs deriving from Taiwanese folk medicinal plants. FEMS Immunol Med Microbiol 43:295–300.

Wang Y, Schellenberg H, Walhorn V (2017) Binding mechanism of PicoGreen to DNA characterized by magnetic tweezers and fluorescence spectroscopy. Eur Biophys J 46:561–566.

Wangchuk P (2019) Plant Alkaloids: Classification, Isolation, and Drug Development. Medicinal Plants 1:131–138.

Warinhomhoun S, Muangnoi C, Buranasudja V (2021) Antioxidant activities and protective effects of dendropachol, a new bisbibenzyl compound from *Dendrobium pachyglossum*, on

hydrogen peroxide-induced oxidative stress in HaCaT keratinocytes. Antioxidants 10:252.

Weerakkody NS, Caffin N, Lambert LK (2011) Synergistic antimicrobial activity of *Galangal* (*Alpinia galanga*), rosemary (*Rosmarinus officinalis*) and lemon iron bark (*Eucalyptus staigerana*) extracts. J Sci Food Agric 91:461–468.

Wheeler RJ, Gluenz E, Gull K (2011) The cell cycle of *Leishmania*: morphogenetic events and their implications for parasite biology. Mol Microbiol 79:647–662.

Xiong Z, Liu W, Zhou L (2016) Mushroom (*Agaricus bisporus*) polyphenoloxidase inhibited by apigenin: Multi-spectroscopic analyses and computational docking simulation. Food Chem 203:430–439.

Xu D, Hu M-J, Wang Y-Q, Cui Y-L (2019) Antioxidant activities of quercetin and its complexes for medicinal application. Molecules 24:1123.

Yadav PN, Liu Z, Rafi MM (2003) A Diarylheptanoid from lesser *Galanga*l (*Alpinia officinarum*) inhibits proinflammatory mediators via inhibition of mitogen-activated protein kinase, p44/42, and transcription factor nuclear factor-κb. J Pharmacol Exp Ther 305:925–931.

Yang D, Rogers M V., Brett SJ, Liew FY (1993) Immunological analysis of the zinc-binding peptides of surface metalloproteinase (gp63) of *Leishmania major*. Immunology 78:582–585.

Yaorong W, Xiaoling L (2019) Anti-tumor mechanism and drug activity analysis of NUTMEG. Bol Malariol y Salud Ambient 59:34-42.

Yi JL, Shi S, Shen YL, et al (2015) Myricetin and methyl eugenol combination enhances the anticancer activity, cell cycle arrest and apoptosis induction of cis-platin against HeLa cervical cancer cell lines. Int J Clin Exp Pathol 8:

Yimdjo MC, Azebaze AG, Nkengfack AE (2004) Antimicrobial and cytotoxic agents from *Calophyllum inophyllum*. Phytochemistry 65:2789–2795.

Yuan H, Ma Q, Ye L, Piao G (2016) The *Traditional Medicine and Modern Medicine from Natural Products*. Molecules 21:559.

Yusoff MM, Ibrahim H, Hamid NA (2011) Chemical characterization and antimicrobial activity of rhizome essential oils of very closely allied zingiberaceae species endemic to borneo: *Alpinia ligulata* K. Schum. and *Alpinia nieuwenhuizii* Val. Chem Biodivers 8:916–923.

Zadrazil J (2010) Nonsteroidal antiinflammatory drugs and the kidney. Vnitr Lek 52:686–90.

Zhou C, Li C, Siva S, et al (2021) Chemical composition, antibacterial activity and study of the interaction mechanisms of the main compounds present in the *Alpinia galanga* rhizomes essential oil. Ind Crops Prod 165:113441.

Zimmermann Franco DC, Gonçalves de Carvalho GS, Rocha PR (2012) Inhibitory effects of resveratrol analogs on mushroom tyrosinase activity. Molecules 17:11816–11825.

Publications

Published:

Gupta MK, Chiranjivi AK, Dutta T, Dubey VK, Rangan L, (2022) Synthesis and characterization of zinc derivatized 3, 5-dihydroxy 4′, 7-dimethoxyflavone and its anti leishmaniasis activity against *Leishmania donovani* ***BioMetals*** 10.1007/s10534-022-00364-x.

Gupta MK, Singh R, Rangan L, (2022) Phytochemical screening, antibacterial, anti-biofilm and quorum sensing inhibiting activity of *Alpinia nigra* leaf extract against infectious pathogen-*Pseudomonas aeruginosa* PAO1 ***Food Control*** 143: 109327.

Gupta MK, Senthilkumar S, Chiranjivi AK, Banik k, Girisa S, Kunnumakkara AK, Dubey VK, Rangan L, (2021) Antioxidant, anti-tyrosinase and anti-inflammatory activities of 3,5-dihydroxy-4′,7-dimethoxyflavone isolated from the leaves of *Alpinia nigra* ***Phytomedicine plus*** 1, (3), 100097.

Sahu S, Rajbonshi MP, Gujre RN, **Gupta MK**, Shelke RG, Ghose A, Rangan L, Pakshirajan K, Mitra S, (2022) Bacterial strains found in the soils of a municipal solid waste dumping site facilitated phosphate solubilization along with cadmium remediation ***Chemosphere*** 287, (3), 132320.

Manuscript under review:

Das A, Saha M, **Gupta MK**, Rangan L, Uppaluri R, Das C, (2022) Comparative Efficacy of Citric acid/Tartaric acid/Malic acid Additive based Polyvinyl alcohol-Starch Composite Films. ***Carbohydrate Polymers***.

Das R, Senapati A, **Gupta MK**, Rangan L, (2022) Study of biomarker for seed germination in non-edible oil crops ***Genetic Resources and Crop Evolution***.

Patent

Senthilkumar S, **Gupta MK**, Boro H, Rangan L, (2021) Device for evaporation and recovery of organic solvents using simple labwares. (**Indian patent application number TEMP/E-1/5498/2021-KOL**)

Das A, Uppaluri VSR, Das C, Saha M, **Gupta MK**, Rangan L, (2021) Cost effective composition of wound dressing compatible polymer hydrogel composite films. (**Indian patent application number 202131059065**)

Conferences Participation/ Presentations:

Gupta MK, Rajkumari J, Rangan L*, Synthesis and characterization of flavone-zinc complex compound and determination of its anti-biofilm efficacy, International conference on Biotechnology for Sustainable Agriculture, Environment and Health (BSAEH-2021) Malaviya National Institute of Technology, Jaipur, India. April 04-08, 2021.

Gupta MK, Chiranjivi AK, Dubey VK, Rangan L, Study of zinc derivatized 3,5-dihydroxy-4',7-dimethoxyflavone against Leishmania parasite. 4th International Conference on Nutraceuticals and Chronic Diseases (INCD-2019), Indian Institute of Technology Guwahati, Assam, India pp 141.

Gupta MK, Rangan L, 3,5-dihydroxy-4'7-dimethoyflavone: Structural characterization, enzyme kinetics, and in-silico approach against melanogenic activity, Indian Plant Science Congress (IPSC 2019) SRM Institute of science and Technology, Chennai pp115.

Gupta MK, Rangan L, 3,5-dihydroxy-4'7-dimethoxyflavone: Isolation and characterization from *Alpinia nigra*, Trends in Biochemical and Biomedical Research (TBBR-2018), Banaras Hindu University, Varanasi pp143.

Conference Publications:

Gupta MK, Rangan L, (2018) 3,5-dihydroxy-4'7-dimethoxyflavone: Isolation and characterization from *Alpinia nigra*, Proceeding of international conference on trends in biochemical and biomedical research: advances and challenges. ***Research Reports***; 2:e1-e205.0.00

NEWGEN-IEDC project grant:

Senthilkumar S, **Gupta MK**, Boro H, Rangan L, (2021) Device for evaporation and recovery of organic solvents using simple labwares.

Gupta MK, Senthilkumar S, Nuzelu, Rangan L, (2022) Development of a Cosmeceutical as a Skin Care Product from Plant Source.

Senapati A, Singh R, **Gupta MK**, Rangan L, (2022) One step ready to use versatile nucleus isolation buffer for plant DNA quantification.

Workshops:

- Nuclear Magnetic Resonance: Technique and its Application North East Centre for Biological Sciences and Healthcare Engineering (NECBH) Indian Institute of Technology Guwahati, Assam, 23rd to 24th August 2021
- Flow Cytometry and its Applications in Biological Research and Clinical Diagnostics" Organized by Trust for Education and Training in Cytometry (TETC) 22nd-28th February 2021.
- Online workshop on Flow Cytometry Techniques and Applications North East Centre for Biological Sciences and Healthcare Engineering (NECBH) Indian Institute of Technology Guwahati, Assam December 21 & 22, 2020.
- Indo-Japan Workshop on Translation Agriculture at IIT Guwahati (2017).
- Intellectual Property Rights- hands on training on patent search, by Research Conclave 2017, IIT Guwahati at IIT Guwahati (March 2017).
- Intellectual Property Rights, by IPR Cell, R&D Section, IIT Guwahati at IIT Guwahati (3rd November 2016).